Investigating and exploiting metabolic vulnerabilities in cancer

A dissertation presented

by

Natalie Janelle German

to

The Division of Medical Sciences

in partial fulfillment of the requirements

for the degree of

Doctor of Philosophy

in the subject of

Biological and Biomedical Sciences

Harvard University

Cambridge, Massachusetts

April 2015

Dissertation Advisor: Dr. Marcia Haigis Natalie Janelle German

Investigating and exploiting metabolic vulnerabilities in cancer

Abstract

Fuel metabolism in healthy cells is not sufficient to sustain the biosynthetic and energetic demands of cancer. For a normal cell to transform to a rapidly dividing tumor cell, metabolism must be dramatically altered in a process called metabolic reprogramming, characterized by increased nutrient uptake and re-purposing. As we move toward a future of personalized medicine, there is new opportunity in targeting the metabolic requirements specific to an individual's tumor. To this end, it is critical to understand molecular drivers that cancer cells hijack to modify metabolism.

In this dissertation, I describe three studies on enzymes and metabolic pathways that shed light on molecular regulation of metabolic reprogramming in cancer. First, we screened for substrates of SIRT4, a mitochondrial sirtuin that promotes metabolic homeostasis and suppresses cancer by mechanisms not well understood. We used proteomics to identify hyperacetylated mitochondrial proteins in SIRT4 knockout mouse tissues compared to wildtype. We find SIRT4 binds and inhibits pyruvate carboxylase, an enzyme important for refueling the TCA cycle in cancer, indicating SIRT4 may target this node in tumor metabolism. Second, we reveal a role for prolyl hyrdoxylase domain (PHD) 3 in coordinating cancer cell addition to fat catabolism. In biochemical and cellular studies, we find PHD3 hydroxylates and activates acetyl-CoA carboxylase (ACC2) to repress fatty acid oxidation (FAO). Loss of this regulatory axis in leukemia enables greater utilization of fatty acids as fuel, and also serves as a liability by rendering

cells susceptible to FAO inhibition. Finally, we used metabolomics to define alterations caused by the diabetes drugs metformin and phenformin to better understand their anti-cancer properties. We analyzed the drugs' effects on cells undergoing neoplastic transformation and on cancer stem cells (CSCs), a small population that possesses predominant tumor-initiation capacity and is selectively inhibited by metformin. We show metformin and phenformin induce changes that oppose cancer cell survival by eliciting a nutrient crisis during transformation and depleting nucleotide triphosphates in CSCs. In sum, these findings contribute to the future potential to impede nutrient switches in cancer, thus turning the metabolic dependencies of cancer cells into metabolic vulnerabilities.

TABLE OF CONTENTS

Abstract iii

Acknowledgements vi

Chapter I: Introduction 1

Chapter II: Acetylation proteomics reveal SIRT4 may have broad deacetylase activity in brown adipose tissue 55

Chapter III: PHD3 hydroxylates and activates acetyl-CoA carboxylase to limit fatty acid oxidation in cancer 82

Chapter IV: Metformin and phenformin deplete tricarboxylic acid cycle and glycolytic intermediates during cell transformation and NTPs in cancer stem cells 118

Chapter V: Discussion 146

Appendix I: SIRT4 coordinates the balance between lipid synthesis and catabolism by repressing malonyl CoA decarboxylase 157

Appendix II: Supplemental data tables and figures to accompany Chapters II-IV 191

ACKNOWLEDGEMENTS

I owe many thanks to Marcia Haigis for her mentorship and ever-present enthusiasm for science. I am grateful for the many opportunities she has given me to attend conferences, teach at Harvard and abroad and explore multiple research projects. I have much gratitude for the members of the Haigis lab- especially Gaëlle Laurent, Noga Ron-Harel, Karina Gonzalez and Jaewon Lee- for their encouragement, helpful discussions and making the lab an enjoyable place to be over the past several years.

I have been very fortunate to collaborate with many excellent scientists throughout Harvard: Rushdia Yusuf, Andreas Janzer, Jlenia Guarnerio, Wilhelm Haas, Kevin Struhl, Pier Paolo Pandolfi, Steve Gygi, Andrew Beck and David Scadden. I give special thanks to Pat Murphy and Bill Kaelin for their close collaborations and for being such nice people to work with. I would like to thank the members of my dissertation advisory committee, Nika Danial, John Blenis and Wade Harper, who provided invaluable guidance and support during my time as a student. Also, many thanks to my dissertation examination committee: Matt Vander Heiden, Brendan Manning and Thomas Michel.

I am incredibly grateful for my close friends Lauren Barclay, Katherine Helming and Arthur Thovmasian with whom I shared the ups and downs that go along with completing our doctorates. Lauren has been a wonderful friend and confidant, and without her grad school would not have been nearly as much fun. Katherine was the first person to make me feel at home in Boston, and she became my inspiration to pursue cancer research in a way that always keeps the patients in mind. Artie was a constant source of support, an example of perseverance and the one person who always helped me

see past the particular stresses of the day and have a brighter outlook. I thank my siblings, Nick, Emily and Chris, for their encouraging words, lightheartedness and joy they shared all the way across the country. Above all, I owe many thanks to my parents, Allen and Cheryl German, for their incredible example of working hard every day and being cheerful in the process.

CHAPTER I

Introduction[1]

It is more relevant than ever to understand how metabolism influences tumor growth. Metabolic dependencies of cancer cells are increasingly being realized as promising candidates for therapeutic interventions in cancer[1-3]. A vast number of studies validate the notion that metabolic dysfunction is not just a consequence of cancer growth but rather a driving factor in tumor progression[4, 5]. Indeed, altered metabolism enables tumor cells to fuel a number of processes, such as amassing a pool of biosynthetic precursors, constructing signaling molecules, generating metabolites for post-translational or epigenetic modifications, and maintaining pH and redox homeostasis[6, 7]. Furthermore, metabolic dysfunction has positioned itself at the forefront of cancer research with the recognition of the undeniable connection between increased cancer incidence and the background of obesity and metabolic disease, pathologies that have reached epidemic proportions in the United States and much of the world[8-11]. It is critical to fully understand the altered metabolism of tumor cells and the pathways that might promote or oppose this metabolic dysfunction.

Central to metabolic regulation in cancer are cellular decisions coordinating fuel preference and utilization. Our cells may be simultaneously exposed to multiple nutrients, and the choice of which fuel to take up and how to use it directs the function of the cell, for example driving growth, energy production, differentiation or stress response[12]. Because altered nutrient consumption and utilization are hallmarks of

[1] This chapter contains modified portions of a review article written by Natalie German that has been submitted for publication in *Current Biology*.

cancer, it is vital to characterize the regulatory nodes that coordinate fuel preference and fate, and to understand how these pathways might contribute to cancer.

Research in the field of cell metabolism has highlighted families of proteins that sense the nutrient state and instigate appropriate metabolic responses. Our cells have evolved diverse enzymes capable of detecting nutrient availability and bioenergetic status and consequently adjusting cellular behavior to promote growth, survival or to deal with stress[13, 14]. Many of these enzymes modulate cell metabolism through post-translational modification of metabolic enzymes, transcription factors or components of signaling pathways. When metabolite-sensing enzymes are dysfunctional, downstream effector proteins can be inappropriately modified, leading to the altered metabolism that characterizes cancer cells[15].

With this landscape in mind, the overarching goal of this thesis was to understand how nutrient sensing pathways in the cell control fuel utilization and furthermore to assess the relevance of these regulatory nodes in cancer. Through studies such as this, our expanding knowledge of how tumor cells use fuel can propel future development of targeted cancer treatments. To discover novel regulatory nodes in cell metabolism, I first focused on two distinct families of regulatory enzymes that are well poised to play pivotal roles in tumor metabolism: sirtuins and prolyl hydroxylase domain (PHD) enzymes. The seven mammalian sirtuins (SIRT1-7) and the three PHDs (PHD1-3) have the unique ability to integrate cellular stress response with coordination of metabolic fitness and homeostasis[16-18]. The role of sirtuins and PHDs as post-translational modifying enzymes may have originated to allow survival under stress, and many of these roles have now been linked to growth regulation in the harsh conditions

experienced by cancer cells[19-21]. In recent years, a number of studies have shown that sirtuins and PHDs not only coordinate cancer cell growth and survival, but also the metabolic state of a tumor[18, 22, 23]. There is growing interest in pinpointing metabolic regulatory nodes that can be targeted in cancer treatment and determining whether enzymes such as sirtuins and PHDs may be promising biomarkers or therapeutic targets in cancer.

Additionally in this thesis, I explored the action of a small molecule modulator of metabolism, metformin, to gain insight to the anti-cancer benefits of interfering with cell metabolism. Metformin is the world's most commonly used diabetes drug that is prescribed 120 million times each year[24]. Multiple retrospective studies have made the perplexing discovery that, compared to diabetic patients treated by other therapeutics, those patients treated with metformin went on to have lower incidences of cancer. Biochemical, cellular and animal studies have supported this finding, showing metformin does indeed have anti-cancer properties. However the direct or indirect mechanisms by which metformin inhibits cancer onset are not entirely clear. Efforts are underway to characterize the metabolic alterations caused by metformin with the hope of making a stronger, more specific drug with even greater anti-cancer effects.

Sirtuin activity is linked to the metabolic state

SIRT1-7 are a family of deacylases and ADP-ribosyltransferases that have been strongly linked to cancer metabolism. All sirtuins share a conserved catalytic core domain but vary in subcellular localization and preferred substrates (Figure 1.1 a)[25]. These differences lead to variations in the ultimate metabolic effect that is coordinated by each sirtuin[19]. SIRT1, 6 and 7 are primarily nuclear and regulate transcription factors

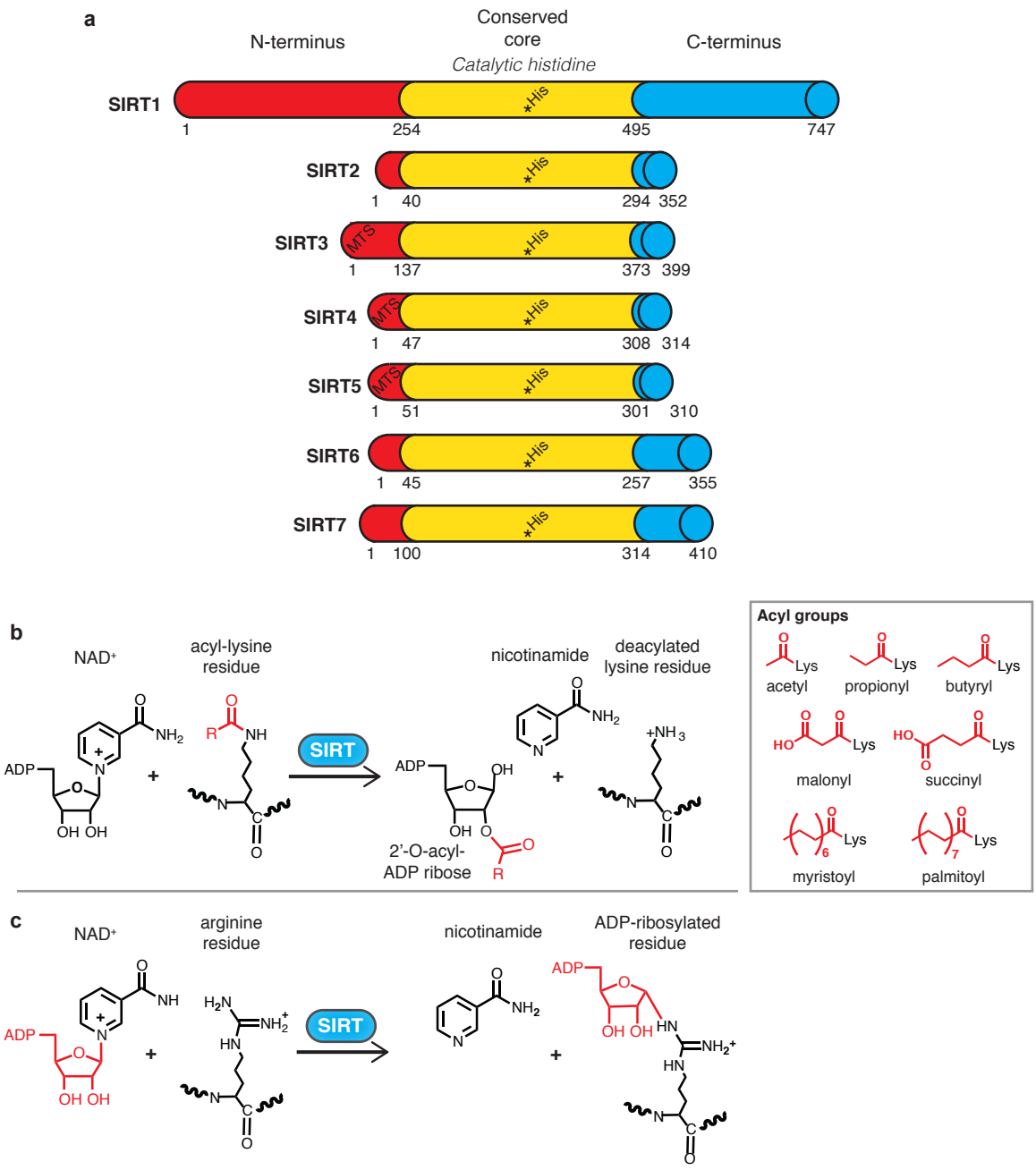

Figure 1.1 | Sirtuin family members and catalytic activities. a, SIRT1-7 domains and conservation. Sirtuins share a conserved catalytic core featuring an active site histidine residue that serves as a proton acceptor. SIRT3-5 have a mitochondrial targeting sequence (MTS) that is cleaved upon mitochondrial import. **b,** During lysine deacylation, sirtuins direct NAD^+ to nucleophilically attack the acylated lysine residue, leading to removal of an acyl modification. NAD^+ is cleaved in the process, forming nicotinamide and 2'-O-acyl ADP-ribose. Sirtuins can potentially remove diverse acyl modifications (inset) from lysine residues. **c,** During ADP-ribosylation, sirtuins use NAD^+ to nucleophilically attack an arginine (shown) or cysteine residue. NAD^+ is cleaved, resulting in release of nicotinamide and transfer of the ADP-ribose portion of NAD^+ to the substrate residue.

and histone modifications to coordinate gene expression programs that direct the cellular metabolic state[26]. Cytosolic functions of SIRT1 have also been identified. SIRT2 is largely cytosolic and coordinates microtubule dynamics as well as the activity of transcription factors residing outside the nucleus[27, 28]. Localization of SIRT3, 4 and 5 in the mitochondrial matrix enables these sirtuins to directly alter the activity of many metabolic enzymes[29].

Sirtuins catalyze NAD^+-dependent deacylation or ADP-ribosylation reactions with varying degrees of substrate versatility[30]. Although most well-studied as lysine deacetylases, certain sirtuins can also remove other acyl modifications from lysine residues including propionyl, butyryl, malonyl, succinyl and the lengthy fatty-acid derived myristoyl and palmitoyl groups among others[31]. SIRT5, for example, is a strong desuccinylase, and SIRT4 was recently reported to function as a lipoamidase by removing lipoyl or biotinyl modifications from lysine residues[32]. Through these processes, sirtuins have been shown to alter substrate activity, localization, stability and protein-protein interactions[33].

Regardless of which type of substrate moiety is modified by sirtuins, a similar NAD^+-dependent reaction mechanism proceeds. During sirtuin-catalyzed deacylation (Figure 1.1 b), nicotinamide adenine dinucleotide (NAD^+) nucleophilically attacks an acyl group of a substrate lysine. The resulting intermediate is cleaved to form 2'-O-acyl-ADP ribose (OAADPR) and nicotinamide, and the acyl group is removed from the lysine residue in the process. In sirtuin-catalyzed ADP-ribosylation (Figure 1.1 c), NAD^+ similarly attacks a substrate arginine or cysteine residue. The ADP-ribose portion of NAD^+ is transferred to the substrate residue, yielding nicotinamide as a side product[34,

35]. At high concentrations, nicotinamide represses sirtuin function via feedback inhibition[36].

Sirtuins are unique sensors of the metabolic state because their NAD^+-dependent enzymatic activity intrinsically couples their function with the metabolic status of the cell or organism[37-41]. According to the metabolic state of the cell, the ratio of NAD toggles between varying amounts of NAD^+ and NADH[42]. NADH is a high energy, reduced form of NAD that can donate electrons to the electron transport chain or convert pyruvate to lactate. NAD^+ is the lower energy, oxidized counterpart required to fuel glycolysis. When the cell uses oxidative metabolism, NADH generated by the TCA cycle and glycolysis donates electrons to complex I of the electron transport chain. This contributes to a proton gradient that will ultimately produce ATP. Upon electron transfer, NADH is oxidized back to NAD^+. In highly glycolytic cells, NAD^+ can alternatively be regenerated from NADH via lactate dehydrogenase (LDH) activity in order to sustain glycolysis. Thus, the NAD^+/NADH ratio provides one readout of the cellular metabolic state.

Due to their dependency on NAD^+, it is not surprising that certain sirtuins are reported to have increased activity in response to high NAD^+ concentrations[43]. For example, SIRT1 in skeletal muscle and brain is activated by exercise, fasting and calorie restriction, conditions with a high NAD^+/NADH ratio[44-46]. In contrast, low NAD^+ levels are observed with obesity and old age, two factors that confer increased risk for many cancers and are also linked to decreased sirtuin activity[47, 48]. Along these lines, growing evidence suggest loss of sirtuin function plays a role in obesity- and age-associated cancers[8, 49]. Tissue or subcellular variations in NAD^+ and NADH levels may lead to differential alterations of sirtuin activities[42]. The existence of distinct

cellular pools of NAD^+ is supported by work showing that mitochondrial NAD^+ is maintained at physiological levels even though cytosolic and nuclear NAD^+ pools are depleted upon genotoxic stress[38].

It is important to point out that sirtuin activity is not solely dependent on NAD^+ levels. Transcriptional regulation, post-translational modification and allosteric regulation are all important physiological regulators of sirtuin activity[50]. In the case of SIRT4, activity does not simply parallel the cellular NAD^+ level. SIRT4 plays a key role in inhibiting fat catabolism when mice are well fed, despite the low levels of NAD^+ expected under this condition[51]. SIRT4 mRNA and protein are also more abundant in mouse tissues under fed versus fasted conditions[52, 53]. It will be important for future studies to reveal further mechanisms by which sirtuin activity is regulated.

Sirtuins and connections to cancer

The associations between cancer metabolism and sirtuins often fall into one of two themes. First, loss of sirtuin activity may result in increased susceptibility to cancer onset. Second, an already established tumor that expresses high levels of some sirtuins may have survival advantages that endow resistance to chemotherapeutics.

Loss of sirtuin activity has been shown to contribute to cancer onset in some cases. The link between sirtuin loss and tumor emergence is evidenced by several models where SIRT1, SIRT2, SIRT3, SIRT4 or SIRT6 knockout (KO) mice are more prone to cancer incidence[17, 54]. In humans, SIRT3 protein and mRNA levels are strongly decreased in breast and ovarian cancer[55]. SIRT4 expression is decreased in lung, breast, bladder and gastric cancer and specific leukemia subtypes[56, 57]. SIRT6 levels are reduced in colon carcinoma and pancreatic cancer[58]. The metabolic state

maintained by sirtuins can be particularly incompatible with the onset of cancer, as discussed further below.

On the other hand, in established tumors it is possible sirtuins have pro-tumorigenic roles by promoting survival under the stress conditions that dominate the cancer cell state. For example, high SIRT1 expression is observed in drug-resistant cancers[59]. In fact, maintaining SIRT1 expression appears so vital for cancer cells that there are no reported deletions of SIRT1 in cancer and only extremely rare instances of SIRT1 mutation[17]. Thus while SIRT1 may counter the onset of cancer, an established tumor can greatly benefit from ramping up SIRT1 expression and inducing pro-survival pathways[60]. Additionally, the mitochondrial sirtuin SIRT3 promotes survival of oral squamous cell carcinoma (OSCC)[61]. While sirtuins in many cases can suppress cancer formation, sirtuins can also benefit the growth of some established tumors depending on the cancer type, stage and accompanying mutations. A more comprehensive understanding of sirtuin functions and relevant targets in cancer may shed light on the pro- or anti-tumorigenic roles of different sirtuins in particular tumor types.

PHD activity is linked to oxygen and the metabolic state

Much like sirtuins, PHDs are perfectly poised to elicit metabolic alterations in response to changing nutrient availability or stress. PHDs are a family of oxygen- and α-ketoglutarate dependent dioxygenases that hydroxylate proline residues of target proteins[62, 63]. The most well studied PHD substrate is hypoxia inducible factor (HIF) α, a key mediator of survival under hypoxia (discussed further below). Other non-HIF substrates are increasingly being identified, as well[64]. The cellular regulation achieved by PHDs illustrates that although hydroxylation is among the smallest post-translational

modifications, it can lead to substantial consequences. Prolyl-hydroxylation results in a region of high electronegativity that alters the pucker of the substrate proline and consequently can modulate protein-protein interactions, stability, activity and localization[63, 65].

There are three main mammalian PHDs (also called egg laying defective nine, or Egln, proteins in reference to their originally described function in egg laying by C. elegans) (Figure 1.2 a)[64]. While all PHDs share a conserved catalytic domain and a modestly conserved middle region, differences exist in localization signals, substrate preference and co-factor affinity. The biological relevance of these differences is only beginning to be realized and raises the possibility that each PHD could achieve unique metabolic regulation. PHD1 and 2 contain long, dissimilar N-terminal regions[66]. This region of PHD1 and 2 includes nuclear localization and nuclear export signals, respectively[67]. All three PHDs show some distribution between the nucleus and cytosol[68]. Interestingly, the rat homolog of PHD3 contains a mitochondrial targeting sequence[69]. Mouse and human PHD3 do not contain this sequence and to date no evidence exists of their localization in the mitochondria. PHD expression is ubiquitous throughout most tissues, but some tissues have a greater abundance of one PHD, highlighting the possibility of tissue-specific roles of each family member. Among the isozymes, cardiac muscle has highest expression of PHD3 and the testis has highest expression of PHD1[70].

The requirement of oxygen for catalysis positions PHDs as perfect mediators of the cellular and metabolic response to changing oxygen levels[21]. During catalysis, PHDs transfer one atom of molecular oxygen to a proline residue of a substrate protein,

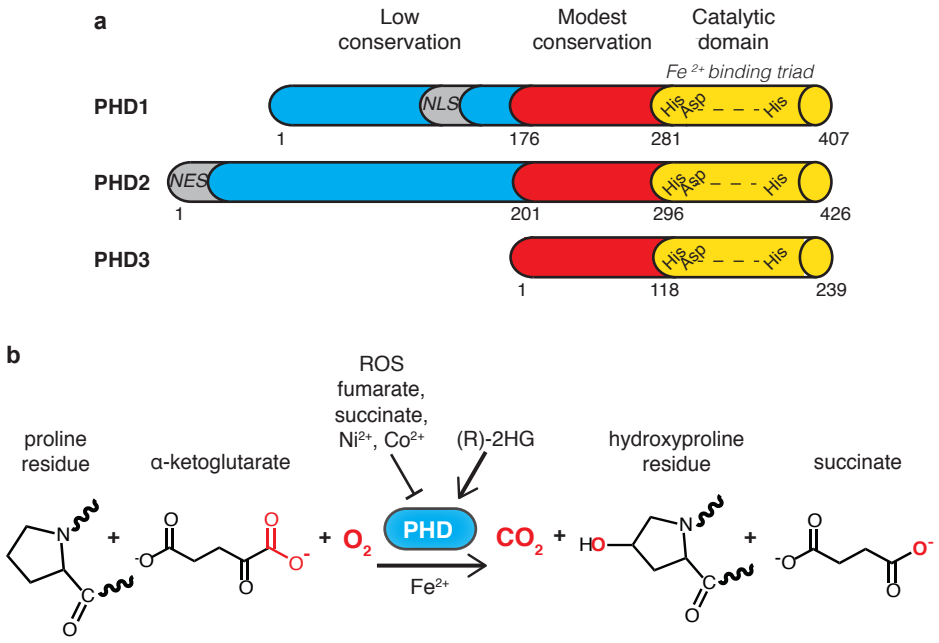

Figure 1.2 | PHD family members and catalytic activity. a, PHD1, 2 and 3 domains and conservation. PHD1 and 2 contain N-terminal regions of low conservation with nuclear localization (NLS) and nuclear export signals (NES), respectively. The C-terminal conserved catalytic domain contains a His-Asp-His catalytic triad to coordinate reduced iron (Fe^{2+}). **b,** To catalyze prolyl hydroxylation, PHDs form a complex with Fe^{2+}, dioxygen and α-ketoglutarate. One oxygen atom contributes to decarboxylation of α-ketoglutarate, yielding succinate and CO_2. The second oxygen atom is transferred to a proline residue of a substrate protein, yielding hydroxyproline. PHD activity is inhibited by reactive oxygen species (ROS) that oxidize iron, TCA cycle intermediates including succinate and fumarate that occupy the α-ketoglutarate binding site, and other doubly charged metal cations that take the place of Fe^{2+}. PHD activity is increased by (R)-2-hydroxyglutarate (R-2HG).

resulting in prolyl-hydroxylation (Figure 1.2 b). The other oxygen atom is transferred to α-ketoglutarate which is subsequently decarboxylated to form carbon dioxide and succinate[62]. Because the PHD catalytic mechanism requires molecular oxygen, a drop in intracellular oxygen levels can decrease PHD activity[71]. PHD1 and 2 are quite sensitive to subtle changes in cellular oxygen levels due to their weak affinity for oxygen. The K_m for oxygen is only slightly higher the normal oxygen concentration in the cell. This suggests PHD1 and 2 normally operate at sub-optimal conditions and any drop in oxygen can make these PHDs much less active[72]. PHD3 remains active during a lower range of oxygen concentrations and is less sensitive to drops in oxygen tension[73]. Thus, a question in the field is whether PHD3 might instead be sensitive to fluctuations in levels of another PHD co-substrate, such as α-ketoglutarate, perhaps enabling differential metabolic regulation based on the cellular nutrient state[74].

PHDs are not solely responsive to oxygen. PHDs are versatile metabolic sensors because their catalytic activity is additionally dependent on several key molecules that can be viewed as indicators of the cellular metabolic state including TCA cycle intermediates and reactive oxygen species (ROS)[21]. Thus, PHD activity can be modulated even under normoxic conditions. Growing evidence indicates PHDs are sensitive to TCA cycle imbalances that can be driven by dysfunctional enzymes in this pathway. For example, at high concentrations, succinate and fumarate competitively inhibit the PHD binding site that is normally occupied by the structurally similar molecule α-ketoglutarate[75, 76]. High levels of the PHD co-substrate α-ketoglutarate are suggested to activate PHDs. Addition of cell-permeable α-ketoglutarate was shown to restore PHD activity in cancer cells where PHDs were otherwise inhibited due to high

succinate levels[77]. Tennant and Gottlieb showed that treating mouse xenografts with esterified, cell-permeable α-ketoglutarate inhibited growth in a PHD3-dependent but HIF-independent mechanism[74]. This suggests PHD3-responsiveness to α-ketoglutarate may have important roles in cancer biology. The related molecule (R)-2-hydroxyglutarate (R-2HG) has been suggested to possibly activate PHDs[78]. R-2HG is normally present at very low in the cell but is produced in high quantities by mutant isoforms of isocitrate dehydrogenase (IDH) 1 and 2, which are observed in several cancers.

PHD enzymatic activity is also intrinsically sensitive to redox status due to the requirement for reduced iron in the catalytic site. The PHD catalytic domain contains a conserved triad of two histidines and one aspartate that coordinate non-heme iron[79]. To enable oxygen binding at this catalytic site, iron must be maintained in the reduced (Fe^{2+}) state, a function achieved by the antioxidants ascorbate (vitamin C) or glutathione[80, 81]. Due to high levels of ROS, these antioxidant molecules can become depleted leading to oxidation of the catalytic iron and inhibition of PHD activity[82]. Additionally, other dually charged cations can occupy the iron-binding site at high concentrations and inhibit PHDs. For example, treatment of cells with cobalt (II) chloride represses PHD activity[83]. In response to changing levels of all these inputs, PHDs have been shown to instigate metabolic changes that restore homeostasis and redox balance.

PHDs and connections to cancer

PHDs have decreased activity in a number of cancers. In some cases, the stress conditions in an established tumor repress PHD activity. In other situations, loss of PHD function is an early step in driving cancer development[5]. In the case of established cancer, PHD activity can be repressed in regions of a tumor experiencing high ROS or

hypoxia due to excessive oxygen consumption or insufficient blood supply[84]. Here, inactivation of PHDs contributes to upregulation of HIF and promotes cellular and metabolic adaptations that enable cancer cell survival. Alternatively, in a healthy cell loss of PHD function can trigger metabolic alterations amenable to transformation. PHDs can be repressed by loss of function mutations in the tumor suppressors succinate dehydrogenase (SDH)[85] or fumarate hydratase (FH)[86]. Mutation of these TCA cycle enzymes leads to a build-up of succinate and fumarate, respectively[18]. Overabundance of these metabolites inhibits PHD function and is linked to neoplastic transformation and HIF-driven metabolic reprogramming. SDH mutations are commonly observed in the neuroendocrine cancers paraganglioma or phaeochromocytoma, and FH mutations cause cutaneous and uterine leiomyomatas and aggressive renal cell carcinoma[87].

PHD3 is repressed in multiple cancers through the additional mechanism of epigenetic silencing. In patient samples from colon cancer, angiocytoma, glioblastoma and multiple myeloma, as well as in cell lines representing prostate cancer, colon cancer and acute myeloid leukemia, PHD3 expression is strongly repressed due to hypermethylation of CpG sites in the gene promoter[88-92]. In the leukemia HL60 cell line, hypermethylation correlates with complete absence of PHD3 mRNA[89]. This mechanism of extensive silencing has not been observed for PHD1 or PHD2 in cancer. Studies such as these highlight the need for future research to characterize the roles of each PHD in different cancer contexts.

Altered glycolysis in cancer

In the 1920s, Otto Warburg made one of the earliest observations of altered cancer cell metabolism[93]. In studies of rapidly proliferating ascites tumor cells, he

measured extraordinarily high glucose uptake and lactate secretion. Whereas these metabolic features were known to be typical of oxygen deprived tissues such as extremely active muscle, here Warburg observed for the first time that cancer cells display increased glycolysis and lactate production even in the presence of ample oxygen. This phenomenon became known as the Warburg effect, and it has since been realized as a general metabolic shift promoting the survival of multiple tumor types[15]. In many cancers, glucose drives biosynthesis and growth; intermediates of glycolysis are directed toward pathways that build macromolecules including nucleotides, antioxidants, lipids and proteins (Figure 1.3). In addition to biosynthesis, glucose contributes to ATP production, generation of signaling molecules and production of lactate[94]. To redirect glucose for anabolism rather than for energy production, a major entry site for glucose-derived pyruvate into the TCA cycle is blocked, effectively boosting the level of glycolytic intermediates that remain in the cytosol rather than being siphoned to the mitochondria for ATP production[95]. In cancer cells, pyruvate is converted in large amounts to lactic acid via lactate dehydrogenase A (LDHA). This reaction generates NAD^+ to allow continued glycolysis[5] and also creates an acidic environment that is proposed to promote tumor cell migration, genetic instability and cancer cell stemness[96-99].

Elevated glycolysis additionally might provide an alternate pathway to maintain ATP production, even under hypoxic conditions in cancer cells. Rapidly growing or metastatic tumors may lack oxygen due to inadequate blood supply or massive oxygen consumption. In the absence of sufficient oxygen, mitochondrial ATP production is limited[71]. To circumvent the hypoxia-driven deficiency in mitochondrial function,

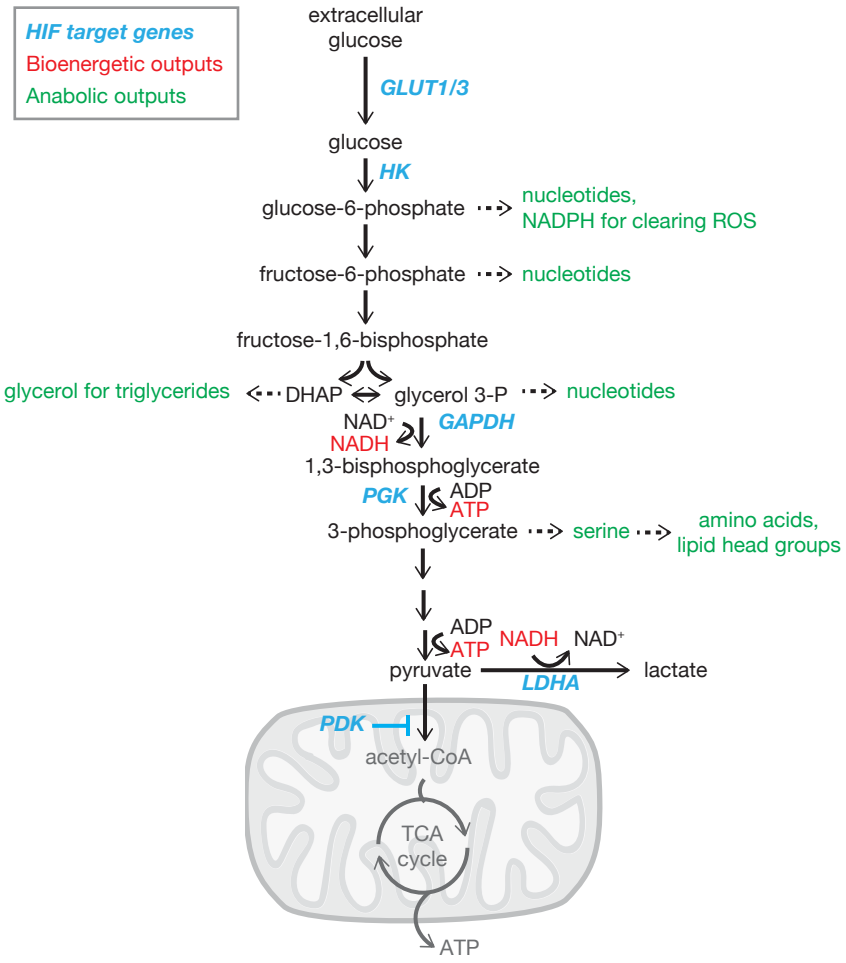

Figure 1.3 | HIF-mediated upregulation of glycolysis in cancer. HIF drives transcription of key metabolic enzymes (blue) in order to boost glycolysis in cancer. In many cancers, increased glyoclytic intermediates fuel anabolic pathways (green) including the generation of nucleotides, amino acids, lipids and antioxidants such as ROS. Glycolysis also generates energy via production of NADH and ATP (red). To promote the build-up of glycolytic intermediates, HIF activates PDK to block entry of pyruvate into the TCA cycle. HIF further activates LDHA to generate lactate as well as NAD^+ required to fuel successive rounds of glycolysis. GLUT= glucose transporter, HK= hexokinase, GAPDH= glyceraldehyde 3-phosphate dehydrogenase, PGK= phosphoglycerate kinase, PDK= pyruvate dehydrogenase kinase, LDHA= lactate dehydrogenase A.

glycolysis may be upregulated to generate ATP via substrate level phosphorylation. The amount of ATP produced by glycolysis is only a fraction of that generated by the electron transport chain; however, greatly induced glycolysis could achieve bioenergetic homeostasis when oxygen is limiting[100].

HIF, PHDs and metabolic stress sensing

The well-known PHD target, hypoxia Inducible Factor (HIF), is a master transcriptional activator of glycolysis with strong links to cancer. HIF acts as an α/β heterodimer[101]. There are three HIFα isoforms, and of these Hif1α and 2α are the most well-studied[21]. Increased levels of HIF1α and 2α are observed in many cancers and correlate with worse prognosis[102]. While overlap exists in many HIF1α and 2α target genes, some genes are exclusively modulated by just one isoform[103]. HIF is normally activated under hypoxia to promote expression of multiple glycolytic genes (Figure 1.3) and boost other pathways that mediate cell survival under low oxygen. However, in many cancers, aberrantly activated HIF facilitates metabolic reprogramming and upregulation of glycolysis even when oxygen levels are sufficient[104].

Physiologically under normoxia, HIF transcriptional activity is limited to a low, basal level (Figure 1.4 a). Cytosolic HIFα is hydroxylated by PHDs and subsequently ubiquitinated by the von Hippel-Lindau (VHL) E3 ubiqutin ligase, targeting HIFα for degradation[105]. In hypoxic tumors or in cancers with disrupted redox status or TCA cycling, PHD activity can be inhibited and HIFα is stabilized (Figure 1.4 b). HIFα translocates to the nucleus and forms a heterodimer with HIFβ (also called aryl hydrocarbon nuclear receptor, ARNT) resulting in a functional transcription factor in

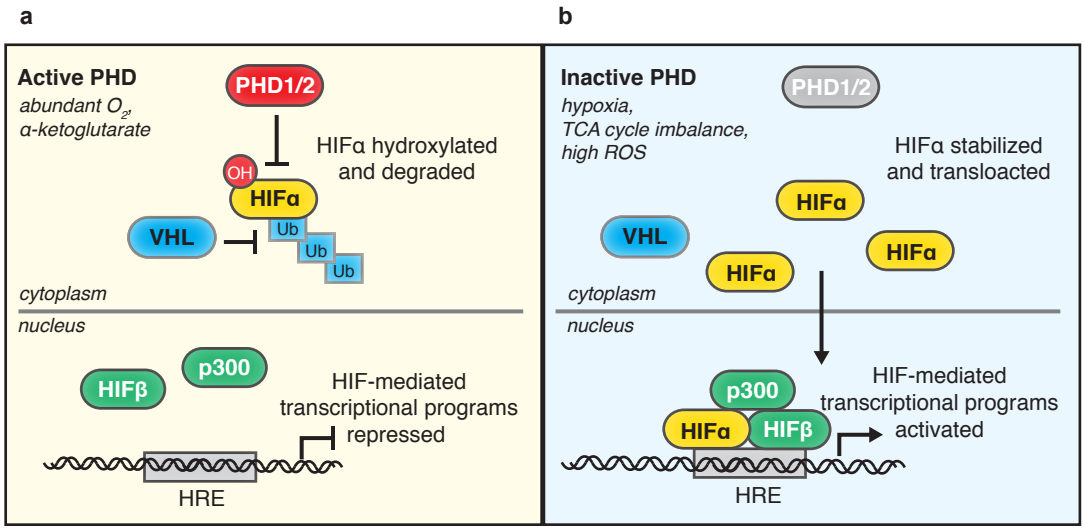

Figure 1.4 | PHD-mediated repression of HIF-driven metabolic reprogramming. a, PHD1 and 2 are the major HIF hydroxylases. PHD activity limits HIF transcriptional activity. Under normoxia and in the presence of the co-substrate α-ketoglutarate, PHDs hydroxylate cytosolic HIFα. This promotes ubiquitination of HIFα by VHL, and HIFα is subsequently degraded by the proteasome. **b,** Loss of PHD activity, such as under hypoxia or in the presence of high succinate, fumarate or ROS, stabilizes HIFα. When HIFα is not hydroxylated, it readily moves to the nucleus and forms a functional transcription factor in complex with HIFβ and p300 on the promoter of genes containing HIF responsive elements (HRE). As a result, HIF-mediated transcriptional programs are activated. VHL= von Hippel-Lindau E3 ubiquitin ligase. OH= prolyl hydroxylation. Ub= ubiquitination. ROS= reactive oxygen species.

complex with the coactivator p300/CBP[70]. This complex binds HIF-responsive elements (HRE) in target gene promoters to activate a transcriptional program that boosts angiogenesis, erythropoiesis and glycolytic metabolism[72]. Interestingly, PHD2 and PHD3 are HIF target genes[79]. It is possible that upregulation of PHDs, particularly PHD2, under hypoxia serves to build a pool of PHDs that can rapidly dampen the HIF signal as soon as adequate oxygen is achieved.

Not all PHDs similarly affect HIF. The range of oxygen sensitivity and differential substrate preference by each PHD leads to dynamic regulation of HIF. In line with great hypoxia-sensitivity, PHD1 and 2 are the major PHDs responsible for HIF hydroxylation and destabilization under normoxia [106, 107]. Under hypoxia, inactivation of PHD1 and 2 promotes HIF and glycolysis, while surprisingly the continued activity of PHD3 was shown to boost HIF function at least in cell culture via hydroxylation of the HIF transactivator PKM2[73]. Protein kinase M2 (PKM2) is the less active, dimeric isoform of the glycolytic enzyme pyruvate kinase that is frequently observed in cancer. PKM2 serves an additional function as a HIF co-activator[108]. Thus, by activating PKM2, PHD3 enhances HIF-driven glycolytic metabolism under hypoxia.

Modulation of HIF by sirtuins

Several studies have shown that the stress- and nutrient-sensing pathways that coordinate HIF activity also intersect with sirtuins at numerous nodes. Elaborate control mechanisms enforced by SIRT1, SIRT3 and SIRT6 counter HIF activity to keep glucose metabolism in check[17]. This interplay is in line with the role of these sirtuins as promoters of oxidative metabolism and mitochondrial function. Loss of sirtuin function

has been shown to shift the cell toward glycolytic metabolism in a process that is amenable to transformation. In cancer cell lines and sirtuin KO mouse models, low expression of SIRT1, 3 and 6 correlates with increased levels of HIF1 target genes[47, 55, 109].

Under normoxia, the nuclear sirtuin SIRT1 inhibits the basal HIF response by promoting stability of the VHL transcript to drive degradation of HIFα[47] and by deacetylating and directly inactivating HIF1α in the nucleus[110]. Under hypoxia, the gradual drop in NAD^+ decreases SIRT1 function and contributes to HIF activation[110], which may synergize with intratumoral PHD inhibition to maximize HIF-driven glycolysis. Also in the nucleus, SIRT6 represses HIF transcriptional activity to limit glycolysis in cancer. To do so, SIRT6 deacetylates histone H3K9 on the promoter of HIF target genes, aiding in gene silencing[109]. Additionally, SIRT6 directly interacts with and inhibits HIF1α on HRE of glycolytic genes. The authors of this study further show that glycolysis is increased upon SIRT6 conditional KO in an $APC^{min/+}$ mouse model of colon cancer and is linked with increased tumor incidence[58].

In the mitochondria, SIRT3 represses HIF-driven glycolysis by coordinating a multipronged strategy to limit ROS (discussed further below). By decreasing ROS, SIRT3 promotes PHD activity and HIF degradation. SIRT3 loss dramatically boosts ROS, which is proposed to deactivate PHD family members and consequently stabilize HIF1α [55, 111]. Indeed, in mouse embryonic fibroblasts (MEFs), SIRT3 KO and the resulting high ROS promote a HIF-mediated transition to the Warburg effect[55].

Alternate fuels and the TCA cycle in cancer

Although elevated glucose consumption is characteristic of many cancer cells, it is increasingly clear that glucose is not the whole story in cancer metabolism. Many cancers, for reasons largely not understood, additionally or alternatively display addiction to fats or amino acids such as glutamine[112, 113]. Physiologically, changes in cellular fuel choice have been shown to direct stress resistance pathways, differentiation, proliferation or adaptation to nutrient availability[12]. Ongoing research in cancer metabolism focuses on identifying molecular determinants that drive use of one fuel versus another, as well as the advantages of using a particular fuel in specific cancer contexts.

One intensely studied use of amino acids and fatty acids in cancer is anaplerosis, the process of refilling the TCA cycle. Anaplerotic pathways provide alternative entry sites to generate TCA cycle intermediates, which are often used for anabolic and bioenergetic purposes in cancer (Figure 1.5). Anaplerosis is required when normal mechanisms for driving the TCA cycle are insufficient[94]. In many healthy tissues, pyruvate dehydrogenase (PDH) is the major enzyme that channels glucose-derived pyruvate into the TCA cycle[114]. PDH converts pyruvate to acetyl-CoA, and then acetyl-CoA condenses with oxaloacetate to form citrate. However, PDH activity is often limited in cancer[115]. Additionally, roadblocks at other steps in the TCA cycle or shunting of metabolites toward biosynthetic pathways can limit production of oxaloacetate, which is needed to fuel subsequent rounds of the TCA cycle[115]. In these cases, PDH alone cannot sustain TCA cycling. In cancer, the TCA cycle can be refueled through at least four major mechanisms: the activity of pyruvate carboxylase, glutaminolysis, reverse TCA cycling and fatty acid oxidation.

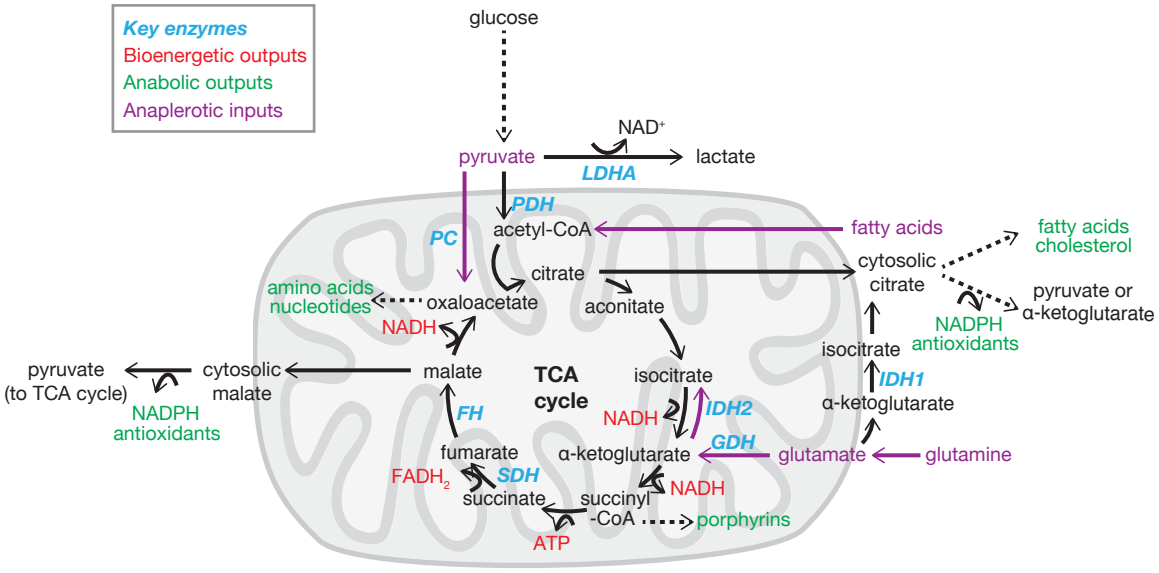

Figure 1.5 | TCA cycle inputs and outputs. TCA cycle flux provides bioenergetic (red) and anabolic outputs (green). NADH and $FADH_2$ generated by the TCA cycle can fuel the electron transport chain and ATP production.TCA cycle intermediates can be siphoned away to generate molecules including fatty acids, cholesterol, amino acids, nucleotides, porphyrins and antioxidants such as NADPH. Normally the TCA cycle is predominantly fueled by conversion of pyruvate to acetyl-CoA via PDH. However, alternate anaplerotic inputs (purple) are required when TCA cycle intermediates are depleted. Anaplerosis is upregulated when TCA cycle enzymes (such as SDH or FH) are inhibited, when pyruvate is shunted from the TCA cycle or when TCA cycle intermediates are depeleted for anabolic or other purposes.

First, the enzyme pyruvate carboxylase (PC) provides an alternate means of generating oxaloacetate to refuel the TCA cycle[116]. PC is a mitochondrial biotin-dependent enzyme that uses bicarbonate to directly convert pyruvate to oxaloacetate[117]. PC-derived oxaloacetate is hypothesized to be particularly important in SDH- or FH-deficient cancers[87]. In these tumors, SDH or FH deficiency limits production of metabolites in the latter half of the TCA cycle, including oxaloacetate. Here, PC provides an additional way to generate oxaloacetate for use in the TCA cycle or for the synthesis of amino acids and nucleotides.

Second, many cancers are dependent on glutamine to amass pools of TCA cycle intermediates that are used for biosynthesis. Glutamine is the most abundant amino acid in serum[118], making it a readily available fuel for many tumors. Glutamine consumption is massively upregulated in particular subsets of cancer including neuroblastoma and basal, but not luminal, breast cancer[119]. To direct glutamine toward the TCA cycle, glutamine can be imported into the mitochondria and deaminated to yield glutamate. Glutamate is converted to α-ketoglutarate by glutamate dehydrogenase (GDH) or transaminases. Then, α-ketoglutarate can proceed through the TCA cycle. Interestingly, evidence suggests PC- and glutamine-driven mechanisms to fuel the TCA cycle are generally mutually exclusive[120]. Thus it has been suggested that PC expression can be used as a biomarker to sort patients in clinical trials for glutamine inhibitors in cancer[121].

Recent studies have shown glutamine not only fuels typical forward TCA cycling, but also reverse TCA cycling. Although the TCA cycle had long been thought to operate in one direction, it is now known that glutamine can fuel the TCA cycle in the reverse

direction in some cancer cells, particularly in response to redox stress, impaired respiration or hypoxia[122-124]. Forward TCA cycling requires acetyl-CoA to condense with oxaloacetate and form citrate. Under harsh conditions, such as proliferating cells in hypoxia, pyruvate is directed almost entirely toward lactate[125]. Acetyl-CoA may be sufficiently depleted such that forward TCA cycling is limited. In this case, an alternate pathway is needed to produce citrate. Citrate is especially essential for cancer cells because it is a key building block for fatty acid synthesis[125]. In cancer cells, glutamine-derived α-ketoglutarate can undergo reductive carboxylation catalyzed by NADPH-dependent isocitrate dehydrogenase (IDH) 1 or 2 to generate citrate[126, 127].

Mitochondrial fatty acid import and oxidation in cancer

In addition to glucose and glutamine, fatty acids have recently been recognized as necessary fuels for specific cancer types. While fatty acid synthesis has long been considered an essential feature of growing tumor cells, fatty acids must also be broken down in subsets of cancer[112]. Fatty acid oxidation (FAO) in the mitochondria generates acetyl-CoA to fuel the TCA cycle, as well as FADH and $NADH_2$ to fuel the electron transport chain. In particular, prostate cancer, colorectal cancer and acute myeloid leukemia (AML) show a strong reliance on FAO[128-130]. This branch of tumor metabolism is far less studied than glucose or glutamine. The prevalence of FAO in cancer warrants further studies to identify molecular pathways that regulate FAO in cancer cells and, furthermore, to understand why fatty acids are the preferred metabolic substrate in specific human cancers.

One key enzyme directing the fate of fatty acids in cancer is carnitine palmitoyl transferase 1 (CPT1), located in the outer mitochondrial membrane[131]. CPT1

catalyzes the rate-limiting step of mitochondrial FAO[132]. Mechanistically, CPT1 attaches carnitine to long chain fatty acyl-CoAs to mediate mitochondrial import (Figure 1.6). A major activator of CPT1 in normal cells is AMP-activated protein kinase, an AMP-sensing enzyme that serves as the bioenergetic rheostat of the cell[133]. Upon sensing a low cellular energy status, AMPK activates FAO and other cellular strategies to boost ATP production. To activate CPT1, AMPK phosphorylates and inhibits acetyl-CoA carboxylase 2 (ACC2)[134]. ACC2 is located at the outer mitochondrial membrane and converts acetyl-CoA to malonyl-CoA, which allosterically inhibits CPT1. When ACC2 is inactivated, CPT1 is turned on and FAO is increased. Of note, short chain fatty acids bypass these regulatory steps and diffuse freely into the mitochondria[135]. Once in the mitochondria, fatty acids are catabolized via multiple rounds of β-oxidation. The vital role of CPT1 in cancer biology is evidenced by its increased expression in specific cancers[136-138], as well as by the finding that pharmacological inhibition of CPT1 suppresses ATP production and induces apoptosis in cancer cell models of glioblastoma[139], Burkitt's lymphoma[140], prostate cancer[137] and AML[129]. Further studies are needed to determine the range of molecular alterations upstream of CPT1 that can boost FAO in cancer.

Growing evidence suggests FAO is not upregulated solely as an energy source. FAO additionally contributes to generation of NADPH, a molecule with antioxidant functions made by channeling fatty acid-derived acetyl-CoA towards citrate-cycling reactions involving TCA cycle enzymes[141-144]. Products of FAO are also suggested to maintain the quality of the mitochondrial membrane and prevent induction of apoptosis[129].

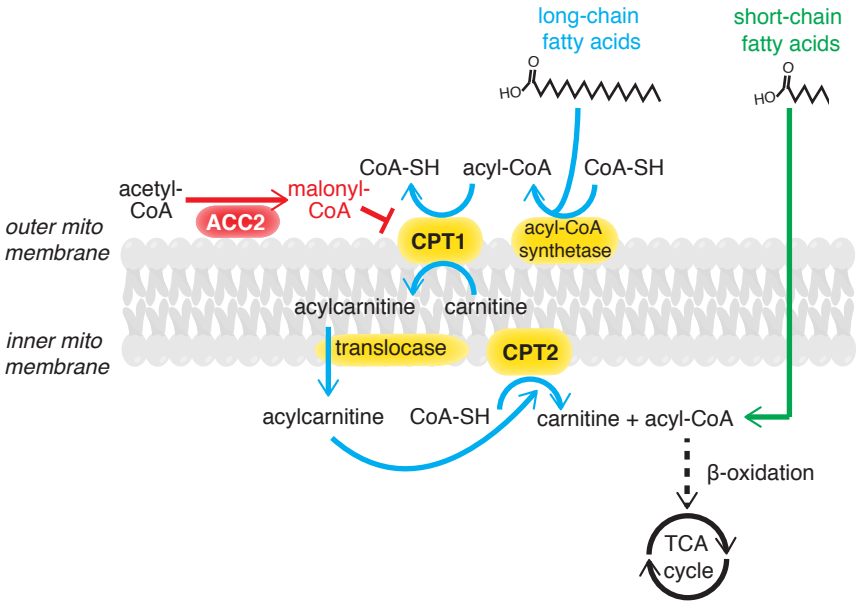

Figure 1.6 | Regulation of long chain versus short chain fatty acid oxidation. Long chain fatty acids must be processed by multiple regulatory steps (blue arrows) in order to be transported to the mitochondrial matrix and undergo fatty acid oxidation. Long chain fatty acids are first charged with a high energy CoA group, which is then replaced with carnitine to mediate transfer across the outer mitochondrial membrane via the enzyme CPT1. CPT1 catalyzes the rate-limiting step of long chain fatty acid oxidation. CPT1 removes the CoA group from the long chain fatty acyl-CoA and replaces it with carnitine. The step is inhibited by malonyl-CoA, the product of ACC2 located at the outer mitochondrial membrane. Once past CPT1, the acylcarnitine is then transported across the inner mitochondrial membrane via a translocase. CPT2 catalyzes removal of carnitine and substitution with CoA. The acyl-CoA is a substrate for fatty acid oxidation in the mitochondrial matrix. Short chain fatty acids bypass these regulatory steps (green arrow) and diffuse freely into the mitochondria. Once in the mitochondria, fatty acids are catabolized via multiple rounds of β-oxidation. CPT= carnitine palmitoyl transferase, ACC2= acetyl-CoA carboxylase 2.

Sirtuin coordination of anaplerosis and alternate fuel sources

Several sirtuins activate TCA cycle flux and anaplerosis. Research in this area has focused on mechanistic characterization of sirtuin substrates in these metabolic pathways, while less is known of the disease relevance of sirtuins and altered anaplerosis. SIRT3 boosts mitochondrial metabolism by deacetylating and activating enzymes involved the TCA cycle, glutaminolysis and fatty acid oxidation[19]. SIRT1 and SIRT6 additionally stimulate FAO[19]. Sirtuin-mediated activation of alternate fuel sources might be expected to serve as an advantage to cancer cells, although these questions have largely been unexplored.

Driving the TCA cycle in reverse by reductive carboxylation is also a sirtuin-modulated process[145]. SIRT1 has recently been shown to promote the use of glutamine for reverse TCA cycling under extreme cellular conditions[145]. In diverse cancer cell lines, prolonged acidosis (pH 6.5), which mimics extensive lactate production, upregulates genes important for reverse TCA cycle flux in a SIRT1-dependent manner. Mechanistically, under low pH SIRT1 deacetylates HIF1α and 2α. Deacetylation inhibits HIF1α but activates HIF2α. By activating HIF2α, SIRT1 triggers expression of key target genes including the glutamine transporter SLC1A5, the mitochondrial glutaminase isoform 1 (GLS1) and IDH1. Thus, the SIRT1/HIF2α axis promotes a metabolic shift to reductive glutamine metabolism in order to maintain levels of TCA cycle intermediates under the harsh conditions experienced by cancer cells.

While other sirtuins boost mitochondrial metabolism, SIRT4 is unique among the sirtuins in its ability to limit TCA cycle flux and anaplerosis at multiple key branch points (Figure 1.7). First, SIRT4 deacetylates and inhibits malonyl-CoA carboxylase (MCD) to

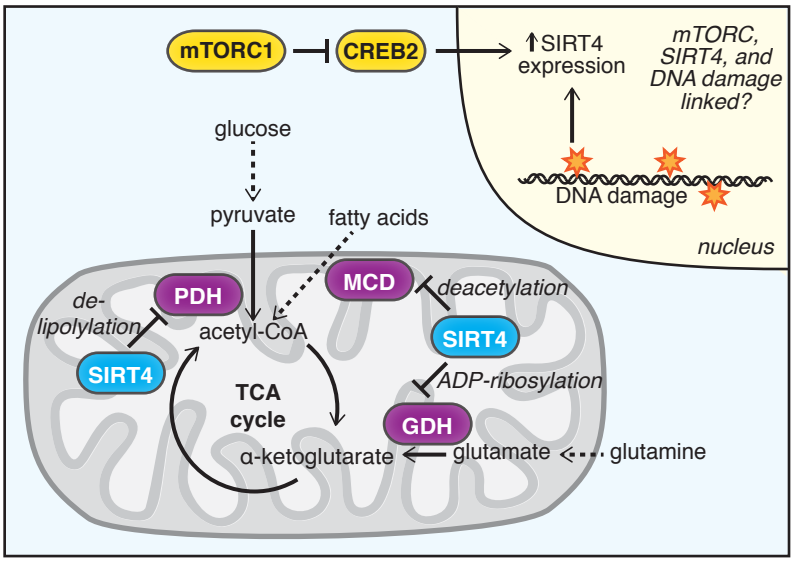

Figure 1.7 | SIRT4 represses TCA cycle anaplerosis at multiple access sites via several catalytic activities. SIRT4 limits entry of glutamine into the TCA cycle, in part by ADP-ribosylating and inhibiting GDH. SIRT4 blocks long chain fatty acid oxidation by deacetylating and inhibiting MCD. This activity of SIRT4 boosts malonyl-CoA levels and blocks fatty acid import into the mitochondria. Finally, SIRT4 limits entry of pyruvate into the TCA cycle by removing a lipoyl modification from PDH. Consequently PDH is repressed. SIRT4 expression is strongly induced in response to various cellular stresses including dysfunctional mTORC1 and DNA damage. The connections between mTORC, DNA damage and SIRT4 repression of anaplerosis are unclear.

repress FAO. MCD converts malonyl-CoA to acetyl-CoA, thus relieving repression of CPT1. When MCD is deacetylated, malonyl-CoA levels increase and FAO is decreased. Second, SIRT4 was recently shown to repress PDH-mediated flux of pyruvate into the TCA cycle. SIRT4 removed lipoyl- and biotinyl-modifications from lysine residues of PDH. The links between cancer metabolism and the effects of SIRT4 on MCD or PDH have not yet been explored.

Finally, SIRT4 limits glutamine anaplerosis by ADP-ribosylating and inhibiting GDH [146]. The ability of SIRT4 to restrict supply of this alternative fuel limits tumorigenesis. In cancer cells, DNA damage dramatically induces SIRT4 expression, and glutamine anaplerosis is inhibited[56]. Consequently, TCA cycle intermediates are depleted and, via mechanisms yet to be elucidated, the cell cycle stalls. This SIRT4-mediated metabolic pause allows time for DNA repair before the cell proceeds through the cell cycle. In the absence of SIRT4, glutamine anaplerosis remains activated even during DNA damage. DNA damage persists and cellular proliferation and transformative properties are increased, possibly due to newly occurring DNA mutations.

In related studies, Csibi et al found that mammalian Target of Rapamycin Complex 1 (mTORC1), a serine/threonine kinase that drives cellular nutrient uptake and proliferation, inhibits SIRT4-mediated repression of anaplerosis. mTORC1 represses SIRT4 expression by inhibiting CREB2, a transcription factor that induces SIRT4[57]. High mTORC1 signaling drives growth in many cancers[147], and in this study mTORC1 was proposed to additionally benefit cancer cell survival by repressing SIRT4 and activating glutaminolysis. In future studies, it will be interesting to examine whether mTOR signaling converges on DNA damage responses via SIRT4.

PHD interconnections with the TCA cycle and anaplerosis

An emerging theme in prolyl hydroxylase research is the ability of PHDs to not only sense alterations in TCA cycle flux, as discussed above, but to reciprocally coordinate TCA cycling. These studies hint that PHDs are capable of influencing metabolic pathways other than glycolysis[18, 148]. For example, PHD3 promotes entry of pyruvate into the TCA cycle by maintaining the stability of the pyruvate dehydrogenase complex (PDC). Specifically, PHD3 interacts with pyruvate dehydrogenase- E1β, and knockdown of PHD3 in breast cancer cells destabilized PDC[149]. This regulation is proposed to occur through physical interaction alone and does not require PHD3 hydroxylase activity.

Some corollary evidence suggests PHDs may play a role in FAO in cancer. Under hypoxia, FAO and mitochondrial metabolism are decreased in tissues such as the myocardia and skeletal muscle to limit ROS production[150]. Huang et al identified HIF1 as a key intermediary of FAO repression in hypoxic hepatocellular carcinoma cell lines[151]. HIF1 decreases expression of two acyl-CoA dehydrogenases involved in catabolism of fatty acids, namely MCAD and LCAD. These findings build upon previous studies indicating HIF1 can limit FAO by dampening expression of PPARα or its obligate binding partner RXR, key regulators of FAO gene transcription[152]. However, PHDs were not implicated as part of this regulatory mechanism. To date, PHDs have not been directly linked to altered FAO in the context of cancer, and PHD substrates in FAO metabolism have not been described.

Electron transport chain flux in cancer

The electron transport chain (ETC) is among the most fundamental machinery required for life. The ETC machinery is our cells' main producer of ATP via oxidative phosphorylation, the main consumer of oxygen and the main generator of ROS[153]. The ETC is comprised of a series of mitochondrial inner membrane-bound protein complexes that catalyze sequential reduction of electron donor molecules in order to power the pumping of protons from the matrix to the mitochondrial intermembrane space (Figure 1.8)[154]. The resulting electrochemical gradient fuels ATP production by Complex V (ATP synthase). The electron donor molecules are NADH and $FADH_2$, generated from catabolism of fuels such as glucose, fats or amino acids. A third, electron donor is glycerol-3-phosphate, a precursor in the synthesis of triglycerides and phospholipids[115]. In mitochondria, electrons are transferred from glycerol 3-phosphate to coenzyme Q in the ETC via the mitochondrial isoform of glycerol-3-phosphate dehydrogenase (GPDH-M)[155]. Despite its important contribution to cellular energy generation, the role of glycerol 3-phosphate in cancer is not well studied.

Despite its fundamental role in biology, the contribution of the ETC to cancer is complex and has been a subject of debate[156]. On one hand it is true that oxidative phosphorylation is frequently decreased in cancer cells due to hypoxia, reduced expression of electron transport machinery or shunting of metabolites toward anabolic pathways rather than bioenergetics[157]. However, there are situations in which some cancer cells are critically dependent on ETC function. For example, Vazquez et al identified subsets of melanoma that express high levels of PGC1α, the master transcriptional activator of mitochondrial biogenesis and oxidative phosphorylation[158]. These high PGC1α melanomas display increased resistance to oxidative stress, highly

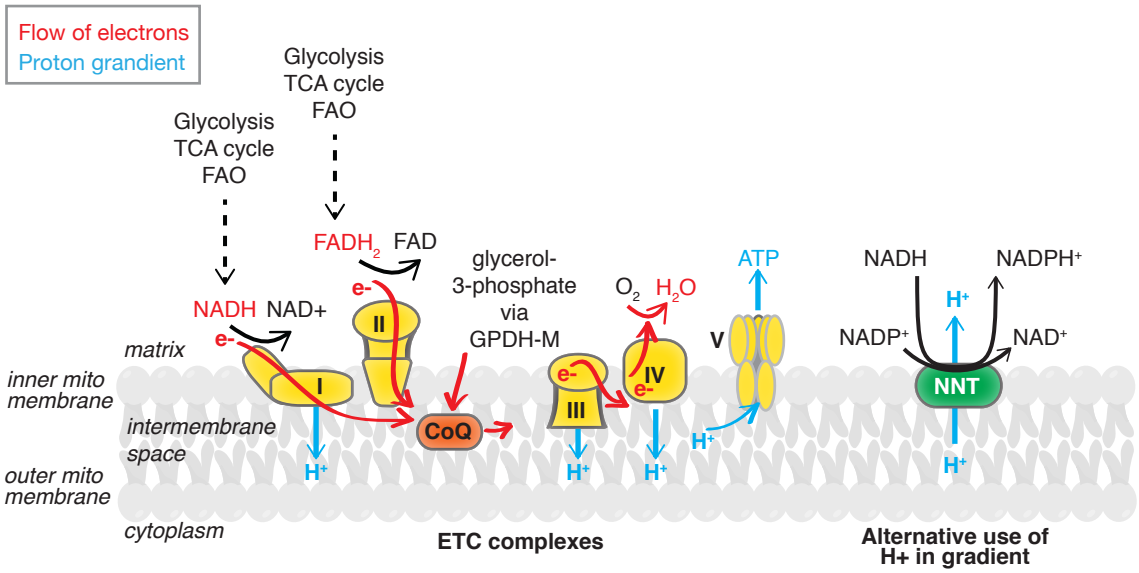

Figure 1.8 | Input and outputs of the electron transport chain. The ETC is fueled by a number of metabolic inputs. NADH and $FADH_2$ are electron donating molecules generated by glycolysis, the TCA cycle and FAO. NADH and $FADH_2$ contribute electrons to Complex I and Complex II, respectively. Glycerol 3-phosphate can also contribute electrons to the ETC upon conversion to the glycolytic intermediate DHAP by GPDH-M. To drive ATP production by oxidative phosphorylation, electrons from these donor molecules are transported through CoQ and the respiratory chain Complexes (shown in yellow) and eventually reach a final acceptor, oxygen. Electron flow drives each complex to pump protons from the matrix to the intermembrane space. The gradient is primarily used to generate ATP as protons flow black across the membrane via Complex V. Alternatively, protons in the intermembrane space can be transported to the matrix by NNT. Proton pumping drives the ability of NNT to convert $NADP^+$ and NADH to NAD^+ and NADPH, thus modulating cofactor balance. GPDH-M= mitochondrial glycerol-3-phosphate dehydrogenase, DHAP= dihydroxyacetone phosphate, NNT= nicotinamide nucleotide transhydrogenase.

aggressive clinical behavior, and sensitivity to pharmacological inhibition of oxidative phosphorylation. Caro et al additionally showed high mitochondrial metabolism and ETC function in subsets of diffuse large B cell lymphoma (DLBCL)[142].

In addition to coordinating cellular bioenergetics, generation of ROS by the electron transport machinery links these proteins to cancer. The role of ROS in cancer is complex, and high ROS have been linked to cancer incidence in numerous studies[159-161]. Stalling or inefficiencies in the ETC can increase ROS production. ROS have both adverse and beneficial consequences on cancer cells, which may in part be determined by the stage of tumor progression or specific cancer-associated mutations[162]. First, at excessive levels ROS can damage cellular machinery including proteins, lipids, DNA and RNA. By causing genetic damage, ROS may have mutagenic and pro-tumorigenic capacities. ROS also serve as important signaling molecules that can drive growth and cell division in cancer[163-165].

While in some contexts ROS boosts cellular transformation and cancer cell growth, high ROS in other contexts acts as a pro-apoptotic signal instructing cancer cells to die[166, 167]. Accelerated metabolism in cancer often generates high ROS. Because ROS can reach toxic concentrations, adaptive mechanisms must be put it place by cancer cells to restore redox homeostasis and allow survival. Therefore, many cancer cells upregulate antioxidant pathways that endow tumors with additional stress protection. In this way, antioxidant programs may actually promote cancer progression of established tumors[168-170]. Of note, the proton gradient generated by the ETC itself can directly be used in antioxidant strategies. The mitochondrial intermembrane protein called nicotinamide nucleotide transhydrogenase (NNT) uses the power provided by the proton

gradient to convert NADH and $NADP^+$ to NAD^+ and NADPH, the latter of which is used to regenerate antioxidants[171]. The distinct roles of ROS in diverse cancer types and stages may help explain the different requirements for ETC machinery and oxidative phosphorylation in these diverse scenarios.

Targeting oxidative metabolism: studies of metformin

Although many tumors display decreased ETC function, a large body of research paradoxically indicates that limiting ETC activity in a healthy cell reduces cancer risk. For example, low Complex I activity due to mitochondrial DNA mutations or treatment with biguanides limits transformation and interferes with tumor cell survival in multiple cancer models[172, 173]. Original support for targeting Complex I in cancer treatment comes from studies of the biguanide metformin. An impressive number of retrospective, epidemiological and laboratory-based studies have revealed that metformin confers cancer-preventative properties[174]. There are several hypotheses to explain the effects of metformin on cancer. One is that metformin decreases systemic insulin levels and thus suppresses insulin-signaling pathways that are linked to cancer onset[175]. These anti-cancer properties are not achieved by all diabetes drugs; sulfonylureas, which instead boost insulin levels as part of diabetes treatment, do not display the same cancer-preventative properties as metformin[176, 177]. Another hypothesis for metformin's mechanism of action, supported by substantial biochemical data, is that metformin directly targets and represses Complex I[178]. Complex I is one site of entry into the ETC. By inhibiting Complex I, metformin decreases ATP production, which may cause anti-cancer effects on its own or through activation of other downstream pathways,

possibly mediated by AMPK[179]. Efforts are underway to determine how metformin might alter cell metabolism to impede cancer onset or progression.

Sirtuin-driven programs for maintaining oxidative metabolism

Several sirtuins have major roles in maintaining ETC function. In the nucleus, Sirt1 promotes oxidative metabolism, mitochondrial biogenesis and ROS defense via coordination of key transcriptional regulators of stress resistance including p53, forkhead homeobox type O (FOXO) proteins, peroxisome proliferator-activated receptor γ coactivator 1α (PGC-1α) and nuclear erythroid factor 2-related factor 2 (NRF2)[54, 180, 181]. Mitochondrial SIRT3 is also a major driver of oxidative phosphorylation. SIRT3 coordinates a multi-faceted post-translational program to maintain ETC function. SIRT3 deacetylates and activates specific subunits in all five ETC complexes to promote efficient electron flow. In addition to limiting ROS production, SIRT3 promotes ROS clearance through upregulation of antioxidant programs. For example, by deacetylating and activating the TCA cycle enzyme IDH2, SIRT3 promotes conversion of isocitrate to α-ketoglutarate in a reaction that simultaneously produces the antioxidant NADPH[182]. Through multiple mechanisms, SIRT1 and 3 increase mitochondrial oxidative capacity, prevent ETC stalling and limit ROS[17, 183-185].

By favoring mitochondrial metabolism over glycolytic metabolism, it is reasonable to hypothesize that, on one hand, SIRT1 and SIRT3 hinder the metabolic switch to glycolytic metabolism that is frequently observed with cellular transformation. However, functional mitochondria are still vital for established an cancer cell population to grow and metastasize[154], and therefore sirtuin-induced upregulation of

mitochondrial metabolism may be one reason why sirtuin expression can benefit many existing cancers.

PHDs, HIF and coordination of the ETC

In line with the role of PHD loss and HIF activation in favoring glycolytic metabolism, a small number of reports suggest HIF additionally represses oxidative phosphorylation in some circumstances. Under hypoxia, HIF acutely represses PGC-1β, a key inducer of mitochondrial biogenesis[186]. Surprisingly, metabolic plasticity enables some restoration of oxidative metabolism in the presence of prolonged HIF activation. While mitochondrial metabolism and oxidative phosphorylation are overall repressed by HIF, residual respiration is optimized due to HIF-mediated activation of a specific isoform of cytochrome c oxidase, COX4-2, which boosts respiration efficiency[187].

Identifying nodes of metabolic reprogramming in cancer

The primary goal of my dissertation work was to investigate novel regulatory nodes that coordinate cell metabolism and explore how these pathways might contribute to cancer. Chapter II of this dissertation describes an unbiased approach to identify new functions of SIRT4. Our lab has previously shown that SIRT4 KO mice have increased propensity toward lung cancer and that SIRT4 KO cells have increased TCA cycle intermediates, but the mechanistic details remain unclear. To this end, we assessed site-specific acetylation of mitochondrial proteins in wildtype and SIRT4 KO mouse tissues. Our approach stems from our finding that SIRT4 has substrate-specific and physiologically relevant deacetylase activity on malonyl-CoA carboxylase (MCD), suggesting the potential for SIRT4 to modify other mitochondrial targets. (The findings about MCD and my contributions to this project are detailed in the Appendix.) For the

first time, we detail the mitochondrial acetylome as it is altered by the presence versus absence of SIRT4. We find SIRT4 loss leads to hyperacetylation of enzymes in the TCA cycle, fatty acid metabolism, the ETC and energy production. We focus on one protein that was additionally found to interact with SIRT4, namely pyruvate carboxylase (PC). PC-mediated anaplerosis has been shown to be particularly relevant in SDH- and FH-deficient cancers and in cancers with low levels of glutaminolysis. This chapter provides insight into regulation of PC by SIRT4 and highlights a number of other proteins of interest in SIRT4 biology.

Chapter III describes the discovery of a novel role for PHD3 in repressing fatty acid oxidation with great significance in acute myeloid leukemia (AML). The effect of PHD3 on fatty acid catabolism is not sensitive to hypoxia and may instead be coordinated by the cellular nutrient state. We find PHD3 interacts with and activates acetyl-CoA carboxylase 2 (ACC2), a key enzyme limiting mitochondrial fatty acid import. Via site-specific hydroxylation, PHD3 activates ACC2 and represses FAO. Mechanistically, PHD3 hydroxylates ACC2 at proline 450, a residue adjacent to the ATP binding site of ACC2. Mutation of this hydroxylation site represses ACC2 activity and blunts the ability of ACC2 to bind ATP. We further show that loss of PHD3 is a common feature of AML, leading to unchecked, dramatically increased FAO that fuels cancer cell survival. We take advantage of the metabolic reliance of low-PHD3 leukemia cells on fatty acids, and show that FAO inhibition kills these cancer cells.

Chapter IV details a metabolomics-based analysis of the effects of the biguanides metformin and phenformin on neoplastic transformation and cancer cell stemness. Metformin is correlated with decreased cancer incidence, and efforts have been made by

numerous labs to understand the anti-cancer benefits of metformin or its more potent relative phenformin. The mechanism of action of biguanides is not entirely clear, but these drugs are proposed to work at least in part through Complex I inhibition. In collaboration with the Kevin Struhl lab at Harvard Medical School, we used metabolomics to assess the alterations caused by metformin and phenformin in cancer. Previous studies have examined the effects of these drugs on existing cancer cells. However, because we aimed to understand the ability of metformin to inhibit cancer onset, we took the novel approach of pre-treating non-tumorigenic cells with metformin or phenformin and then inducing cellular transformation. We find both metformin and phenformin limit cellular transformation, and we present here the metabolic alterations linked with biguanide treatment that appear to be incompatible with transformation. Additionally, we studied the metabolic effects of biguanides on cancer stem cells, a small population of cells that possess the predominant tumor-initiating capacity and are a major cause of therapeutic resistance and relapse[188]. This chapter reveals the metabolic effects of biguanides and furthermore highlights metabolic vulnerabilities during transformation or in cancer stem cells that could be targeted in future studies.

Together the studies presented in this dissertation enhance our understanding of metabolic regulatory nodes in the cell. Our knowledge of metabolic crux points in cancer is generating an increasingly clear view of the metabolic liabilities that can potentially be targeted in cancer treatment. For example, metformin is currently the subject of multiple ongoing clinical trials in cancer treatment (as of March 2015, www.clinicaltrials.gov lists over 100 such trials in its database). Additionally, initial success in using an inhibitor of mutant IDH2 to treat AML[189] set a precedent for impeding metabolic pathways in the

future. Further research of metabolic regulators such as sirtuins and PHDs will surely aid in the pursuit of therapeutics directed toward cancer metabolism. On one hand, studies of these enzymes have revealed interconnected metabolic and signaling pathways that drive tumor biology and could be specifically targeted in cancer treatment. On the other hand, sirtuin or PHD expression could be considered for its utility as a metabolic biomarker to designate the most promising therapeutic approach in a new era of metabolically based precision medicine.

References

1. Vander Heiden, M. G. (2011). Targeting cancer metabolism: a therapeutic window opens. Nat Rev Drug Discov *10*, 671–684.

2. Cheong, H., Lu, C., Lindsten, T., and Thompson, C. B. (2012). Therapeutic targets in cancer cell metabolism and autophagy. Nat Biotechnol *30*, 671–678.

3. Zhao, Y., Butler, E. B., and Tan, M. (2013). Targeting cellular metabolism to improve cancer therapeutics. Cell Death Dis *4*, e532.

4. Dang, C. V. (2012). Links between metabolism and cancer. Genes & Development *26*, 877–890.

5. Jones, R. G., and Thompson, C. B. (2009). Tumor suppressors and cell metabolism: a recipe for cancer growth. Genes & Development *23*, 537–548.

6. Cairns, R. A., Harris, I. S., and Mak, T. W. (2011). Regulation of cancer cell metabolism. Nat Rev Cancer *11*, 85–95.

7. Kroemer, G., and Pouysségur, J. (2008). Tumor Cell Metabolism: Cancer"s Achilles" Heel. Cancer Cell *13*, 472–482.

8. Hursting, S. D., and Berger, N. A. (2010). Energy Balance, Host-Related Factors, and Cancer Progression. Journal of Clinical Oncology *28*, 4058–4065.

9. Haslam, D. W., and James, W. P. T. (2005). Obesity. The Lancet *366*, 1197–1209.

10. LeRoith, D., Novosyadlyy, R., Gallagher, E., Lann, D., Vijayakumar, A., and Yakar, S. (2008). Obesity and Type 2 Diabetes are Associated with an Increased Risk of Developing Cancer and a Worse Prognosis; Epidemiological and Mechanistic Evidence. Exp Clin Endocrinol Diabetes *116*, S4–S6.

11. Calle, E. E., Rodriguez, C., Walker-Thurmond, K., and Thun, M. J. (2003). Overweight, obesity, and mortality from cancer in a prospectively studied cohort of U.S. adults. N. Engl. J. Med. *348*, 1625–1638.

12. Stanley, I. A., Ribeiro, S. M., Giménez-Cassina, A., Norberg, E., and Danial, N. N. (2013). Changing appetites: the adaptive advantages of fuel choice. Trends in Cell Biology *24*, 118–127.

13. Tsalikis, J., Croitoru, D. O., Philpott, D. J., and Girardin, S. E. (2013). Nutrient sensing and metabolic stress pathways in innate immunity. Cell. Microbiol. *15*, 1632–1641.

14. Ochocki, J. D., and Simon, M. C. (2013). Nutrient-sensing pathways and metabolic regulation in stem cells. The Journal of Cell Biology *203*, 23–33.

15. Cantor, J. R., and Sabatini, D. M. (2012). Cancer Cell Metabolism: One Hallmark, Many Faces. Cancer Discovery *2*, 881–898.

16. Chang, H.-C., and Guarente, L. (2014). SIRT1 and other sirtuins in metabolism. Trends in Endocrinology & Metabolism *25*, 138–145.

17. Roth, M., and Chen, W. Y. (2013). Sorting out functions of sirtuins in cancer. Oncogene *33*, 1609–1620.

18. Boulahbel, H., Durán, R. V., and Gottlieb, E. (2009). Prolyl hydroxylases as regulators of cell metabolism. Biochem. Soc. Trans. *37*, 291–294.

19. Houtkooper, R. H., Pirinen, E., and Auwerx, J. (2012). Sirtuins as regulators of metabolism and healthspan. Nature Publishing Group *13*, 225–238.

20. Bosch-Presegue, L., and Vaquero, A. (2013). Sirtuins in stress response: guardians of the genome. Oncogene *33*, 3764–3775.

21. Kaelin, W. G., Jr., and Ratcliffe, P. J. (2008). Oxygen Sensing by Metazoans: The Central Role of the HIF Hydroxylase Pathway. Molecular Cell *30*, 393–402.

22. Gonfloni, S., Iannizzotto, V., Maiani, E., Bellusci, G., Ciccone, S., and Diederich, M. (2014). P53 and Sirt1: Routes of metabolism and genome stability. Biochem. Pharmacol. *92*, 149–156.

23. Cha, Y. I., and Kim, H.-S. (2013). Emerging role of sirtuins on tumorigenesis: possible link between aging and cancer. BMB Rep *46*, 429–438.

24. Dowling, R. J. O., Goodwin, P. J., and Stambolic, V. (2011). Understanding the benefit of metformin use in cancer treatment. BMC Med *9*, 33.

25. North, B. J., and Verdin, E. (2004). Sirtuins: Sir2-related NAD-dependent protein deacetylases. Genome Biol. *5*, 224.

26. Nakagawa, T., and Guarente, L. (2011). Sirtuins at a glance. Journal of Cell Science *124*, 833–838.

27. North, B. J., Marshall, B. L., Borra, M. T., Denu, J. M., and Verdin, E. (2003). The human Sir2 ortholog, SIRT2, is an NAD+-dependent tubulin deacetylase. Molecular Cell *11*, 437–444.

28. Inoue, T., Hiratsuka, M., Osaki, M., and Oshimura, M. (2014). The Molecular Biology of Mammalian SIRT Proteins: SIRT2 Functions on Cell Cycle Regulation. Cell Cycle *6*, 1011–1018.

29. He, W., Newman, J. C., Wang, M. Z., Ho, L., and Verdin, E. (2012). Mitochondrial sirtuins: regulators of protein acylation and metabolism. Trends in Endocrinology & Metabolism *23*, 467–476.

30. Sebastian, C., Satterstrom, F. K., Haigis, M. C., and Mostoslavsky, R. (2012). From Sirtuin Biology to Human Diseases: An Update. Journal of Biological Chemistry *287*, 42444–42452.

31. Feldman, J. L., Baeza, J., and Denu, J. M. (2013). Activation of the Protein Deacetylase SIRT6 by Long-chain Fatty Acids and Widespread Deacylation by Mammalian Sirtuins. Journal of Biological Chemistry *288*, 31350–31356.

32. Mathias, R. A., Greco, T. M., Oberstein, A., Budayeva, H. G., Chakrabarti, R., Rowland, E. A., Kang, Y., Shenk, T., and Cristea, I. M. (2014). Sirtuin 4 Is a Lipoamidase Regulating Pyruvate Dehydrogenase Complex Activity. Cell *159*, 1615–1625.

33. Bosch-Presegue, L., and Vaquero, A. (2011). The Dual Role of Sirtuins in Cancer. Genes & Cancer *2*, 648–662.

34. Sauve, A. A. (2010). Sirtuin chemical mechanisms. Biochimica et Biophysica Acta (BBA) - Proteins and Proteomics *1804*, 1591–1603.

35. Hassa, P. O., Haenni, S. S., Elser, M., and Hottiger, M. O. (2006). Nuclear ADP-Ribosylation Reactions in Mammalian Cells: Where Are We Today and Where Are We Going? Microbiology and Molecular Biology Reviews *70*, 789–829.

36. Bitterman, K. J. (2002). Inhibition of Silencing and Accelerated Aging by Nicotinamide, a Putative Negative Regulator of Yeast Sir2 and Human SIRT1. Journal of Biological Chemistry *277*, 45099–45107.

37. Nakagawa, T., Lomb, D. J., Haigis, M. C., and Guarente, L. (2009). SIRT5 Deacetylates Carbamoyl Phosphate Synthetase 1 and Regulates the Urea Cycle. Cell *137*, 560–570.

38. Yang, H., Yang, T., Baur, J. A., Perez, E., Matsui, T., Carmona, J. J., Lamming, D. W., Souza-Pinto, N. C., Bohr, V. A., Rosenzweig, A., et al. (2007). Nutrient-

Sensitive Mitochondrial NAD+ Levels Dictate Cell Survival. Cell *130*, 1095–1107.

39. Van Gool, F., Gallí, M., Gueydan, C., Kruys, V., Prevot, P.-P., Bedalov, A., Mostoslavsky, R., Alt, F. W., De Smedt, T., and Leo, O. (2009). Intracellular NAD levels regulate tumor necrosis factor protein synthesis in a sirtuin-dependent manner. Nat Med *15*, 206–210.

40. Nakahata, Y., Sahar, S., Astarita, G., Kaluzova, M., and Sassone-Corsi, P. (2009). Circadian control of the NAD+ salvage pathway by CLOCK-SIRT1. Science *324*, 654–657.

41. Ramsey, K. M., Yoshino, J., Brace, C. S., Abrassart, D., Kobayashi, Y., Marcheva, B., Hong, H.-K., Chong, J. L., Buhr, E. D., Lee, C., et al. (2009). Circadian clock feedback cycle through NAMPT-mediated NAD+ biosynthesis. Science *324*, 651–654.

42. Haigis, M. C., and Guarente, L. P. (2006). Mammalian sirtuins--emerging roles in physiology, aging, and calorie restriction. Genes & Development *20*, 2913–2921.

43. Houtkooper, R. H., and Auwerx, J. (2012). Exploring the therapeutic space around NAD. The Journal of Cell Biology *199*, 205–209.

44. Cantó, C., and Auwerx, J. (2012). Targeting sirtuin 1 to improve metabolism: all you need is NAD(+)? Pharmacol. Rev. *64*, 166–187.

45. Cohen, D. E., Supinski, A. M., Bonkowski, M. S., Donmez, G., and Guarente, L. P. (2009). Neuronal SIRT1 regulates endocrine and behavioral responses to calorie restriction. Genes & Development *23*, 2812–2817.

46. Cantó, C., Jiang, L. Q., Deshmukh, A. S., Mataki, C., Coste, A., Lagouge, M., Zierath, J. R., and Auwerx, J. (2010). Interdependence of AMPK and SIRT1 for Metabolic Adaptation to Fasting and Exercise in Skeletal Muscle. Cell Metabolism *11*, 213–219.

47. Gomes, A. P., Price, N. L., Ling, A. J. Y., Moslehi, J. J., Montgomery, M. K., Rajman, L., White, J. P., Teodoro, J. S., Wrann, C. D., Hubbard, B. P., et al. (2013). Declining NAD+ Induces a Pseudohypoxic State Disrupting Nuclear-Mitochondrial Communication during Aging. Cell *155*, 1624–1638.

48. Kendrick, A. A., Choudhury, M., Rahman, S. M., McCurdy, C. E., Friederich, M., Van Hove, J. L. K., Watson, P. A., Birdsey, N., Bao, J., Gius, D., et al. (2011). Fatty liver is associated with reduced SIRT3 activity and mitochondrial protein hyperacetylation. Biochem. J. *433*, 505–514.

49. Lavu, S., Boss, O., Elliott, P. J., and Lambert, P. D. (2008). Sirtuins — novel therapeutic targets to treat age-associated diseases. Nat Rev Drug Discov *7*, 841–

853.

50. Flick, F., and Lüscher, B. (2012). Regulation of sirtuin function by posttranslational modifications. Front. Pharmacol. *3*.

51. Laurent, G., German, N. J., Saha, A. K., de Boer, V. C. J., Davies, M., Koves, T. R., Dephoure, N., Fischer, F., Boanca, G., Vaitheesvaran, B., et al. (2013). SIRT4 Coordinates the Balance between Lipid Synthesis and Catabolism by Repressing Malonyl CoA Decarboxylase. Molecular Cell *50*, 686–698.

52. Ho, L., Titus, A. S., Banerjee, K. K., George, S., Lin, W., Deota, S., Saha, A. K., Nakamura, K., Gut, P., Verdin, E., et al. (2013). SIRT4 regulates ATP homeostasis and mediates a retrograde signaling via AMPK. Aging (Albany NY) *5*, 835–849.

53. Laurent, G., de Boer, V. C. J., Finley, L. W. S., Sweeney, M., Lu, H., Schug, T. T., Cen, Y., Jeong, S. M., Li, X., Sauve, A. A., et al. (2013). SIRT4 Represses Peroxisome Proliferator-Activated Receptor Activity To Suppress Hepatic Fat Oxidation. Molecular and Cellular Biology *33*, 4552–4561.

54. Chen, W., Yuan, H., and Su, L. (2013). The emerging and diverse roles of sirtuins in cancer: a clinical perspective. OTT, 1399.

55. Finley, L. W. S., Carracedo, A., Lee, J., Souza, A., Egia, A., Zhang, J., Teruya-Feldstein, J., Moreira, P. I., Cardoso, S. M., Clish, C. B., et al. (2011). SIRT3 Opposes Reprogramming of Cancer Cell Metabolism through HIF1α Destabilization. Cancer Cell *19*, 416–428.

56. Jeong, S. M., Xiao, C., Finley, L. W. S., Lahusen, T., Souza, A. L., Pierce, K., Li, Y.-H., Wang, X., Laurent, G., German, N. J., et al. (2013). SIRT4 Has Tumor-Suppressive Activity and Regulates the Cellular Metabolic Response to DNA Damage by Inhibiting Mitochondrial Glutamine Metabolism. Cancer Cell *23*, 450–463.

57. Csibi, A., Fendt, S.-M., Li, C., Poulogiannis, G., Choo, A. Y., Chapski, D. J., Jeong, S. M., Dempsey, J. M., Parkhitko, A., Morrison, T., et al. (2013). The mTORC1 Pathway Stimulates Glutamine Metabolism and Cell Proliferation by Repressing SIRT4. Cell *153*, 840–854.

58. Sebastian, C., Zwaans, B. M. M., Silberman, D. M., Gymrek, M., Goren, A., Zhong, L., Ram, O., Truelove, J., Guimaraes, A. R., Toiber, D., et al. (2012). The Histone Deacetylase SIRT6 Is a Tumor Suppressor that Controls Cancer Metabolism. Cell *151*, 1185–1199.

59. Chu, F. (2005). Control of Multidrug Resistance Gene mdr1 and Cancer Resistance to Chemotherapy by the Longevity Gene sirt1. Cancer Research *65*, 10183–10187.

60. Jang, K. Y., Noh, S. J., Lehwald, N., Tao, G.-Z., Bellovin, D. I., Park, H. S., Moon, W. S., Felsher, D. W., and Sylvester, K. G. (2012). SIRT1 and c-Myc Promote Liver Tumor Cell Survival and Predict Poor Survival of Human Hepatocellular Carcinomas. PLoS ONE *7*, e45119.

61. Alhazzazi, T. Y., Kamarajan, P., Joo, N., Huang, J.-Y., Verdin, E., D'Silva, N. J., and Kapila, Y. L. (2010). Sirtuin-3 (SIRT3), a novel potential therapeutic target for oral cancer. Cancer *117*, 1670–1678.

62. McNeill, L. A., Hewitson, K. S., Gleadle, J. M., Horsfall, L. E., Oldham, N. J., Maxwell, P. H., Pugh, C. W., Ratcliffe, P. J., and Schofield, C. J. (2002). The use of dioxygen by HIF prolyl hydroxylase (PHD1). Bioorganic & medicinal chemistry letters *12*, 1547–1550.

63. Loenarz, C., and Schofield, C. J. (2011). Physiological and biochemical aspects of hydroxylations and demethylations catalyzed by human 2-oxoglutarate oxygenases. Trends in Biochemical Sciences *36*, 7–18.

64. Wong, B. W., Kuchnio, A., Bruning, U., and Carmeliet, P. (2012). Emerging novel functions of the oxygen-sensing prolyl hydroxylase domain enzymes. Trends in Biochemical Sciences, 1–9.

65. Gorres, K. L., and Raines, R. T. (2010). Prolyl 4-hydroxylase. Critical Reviews in Biochemistry and Molecular Biology *45*, 106–124.

66. Villar, D., Vara-Vega, A., Landázuri, M. O., and Del Peso, L. (2007). Identification of a region on hypoxia-inducible-factor prolyl 4-hydroxylases that determines their specificity for the oxygen degradation domains. Biochem. J. *408*, 231–240.

67. Yasumoto, K.-I., Kowata, Y., Yoshida, A., Torii, S., and Sogawa, K. (2009). Role of the intracellular localization of HIF-prolyl hydroxylases. Biochimica et Biophysica Acta (BBA) - Molecular Cell Research *1793*, 792–797.

68. Metzen, E. (2003). Intracellular localisation of human HIF-1alpha hydroxylases: implications for oxygen sensing. Journal of Cell Science *116*, 1319–1326.

69. Freeman, R. S., Hasbani, D. M., Lipscomb, E. A., Straub, J. A., and Xie, L. (2003). SM-20, EGL-9, and the EGLN family of hypoxia-inducible factor prolyl hydroxylases. Mol. Cells *16*, 1–12.

70. Myllyharju, J., and Koivunen, P. (2013). Hypoxia-inducible factor prolyl 4-hydroxylases: common and specific roles. Biol. Chem. *394*, 435–448.

71. Majmundar, A. J., Wong, W. J., and Simon, M. C. (2010). Hypoxia-inducible factors and the response to hypoxic stress. Molecular Cell *40*, 294–309.

72. Fraisl, P., Aragonés, J., and Carmeliet, P. (2009). Inhibition of oxygen sensors as

a therapeutic strategy for ischaemic and inflammatory disease. Nat Rev Drug Discov *8*, 139–152.

73. Luo, W., Hu, H., Chang, R., Zhong, J., Knabel, M., O'Meally, R., Cole, R. N., Pandey, A., and Semenza, G. L. (2011). Pyruvate kinase M2 is a PHD3-stimulated coactivator for hypoxia-inducible factor 1. Cell *145*, 732–744.

74. Tennant, D. A., and Gottlieb, E. (2010). HIF prolyl hydroxylase-3 mediates alpha-ketoglutarate-induced apoptosis and tumor suppression. J Mol Med *88*, 839–849.

75. Xiao, M., Yang, H., Xu, W., Ma, S., Lin, H., Zhu, H., Liu, L., Liu, Y., Yang, C., Xu, Y., et al. (2012). Inhibition of -KG-dependent histone and DNA demethylases by fumarate and succinate that are accumulated in mutations of FH and SDH tumor suppressors. Genes & Development *26*, 1326–1338.

76. Koivunen, P., Hirsilä, M., Remes, A. M., Hassinen, I. E., Kivirikko, K. I., and Myllyharju, J. (2007). Inhibition of hypoxia-inducible factor (HIF) hydroxylases by citric acid cycle intermediates: possible links between cell metabolism and stabilization of HIF. J. Biol. Chem. *282*, 4524–4532. Available at: http://eutils.ncbi.nlm.nih.gov/entrez/eutils/elink.fcgi?dbfrom=pubmed&id=17182618&retmode=ref&cmd=prlinks.

77. MacKenzie, E. D., Selak, M. A., Tennant, D. A., Payne, L. J., Crosby, S., Frederiksen, C. M., Watson, D. G., and Gottlieb, E. (2007). Cell-Permeating -Ketoglutarate Derivatives Alleviate Pseudohypoxia in Succinate Dehydrogenase-Deficient Cells. Molecular and Cellular Biology *27*, 3282–3289.

78. Losman, J. A., Looper, R. E., Koivunen, P., Lee, S., Schneider, R. K., McMahon, C., Cowley, G. S., Root, D. E., Ebert, B. L., and Kaelin, W. G. (2013). (R)-2-Hydroxyglutarate Is Sufficient to Promote Leukemogenesis and Its Effects Are Reversible. Science *339*, 1621–1625.

79. Schofield, C. J., and Ratcliffe, P. J. (2004). Oxygen sensing by HIF hydroxylases. Nature Publishing Group *5*, 343–354.

80. Pagé, E. L., Chan, D. A., Giaccia, A. J., Levine, M., and Richard, D. E. (2008). Hypoxia-inducible factor-1alpha stabilization in nonhypoxic conditions: role of oxidation and intracellular ascorbate depletion. Molecular Biology of the Cell *19*, 86–94.

81. Knowles, H. J., Raval, R. R., Harris, A. L., and Ratcliffe, P. J. (2003). Effect of ascorbate on the activity of hypoxia-inducible factor in cancer cells. Cancer Research *63*, 1764–1768.

82. Gao, P., Zhang, H., Dinavahi, R., Li, F., Xiang, Y., Raman, V., Bhujwalla, Z. M., Felsher, D. W., Cheng, L., Pevsner, J., et al. (2007). HIF-dependent antitumorigenic effect of antioxidants in vivo. Cancer Cell *12*, 230–238.

83. Wang, G. L., and Semenza, G. L. (1993). Desferrioxamine induces erythropoietin gene expression and hypoxia-inducible factor 1 DNA-binding activity: implications for models of hypoxia signal transduction. Blood *82*, 3610–3615.

84. Esteban, M. A., and Maxwell, P. H. (2005). HIF, a missing link between metabolism and cancer. Nat Med *11*, 1047–1048.

85. Selak, M. A., Armour, S. M., MacKenzie, E. D., Boulahbel, H., Watson, D. G., Mansfield, K. D., Pan, Y., Simon, M. C., Thompson, C. B., and Gottlieb, E. (2005). Succinate links TCA cycle dysfunction to oncogenesis by inhibiting HIF-α prolyl hydroxylase. Cancer Cell *7*, 77–85.

86. Isaacs, J. S., Jung, Y. J., Mole, D. R., Lee, S., Torres-Cabala, C., Chung, Y.-L., Merino, M., Trepel, J., Zbar, B., Toro, J., et al. (2005). HIF overexpression correlates with biallelic loss of fumarate hydratase in renal cancer: Novel role of fumarate in regulation of HIF stability. Cancer Cell *8*, 143–153.

87. King, A., Selak, M. A., and Gottlieb, E. (2006). Succinate dehydrogenase and fumarate hydratase: linking mitochondrial dysfunction and cancer. Oncogene *25*, 4675–4682.

88. Rawluszko, A. A., Bujnicka, K. E., Horbacka, K., Krokowicz, P., and Jagodziński, P. P. (2013). Expression and DNA methylation levels of prolyl hydroxylases PHD1, PHD2, PHD3 and asparaginyl hydroxylase FIH in colorectal cancer. BMC Cancer *13*, 526.

89. Huang, K. T., Mikeska, T., Dobrovic, A., and Fox, S. B. (2010). DNA methylation analysis of the HIF-1α prolyl hydroxylase domain genes PHD1, PHD2, PHD3 and the factor inhibiting HIF gene FIH in invasive breast carcinomas. Histopathology *57*, 451–460.

90. Place, T. L., Fitzgerald, M. P., Venkataraman, S., Vorrink, S. U., Case, A. J., Teoh, M. L. T., and Domann, F. E. (2011). Aberrant Promoter CpG Methylation Is a Mechanism for Impaired PHD3 Expression in a Diverse Set of Malignant Cells. PLoS ONE *6*, e14617.

91. Hatzimichael, E., Dasoula, A., Shah, R., Syed, N., Papoudou-Bai, A., Coley, H. M., Dranitsaris, G., Bourantas, K. L., Stebbing, J., and Crook, T. The prolyl-hydroxylase EGLN3 and not EGLN1 is inactivated by methylation in plasma cell neoplasia. European Journal of Haematology *84*, 47–51.

92. Henze, A.-T., Garvalov, B. K., Seidel, S., Cuesta, A. M., Ritter, M., Filatova, A., Foss, F., Dopeso, H., Essmann, C. L., Maxwell, P. H., et al. (2014). Loss of PHD3 allows tumours to overcome hypoxic growth inhibition and sustain proliferation through EGFR. Nat Comms *5*, 5582.

93. Warburg, O. (1956). On the origin of cancer cells. Science *123*, 309–314.

94. DeBerardinis, R. J., Lum, J. J., Hatzivassiliou, G., and Thompson, C. B. (2008). The Biology of Cancer: Metabolic Reprogramming Fuels Cell Growth and Proliferation. Cell Metabolism *7*, 11–20.

95. McFate, T., Mohyeldin, A., Lu, H., Thakar, J., Henriques, J., Halim, N. D., Wu, H., Schell, M. J., Tsang, T. M., Teahan, O., et al. (2008). Pyruvate dehydrogenase complex activity controls metabolic and malignant phenotype in cancer cells. J. Biol. Chem. *283*, 22700–22708.

96. Estrella, V., Chen, T., Lloyd, M., Wojtkowiak, J., Cornnell, H. H., Ibrahim-Hashim, A., Bailey, K., Balagurunathan, Y., Rothberg, J. M., Sloane, B. F., et al. (2013). Acidity Generated by the Tumor Microenvironment Drives Local Invasion. Cancer Research *73*, 1524–1535.

97. Rofstad, E. K. (2006). Acidic Extracellular pH Promotes Experimental Metastasis of Human Melanoma Cells in Athymic Nude Mice. Cancer Research *66*, 6699–6707.

98. Dai, C., Sun, F., Zhu, C., and Hu, X. (2013). Tumor Environmental Factors Glucose Deprivation and Lactic Acidosis Induce Mitotic Chromosomal Instability – An Implication in Aneuploid Human Tumors. PLoS ONE *8*, e63054.

99. Martinez-Outschoorn, U. E., Prisco, M., Ertel, A., Tsirigos, A., Lin, Z., Pavlides, S., Wang, C., Flomenberg, N., Knudsen, E. S., Howell, A., et al. (2014). Ketones and lactate increase cancer cell "stemness," driving recurrence, metastasis and poor clinical outcome in breast cancer. Cell Cycle *10*, 1271–1286.

100. Seyfried, T. N., and Shelton, L. M. (2010). Cancer as a metabolic disease. Nutr Metab (Lond) *7*, 7.

101. Wang, G. L., Jiang, B. H., Rue, E. A., and Semenza, G. L. (1995). Hypoxia-inducible factor 1 is a basic-helix-loop-helix-PAS heterodimer regulated by cellular O_2 tension. Proc. Natl. Acad. Sci. U.S.A. *92*, 5510–5514.

102. Semenza, G. L. (2003). Targeting HIF-1 for cancer therapy. Nat Rev Cancer *3*, 721–732.

103. Loboda, A., Jozkowicz, A., and Dulak, J. (2010). HIF-1 and HIF-2 transcription factors — Similar but not identical. Mol. Cells *29*, 435–442.

104. Masson, N., and Ratcliffe, P. J. (2014). Hypoxia signaling pathways in cancer metabolism: the importance of co-selecting interconnected physiological pathways. Cancer Metab *2*, 3.

105. Masson, N., Willam, C., Maxwell, P. H., Pugh, C. W., and Ratcliffe, P. J. (2001). Independent function of two destruction domains in hypoxia-inducible factor-alpha chains activated by prolyl hydroxylation. The EMBO Journal *20*, 5197–5206.

106. Berra, E., Benizri, E., Ginouvès, A., Volmat, V., Roux, D., and Pouysségur, J. (2003). HIF prolyl‐hydroxylase 2 is the key oxygen sensor setting low steady‐state levels of HIF‐1α in normoxia. The EMBO Journal *22*, 4082–4090.

107. Appelhoff, R. J. (2004). Differential Function of the Prolyl Hydroxylases PHD1, PHD2, and PHD3 in the Regulation of Hypoxia-inducible Factor. Journal of Biological Chemistry *279*, 38458–38465.

108. Luo, W., and Semenza, G. L. (2012). Emerging roles of PKM2 in cell metabolism and cancer progression. Trends in Endocrinology & Metabolism *23*, 560–566.

109. Zhong, L., D'Urso, A., Toiber, D., Sebastian, C., Henry, R. E., Vadysirisack, D. D., Guimaraes, A., Marinelli, B., Wikstrom, J. D., Nir, T., et al. (2010). The Histone Deacetylase Sirt6 Regulates Glucose Homeostasis via Hif1α. Cell *140*, 280–293.

110. Lim, J.-H., Lee, Y.-M., Chun, Y.-S., Chen, J., Kim, J.-E., and Park, J.-W. (2010). Sirtuin 1 Modulates Cellular Responses to Hypoxia by Deacetylating Hypoxia-Inducible Factor 1α. Molecular Cell *38*, 864–878.

111. Bell, E. L., Emerling, B. M., Ricoult, S. J. H., and Guarente, L. (2011). SirT3 suppresses hypoxia inducible factor 1α and tumor growth by inhibiting mitochondrial ROS production. Oncogene *30*, 2986–2996.

112. Carracedo, A., Cantley, L. C., and Pandolfi, P. P. (2013). Cancer metabolism: fatty acid oxidation in the limelight. Nat Rev Cancer *13*, 227–232.

113. Wise, D. R., and Thompson, C. B. (2010). Glutamine addiction: a new therapeutic target in cancer. Trends in Biochemical Sciences *35*, 427–433.

114. Patel, M. S., and Roche, T. E. (1990). Molecular biology and biochemistry of pyruvate dehydrogenase complexes. FASEB J. *4*, 3224–3233.

115. Lunt, S. Y., and Vander Heiden, M. G. (2011). Aerobic Glycolysis: Meeting the Metabolic Requirements of Cell Proliferation. Annu. Rev. Cell Dev. Biol. *27*, 441–464.

116. Marin-Valencia, I., Roe, C. R., and Pascual, J. M. (2010). Pyruvate carboxylase deficiency: Mechanisms, mimics and anaplerosis. Molecular Genetics and Metabolism *101*, 9–17.

117. Jitrapakdee, S., St Maurice, M., Rayment, I., Cleland, W. W., Wallace, J. C., and Attwood, P. V. (2008). Structure, mechanism and regulation of pyruvate carboxylase. Biochem. J. *413*, 369.

118. Bergström, J., Fürst, P., Norée, L. O., and Vinnars, E. (1974). Intracellular free amino acid concentration in human muscle tissue. J Appl Physiol *36*, 693–697.

119. Hensley, C. T., Wasti, A. T., and DeBerardinis, R. J. (2013). Glutamine and cancer: cell biology, physiology, and clinical opportunities. J. Clin. Invest. *123*, 3678–3684.

120. Cheng, T., Sudderth, J., Yang, C., Mullen, A. R., Jin, E. S., Matés, J. M., and DeBerardinis, R. J. (2014). Pyruvate carboxylase is required for glutamine-independent growth of tumor cells. Proc. Natl. Acad. Sci. U.S.A. *108*, 8674–8679.

121. Elhammali, A., Ippolito, J. E., Collins, L., Crowley, J., Marasa, J., and Piwnica-Worms, D. (2014). A High-Throughput Fluorimetric Assay for 2-Hydroxyglutarate Identifies Zaprinast as a Glutaminase Inhibitor. Cancer Discovery *4*, 828–839.

122. Fendt, S. M., Bell, E. L., Keibler, M. A., Davidson, S. M., Wirth, G. J., Fiske, B., Mayers, J. R., Schwab, M., Bellinger, G., Csibi, A., et al. (2013). Metformin Decreases Glucose Oxidation and Increases the Dependency of Prostate Cancer Cells on Reductive Glutamine Metabolism. Cancer Research *73*, 4429–4438.

123. Fendt, S.-M., Bell, E. L., Keibler, M. A., Olenchock, B. A., Mayers, J. R., Wasylenko, T. M., Vokes, N. I., Guarente, L., Heiden, M. G. V., and Stephanopoulos, G. (2013). Reductive glutamine metabolism is a function of the α-ketoglutarate to citrate ratio in cells. Nat Comms *4*.

124. Gameiro, P. A., Laviolette, L. A., Kelleher, J. K., Iliopoulos, O., and Stephanopoulos, G. (2013). Cofactor balance by nicotinamide nucleotide transhydrogenase (NNT) coordinates reductive carboxylation and glucose catabolism in the tricarboxylic acid (TCA) cycle. Journal of Biological Chemistry *288*, 12967–12977.

125. Metallo, C. M., Gameiro, P. A., Bell, E. L., Mattaini, K. R., Yang, J., Hiller, K., Jewell, C. M., Johnson, Z. R., Irvine, D. J., Guarente, L., et al. (2012). Reductive glutamine metabolism by IDH1 mediates lipogenesis under hypoxia. Nature *481*, 380–384.

126. Mullen, A. R., Wheaton, W. W., Jin, E. S., Chen, P.-H., Sullivan, L. B., Cheng, T., Yang, Y., Linehan, W. M., Chandel, N. S., and DeBerardinis, R. J. (2012). Reductive carboxylation supports growth in tumour cells with defective mitochondria. Nature *481*, 385–388.

127. Wise, D. R., Ward, P. S., Shay, J. E. S., Cross, J. R., Gruber, J. J., Sachdeva, U. M., Platt, J. M., DeMatteo, R. G., Simon, M. C., and Thompson, C. B. (2011). Hypoxia promotes isocitrate dehydrogenase-dependent carboxylation of α-ketoglutarate to citrate to support cell growth and viability. Proc. Natl. Acad. Sci. U.S.A. *108*, 19611–19616.

128. Liu, Y., Zuckier, L. S., and Ghesani, N. V. (2013). Dominant uptake of fatty acid over glucose by prostate cells: a potential new diagnostic and therapeutic

approach. Anticancer Research, 1–6.

129. Samudio, I., Harmancey, R., Fiegl, M., Kantarjian, H., Konopleva, M., Korchin, B., Kaluarachchi, K., Bornmann, W., Duvvuri, S., Taegtmeyer, H., et al. (2010). Pharmacologic inhibition of fatty acid oxidation sensitizes human leukemia cells to apoptosis induction. J. Clin. Invest. *120*, 142–156.

130. Holla, V. R., Wu, H., Shi, Q., Menter, D. G., and DuBois, R. N. (2011). Nuclear Orphan Receptor NR4A2 Modulates Fatty Acid Oxidation Pathways in Colorectal Cancer. Journal of Biological Chemistry *286*, 30003–30009.

131. Peluso, G., Nicolai, R., Reda, E., Benatti, P., Barbarisi, A., and Calvani, M. (2000). Cancer and anticancer therapy-induced modifications on metabolism mediated by carnitine system. J. Cell. Physiol. *182*, 339–350.

132. Lochner, M., Berod, L., and Sparwasser, T. (2015). Fatty acid metabolism in the regulation of T cell function. Trends Immunol. *36*, 81–91.

133. Ruderman, N., and Prentki, M. (2004). AMP kinase and malonyl-CoA: targets for therapy of the metabolic syndrome. Nat Rev Drug Discov *3*, 340–351.

134. Cho, Y. S., Lee, J. I., Shin, D., Kim, H. T., Cheon, Y. H., Seo, C. I., Kim, Y. E., Hyun, Y.-L., Lee, Y. S., Sugiyama, K., et al. (2007). Crystal structure of the biotin carboxylase domain of human acetyl-CoA carboxylase 2. Proteins *70*, 268–272.

135. O'Donnell, J. M., Alpert, N. M., White, L. T., and Lewandowski, E. D. (2002). Coupling of Mitochondrial Fatty Acid Uptake to Oxidative Flux in the Intact Heart. Biophysical Journal *82*, 11–18.

136. Linher-Melville, K., Zantinge, S., Sanli, T., Gerstein, H., Tsakiridis, T., and Singh, G. (2011). Establishing a relationship between prolactin and altered fatty acid β-oxidation via carnitine palmitoyl transferase 1 in breast cancer cells. BMC Cancer *11*, 56.

137. Schlaepfer, I. R., Rider, L., Rodrigues, L. U., Gijon, M. A., Pac, C. T., Romero, L., Cimic, A., Sirintrapun, S. J., Glode, L. M., Eckel, R. H., et al. (2014). Lipid Catabolism via CPT1 as a Therapeutic Target for Prostate Cancer. Molecular Cancer Therapeutics *13*, 2361–2371.

138. Zaugg, K., Yao, Y., Reilly, P. T., Kannan, K., Kiarash, R., Mason, J., Huang, P., Sawyer, S. K., Fuerth, B., Faubert, B., et al. (2011). Carnitine palmitoyltransferase 1C promotes cell survival and tumor growth under conditions of metabolic stress. Genes & Development *25*, 1041–1051.

139. Pike, L. S., Smift, A. L., Croteau, N. J., Ferrick, D. A., and Wu, M. (2011). Inhibition of fatty acid oxidation by etomoxir impairs NADPH production and increases reactive oxygen species resulting in ATP depletion and cell death in

human glioblastoma cells. BBA - Bioenergetics *1807*, 726–734.

140. Pacilli, A., Calienni, M., Margarucci, S., D'Apolito, M., Petillo, O., Rocchi, L., Pasquinelli, G., Nicolai, R., Koverech, A., Calvani, M., et al. (2013). Carnitine-Acyltransferase System Inhibition, Cancer Cell Death, and Prevention of Myc-Induced Lymphomagenesis. JNCI Journal of the National Cancer Institute *105*, 489–498.

141. Schafer, Z. T., Grassian, A. R., Song, L., Jiang, Z., Gerhart-Hines, Z., Irie, H. Y., Gao, S., Puigserver, P., and Brugge, J. S. (2009). Antioxidants and metabolic defects Nature 2009. Nature *461*, 109–113.

142. Caro, P., Kishan, A. U., Norberg, E., Stanley, I. A., Chapuy, B., Ficarro, S. B., Polak, K., Tondera, D., Gounarides, J., Yin, H., et al. (2012). Metabolic Signatures Uncover Distinct Targets in Molecular Subsets of Diffuse Large B Cell Lymphoma. Cancer Cell *22*, 547–560.

143. Jeon, S.-M., Chandel, N. S., and Hay, N. (2012). AMPK regulates NADPH homeostasis to promote tumour cell survival during energy stress. Nature *485*, 661–665.

144. Zaugg, K., Yao, Y., Reilly, P. T., Kannan, K., Kiarash, R., Mason, J., Huang, P., Sawyer, S. K., Fuerth, B., Faubert, B., et al. (2011). Carnitine palmitoyltransferase 1C promotes cell survival and tumor growth under conditions of metabolic stress. Genes & Development *25*, 1041–1051.

145. Corbet, C., Draoui, N., Polet, F., Pinto, A., Drozak, X., Riant, O., and Feron, O. (2014). The SIRT1/HIF2 Axis Drives Reductive Glutamine Metabolism under Chronic Acidosis and Alters Tumor Response to Therapy. Cancer Research *74*, 5507–5519.

146. Haigis, M. C., Mostoslavsky, R., Haigis, K. M., Fahie, K., Christodoulou, D. C., Murphy, A. J., Valenzuela, D. M., Yancopoulos, G. D., Karow, M., Blander, G., et al. (2006). SIRT4 Inhibits Glutamate Dehydrogenase and Opposes the Effects of Calorie Restriction in Pancreatic β Cells. Cell *126*, 941–954.

147. Menon, S., and Manning, B. D. (2009). Common corruption of the mTOR signaling network in human tumors. Oncogene *27*, S43–S51.

148. Durán, R. V., MacKenzie, E. D., Boulahbel, H., Frezza, C., Heiserich, L., Tardito, S., Bussolati, O., Rocha, S., Hall, M. N., and Gottlieb, E. (2012). HIF-independent role of prolyl hydroxylases in the cellular response to amino acids. Oncogene *32*, 4549–4556.

149. Kikuchi, D., Minamishima, Y. A., and Nakayama, K. (2014). Prolyl-hydroxylase PHD3 interacts with pyruvate dehydrogenase (PDH)-E1β and regulates the cellular PDH activity. Biochemical and Biophysical Research Communications *451*, 288–294.

150. Morash, A. J., Kotwica, A. O., and Murray, A. J. (2013). Tissue-specific changes in fatty acid oxidation in hypoxic heart and skeletal muscle. AJP: Regulatory, Integrative and Comparative Physiology *305*, R534–R541.

151. Huang, D., Li, T., Li, X., Zhang, L., Sun, L., He, X., Zhong, X., Jia, D., Song, L., Semenza, G. L., et al. (2014). HIF-1-Mediated Suppression of Acyl-CoA Dehydrogenases and Fatty Acid Oxidation Is Critical for Cancer Progression. Cell Reports *8*, 1930–1942.

152. Huss, J. M., Levy, F. H., and Kelly, D. P. (2001). Hypoxia inhibits the peroxisome proliferator-activated receptor alpha/retinoid X receptor gene regulatory pathway in cardiac myocytes: a mechanism for O2-dependent modulation of mitochondrial fatty acid oxidation. J. Biol. Chem. *276*, 27605–27612.

153. Hamanaka, R. B., and Chandel, N. S. (2009). Mitochondrial reactive oxygen species regulate hypoxic signaling. Current Opinion in Cell Biology *21*, 894–899.

154. Wallace, D. C. (2012). Mitochondria and cancer. Nat Rev Cancer *12*, 685–698.

155. Murphy, M. P. (2009). How mitochondria produce reactive oxygen species. Biochem. J. *417*, 1–13.

156. Gaude, E., and Frezza, C. (2014). Defects in mitochondrial metabolism and cancer. Cancer Metab *2*, 10.

157. Solaini, G., Sgarbi, G., and Baracca, A. (2011). Oxidative phosphorylation in cancer cells. Biochimica et Biophysica Acta (BBA) - Bioenergetics *1807*, 534–542.

158. Vazquez, F., Lim, J.-H., Chim, H., Bhalla, K., Girnun, G., Pierce, K., Clish, C. B., Granter, S. R., Widlund, H. R., Spiegelman, B. M., et al. (2013). PGC1α Expression Defines a Subset of Human Melanoma Tumors with Increased Mitochondrial Capacity and Resistance to Oxidative Stress. Cancer Cell *23*, 287–301.

159. Waris, G., and Ahsan, H. (2006). Reactive oxygen species: role in the development of cancer and various chronic conditions. J Carcinog *5*, 14.

160. Liou, G.-Y., and Storz, P. (2010). Reactive oxygen species in cancer. Free Radic Res *44*, 479–496.

161. Burhans, W. C., and Weinberger, M. (2007). DNA replication stress, genome instability and aging. Nucleic Acids Research *35*, 7545–7556.

162. Sullivan, L. B., and Chandel, N. S. (2014). Mitochondrial reactive oxygen species and cancer. Cancer Metab *2*, 17.

163. Bae, Y. S., Kang, S. W., Seo, M. S., Baines, I. C., Tekle, E., Chock, P. B., and Rhee, S. G. (1997). Epidermal growth factor (EGF)-induced generation of hydrogen peroxide. Role in EGF receptor-mediated tyrosine phosphorylation. J. Biol. Chem. *272*, 217–221.

164. Finkel, T. (2003). Oxidant signals and oxidative stress. Current Opinion in Cell Biology *15*, 247–254.

165. Sundaresan, M., Yu, Z. X., Ferrans, V. J., Irani, K., and Finkel, T. (1995). Requirement for generation of H2O2 for platelet-derived growth factor signal transduction. Science *270*, 296–299.

166. Jeong, S.-Y., and Seol, D.-W. (2008). The role of mitochondria in apoptosis. BMB Rep *41*, 11–22.

167. Kaminskyy, V. O., and Zhivotovsky, B. (2014). Free radicals in cross talk between autophagy and apoptosis. Antioxidants & Redox Signaling *21*, 86–102.

168. DeNicola, G. M., Karreth, F. A., Humpton, T. J., Gopinathan, A., Wei, C., Frese, K., Mangal, D., Yu, K. H., Yeo, C. J., Calhoun, E. S., et al. (2011). Oncogene-induced Nrf2 transcription promotes ROS detoxification and tumorigenesis. Nature *475*, 106–109.

169. Son, J., Lyssiotis, C. A., Ying, H., Wang, X., Hua, S., Ligorio, M., Perera, R. M., Ferrone, C. R., Mullarky, E., Shyh-Chang, N., et al. (2013). Glutamine supports pancreatic cancer growth through a KRAS-regulated metabolic pathway. Nature *496*, 101–105.

170. Glasauer, A., Sena, L. A., Diebold, L. P., Mazar, A. P., and Chandel, N. S. (2013). Targeting SOD1 reduces experimental non–small-cell lung cancer. J. Clin. Invest. *124*, 117–128.

171. Lopert, P., and Patel, M. (2014). Nicotinamide Nucleotide Transhydrogenase (Nnt) Links the Substrate Requirement in Brain Mitochondria for Hydrogen Peroxide Removal to the Thioredoxin/Peroxiredoxin (Trx/Prx) System. Journal of Biological Chemistry *289*, 15611–15620.

172. Birsoy, K., Possemato, R., Lorbeer, F. K., Bayraktar, E. C., Thiru, P., Yucel, B., Wang, T., Chen, W. W., Clish, C. B., and Sabatini, D. M. (2014). Metabolic determinants of cancer cell sensitivity to glucose limitation and biguanides. Nature *508*, 108–112.

173. Iommarini, L., Kurelac, I., Capristo, M., Calvaruso, M. A., Giorgio, V., Bergamini, C., Ghelli, A., Nanni, P., De Giovanni, C., Carelli, V., et al. (2014). Different mtDNA mutations modify tumor progression in dependence of the degree of respiratory complex I impairment. Human Molecular Genetics *23*, 1453–1466.

174. Pollak, M. (2013). Potential applications for biguanides in oncology. J. Clin. Invest. *123*, 3693–3700.

175. Gong, J., Robbins, L. A., Lugea, A., Waldron, R. T., Jeon, C. Y., and Pandol, S. J. (2014). Diabetes, pancreatic cancer, and metformin therapy. Front Physiol *5*, 426.

176. Bowker, S. L., Majumdar, S. R., Veugelers, P., and Johnson, J. A. (2006). Increased cancer-related mortality for patients with type 2 diabetes who use sulfonylureas or insulin. Diabetes Care *29*, 254–258.

177. Ruiter, R., Visser, L. E., van Herk-Sukel, M. P. P., Coebergh, J. W. W., Haak, H. R., Geelhoed-Duijvestijn, P. H., Straus, S. M. J. M., Herings, R. M. C., and Stricker, B. H. C. (2011). Lower Risk of Cancer in Patients on Metformin in Comparison With Those on Sulfonylurea Derivatives: Results from a large population-based follow-up study. Diabetes Care *35*, 119–124.

178. Wheaton, W. W., Weinberg, S. E., Hamanaka, R. B., Soberanes, S., Sullivan, L. B., Anso, E., Glasauer, A., Dufour, E., Mutlu, G. M., Budigner, G. S., et al. (2014). Metformin inhibits mitochondrial complex I of cancer cells to reduce tumorigenesis. Elife *3*, e02242.

179. Rena, G., Pearson, E. R., and Sakamoto, K. (2013). Molecular mechanism of action of metformin: old or new insights? Diabetologia *56*, 1898–1906.

180. Kulkarni, S. R., Donepudi, A. C., Xu, J., Wei, W., Cheng, Q. C., Driscoll, M. V., Johnson, D. A., Johnson, J. A., Li, X., and Slitt, A. L. (2014). Fasting Induces Nuclear Factor E2-Related Factor 2 and ATP-Binding Cassette Transporters viaProtein Kinase A and Sirtuin-1 in Mouse and Human. Antioxidants & Redox Signaling *20*, 15–30.

181. Nemoto, S., Fergusson, M. M., and Finkel, T. (2005). SIRT1 Functionally Interacts with the Metabolic Regulator and Transcriptional Coactivator PGC-1. Journal of Biological Chemistry *280*, 16456–16460.

182. Yu, W., Dittenhafer-Reed, K. E., and Denu, J. M. (2012). SIRT3 Protein Deacetylates Isocitrate Dehydrogenase 2 (IDH2) and Regulates Mitochondrial Redox Status. Journal of Biological Chemistry *287*, 14078–14086.

183. Finley, L. W. S., Haas, W., Desquiret-Dumas, V., Wallace, D. C., Procaccio, V., Gygi, S. P., and Haigis, M. C. (2011). Succinate Dehydrogenase Is a Direct Target of Sirtuin 3 Deacetylase Activity. PLoS ONE *6*, e23295–6.

184. Brenmoehl, J., and Hoeflich, A. (2013). Dual control of mitochondrial biogenesis by sirtuin 1 and sirtuin 3. Mitochondrion *13*, 755–761.

185. Chau, M. D. L., Gao, J., Yang, Q., Wu, Z., and Gromada, J. (2010). Fibroblast growth factor 21 regulates energy metabolism by activating the AMPK-SIRT1-

PGC-1alpha pathway. Proc. Natl. Acad. Sci. U.S.A. *107*, 12553–12558.

186. Zhang, H., Gao, P., Fukuda, R., Kumar, G., Krishnamachary, B., Zeller, K. I., Dang, C. V., and Semenza, G. L. (2007). HIF-1 Inhibits Mitochondrial Biogenesis and Cellular Respiration in VHL-Deficient Renal Cell Carcinoma by Repression of C-MYC Activity. Cancer Cell *11*, 407–420.

187. Fukuda, R., Zhang, H., Kim, J.-W., Shimoda, L., Dang, C. V., and Semenza, G. L. (2007). HIF-1 Regulates Cytochrome Oxidase Subunits to Optimize Efficiency of Respiration in Hypoxic Cells. Cell *129*, 111–122.

188. ElShamy, W. M., and Duhé, R. J. (2013). Overview: Cellular plasticity, cancer stem cells and metastasis. Cancer Letters *341*, 2–8.

189. Wang, F., Travins, J., DeLaBarre, B., Penard-Lacronique, V., Schalm, S., Hansen, E., Straley, K., Kernytsky, A., Liu, W., Gliser, C., et al. (2013). Targeted inhibition of mutant IDH2 in leukemia cells induces cellular differentiation. Science *340*, 622–626.

CHAPTER II

Acetylation proteomics reveal SIRT4 may have broad deacetylase activity in brown adipose tissue

Natalie J. German[1] and Marcia C. Haigis[1]

[1]Department of Cell Biology Harvard Medical School, Boston, MA 02115, USA

Natalie German conceived, designed and performed all experiments with assistance from Cell Signaling Technologies in conducting the AcetylScan.

Abstract

SIRT4 is a mitochondrial member of the sirtuin family of NAD^+-dependent deacylases and ADP-ribosyltransferases. Although originally studied as an ADP-ribosyltransferase, we recently showed SIRT4 acts as a substrate-specific deacetylase of malonyl CoA decarboxylase with dramatic impacts on lipid metabolism, onset of obesity and exercise capacity. This raises the possibility that SIRT4 may possess deacetylase activity toward additional targets. Here we use an immunoaffinity-based label-free quantitative LC-MS/MS approach to identify changes in mitochondrial protein acetylation between wildtype (WT) and SIRT4 knockout (KO) tissues. This study identified 1,259 unique acetylated peptides in brown adipose tissue (BAT) and liver of WT and KO mice. In the absence of SIRT4, lysine acetylation was significantly increased by at least 1.5-fold in 94 proteins in BAT and 25 proteins in liver. A number of enzymes that coordinate the TCA cycle, fatty acid metabolism, the electron transport chain and the mitochondrial proton gradient are hyperacetylated in SIRT4 KO tissues. We show one candidate substrate, pyruvate carboxylase (PC), interacts with SIRT4 and displays elevated acetylation and activity in SIRT4 KO tissues. PC is a mitochondrial biotin-dependent enzyme that catalyzes conversion of pyruvate to oxaloacetate. Through this reaction, PC serves to replenish the TCA cycle, which has been linked to maintaining anaplerosis in cancer as well as driving gluconeogenesis in liver and lipogenesis in adipose. Altered post-translational modification of PC and other mitochondrial proteins potentially targeted by SIRT4 supports the role of SIRT4 as a substrate-specific deacetylase capable of fine-tuning cell metabolism.

Introduction

The sirtuin family of NAD^+-dependent deacylases and ADP-ribosyltransferases are master regulators of metabolism in response to nutrient or redox stresses[1]. The seven mammalian sirtuins share a conserved catalytic core domain, but have differences in localization, substrate preference and the range of enzymatic activities they possess[2, 3]. Lysine deacetylation is the most common activity of sirtuins, in line with the finding that acetylation is an incredibly abundant post-translational modification in the cell[4]. Hundreds of mitochondrial proteins are acetylated, including enzymes from all major metabolic pathways such as the TCA cycle, oxidative phosphorylation, amino acid metabolism and fatty acid oxidation[5]. Modulation of acetylation status is recognized as a major regulator of mitochondrial protein activity and metabolism[6]. As deacetylases, sirtuins contribute to a reversible mode of regulation for potentially numerous proteins.

The mitochondrial sirtuin SIRT4 has been implicated in the regulation of glutaminolysis, lipid metabolism and the DNA damage response[7]. SIRT4 also has tumor suppressor functions at least in part through limiting glutamine utilization[8]. Despite the striking phenotypes of SIRT4 KO mice, the enzymatic activity of SIRT4 is not completely understood. SIRT4 does not demonstrate broad or robust in vitro deacetylase activity on known substrates of other sirtuins and instead was first shown to act as a mono-ADP-ribosyltransferase[9]. However, we recently showed SIRT4 does indeed possess substrate-specific deacetylase activity toward malonyl coA decarboxylase (MCD), a major coordinator of lipid homeostasis[10]. Likewise, a peptide screen of all 7 sirtuins by Rauh et al found recombinant SIRT4, but not the catalytically inactive H161Y SIRT4 point mutant, has NAD^+-dependent deacetylase activity toward select peptides in

vitro[11]. These findings suggest other substrates of SIRT4 activity remain to be discovered.

Here, we examined SIRT4-dependent changes in protein acetylation to cast light on potential novel substrates and functions of SIRT4. We took a global approach by assessing SIRT4-dependent acetylation changes in BAT and liver mitochondria from WT and SIRT4 KO mice. We used a robust immunoaffinity method to enrich mitochondrial acetylated peptides for analysis by LC-MS/MS. We show that a number of enzymes with roles in metabolism and bioenergetics are hyperacetylated in the absence of SIRT4, pointing to new biologies that may be coordinated by substrate-specific SIRT4 deacetylase activity.

Results

SIRT4 loss alters the mitochondrial acetylome

In order to identify mitochondrial proteins that are differentially acetylated in response to SIRT4, we performed a large-scale acetylation proteomics survey developed by Cell Signaling Technology called an AcetylScan (Figure 2.1 a)[12]. Mitochondria were extracted from BAT and liver of ad-libitum fed 6-month-old C57BL/6 female WT and SIRT4 KO mouse (n=2). These tissues were of particular interest due to their vital roles in regulating the organismal metabolic state. Next, mitochondrial extracts were normalized by protein content, trypsin-digested, immunoprecipitated with anti-acetyllysine antibody loaded on resin, and subjected to LC-MS/MS analysis on an LTQ-Orbitrap mass spectrometer. Levels of acetylated peptides were normalized by median-centering. This method identified 1,259 unique acetylated peptides across all samples.

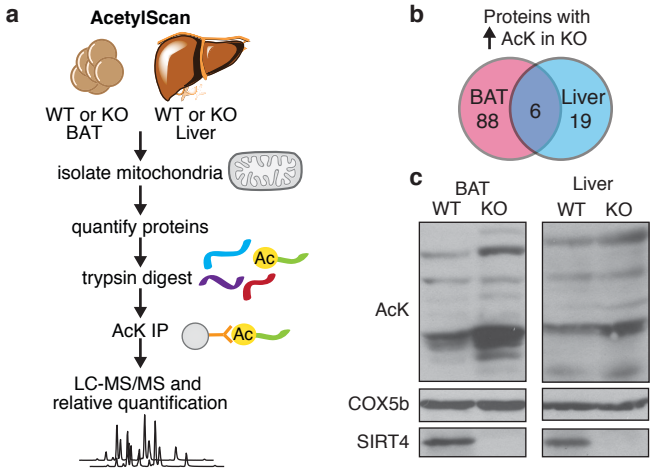

d

Name	Description	BAT AcK site	BAT Fold change	BAT pvalue	Liver AcK site	Liver Fold change	Liver pvalue
TCA cycle and anaplerosis							
DLST	dihydrolipoamide S-succinyltransferase	268, 274	2.77	0.043	268, 273	2.17	0.008
		268, 273	2.38	0.002			
		227	2.10	<0.001			
		273	2.09	0.001			
Lipid metabolism							
HADHA	mitochondrial trifunctional protein α	406, 411	5.49	0.002	460	1.95	0.028
		457	2.47	0.002			
		129	2.17	<0.001			
		516	2.02	0.002			
		759	1.96	0.002			
		249	1.71	0.016			
		303	1.66	0.001			
HADHSC	L-3-hydroxyacyl-Co A dehydrogenase	185	1.83	0.006	206	1.56	<0.001
		206	1.79	0.011			
Chaperone							
HSP60	heat shock protein 1 (chaperonin)	387	1.54	0.010	369	1.78	0.010
Waste and ROS clearance							
TXNRD2	thioredoxin reductase 2 precursor	153	1.83	0.004	153	1.52	0.014
Other small molecule metabolism							
BPHL	biphenyl hydrolase-like (serine hydrolase)	126	1.91	0.041	126	1.82	0.041

Figure 2.1 | AcetylScan to identify differentially acetylated proteins in SIRT4 WT and KO BAT and liver. a, An acetylation proteomics study (AcetylScan) was performed to identify and quantify site-specific changes in mitochondrial protein acetylation with SIRT4 loss. Mitochondria were extracted from fresh SIRT4 WT and KO BAT or liver (n=2). Following protein quantification and normalization, lysates were fragmented by trypsin digest and the peptides were subjected to immunoprecipitation by resin-bound acetyl-lysine (AcK) antibody. Immunopurified peptides were analyzed by LC-MS/MS, and relative quantification of site-specific acetylation was determined. **b,** Venn diagram depicting the number of proteins with at least one AcK site signficantly (p-value < 0.05) increased in SIRT4 KO BAT (magenta), liver (blue) or both compared to WT. The median-centered fold change cut-off was set at 1.5-fold increase. **c,** Differential mitochondrial acetylation as assessed by Western blot. Mitochondria were extracted from snap frozen WT and SIRT4 KO liver or BAT and lysed in NP40 buffer containing the deacetylase inhibitors nicotinamide and trichostatin A. Equal quantities of mitochondrial lysate were analyzed to assess global acetylated lysine changes. **d,** Table of the proteins found to be hyperacetylated in both SIRT4 KO BAT and liver. Fold change is the normalized, median-centered fold change over WT.

To assess the tissue specificity of SIRT4-directed differential acetylation, we compared the acetylation profiles of BAT and liver. The AcetylScan revealed 94 proteins were significantly hyperacetylated by at least 1.5-fold in SIRT4 KO BAT, compared to 25 proteins in SIRT4 KO liver (Figure 2.1 b). Only 6 proteins were shown by the AcetylScan to be hyperacetylated in both tissues of SIRT4 KO mice, suggesting substantial tissue-dependent differences in SIRT4 activity. The 6 proteins with increased acetylation of at least one lysine residue in both SIRT4 KO BAT and liver include DLST, a component of the TCA cycle enzyme α-ketoglutarate dehydrogenase, as well as HADHA and HADHSC, enzymes required for oxidation of long chain and short chain fatty acids, respectively (Figure 2.1 d). Sequences and data on all significantly altered acetylated peptides can be found in Supplemental Tables 2.1 and 2.2.

To test the finding that SIRT4 loss is linked to particularly strong hyperacetylation in BAT compared to liver, we examined mitochondrial acetylation in these tissues by Western blot. Similar to previous reports, global levels of mitochondrial acetylation in liver were similar between WT and SIRT4 KO lysates[13]. Strikingly, Western blot analysis of mitochondrial lysates from WT and SIRT4 KO BAT demonstrated increased acetylation in SIRT4 KO BAT (Figure 2.1 c). Of note, nearly all hyperacetylated proteins elucidated by this strategy were found to have another acetyllysine site with relatively unchanged levels (a non-significant, less than 1.5 fold difference) in SIRT4 KO tissues, suggesting altered post-translational modification rather than upregulated translation is the reason for differential acetylation.

Pathway analysis of hyperacetylated proteins in SIRT4 KO BAT point to TCA cycle regulation

To gain insight to the functional significance of hyperacetylation upon SIRT4 loss in BAT, we analyzed the AcetylScan results to assess whether the hyperacetylated proteins shared related functions. Rather than representing a broad range of mitochondrial programs, the hyperacetylated proteins were predominantly members of mitochondrial metabolic pathways (Figure 2.2 a). The majority of the hyperacetylated proteins were enzymes in the TCA cycle and anaplerosis, lipid metabolism, the electron transport chain (ETC) and mitochondrial proton gradient and, finally, amino acid metabolism. Supporting this observation, the individual peptides with the greatest increase in acetylation in SIRT4 KO BAT were from proteins in many of these pathways (Figure 2.2 b).

Alterations in lipid metabolism and amino acid metabolism enzymes are in line with previous reports showing SIRT4 limits fatty acid oxidation and glutaminolysis. However, the TCA cycle and anaplerosis stood out for representing the greatest portion of hyperacetylated peptides as well as for being little explored in terms of SIRT4 regulation. 17 enzymes involved in the TCA cycle and anaplerosis were hyperacetylated on at least one site in SIRT4 KO BAT (Figure 2.2 c). Of note, only three of these sites (ACO2 K138, CS K393 and DLST K373) were also differentially acetylated in a similar acetylomics analysis comparing SIRT3 WT and KO tissues[14]. This suggests the acetylated residues found in our study may be specific to SIRT4 and not mitochondrial sirtuins in general.

Pyruvate carboxylase interacts with SIRT4 and is hyperacetylated in SIRT4 KO tissues

The acetylation proteomics suggest SIRT4 may directly bind and alter the acetylation status of candidate proteins in the TCA cycle and other metabolic pathways.

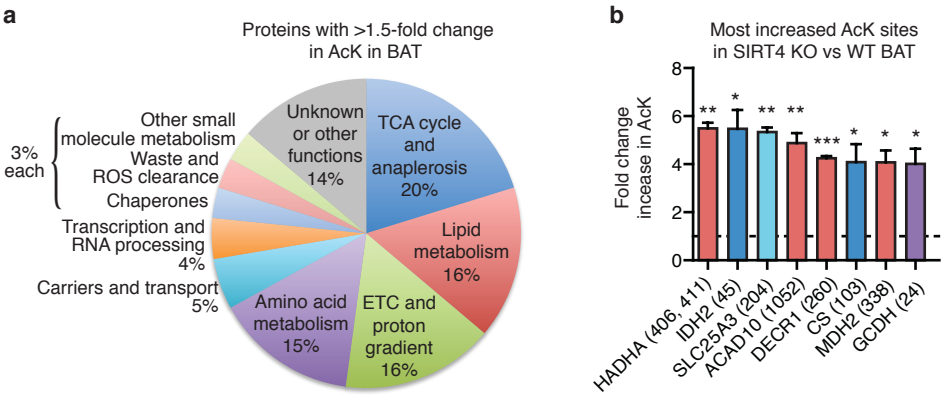

c

TCA cycle and anaplerosis enzymes with increased AcK in KO BAT

Name	Description	# of sites with increased AcK
ACO2	aconitase 2, mitochondrial	9
ACSS1	acyl-CoA synthetase short-chain family member 1	1
ACSS3	acyl-CoA synthetase short-chain family member 3	1
CS	citrate synthase	2
DLAT	dihydrolipoamide S-acetyltransferase	1
DLD	dihydrolipoamide dehydrogenase	3
DLST	dihydrolipoamide S-succinyltransferase	4
FH	fumarate hydratase 1	1
IDH2	isocitrate dehydrogenase 2 (NADP+), mitochondrial	2
IDH3A	isocitrate dehydrogenase 3 (NAD+) alpha	1
IDH3B	isocitrate dehydrogenase 3, beta subunit	1
IDH3G	isocitrate dehydrogenase 3 (NAD+), gamma	1
MDH2	malate dehydrogenase 2, NAD (mitochondrial)	4
PC	pyruvate carboxylase	2
PDHA1	pyruvate dehydrogenase E1 alpha 1	4
SCS-beta	succinate-CoA ligase, ADP-forming, beta subunit	1
SDHA	succinate dehydrogenase Fp subunit	3

Figure 2.2 | Top proteins and pathways with increased lysine acetylation in SIRT4 KO BAT. a, Pie chart depicting the pathways represented by the 94 mitochondrial proteins with significantly increased lysine acetylation in SIRT4 KO versus WT BAT. Enzymes involved in the TCA cycle and anaplerosis represent the greatest portion. **b,** AcK sites with the greatest increase in SIRT4 KO BAT, based on the median-centered normalized fold change values. The acetylated residue is listed in parenthesis. **c,** TCA cycle and anaplerosis enzymes with significantly increased lysine acetylation of at least one site in SIRT4 KO BAT. *$p < 0.05$, **$p < 0.01$, *** $p < 0.001$. Error bars indicate SEM.

To prioritize identification of potential substrates, we took an unbiased approach to assess SIRT4 interacting proteins using immunoprecipitation and mass spectrometry. Stably overexpressed HA-tagged SIRT4 or mitochondrial HA-tagged DsRed control protein was immunoprecipitated from HEK-293T cells. Co-immunoprecipitated proteins were resolved by SDS-PAGE, Coomassie stained, and analyzed by mass spectrometry. This led to the identification of pyruvate carboxylase (PC) as a top mitochondrial protein that interacted specifically with SIRT4 but not DsRed control protein (Figure 2.3 a). Moreover, SIRT4 KO BAT lysates demonstrated elevated PC acetylation in the AcetylScan, leading us to examine the regulation of PC by SIRT4 (Supplemental Table 2.1).

PC is a biotin-containing mitochondrial enzyme that catalyzes the conversion of pyruvate and bicarbonate to oxaloacetate[15]. PC provides one way to replenish the TCA cycle when intermediates have been shunted away for macromolecule synthesis or when deficiencies in metabolic enzymes lead to incomplete TCA cycling[16]. By providing oxaloacetate, PC in liver also catalyzes the first committed step of gluconeogenesis[17]. In brown and white adipose, PC provides oxaloacetate for lipogenesis and to promote pyruvate-cycling. Cycling of pyruvate and its TCA cycle derivatives, including oxaloacetate, malate, and citrate, between the mitochondria and cytoplasm produces cytosolic NADPH, a co-factor important in biosynthetic reactions and antioxidant defense programs[18]. Thus, SIRT4 regulation of PC has the potential to coordinate a number of metabolic programs.

To examine the interaction between SIRT4 and PC, we first validated binding by immunoprecipitating transiently overexpressed Flag-SIRT4, Flag-SIRT5 or empty vector

a **SIRT4 interacting proteins**

Protein name	Description	Unique peptides	Differential AcK in T4-KO, p< 0.05
HSP60	heat shock 60kDa protein 1 (chaperonin)	15	yes, BAT and liver
PC	pyruvate carboxylase	7	yes, BAT
SLC27A2	solute carrier family 27 (fatty acid transporter), member 2	3	yes, liver
GTF2i	general transcription factor IIi	22	no
HNRNPU	heterogenous nuclear ribonuclear protein U	7	no
TUBA4A	tubulin, alpha 4	3	no
UBC	ubiquitin C	3	no

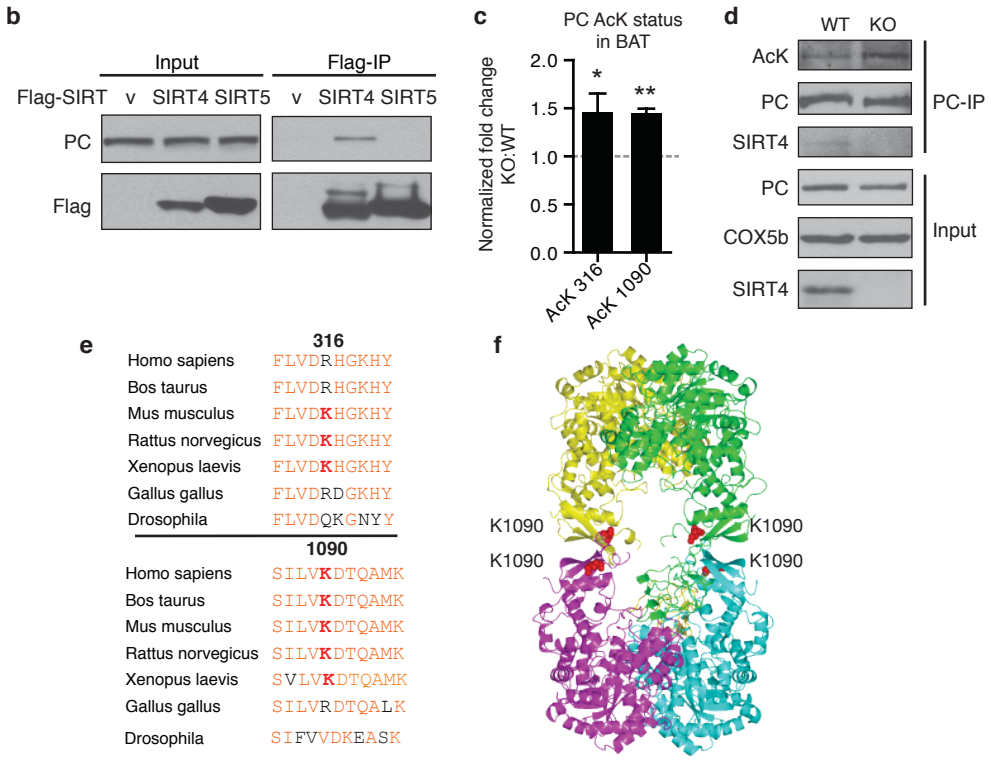

Figure 2.3 | Pyruvate carboxylase interacts with SIRT4 and is hyperacetlated in SIRT4 KO BAT. a, SIRT4 interacting proteins identified by LC-MS/MS following co-immunoprecipitation with HA-SIRT4 but not HA-DsRed control protein in 293T cell lysates. A portion of the interacting proteins, including PC, show >1.5-fold significantly increased acetylation ($p < 0.05$) of at least one lysine residue in the AcetylScan. **b,** PC interacts with SIRT4. Flag-tagged SIRT4, SIRT5 or empty vector was transiently overexpressed in 293T cells. Following immunoprecipitation with anti-Flag resin, the interaction between SIRT4 and PC was detected by Western blot. **c**, PC is hyper-acetylated at K316 and K1090 in SIRT4 KO BAT, as assessed by the AcetylScan. **d,** PC interacts with endogenous SIRT4 and is hyper-acetylated in SIRT4 KO BAT. Mitochondria were extracted from WT and SIRT4 KO BAT, then lysed in NP40 buffer. PC was immunoprecipitated and analyzed by SDS-PAGE and Western blot with a pan acetyl-lysine antibody. **e,** Conservation of K1090 and K316 in PC. K316 is conserved in mouse, rat and frog but not in human. K1090 is conserved in the PC tetramerization domain in several vertebrate species, and the residue may be conserved but shifted in drosophila. K1090 and K316 are highlighted in red. Other conserved residues are in orange. **f,** Molecular modeling to evaluate the location of K1090 (red) in the tetrameric interface of human PC (PDB: 3BG3). PC monomers are in yellow, green, cyan and magenta. *$p < 0.05$, **$p < 0.01$. Error bars indicate SEM.

from 293T cells and blotting for endogenous PC (Figure 2.3 b). Here, PC interacted specifically with SIRT4. The AcetylScan showed two PC residues were hyperacetylated in SIRT4 KO BAT: K316 and K1090 (Figure 2.3 c). We confirmed the change in acetylation by immunoprecipitating PC from WT and SIRT4 KO BAT and immunoblotting with a pan-acetyllysine antibody (Figure 2.3 d). This analysis also demonstrated that SIRT4 co-immunoprecipitates with PC in WT tissue, confirming the endogenous interaction between these proteins.

We next assessed conservation of the PC acetyllysine residues to gain insight into the relevance of these sites (Figure 2.3 e). K316, located in the ATP-grasp region of PC, is present in mouse, rat and frog, but is not conserved in human or other vertebrates. Residue K316 residue was previously shown to be acetylated in fasted mice[19]. Interestingly, K316 in mouse is changed to arginine in human, which mimics a constitutively deacetylated lysine. K1090 is located in the PC tetramerization domain and conserved in multiple vertebrate species from human to frog. To gain mechanistic insight into how acetylation status of K1090 could modulate human PC, we mapped this site in the published human PC crystal structure (PDB: 3BG3) (Figure 2.3 f)[20]. Its position in the interface between PC monomers suggests it may play a role in formation of the functional PC homotetramer. Therefore, SIRT4-mediated coordination of PC K1090 acetylation status might have strong functional significance.

SIRT4-mediated regulation of PC activity

To evaluate the link between SIRT4 and PC activity, we performed an in vitro PC activity assay based on the production of ^{14}C-oxaloacetate from ^{14}C-bicarbonate (Figure 2.4 a). In preliminary studies, PC activity trends toward being increased in SIRT4 KO

Figure 2.4 | SIRT4 inhibits PC activity in mouse tissues. a-b, PC activity trends towards an increase in SIRT4 KO BAT as measured in a radioactivity-based carbon fixation assay with 50 μg mitochondrial extracts. Western blot shows SIRT4 KO, PC levels and the Complex III Rieske subunit loading control. n=2 experimental replicates. **b,** Schematic of the spectrophotometric citrate synthase-coupled PC activity assay performed with mouse liver mitochondrial lysates. PC converts contain uses ATP and bicarbonate to convert pyruvate to oxaloacetate. Exogenous citrate synthase uses acetyl-CoA in the reaciton mix to convert oxaloacetate to citrate. Free CoA is released in the process. 5,5'-dithiobis-(2-nitrobenzoic acid) (DTNB) reacts with the thiol group of free CoA and generates TNB^{2-}, a yellow product quantified by absorbance at A= 412nm. **c,** Optimization of the citrate synthase-coupled PC activity assay. Bovine PC (Sigma) was spiked into cuvettes containing the reaction components plus vehicle or the PC inhibitors avidin or phenylacetic acid. An additional sample was measured without pyruvate. Activity was monitored by measuring the absorbance at A= 412nm every 15 s for 9 minutes. **d,** Initial rate of PC activity based on the data shown in **(c)**. **e,** PC activity is increased in SIRT4 KO liver mitochondrial extracts. Western blot shows SIRT4 KO, PC levels and Hsp60 loading control. n=3 biological replicates, each measured in triplicate. **f,** Sites K319, K434 and K1061 in PC trend toward increased acetylation in SIRT4 KO liver, as assessed by the AcetylScan. **g,** Endogenous SIRT4 co-immunoprecipitates with endogenous PC that was affinity purified from WT mouse liver using PC-antibody and IgG resin. ***$p < 0.001$. Error bars indicate SEM.

Figure 2.4 (Continued).

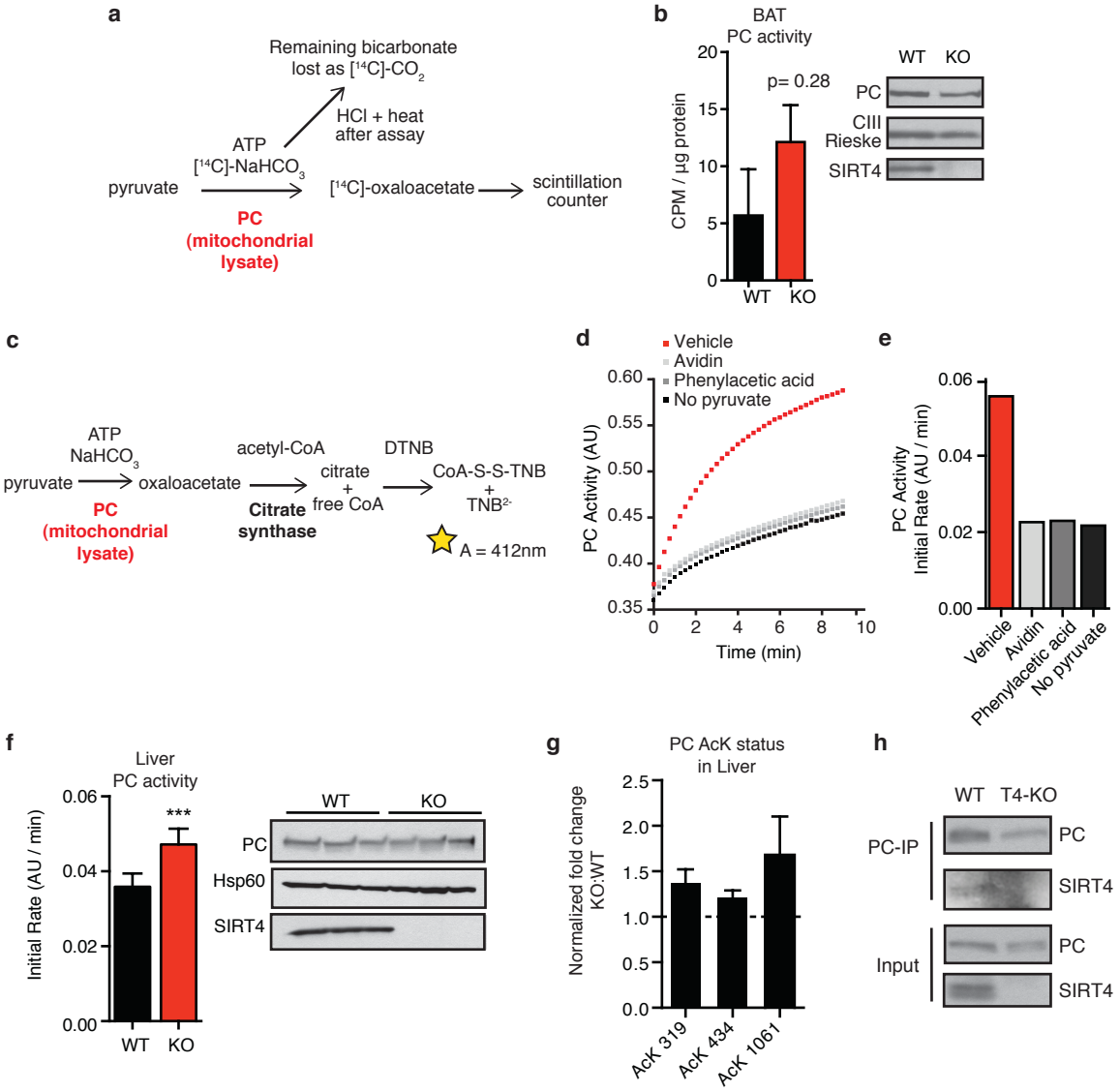

BAT mitochondrial lysates (Figure 2.4 b). Alternatively, we assessed PC activity using a citrate-synthase coupled, absorbance-based enzymatic assay in liver (Figure 2.4 c). The high abundance of PC in liver makes this assay possible, rather than requiring a radioactivity-based method. The citrate synthase-coupled assay was optimized using commercially available bovine PC in the presence or absence of the PC inhibitors avidin and phenylacetic acid as well as in the absence of the substrate pyruvate (Figure 2.4 d-e). In SIRT4 KO liver, we observed a significant increase in PC activity (Figure 2.4 f), suggesting a model in which SIRT4-mediated deacetylation of PC represses PC activity. Of note, three PC lysine residues trend toward being hyperacetylated in SIRT4 KO liver, specifically K319 in the ATP-grasp region, K434 in the biotin carboxylation domain and K1061 in the PC tetramerization domain (Figure 2.4 g). To test the possibility that SIRT4 directly binds and represses SIRT4 in liver, we performed immunoprecipitation of PC from WT and SIRT4 KO liver and Western blotted for endogenous SIRT4. PC interacted with SIRT4 in WT liver (Figure 2.4 h), suggesting SIRT4 could indeed directly modulate PC.

Through inhibition of PC, SIRT4 might be expected to limit PC-mediated anaplerotic flux. To assess the role of SIRT4 in regulating flux through PC, we performed U-^{13}C-labeled glucose metabolic flux analyses on transformed WT and SIRT4 KO MEFs. 24 h after incubation with labeled glucose, metabolites were extracted, and we assessed the abundance of 3-carbon labeled citrate (generated from flux through PC) as well as 5-carbon labeled citrate (generated from flux through both PC and PDH)[21] (Figure 2.5). A small but significant increase was observed in 5-carbon labeled citrate in KO MEFs, indicating activity of PC, PDH or both is increased. However, the low levels of +3 and +5

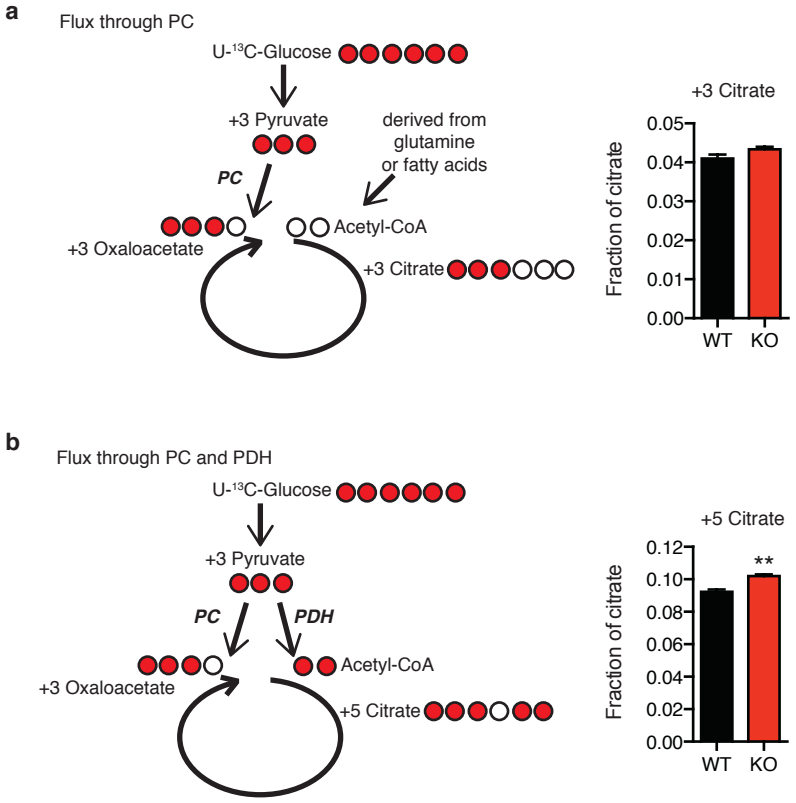

Figure 2.5 | Anaplerotic flux through PC in WT and SIRT4 KO MEFs. a-b, U-^{13}C-labeled glucose metabolic flux analysis on transformed WT and SIRT4 KO MEFs. 24 h after incubation with labeled glucose, metabolites were extracted, analyzed by mass spectrometry and normalized to cell number in parallel plates. 3-carbon labeled citrate indicates flux of glucose-derived pyruvate through PC **(a)**. 5-carbon labeled citrate indicates flux through both PC and PDH. Data are presented as a fraction of total citrate **(b)** (n = 3). **p < 0.01. Error bars indicate SEM.

citrate are consistent with PC activity not playing a major role in anaplerosis in these MEFs. Therefore, we moved to a more suitable cell model to assess the effect of SIRT4 on PC activity.

To examine the role of SIRT4 on PC in a relevant cell model, we used the Huh7 hepatocellular carcinoma cell line, which were reported to display high PC-mediated anaplerosis[22]. The dependency on PC rather than glutaminolysis for anaplerosis enables these cells to grow normally even in the absence of glutamine (Figure 2.6 a), whereas cells with low PC anaplerosis such as 293T experience growth inhibition upon glutamine withdrawal (Figure 2.6 b). In Huh7 cells, preliminary PC activity assay results show transient SIRT4 overexpression induces a trend toward decreased PC activity (Figure 2.6 c). Reduced PC function is known to boost pyruvate and lactate levels[16]. Because SIRT4 inhibits PC, we predicted overexpression of SIRT4 would block PC-mediated anaplerosis and shunt pyruvate toward lactate (Figure 2.6 d). Fitting with this hypothesis, we found overexpression of SIRT4, but not the catalytically inactive mutant H161Y, increased lactate production in Huh7 cells (Figure 2.6 e). The change in lactate was not accompanied by increased glucose uptake (Figure 2.6 f), indicating the increased lactate production was indeed due to altered pyruvate flux rather than altered glucose metabolism as a whole. Together, these data suggest SIRT4 inhibits PC-flux and potentially serves as a central gatekeeper of pyruvate anaplerosis.

To assess the potential impact of PC repression on whole body metabolism, we performed pyruvate tolerance tests (PTT) on WT and SIRT4 KO mice. PTT measures the production of glucose following intraperitoneal injection of pyruvate in fasted mice. Because this process requires PC flux[17], we hypothesized hyperactive PC in SIRT4 KO

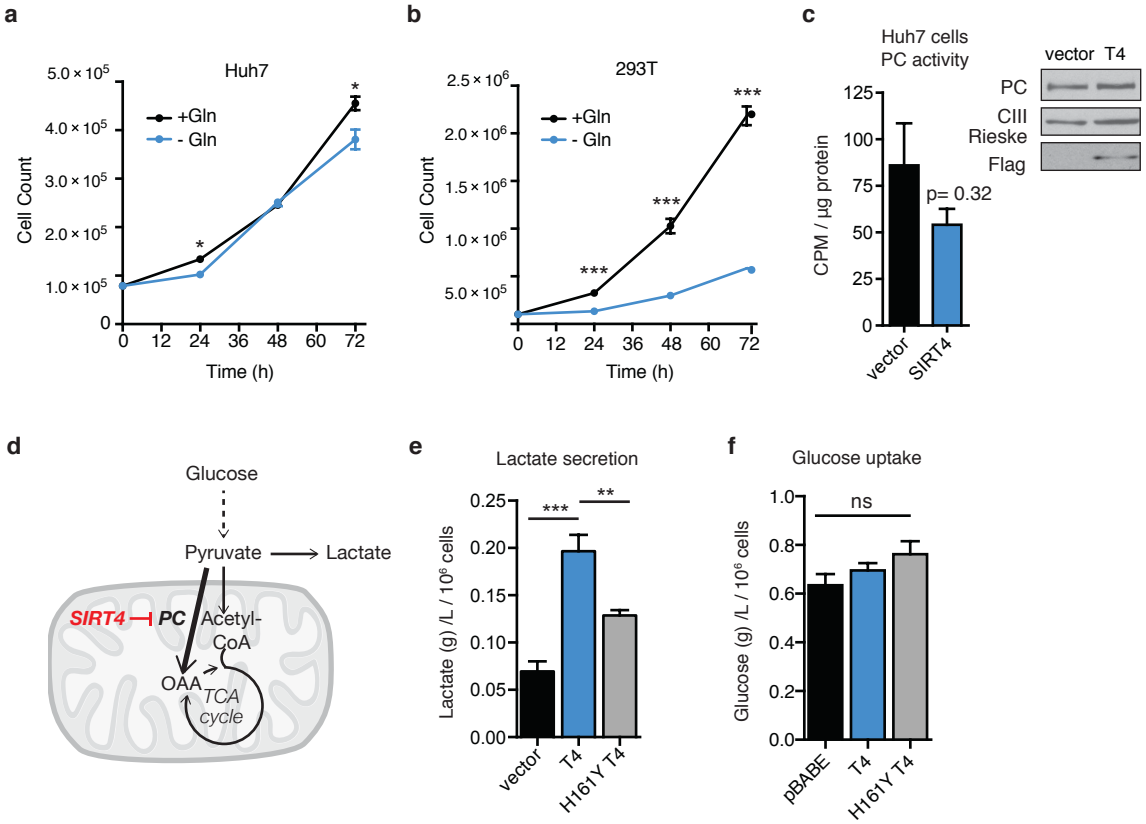

Figure 2.6 | SIRT4 regulates metabolic outputs in the PC-dependent Huh7 cell line. **a,** Growth curves of Huh7 cells in media +/- glutamine for 72 h, demonstrating the glutamine-independence of this cell line. **b,** Growth curves of 293T cells in media +/- glutamine for 72 h, demonstrating the high reliance on glutamine of this cell line. **c,** PC activity trends toward a decrease in Huh7 cells transiently overexpressing Flag-SIRT4. 30 µg mitochondrial extracts were used in the radioactivity-based PC assay. Western blot shows Flag-SIRT4, PC and the Complex III Rieske subunit loading control. n=2. **d,** Model of the effect of SIRT4 on PC. SIRT4 inhibits PC, possibly repressing anaplerosis and shunting pyruvate toward lactate. **e-f,** Lactate production **(e)** and glucose uptake **(f)** in Huh7 cells stably overexpressing vector, SIRT4 or catalytic mutant H161Y SIRT4. Prior to the assay, cells were split to a 6 well plate, n=5. The next morning, cells were placed in fresh media lacking glutamine. After 6 hr, the media was collected, and glucose and lactate were measured on the Nova flux analyzer. Values were normalized to cell count. *$p < 0.05$, ** $p < 0.01$, ***$p < 0.001$. Error bars indicate SEM.

mice would boost the gluconeogenic output. Upon pyruvate injection, SIRT4 KO mice reach higher blood glucose levels than WT (Figure S2.1 a-b). Blood glucose was particularly high in SIRT4 KO female mice (Figure S2.1 a). Because hyperglycemia following pyruvate injection could also result from alteration of other gluconeogenic enzymes or reduced insulin sensitivity, we cannot rule out the possibility that the PTT results are due to a defect unrelated to PC. Of note, however, WT and SIRT4 KO mice on a normal chow diet show no difference in glucose tolerance tests or insulin tolerance tests (data not shown), supporting the hypothesis that this alteration is specific to gluconeogenesis and not a defect in tissue glucose uptake.

Discussion

Contrary to previous reports that SIRT4 is a weak deacetylase, our data suggest SIRT4 is a biologically relevant, tissue-specific deacetylase with major impacts on cellular metabolism and bioenergetics. The finding that SIRT4 extensively modulates acetylation in BAT, combined with our previous report that SIRT4 deacetylates MCD in white adipose tissue, points to the presence of a molecular component in adipose that is key to SIRT4 activation. It is possible that the high lipid content in adipose boosts SIRT4 activity, similar to the way in which fatty acids boost SIRT6 activity in vitro. Alternatively, as a sensor of nutrient overload and DNA damage, SIRT4 deacetylase activity may be instigated by a stress condition that is generally more prevalent in adipose than other tissues.

Future studies are needed to validate and explore the biological relevance of the multiple acetylated proteins modulated by SIRT4. Additionally, the role of SIRT4 in liver should not be entirely discounted. Although SIRT4 activity appears be greater in BAT,

we detected site-specific hyperacetylation in SIRT4 KO liver, particularly in proteins regulating the electron transport chain and lipid metabolism (Figure S2.2 a). We observed a particularly striking increase in acetylation of nicotinamide nucleotide transhydrogenase (NNT) (Figure S2.2 b), in line with a published peptide library screen showing recombinant SIRT4 deacetylates an NNT peptide in an NAD^+-dependent manner[11]. Strikingly, we find NNT is hyperacetylated over 150-fold at residue K70 and 7-fold at K433 in SIRT4 KO liver (Figure S2.2 c). These residues are well conserved across species (Figure S2.2 d) and located in the mitochondrial matrix domain of NNT[23], suggesting accessibility to SIRT4. NNT is an inner-mitochondrial membrane bound protein that transfers reducing equivalents from NADH to $NADP^+$, generating NAD^+ and NADPH (Figure S2.2 e)[24-26]. Thus, by coordinating NNT and cofactor balance, SIRT4 has potential to direct the redox status and metabolic state of the cell.

The finding that SIRT4 interacts with and represses PC supports a developing theme in sirtuin research that the major function of SIRT4 is to limit mitochondrial oxidative metabolism. While most sirtuins promote oxidative metabolism under low nutrient conditions, SIRT4 is emerging as a counterbalance that limits oxidative metabolism in the presence of adequate nutrients by repressing glutaminolysis, fatty acid oxidation and PDH, as was shown very recently[27]. We now add PC to this model. Future studies are needed to determine the scope of the SIRT4/PC regulatory axis in both physiological and pathological state. Loss of SIRT4 and upregulation of PC might be expected to contribute to pathogenesis of a diabetic state in patients. Furthermore, SIRT4 loss in cancer may promote flux through PC and may be particularly advantageous to cancers that rely on this route for anaplerosis. To understand the role of SIRT4 in cancer,

it will be important for future studies to assess metabolic flux and cancer viability in PC-dependent cancer models upon modulation of SIRT4. In sum, our work uncovers multiple potential metabolic substrates of SIRT4 deacetylase activity and suggests many new biologies that may be impacted by this sirtuin.

Acknowledgements

We thank Alexandra Bause for technical assistance with mouse studies. We thank Priscilla Yang at Harvard Medical School for Huh7 cells. We thank Jeffrey Silva and Cell Signaling Technology for assistance with the AcetylScan. We thank Sarah-Maria Fendt at MIT for assistance with metabolic flux experiments. We thank Jason Locasale, formally at Harvard Medical School, for helpful discussions and suggestions.

Materials and methods

Mice. Female 22-26 week-old C57BL/6 WT and SIRT4 KO mice that were fed ad-libitum were used for the AcetylScan and all other experiments, except those assessing the role of PC in BAT. For these studies the 129 mouse strain was more readily available. All animal experiments were performed in accordance with institutional guidelines.

AcetylScan and statistical analysis. Acetylation proteomics were performed as previously described using the platform developed by Cell Signaling Technology[12, 28]. Liver and BAT from WT and SIRT4 KO mice were analyzed (n=2). Label-free quantification was done by comparing peak intensities of the same peptide ion in each sample. Raw values from the mass spectrometry were used to calculate significance ($p < 0.05$, using n=2). Non-mitochondrial proteins were manually filtered and excluded from the dataset. Fold changes in lysine acetylation were calculated from the median-centered normalized data.

Crude mitochondrial extraction. Mitochondria were isolated from mouse tissue using differential centrifugation. Briefly, mice were euthanized by cervical dislocation. Liver and BAT were dissected and immediately frozen in liquid nitrogen. For mitochondrial extraction, tissues were homogenized in ice-cold mitochondrial isolation buffer (225 mM mannitol, 75 mM sucrose, 10 mM MOPS, 1 mM EGTA, 0.5% BSA, pH 7.2) containing protease and phosphatase inhibitors as well as 1 mM DTT, 10 mM nicotinamide and 400 nM trichostatin A. Homogenates were centrifuged 10 min at 1,000 x g. Mitochondria were in the supernatant. A second extraction and centrifugation were performed. The supernatants were combined and spun 10 min at 1,000 x g. Finally the supernatant was centrifuged 15 min at 8,000 x g to pellet the mitochondria.

Reagents and constructs. For transient overexpression studies, Fugene 6 (Roche) was used to transfect 293T cells. Huh7 cells were transfected with X-tremeGENE HP (Roche). pCMV empty vector and constructs containing Flag-SIRT4, Flag-SIRT4 H161Y and Flag-SIRT5 were previously described[9].

Cell culture. 293T cells were cultured in 4.5 g/L glucose DMEM containing pyruvate (Invitrogen) supplemented with 10% FBS and penicillin/streptomycin. Huh7 cells were cultured in 4.5 g/L glucose DMEM without pyruvate (Invitrogen) supplemented with 10% FBS and penicillin/streptomycin. MEFs were isolated from WT and SIRT4 KO littermate embryos and transformed as previously described[8] MEFs were cultured in 4.5 g/L DMEM containing supplemented with 10% FBS, b-mercaptoethanol and penicillin/streptomycin.

Immunoprecipitation, western blotting and antibodies. Cells or tissue mitochondrial extracts were lysed in 1% NP40 buffer (150 mM NaCl, 50 mM Tris, pH 8.0) containing

10 mM nicotinamide, 400 nM trichostatin A and protease inhibitor cocktail (Roche), except for Western blots of PC activity assays in which cells were lysed in the activity assay buffer. Protein concentrations were assessed by BCA assay (Pierce) and equal quantities were loaded on a 4-15% Criterion Tris-HCl gel for electrophoresis. Proteins were transferred to nitrocellulose membrane for immunoblotting. Western blotting was performed using antibodies against Flag-M2 (Sigma no. F-3165), PC (Santa Cruz no. sc-271493), Cox5b (MitoSciences no. MS503), acetyl-lysine (CST no. 9441), CIII Rieske (MitoSciences no. MS305) and Hsp60 (Abcam no. ab3080-500). For immunoprecipitations of transiently overexpressed HA- or Flag-tagged proteins, lysates were immunoprecipitated using EZview anti-HA Affinity Gel (Sigma no. E6779) or EZview anti-Flag M2 Affinity Gel (Sigma no. F2426). For endogenous immunoprecipitations, lysates were immunoprecipitated with PC antibody (Santa Cruz no. sc-271493).

Immunoprecipitation and mass spectrometry to identify SIRT4 interactors. To identify SIRT4 interacting proteins, HA-SIRT4 or HA-DsRed control protein was stably overexpressed in 293T cells. Cell lysates were collected and immunoprecipitated with anti-HA EzView resin. Bound material was washed twice in a high salt wash containing 300 mM NaCl, followed by two washes at 150 mM NaCl. Immunoprecipitated material was separated by SDS-PAGE. The Coomassie stained band was excised, analyzed by LC-MS2 and searched against the Uniprot Human database.

^{13}C glucose flux tracing. Metabolic flux with SIRT4 WT and KO MEFs was performed as previously described[29]. Prior to the analysis, MEFs were cultured in pyruvate-free DMEM containing 4.5 g/L glucose supplemented with 10% FBS, β-mercaptoethanol and

penicillin/streptomycin. Cells were split into parallel 6-well plates for flux and for cell counting. For flux studies, cells were rinsed in PBS and replaced with flux media containing glucose-free DMEM containing glutamine and supplement with labeled glucose, dialyzed FBS, β-mercaptoethanol and penicillin/streptomycin. 24 hr later metabolites were harvested for analysis and cells were counted in the parallel plates.

Lactate secretion and glucose uptake measurements. Lactate and glucose levels in culture media were measured using the BioProfile FLEX analyzer (Nova Biomedical) compared to blank media that had not been exposed to cells. Fresh, glutamine-free media was added to a 6-well plate of subconfluent cells, and 6 hr later media was collected for analysis and normalized to cell number.

Pyruvate tolerance tests. Mice were fasted for 16-18 hr overnight before the PTT. Following intraperitoneal injection of 2 g/kg sodium pyruvate, tail vein blood glucose was measured at 15 min intervals using a One-Touch glucometer. Results were normalized to initial blood glucose levels at time 0.

Spectrophotometric-based PC activity assay. Reactions were performed as previously described[30] with the following exceptions. Samples were incubated with 90 mM Tris-HCl, 100 mM NaHCO3, 50 mM MgCl2, 500 mM acetyl-CoA, 25 mM DTNB, 50 mM ATP, 50 mM pyruvate and 1 unit/ml citrate synthase (C3260, Sigma, Porcine). Reactions were initiated by the addition of 75 μg mitochondrial protein lysate. Oxaloacetate formed by PC is measured in the presence of excess citrate synthase, which reacts with acetyl CoA to yield citrate and free CoA. CoA reduces DTNB, generating a colored product measured at A=412 nm.

Radioactivity-based PC activity assay. Reactions were performed as previously

described[31] with the following exception. Samples were incubated 30 min at 37˚ in a Thermomixer (Eppendorf) at 1000 rpm. Samples were quenched with 30 μl of 1 N HCl and heated for 60 min at 90˚ with lids open to allow carbon dioxide to escape. Background control samples lacked pyruvate and acetyl CoA. PC activity was calculated as incorporation of [^{14}C]bicarbonate into [^{14}C]oxaloacetate (the acid and heat stable product) as measured by scintillation counting.

Molecular modeling. Using CCP4mg molecular graphic software, the homotetrameric form of human PC (PDB: 3BG3) was analyzed to highlight the position of acetylated residues. The structure depicts the C-terminal portion of PC, missing only the N-terminal biotin carboxylation domain.

*Statistical analysis***.** Unpaired two-tailed Student's t tests were used. All experiments were performed at least two to three times.

Growth rates. For growth-rate analysis, Huh7 or 293T cells were plated in the wells of a 12 well plate (25,000 cells/well). At indicated times, cells were trypsinized and counted.

References

1. Houtkooper, R. H., Pirinen, E., and Auwerx, J. (2012). Sirtuins as regulators of metabolism and healthspan. Nature Publishing Group *13*, 225–238.

2. North, B. J., and Verdin, E. (2004). Sirtuins: Sir2-related NAD-dependent protein deacetylases. Genome Biol. *5*, 224.

3. Choudhary, C., Weinert, B. T., Nishida, Y., Verdin, E., and Mann, M. (2014). The growing landscape of lysine acetylation links metabolism and cell signalling. Nature Publishing Group *15*, 536–550.

4. Choudhary, C., Kumar, C., Gnad, F., Nielsen, M. L., Rehman, M., Walther, T. C., Olsen, J. V., and Mann, M. (2009). Lysine Acetylation Targets Protein Complexes and Co-Regulates Major Cellular Functions. Science *325*, 834–840.

5. Zhao, S., Xu, W., Jiang, W., Yu, W., Lin, Y., Zhang, T., Yao, J., Zhou, L., Zeng, Y., Li, H., et al. (2010). Regulation of Cellular Metabolism by Protein Lysine

Acetylation. Science *327*, 1000–1004.

6. Yang, X. J. (2004). The diverse superfamily of lysine acetyltransferases and their roles in leukemia and other diseases. Nucleic Acids Research *32*, 959–976.

7. Zhu, Y., Yan, Y., Principe, D. R., Zou, X., Vassilopoulos, A., and Gius, D. (2014). SIRT3 and SIRT4 are mitochondrial tumor suppressor proteins that connect mitochondrial metabolism and carcinogenesis. Cancer Metab *2*, 15.

8. Jeong, S. M., Xiao, C., Finley, L. W. S., Lahusen, T., Souza, A. L., Pierce, K., Li, Y.-H., Wang, X., Laurent, G., German, N. J., et al. (2013). SIRT4 Has Tumor-Suppressive Activity and Regulates the Cellular Metabolic Response to DNA Damage by Inhibiting Mitochondrial Glutamine Metabolism. Cancer Cell *23*, 450–463.

9. Haigis, M. C., Mostoslavsky, R., Haigis, K. M., Fahie, K., Christodoulou, D. C., Murphy, A. J., Valenzuela, D. M., Yancopoulos, G. D., Karow, M., Blander, G., et al. (2006). SIRT4 Inhibits Glutamate Dehydrogenase and Opposes the Effects of Calorie Restriction in Pancreatic β Cells. Cell *126*, 941–954.

10. Laurent, G., German, N. J., Saha, A. K., de Boer, V. C. J., Davies, M., Koves, T. R., Dephoure, N., Fischer, F., Boanca, G., Vaitheesvaran, B., et al. (2013). SIRT4 Coordinates the Balance between Lipid Synthesis and Catabolism by Repressing Malonyl CoA Decarboxylase. Molecular Cell *50*, 686–698.

11. Rauh, D., Fischer, F., Gertz, M., Lakshminarasimhan, M., Bergbrede, T., Aladini, F., Kambach, C., Becker, C. F. W., Zerweck, J., Schutkowski, M., et al. (2013). An acetylome peptide microarray reveals specificities and deacetylation substrates for all human sirtuin isoforms. Nat Comms *4*.

12. Stokes, M. P., Farnsworth, C. L., Moritz, A., Silva, J. C., Jia, X., Lee, K. A., Guo, A., Polakiewicz, R. D., and Comb, M. J. (2012). PTMScan Direct: Identification and Quantification of Peptides from Critical Signaling Proteins by Immunoaffinity Enrichment Coupled with LC-MS/MS. Molecular & Cellular Proteomics *11*, 187–201.

13. Lombard, D. B., Alt, F. W., Cheng, H. L., Bunkenborg, J., Streeper, R. S., Mostoslavsky, R., Kim, J., Yancopoulos, G., Valenzuela, D., Murphy, A., et al. (2007). Mammalian Sir2 Homolog SIRT3 Regulates Global Mitochondrial Lysine Acetylation. Molecular and Cellular Biology *27*, 8807–8814.

14. Rardin, M. J., Newman, J. C., Held, J. M., Cusack, M. P., Sorensen, D. J., Li, B., Schilling, B., Mooney, S. D., Kahn, C. R., Verdin, E., et al. (2013). Label-free quantitative proteomics of the lysine acetylome in mitochondria identifies substrates of SIRT3 in metabolic pathways. Proc. Natl. Acad. Sci. U.S.A. *110*, 6601–6606.

15. Jitrapakdee, S., St Maurice, M., Rayment, I., Cleland, W. W., Wallace, J. C., and

Attwood, P. V. (2008). Structure, mechanism and regulation of pyruvate carboxylase. Biochem. J. *413*, 369.

16. Marin-Valencia, I., Roe, C. R., and Pascual, J. M. (2010). Pyruvate carboxylase deficiency: Mechanisms, mimics and anaplerosis. Molecular Genetics and Metabolism *101*, 9–17.

17. Kumashiro, N., Beddow, S. A., Vatner, D. F., Majumdar, S. K., Cantley, J. L., Guebre-Egziabher, F., Fat, I., Guigni, B., Jurczak, M. J., Birkenfeld, A. L., et al. (2013). Targeting pyruvate carboxylase reduces gluconeogenesis and adiposity and improves insulin resistance. Diabetes *62*, 2183–2194.

18. Jensen, M. V., Joseph, J. W., Ilkayeva, O., Burgess, S., Lu, D., Ronnebaum, S. M., Odegaard, M., Becker, T. C., Sherry, A. D., and Newgard, C. B. (2006). Compensatory responses to pyruvate carboxylase suppression in islet beta-cells. Preservation of glucose-stimulated insulin secretion. J. Biol. Chem. *281*, 22342–22351.

19. Kim, S. C., Sprung, R., Chen, Y., Xu, Y., Ball, H., Pei, J., Cheng, T., Kho, Y., Xiao, H., and Xiao, L. (2006). Substrate and Functional Diversity of Lysine Acetylation Revealed by a Proteomics Survey. Molecular Cell *23*, 607–618.

20. Xiang, S., and Tong, L. (2008). Crystal structures of human and Staphylococcus aureus pyruvate carboxylase and molecular insights into the carboxyltransfer reaction. Nat Struct Mol Biol *15*, 295–302.

21. Wise, D. R., Ward, P. S., Shay, J. E. S., Cross, J. R., Gruber, J. J., Sachdeva, U. M., Platt, J. M., DeMatteo, R. G., Simon, M. C., and Thompson, C. B. (2011). Hypoxia promotes isocitrate dehydrogenase-dependent carboxylation of α-ketoglutarate to citrate to support cell growth and viability. Proc. Natl. Acad. Sci. U.S.A. *108*, 19611–19616.

22. Cheng, T., Sudderth, J., Yang, C., Mullen, A. R., Jin, E. S., Matés, J. M., and DeBerardinis, R. J. (2011). Pyruvate carboxylase is required for glutamine-independent growth of tumor cells. Proc. Natl. Acad. Sci. U.S.A. *108*, 8674–8679.

23. The UniProt Consortium (2015). UniProt: a hub for protein information. Nucleic Acids Research *43*, D204–D212.

24. Wallace, D. C. (2012). Mitochondria and cancer. Nat Rev Cancer *12*, 685–698.

25. Gameiro, P. A., Laviolette, L. A., Kelleher, J. K., Iliopoulos, O., and Stephanopoulos, G. (2013). Cofactor balance by nicotinamide nucleotide transhydrogenase (NNT) coordinates reductive carboxylation and glucose catabolism in the tricarboxylic acid (TCA) cycle. Journal of Biological Chemistry *288*, 12967–12977.

26. Yin, F., Sancheti, H., and Cadenas, E. (2012). Silencing of nicotinamide nucleotide

transhydrogenase impairs cellular redox homeostasis and energy metabolism in PC12 cells. Biochimica et Biophysica Acta (BBA) - Bioenergetics *1817*, 401–409.

27. Mathias, R. A., Greco, T. M., Oberstein, A., Budayeva, H. G., Chakrabarti, R., Rowland, E. A., Kang, Y., Shenk, T., and Cristea, I. M. (2014). Sirtuin 4 Is a Lipoamidase Regulating Pyruvate Dehydrogenase Complex Activity. Cell *159*, 1615–1625.

28. Schwer, B., Eckersdorff, M., Li, Y., Silva, J. C., Fermin, D., Kurtev, M. V., Giallourakis, C., Comb, M. J., Alt, F. W., and Lombard, D. B. (2009). Calorie restriction alters mitochondrial protein acetylation. Aging Cell *8*, 604–606.

29. Csibi, A., Fendt, S.-M., Li, C., Poulogiannis, G., Choo, A. Y., Chapski, D. J., Jeong, S. M., Dempsey, J. M., Parkhitko, A., Morrison, T., et al. (2013). The mTORC1 Pathway Stimulates Glutamine Metabolism and Cell Proliferation by Repressing SIRT4. Cell *153*, 840–854.

30. Payne, J., and Morris, J. G. (1969). Pyruvate carboxylase in Rhodopseudomonas spheroides. J. Gen. Microbiol. *59*, 97–101.

31. Mackall, J. C., and Lane, M. D. (1977). Role of pyruvate carboxylase in fatty acid synthesis: alterations during preadipocyte differentiation. Biochemical and Biophysical Research Communications *79*, 720–725.

CHAPTER III

PHD3 hydroxylates acetyl-CoA carboxylase to limit fatty acid oxidation in cancer

Natalie J. German[1], J. Patrick Murphy[1], Rushdia Z. Yusuf[2], Lydia W.S. Finley[1†], Jlenia Guarnerio[3], Gaëlle Laurent[1], Wilhelm Haas[1], Pier Paolo Pandolfi[3], Andrew H. Beck[4], Steven P. Gygi[1], David Scadden[2], William G. Kaelin Jr[56], Marcia C. Haigis[1]

[1]Department of Cell Biology, Harvard Medical School, Boston, MA 02115; [2]Stem Cell and Regenerative Biology Department, Harvard Stem Cell Institute, Harvard University, Cambridge, MA 02138; Center for Regenerative Medicine, Massachusetts General Hospital, Boston, MA 02114; [3]Cancer Research Institute, Beth Israel Deaconess Cancer Center, Department of Medicine and Pathology, Beth Israel Deaconess Medical Center, Harvard Medical School, Boston, MA, 02115; [4] Department of Pathology, Beth Israel Deaconess Medical Center and Harvard Medical School, Boston, MA, 02115; [5]Department of Medical Oncology, Dana-Farber Cancer Institute, Boston, MA 02215; [6]Howard Hughes Medical Institute, Chevy Chase, MD 20815; †Current address: Cancer Biology and Genetics Program, Memorial Sloan-Kettering Cancer Center, New York, NY 10065

This work is a revised and extended version of a manuscript recently submitted for publication. Natalie German performed the experiments described in this chapter, with help from Patrick Murphy and Wilhelm Haas (mass spectrometry), Rushdia Yusuf and Jlenia Guarnerio (provided leukemia cell lines and assisted with ongoing mouse studies) and Lydia Finley and Gaëlle Laurent (technical assistance).

Abstract

In cancer, cell metabolism is fundamentally altered to drive biosynthetic, bioenergetic and signaling pathways[1, 2]. While much research has focused on the use of glucose and glutamine by tumor cells[3-5], a substantial subset of cancers, for reasons largely not understood, have a high capacity and preference for fat oxidation[6]. Our knowledge of molecular pathways that drive dependency of fatty acid oxidation in cancers is limited, demonstrating a critical need to identify these regulatory nodes. Here we reveal a novel role for prolyl hyrdoxylase domain (PHD) 3 in inhibiting fatty acid oxidation (FAO) in cancers. PHDs are α-ketoglutarate-dependent dioxygenases that modify proline residues of target proteins and have been linked to fuel switching in cancer[7, 8]. We find PHD3 hydroxylates and activates acetyl-CoA carboxylase (ACC2), an enzyme that inhibits mitochondrial FAO[9]. Site-specific hydroxylation at Pro450 results in full ATP binding and activation of ACC2. We find this regulatory axis is not sensitive to hypoxia or the transcriptional regulator hypoxia inducible factor (HIF), but rather is sensitive to cellular nutrient status. Under nutrient replete conditions, PHD3 acts through ACC2 to drive a switch that represses FAO. We show PHD3 expression is strongly decreases in acute myeloid leukemia (AML). Low-PHD3 AML cell lines display altered ACC2, elevated FAO regardless of external nutrient cues and sensitivity to treatment with FAO inhibitors. Thus, loss of the PHD3/ACC2 regulatory axis in leukemia enables greater utilization of fatty acids as fuel, but also serves as a metabolic liability by rendering cells susceptible to FAO inhibition.

Introduction

Elevated fatty acid uptake and utilization are hallmarks of several subsets of cancer[6, 10]. Amplified fatty acid catabolism may promote cancer cell survival via several mechanisms including by providing ATP, maintaining mitochondrial membrane quality or building a pool of citrate that is used for the production of the antioxidant molecule NADPH[11-15]. However, our knowledge of the metabolic drivers enabling altered FAO in cancer is lacking, highlighting a critical unmet area of cancer research. It is vital to elucidate the regulatory nodes that coordinate fatty acid preference and fate, and to understand how these pathways might contribute to cancer.

PHDs (also called EGLN1-3) are a conserved class of oxygen- and α-ketoglutarate dependent enzymes that perfectly poised to modulate metabolism in cancer. PHD family members are well known to regulate glycolytic metabolism through prolyl hydroxylation of the master transcriptional regulator hypoxia inducible factor (HIF)[7, 8]. Hypoxia and a number of mutations in cancer that alter levels of TCA cycle intermediates inhibit the activity of PHD family members, thus stabilizing HIFα and triggering a transcriptional program to increase glycolysis and anabolism while limiting mitochondrial bioenergetics[16-19]. PHD1 and 2 are quite sensitive to subtle changes in oxygen levels due to their weak affinity for oxygen, positioning these enzymes as prime mediators of the cellular and metabolic response to changing oxygen levels[7]. However, in most cell types PHD3 (also called EGLN3) is not a major HIF hydroxylase and is less sensitive to low oxygen than other PHDs[20, 21], raising the question as to what other pathways PHD3 may coordinate. In vitro studies indicate PHD3 has lower affinity for the co-substrate α-ketoglutarate than other PHDs, a characteristic that suggests PHD3 might be sensitive to fluctuations in the cellular nutrient state[22]. Recent studies indicate

PHD3 can bind and regulate other targets with potential disease relevance including pyruvate kinase M2 (PKM2) and pyruvate dehydrogenase (PDH)-E1β, demonstrating broader specificity of these enzymes[20, 23]. Therefore, in this study we aimed to identify novel PHD3 substrates that may impact cellular metabolism in cancer.

Results

PHD3 binds and modifies ACC by site-specific prolyl hydroxylation

In order to determine novel PHD3 substrates, we performed immunoprecipitation of PHD3 followed by liquid chromatography tandem mass spectrometry (LC-MS2) and detected a novel interaction with acetyl-CoA carboxylase (ACC). ACC specifically interacted with PHD3 but not PHD1, PHD2 or anti-HA affinity resin alone, as verified by Western blot (Figure 3.1 a, Table 3.1). Although PHDs are commonly associated with glucose metabolism, this interaction was perplexing in that it suggests PHD3 may be directly linked to fat metabolism. ACC is a key regulator of fatty acid homeostasis that directs the cell to catabolize or synthesize fatty acids. ACC converts acetyl-coA to malonyl-CoA, which serves as a precursor for fat synthesis and an inhibitor of fatty acid oxidation (FAO)[24-26].

We considered the possibility that PHD3 modifies ACC by prolyl hydroxylation. To this end, we analyzed PHD3-responsive changes in prolyl hydroxylation. We identify for the first time that ACC is prolyl-hydroxylated and that this modification is present in a PHD3-dependent manner (Figure 3.1 b). Hydroxylation of endogenous ACC is decreased upon knockdown of PHD3 by two different hairpins, as detected by immunoprecipitation and Western blot with a pan-hydroxyproline antibody (Figure 3.1 b, extent of knockdown by each hairpin shown in Figure S3.1 a-b). Accordingly,

Figure 3.1 | ACC interacts with PHD3 and is modified by site-specific hydroxylation at Pro450. a, Interaction between ACC and PHD3. HA-tagged PHD1-3 or empty vector were transfected in 293T cells, immunoprecipitated with anti-HA affinity resin, and interactions were detected by immunoblotting for ACC. **b,** Endogenous ACC hydroxylation was measured in 293T cells in complete media following stable PHD3 knockdown by two different shRNA or non-targeting control. **c,** Endogenous ACC hydroxylation in 293T cells in serum-free, low glucose media transiently overexpressing HA-PHD3 or vector. ACC was immunoprecipitated by ACC antibody and Protein G affinity resin. Hydroxylation was detected by immunoblot with hydroxyproline (OH-Pro) antibody. **d,** Endogenous ACC hydroxylation in 293T cells in serum-free, low glucose media transiently overexpressing wild type PHD3 or catalytically inactive PHD3 mutants (R206K and H196A). **e,** Hydroxylation of endogenous ACC1 versus ACC2 was assessed by immunoprecipitation with isoform-specific antibodies and immunoblotting with OH-Pro antibody. 293T cells were pre-treated 12 h with serum-free, low glucose media prior to IP. **f-g,** Representative mass spectra identifying the hydroxylated and non-hydroxylated versions of residue P450 in ACC2 peptides. OH-Pro sites were identified by the expected +15.9949 molecular weight shift. 'b' fragments (blue) contain the N-terminal amino acid of the peptide and are labeled from the amino to the carboxyl terminus. 'y' fragments (green) contain the C-terminal amino acid of the peptide are labled from the carboxyl to the amino terminus. **h,** ACC2 hydroxyproline residues detected by mass spectrometry following transient overexpression of ACC2 in 293T cells and immunoprecipitation with ACC antibody. **i,** Diagram shows the location of OH-Pro residues in ACC2 domains. **j,** Hydroxylation of transiently overexpressed WT ACC2 or proline to alanine point mutants. Overexpressed ACC2 was immunoprecipitated with ACC antibody. Hydroxylation was assessed by immunoblot. **k,** In vitro reconstituted hydroxylation assay with ACC2 peptides containing the indicated proline residue and recombinant PHD3 (n = 2). Xcorr = cross correlation score. BT = biotin transferase domain. BCCP = biotin carboxyl carrier protein. ***$p < 0.001$. Error bars indicate SEM.

Figure 3.1 (Continued).

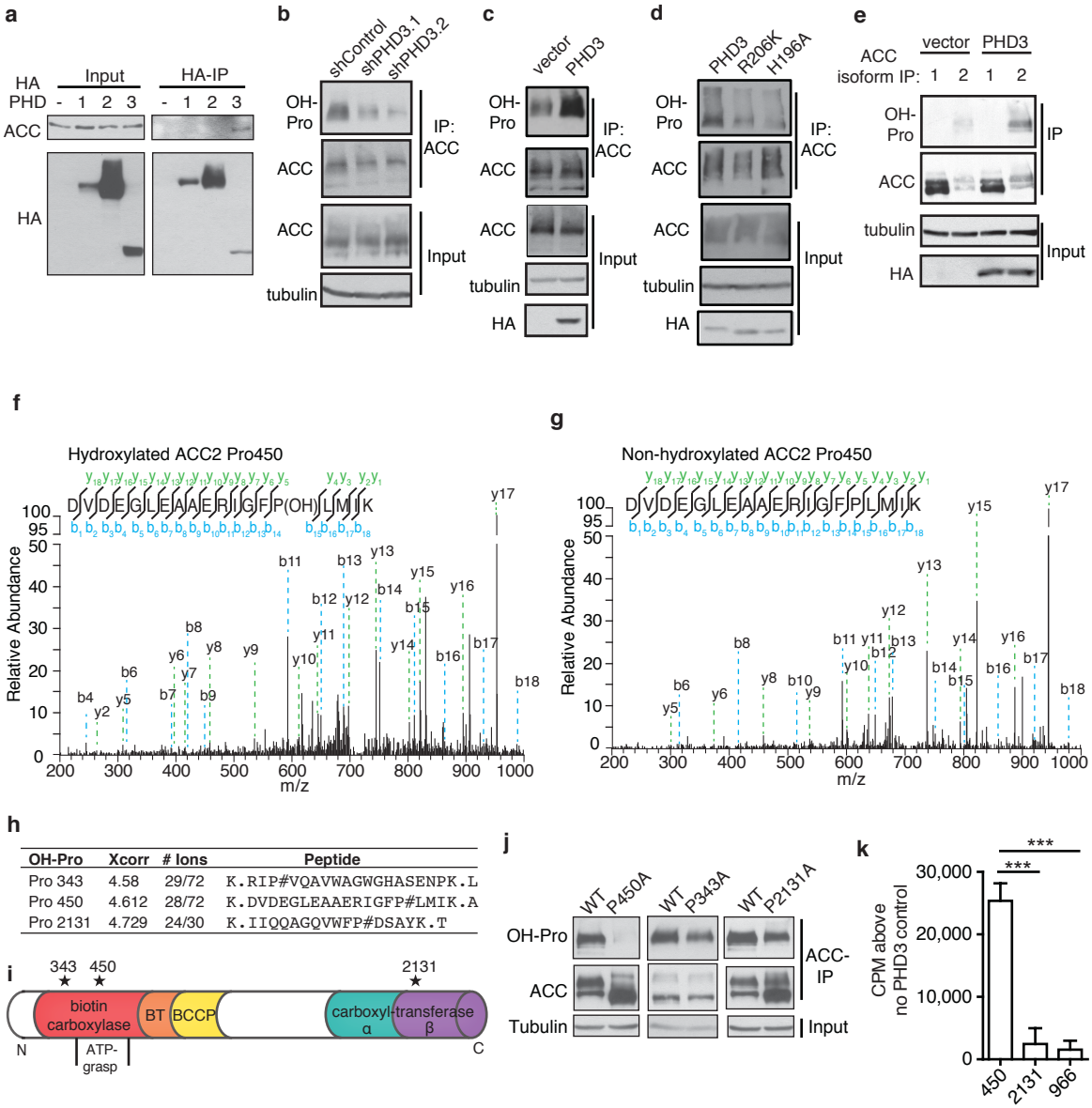

Table 3.1 | PHD3-interacting peptides indistinguishable between ACC1 and 2 isozymes.

Xcorr	ΔCorr	# Ions	Redundancy	Peptide
4.518	0.54	33/88	8	R.ITSENPDEGFKPSSGTVQELNFR.S
3.168	0.392	16/24	12	R.DFTVASPAEFVTR.F
2.409	0.071	15/24	9	K.EASFEYLQNEGER.L
2.221	0.415	16/18	9	R.AIGIGAYLVR.L
1.757	0.124	8/14	8	K.DMYDQVLK.F

Peptides were filtered using Xcorr and ΔCorr. Xcorr= cross correlation score. ΔCorr= delta correlation.

hydroxylation is increased with PHD3 overexpression (Figure 3.1 c), while two previously characterized catalytically inactive PHD3 mutants, H196A and R206K[27, 28], did not augment ACC hydroxylation to the same extent as wild type PHD3 (Figure 3.1 d).

ACC is present in two spatially and functionally distinct isoforms. Cytosolic ACC1 provides malonyl-CoA for fatty acid synthesis, while ACC2 at the outer mitochondrial membrane generates malonyl-CoA to inhibit the fatty acid transport protein CPT1[24]. Several PHD3-interacting peptides that we found by mass spectrometry are shared between ACC1 and ACC2 (Table 3.1). Thus, we interrogated whether PHD3 hydroxylates ACC1 or ACC2. Immunoprecipitation of endogenous ACC1 or ACC2 by isoform-specific antibodies showed hydroxylation was particular to ACC2 and also stronger in the presence versus absence of PHD3 (Figure 3.1 e), showing PHD3 is a clear modulator of ACC2 hydroxylation status.

We next used LC-MS2 to map ACC2 proline residues that were modified by hydroxylation, as detected by a +15.9949 molecular weight shift compared to an unmodified peptide (representative spectra in Figure 3.1 f-g). We found three hydroxylated prolines with greater than 5 redundant peptides per hydroxylation site: prolines 343, 450 and 2131 of ACC2 (Figure 3.1 h). These sites are located in the biotin carboxylase, ATP-grasp and carboxyltransferase domains, respectively (Figure 3.1 i). To validate hydroxylation of these residues, we generated proline to alanine ACC2 point mutants at each putative hydroxylation site. Immunoprecipitation of wild type or mutant ACC2 revealed P450A mutagenesis most dramatically decreased the level of hydroxylation compared to P343A and P2131A variants (Figure 3.1 j). Using a

reconstituted in vitro radioactivity-based hydroxylation assay, we determined that recombinant PHD3 could hydroxylate a synthetic ACC2 peptide containing P450, but not a peptide containing P2131 or a control ACC2 proline-containing peptide (P966) (Figure 3.1 k). Together these data demonstrate P450 is a major site of PHD3 hydroxylation, suggesting that modification of this residue may coordinate ACC2 function.

Hydroxylation at residue P450 promotes ACC2 activity and ATP binding

At only 16 daltons, prolyl hydroxylation is among the smallest of all posttranslational modifications. Nevertheless, the electronegativity it imparts alters the pucker of the modified proline residue and induces larger-scale conformational changes significant enough to alter protein-protein interactions, substrate stability or activity[8, 29]. Thus, we investigated the mechanism by which site-specific hydroxylation might regulate ACC2 activity. Residue P450 is conserved from yeast to human (Figure 3.2 a) and is located in the ATP-grasp domain, a 196 amino acid region within the biotin carboxylase domain that includes nucleotide-binding amino acids at residues 458-463[30]. We mapped site P450 in the published human ACC2 biotin carboxylase domain crystal structure (PDB: 3JRW)[31] superposed with the *e. coli* ATP-bound ACC biotin carboxylase domain (PDB: 1DV2)[32]. This modeling revealed P450 is in close proximity to the catalytic site ATP (Figure 3.2 b). P450 caps the adenine ring of ATP, while the phosphate groups of ATP abut the previously described nucleotide-binding site within ACC2. The proximity of P450 and ATP led us to hypothesize that hydroxylation modulates that ability of ACC2 to bind ATP. To assess this hypothesis, we purified ATP-binding proteins from dialyzed cell lysates using ATP affinity chromatography and Western blotted to determine levels of ACC bound by the ATP-linked resin. We found

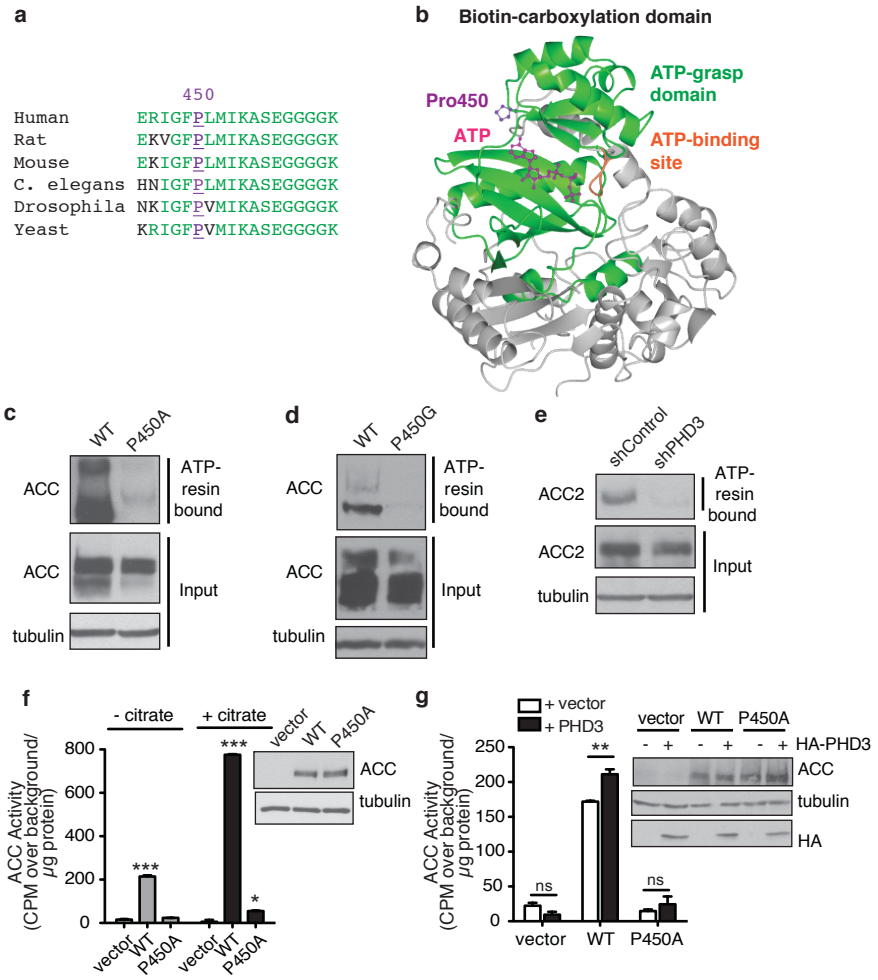

Figure 3.2 | Hydroxylation at site P450 promotes ACC2 activity and ATP binding. a, Conservation of P450 in the ATP grasp domain. Alignment shows the ACC2 isoform in human, rat and mouse, and ACC in C. elegans, drosophila and S. cerevisiae, organisms lacking distinct ACC1/2 isoforms. P450 highlighted in purple. **b,** Molecular modeling to evaluate the location of P450 (purple) in the human ACC2 ATP-grasp domain (green) relative to ATP (magenta) and known nucleotide binding residues (orange). **c-d,** ATP-affinity of wild type and P450A **(c)** or P450G **(d)** ACC2 point mutant from transiently transfected 293T cells, as assessed by immunoprecipitation with ATP-affinity resin and immunoblot with ACC antibody. **e,** ATP-affinity of endogenous ACC2 from 293T cells stably expressing shRNA against PHD3 or non-targeting control. Levels of immunoprecipitated ACC2 were analyzed by immunoblot with ACC2 antibody. **f,** ACC activity was measured in 293T cell lysates overexpressing vector, wild type ACC2 or P450A mutant (n = 3). Reactions were done ± the ACC allosteric activator citrate (2 mM). Western blots show overrexpressed ACC2. **g,** ACC activity in 293T cell lysates co-overexpressing vector, ACC2 or P450A along with either HA-PHD3 or empty vector (n = 4). Reactions were done with citrate. Western blots show overexpressed ACC2 and HA-PHD3. *p < 0.05, **p < 0.01, ***p < 0.001. Error bars indicate SEM.

that ACC2 lacking the major hydroxylation site upon P450 mutation to alanine or glycine showed decreased ATP binding versus wild type ACC2 (Figure 3.2 c-d), demonstrating the importance of this residue for ATP binding. Strikingly, knockdown of PHD3 also diminished ATP-binding by endogenous ACC2 (Figure 3.2 e), further demonstrating that hydroxylation of P450 is critical for ACC binding to ATP. Together these data indicate PHD3 may activate ACC2 by enabling greater affinity for the co-substrate ATP.

To evaluate whether PHD3 promotes ACC enzymatic activity, we performed in vitro ACC activity assays based on the production of [^{14}C]malonyl-CoA from [^{14}C]bicarbonate and acetyl-CoA. Although endogenous ACC activity was barely detectable in whole cell lysates, overexpression of ACC2 enabled measurement of enzymatic activity. ACC2 was activated by citrate, a known allosteric modulator[33], while P450A mutation strongly decreased ACC activity (Figure 3.2 f). When assaying the effect of PHD3 on ACC2 function, we found PHD3 overexpression amplified wild type ACC2 activity (Figure 3.2 g), but had no effect on the P450A variant. Our data collectively support the model that PHD3 boosts ACC2 activity via site-specific hydroxylation of P450.

PHD3 represses long chain fatty acid oxidation

Via production of malonyl-CoA, ACC2 is implicated in regulation of the carnitine shuttle that transports long chain fatty acids into the mitochondrial matrix for oxidation[33]. Malonyl-CoA generated by ACC2 allosterically inhibits CPT1, an outer mitochondrial membrane-bound component of the carnitine shuttle that serves as the rate-limiting enzyme in FAO. Thus, high ACC2 activity decreases FAO. Therefore, we hypothesized that FAO is repressed when ACC2 is hydroxylated and activated by PHD3.

To test if the PHD3/ACC2 regulatory axis impacts fatty acid utilization, we measured oxidation of the fatty acid palmitate upon PHD3 modulation. Knockdown of PHD3 enhanced palmitate oxidation in 293T cells (Figure 3.3 a, Figure S3.1 a-b). This result showed that PHD3 has an inhibitory effect on FAO, a finding confirmed in HepG2 cells (Figure 3.3 b, Figure S3.2 a). Of note, PHD3 modulates FAO at a magnitude similar to that observed in studies of known lipid metabolism regulators including ACC2, adiponectin and sirtuins[34-37]. PHD1 and PHD2 gene expression were not consistently altered by PHD3 knockdown, indicating the effect on FAO was not due to over-compensation by other PHDs (Figure S3.1 a). To assess the role of ACC2 P450 prolyl hydroxylation in FAO, we performed FAO experiments in 293T cells overexpressing wild type or mutant ACC2. While overexpression of wild type ACC2 decreased palmitate oxidation, the P450A mutant lacking the major hydroxylation site had blunted ability to repress FAO (Figure 3.3 c). By contrast, mutations P343A and P2131A had no effect on FAO (Figure S3.3 a-b).

Since ACC2 gates long chain fatty acid import into the mitochondria, whereas short chain fatty acids can freely diffuse, we probed whether PHD3 specifically modulates oxidation of long chain fatty acids. Comparison of 16-carbon palmitate oxidation versus 6-carbon hexanoate oxidation revealed PHD3 knockdown only boosts long chain FAO (Figure 3.3 d). Consistent with the biochemical and mass spectrometry studies showing that ACC2, but not ACC1, is hydroxylated by PHD3, we observed no effect of PHD3 on fatty acid synthesis in cell lines tested- a process mediated by ACC1 (Figure 3.3 e-f). Together the data suggests a model in which PHD3 hydroxylates and

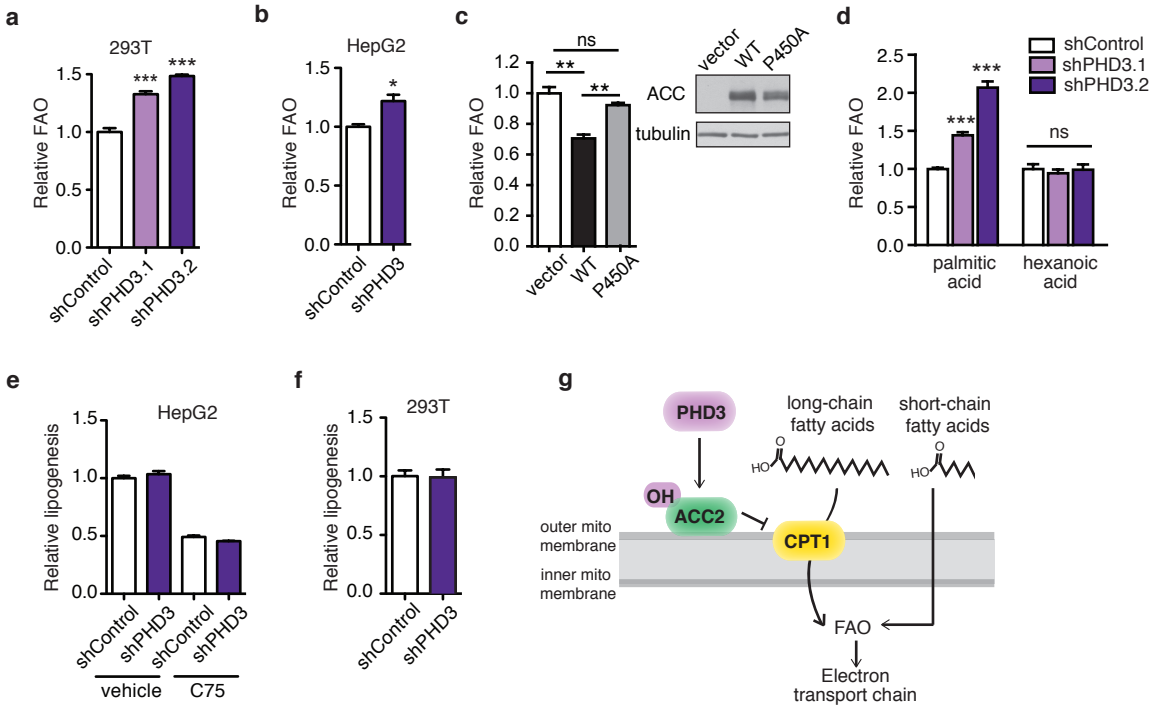

Figure 3.3 | PHD3 represses long chain fatty acid oxidation. a, Palmitate oxidation by 293T cells stably expressing shRNA against PHD3 (shPHD3.1 and shPHD3.2) or non-targeting control (n = 4). **b,** Palmitate oxidation in HepG2 cells with PHD3 knockdown (n = 3). **c,** Palmitate oxidation in complete media in 293T cells transiently overexpressing wild type ACC2 or ACC2 lacking the P450 hydroxylation sites (n = 3). Western blots show levels of overexpressed ACC2. **d,** Impact of PHD3 on long chain versus short chain FAO. Oxidation of long chain palmitic acid and short chain hexanoic acid was assessed in 293T cells stably expressing shPHD3 or non-targeting control shRNA (n = 3). **e-f,** Lipid synthesis from acetate in HepG2 **(e)** or 293T **(f)** cells with stable PHD3 knockdown by shRNA or non-targeting control (n = 3). C75 = fatty acid synthase inhibitor (20 μM). **g,** Model of the effect of PHD3 on long chain FAO via ACC2 hydroxylation. PHD3 hydroxylates and activates ACC2 to limit long chain fatty acid mitochondrial import, but not import of short chain fatty acids which bypass regulatory mechanisms. *p < 0.05, ***p < 0.001. Error bars indicate SEM.

activates ACC2, limiting flux of long chain fatty acids into the mitochondria (Figure 3.3 g).

PHD3 represses FAO in a manner insensitive to hypoxia and HIF, but sensitive to cellular nutrient status

We next aimed to identify physiological stimuli that might modulate the ability of PHD3 to activate ACC2 and inhibit FAO. First, we used a multifaceted approach to systematically assess whether the elevated FAO caused by PHD3 knockdown was sensitive to hypoxia or occurred via HIF stabilization. We found PHD3 repression of FAO was not sensitive to hypoxia, and PHD3 knockdown still led to increased FAO even under 1% O_2 (Figure 3.4 a). Additionally, HIF1/2α protein levels were not changed with PHD3 knockdown under our experimental conditions (Figure 3.4 b), suggesting the effects of PHD3 on FAO are not due to altered HIF. Further, PHD3 modulates FAO in cellular systems where HIF is either constitutively stabilized or inactivated. We found PHD3 knockdown boosts FAO in 786-O von Hippel-Lindau (VHL)-deficient renal carcinoma cells with stabilized HIF[38] (Figure 3.4 c, Figure S3.2 b). Additionally, PHD3 alters FAO in mouse hepatoma 4 (B13NBii1) arylhydrocarbon receptor nuclear translocator (ARNT, also known as HIFβ) null cells, which lack functional HIF1 transcriptional activity[39] (Figure 3.4 d-e, Figure S3.2 c). The absence of HIF transcriptional activity in ARNT -/- cells was validated by treatment with $CoCl_2$, which stabilizes HIFα, but in these cells was found not to induce HIF target genes including phosphoglycerate kinase 1 (PGK1) and hexokinase 2 (HK2) (Fig. S3.2 c). Together, these multiple lines of data indicate PHD3 repression of FAO is not sensitive to hypoxia and not dependent on HIF.

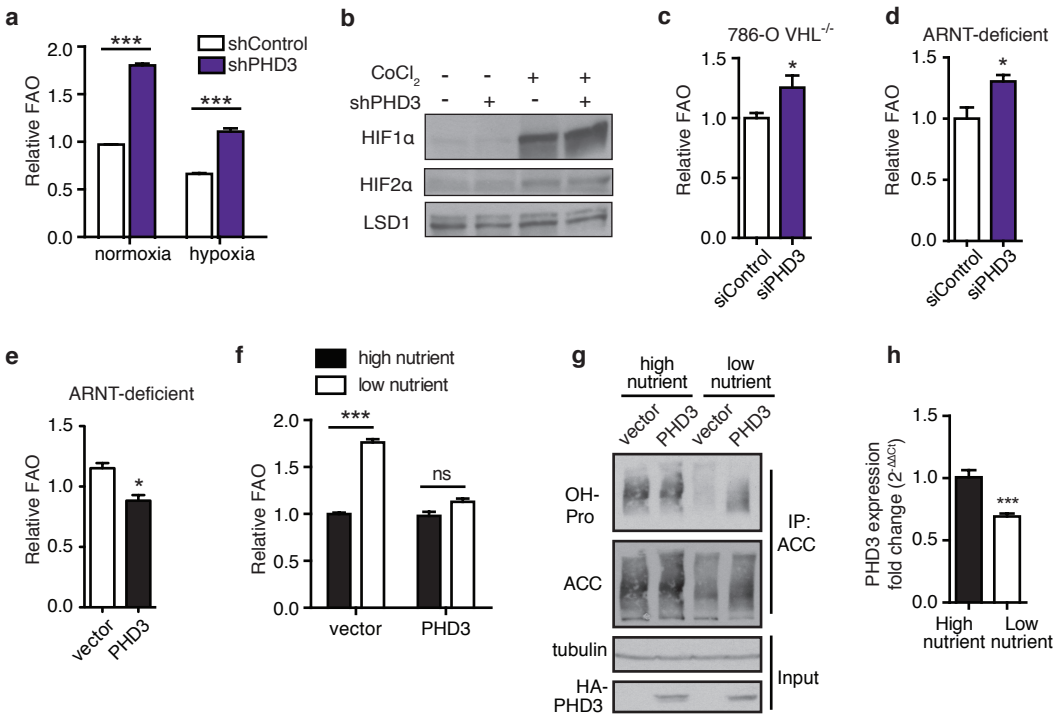

Figure 3.4 | PHD3 modulation of FAO is not sensitive to hypoxia or HIF, but is sensitive to nutrient status. a, Palmitate oxidation in 293T cells following 12 hr pre-incubation in normoxia or hypoxia (1% O_2). For 2 hr FAO analysis, cells were again maintained under normoxia or hypoxia (n = 4). **b,** Immunoblot of HIF1α and 2α levels in 293T cells with PHD3 knockdown or control. Bands representing HIF1/2α were made more visible by 4 hr treatment with 250 μM $CoCl_2$. **c,** Palmitate oxidation in 786-O $VHL^{-/-}$ cells with constitutively stabilized HIF. Cells were transiently transfected with Dharmacon siGENOME SMARTpool EGLN3 siRNA (siPHD3) or Non-Targeting siRNA Pool #2 (siControl), and FAO was assessed 48 hr later (n = 3). **d-e,** Effect of PHD3 levels on palmitate oxidation in complete media in ARNT-deficient cells, which have constitutively inactive HIF. FAO was assessed following transfection with siPHD3 or siControl **(d)** or with human HA-PHD3 or vector **(e)** (n = 3). **f,** FAO in high nutrient conditions (complete media containing 4.5 g/L glucose) or low nutrient conditions (serum-free media containing 1 g/L glucose) in transiently transfected ARNT-deficient cells. In empty vector-treated cells, FAO is limited under a high nutrient state and increased under low nutrient conditions. PHD3 overexpression blunts the increase in FAO. **g,** ACC is more hydroxylated in hight nutrient versus low nutrient media, suggesting endogenous PHD3 is activated by a nutrient replete state. PHD3 overexpression enables hydroxylation under low nutrient conditions. Endogenous ACC hydroxylation was measured in 293T cells treated for 12 h in high or low nutrient media, as described above, and also transiently overexpressing HA-PHD3 or vector. **h,** PHD3 gene expression in high versus low nutrient media, as described above. *$p < 0.05$, ***$p < 0.001$. Error bars indicate SEM.

We next considered the possibility that PHD3 limits FAO in a manner linked to the nutrient state of the cell. Physiologically, in many tissues fatty acids are not a major fuel choice under nutrient replete conditions but rather are reserved for utilization under fasting or nutrient deprivation to allow restoration of metabolic homeostasis[37]. Nutrient availability and the bioenergetic status of the cell result in major changes in catabolism or anabolism that are often mediated by post-translational modification of metabolic enzymes. Recent reports indicate that PHD enzymes, beyond oxygen sensing, are also responsive to the cellular nutrient status. This family of enzymes have potential roles as versatile metabolic sensors because their catalytic activity is dependent on several key molecules that can be viewed as indicators of the metabolic state including TCA cycle intermediates and reactive oxygen species[7]. In response to changing levels of all these inputs, PHDs have been shown to instigate metabolic changes that restore homeostasis and redox balance.

With this landscape in mind, we assessed whether PHD3 activity toward ACC2 and FAO is sensitive to the cellular nutrient status. In ARNT-/- hepatoma cells expressing endogenous levels of PHD3, we observed FAO is limited to a basal level under high nutrient conditions with complete media, but reaches higher levels under low nutrient conditions, consisting of serum-free, low glucose media (Figure 3.4 f). However, forcing PHD3 overexpression blunts the increase in FAO that otherwise occurs in a low nutrient state (Figure 3.4 f). This raises the possibility that PHD3 is sensitive to nutrient availability and bioenergetic status and consequently adjusts fatty acid utilization. Our data fits the hypothesis that greater activity of endogenous PHD3 in the presence of

abundant nutrients restricts FAO, while reduced PHD3 activity upon nutrient deprivation causes repression of FAO to be lifted.

We next examined ACC hydroxylation under high and low nutrient conditions. ACC is strongly hydroxylated by endogenous PHD3 in 293T cells grown in complete media, but less hydroxylated in cells grown in serum-free, low glucose media (Figure 3.4 g), suggesting PHD3 is active under nutrient replete conditions. In low nutrient conditions, overexpressing PHD3 restores the level of hydroxylation to nearly that of cells in the high nutrient state (Figure 3.4 g). Thus, our data suggest endogenous PHD3 hydroxylates ACC2 under nutrient replete conditions to limit FAO, but is less active under nutrient deprivation. This model is further supported by the observation that PHD3 expression is higher in 293T cells grown in complete media compared to low nutrient media (Figure 3.4 h).

Low PHD3 expression in AML is linked to altered ACC2 and largely elevated FAO

FAO is increased as part of metabolic reprogramming in cancers such as diffuse large B-cell lymphoma (DLBCL) subtypes, prostate cancer, colorectal cancer, acute myeloid leukemia (AML) and subsets of aggressive breast cancer, but the underlying mechanisms are largely unknown[6, 12, 40, 41]. Moreover, recent studies suggest leukemia can be characterized by enhanced dependence on FAO, and that inhibition of FAO increases sensitivity to pharmacological induction of apoptosis both in cell culture and in a murine model of human AML[15, 42]. Thus we probed whether cancer cell dependence on FAO was linked to PHD3 status. Analysis of the Ramaswamy Multi-Cancer dataset[43] from the Oncomine cancer microarray database (http://www.oncomine.org) indicated AML has the lowest PHD3 expression compared to

a panel of other cancerous tissues (Figure 3.5 a). Valk Leukemia (285 AML and 8 normal marrow samples) and Andersson Leukemia (23 AML and 6 normal marrow samples) datasets also show decreased PHD3 mRNA levels in AML compared to normal marrow patient samples (Figure 3.5 b-c)[44, 45].

To investigate the relevance of decreased PHD3 in leukemia, we examined the metabolic consequences of low PHD3 expression in a panel of leukemia cell lines. Gene expression studies revealed PHD3 is nearly undetectable in panel of AML cell lines (MOLM14, KG1, THP1) compared to the K562 chronic myeloid leukemia (CML) cell line (Figure 3.5 d). Low-PHD3 AML cell lines show reduced ACC hydroxylation and ATP binding (Figure 3.5 e-f). Additionally, low PHD3 expression in AML cells correlates with markedly increased palmitate oxidation (Figure 3.5 g).

Low PHD3 expression in AML indicates insensitivity to physiological nutrient cues and highlights a dependency on FAO that can be therapeutically targeted

We hypothesized that low-PHD3 leukemia cells possessed a metabolic liability rooted by their dependency on FAO. Thus we examined their sensitivity to etomoxir or ranolazine, FAO inhibitors that have shown success in treating angina and heart disease, respectively[6, 46, 47]. Etomoxir represses FAO by inhibiting CPT1 to limit the uptake and oxidation of long chain fatty acids, and ranolazine inhibits 3-ketoacylthiolase, the enzyme catalyzing the final step in each round of β-oxidation[6]. 96 hr inhibition of FAO by etomoxir led to substantial cell death in low-PHD3 leukemia cells but not K562 leukemia cells with higher PHD3 (Figure 3.6 a-b). Along these lines, 96 hr treatment with ranolazine also drastically reduced cell viability in low-PHD3 leukemia cells while viability was largely maintained for K562 cells (Figure 3.6 c-d). Sensitivity to FAO

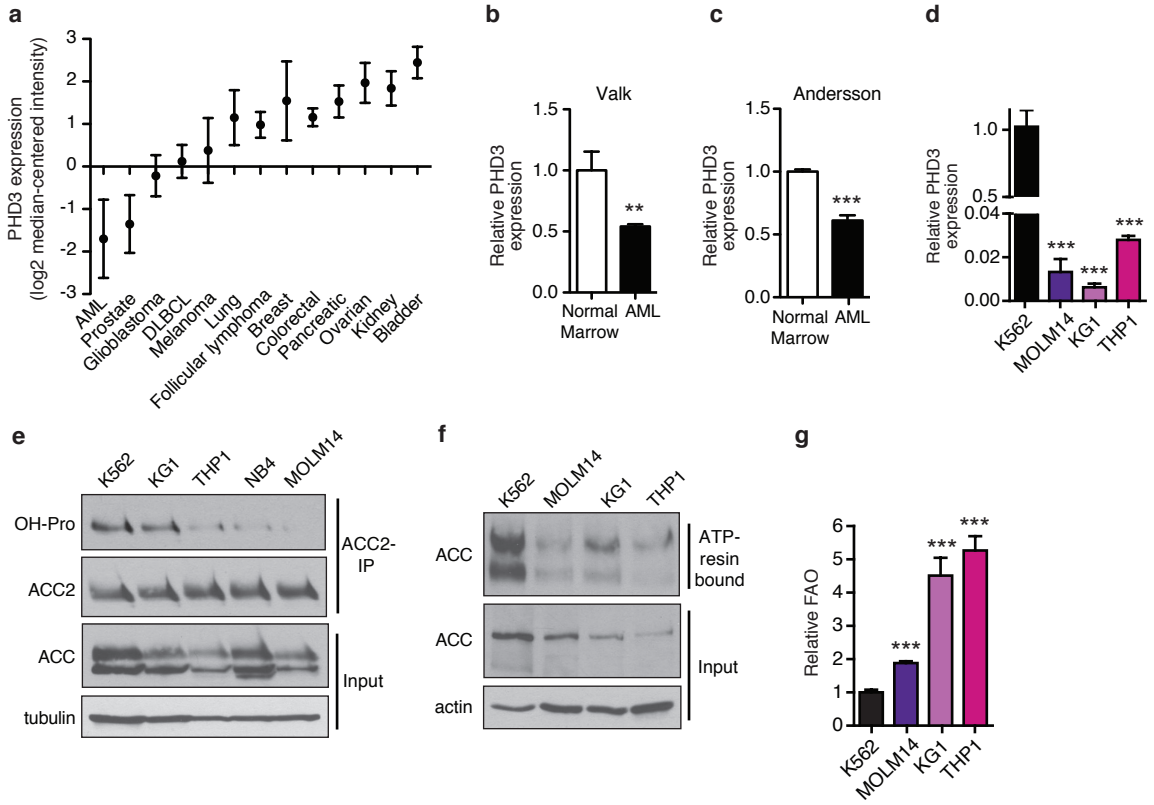

Figure 3.5 | PHD3 expression is strongly repressed in AML, contributing to increased FAO and altered ACC. a, Gene expression of PHD3 in patient samples across cancer types. Data obtained from the Ramaswamy multi-type cancer analysis on Oncomine. **b-c,** Relative PHD3 gene expression in normal marrow versus AML patient samples. Data obtained from Valk and Andersson Leukemia Oncomine datasets. **d,** PHD3 gene expression in leukemia cells. K562= CML cell line (black bar). MOLM14, KG1 and THP1= AML cell lines (purple/magenta bars). **e,** Endogenous ACC2 hydroxylation was measured in leukemia cell lines. ACC2 was immunoprecipitated with ACC2 antibody, and hydroxyproline was assessed by immunoblot with OH-Pro antibody. Because the ACC2 antibody cannot detect endogneous levels of ACC2 in whole cell lysates, an ACC antibody was used instead to show input. **f,** ATP-affinity of endogenous ACC in leukemia cell lines, as assessed by immunoprecipitation with ATP-affinity resin and immunoblot with ACC antibody. **g,** Palmitate oxidation by leukemia cell lines in complete RPMI media (n = 3). $^{**}p < 0.01$, $^{***}p < 0.001$. Error bars indicate SEM.

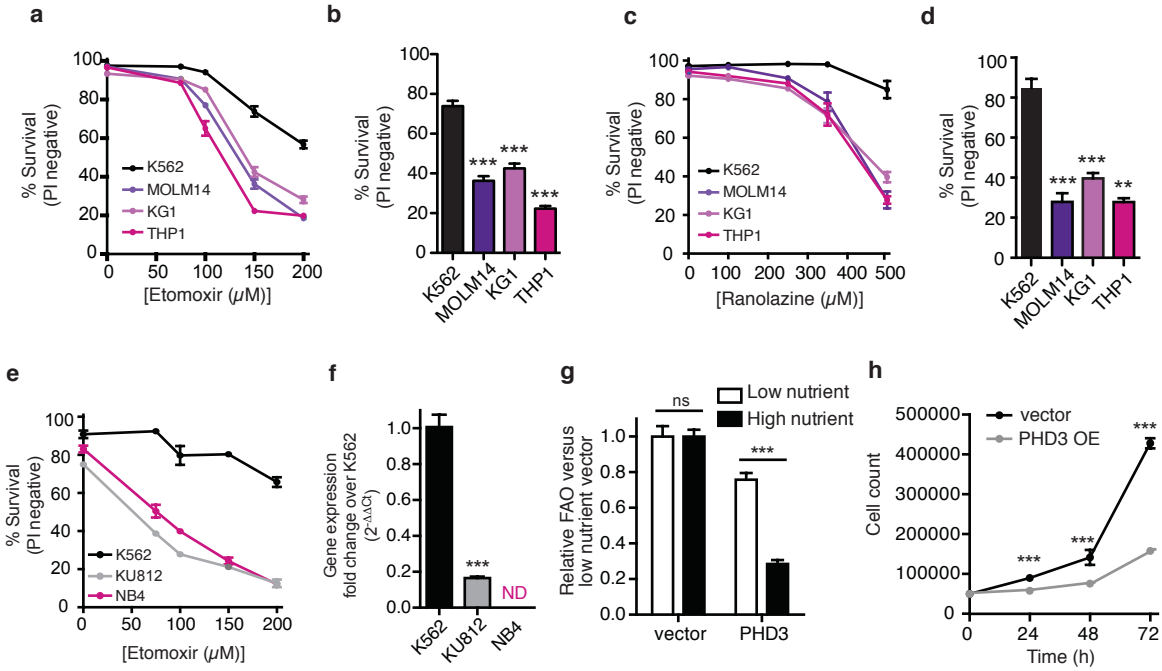

Figure 3.6 | Low PHD3 expression in AML indicates insensitivity to physiological nutrient cues and highlights a dependency on FAO that can be therapeutically targeted. a, Viability of leukemia cells assessed by PI staining after 96 hr treatment with indicated doses of etomoxir (n = 3). All data points with drug treatment are significant by $p < 0.001$ for all cell lines compared to K562. **b,** Plot of data shown in **(a)** highlighting sensitivity to 150 μM etomoxir. **c,** Viability of leukemia cells after 96 hr treatment with indicated doses of ranolazine (n = 3). All data points with drug treatment are significant by $p < 0.05$ for all cell lines compared to K562. **d,** Plot of data shown in **(c)** highlighting sensitivity to 500 μM ranolazine. **e,** Viability of high PHD3 CML cell line (K562) compared to low PHD3 CML cell line (KU812) and low PHD3 AML cell lines (NB4) following 96 hr treatment with etomoxir (n = 3). All data points with drug treatment are significant by $p < 0.01$ for all cell lines compared to K562. **f,** Relative PHD3 gene expression in K562, KU812 and NB4 leukemia cell lines. ND = not detectable. **g,** Restoring PHD3 expression in MOLM14 cells enables nutrient-sensitive modulation of FAO. Palmitate oxidation was assessed in MOLM14 cells stably overexpressing vector or PHD3 in high nutrient conditions (complete RPMI containing 1 g/L glucose) or low nutrient conditions (serum-free RPMI containing 0.2 g/L glucose) (n = 3). **h,** Growth curves of MOLM14 cells stably overexpressing empty vector or PHD3 (n=3), grown in complete media. **$p < 0.01$, ***$p < 0.001$. Error bars indicate SEM.

inhibition was more strongly linked to PHD3 status than to classification as AML or CML. A CML cell line with low PHD3 expression, KU812, was in fact sensitive to treatment with etomoxir and more closely mimicked another low-PHD3 AML cell line (NB4) rather than a high-PHD3 CML line (K562) (Figure 3.6 e-f).

Our findings suggest PHD3 serves as a metabolic toggle to repress FAO under high nutrient conditions (Figure 3.4 f-g). Therefore, we assessed whether this nutrient switch is defective in AML cells with low PHD3 expression. Indeed, MOLM14 cells, which are almost entirely deficient of PHD3 expression, show a loss of sensitivity to external nutrient cues and display consistently elevated FAO under both high and low nutrient conditions (Figure 3.6 g). Strikingly, restoring PHD3 levels via overexpression reestablishes sensitivity to nutrient status and enables repression of FAO under high nutrient conditions (Figure 3.6 g). Overexpression of PHD3 in low-PHD3 AML cells also decreases cancer cell proliferation, demonstrating the susceptibility of tumor cells with low PHD3 to inhibition of FAO (Figure 3.6 h). Collectively, our data show low PHD3 expression in AML indicates a loss of metabolic plasticity, sustained elevation of FAO and susceptibility to treatment with pharmacological inhibitors of FAO.

Discussion

In this work, we elucidate a novel mechanism by which PHD3 directly regulates fatty acid oxidation: via hydroxylation and activation of ACC2. Mechanistically, PHD3 induces a switch in fat metabolism by hydroxylating residue P450 of ACC2 to boost its ATP affinity and enzymatic activity. P450 is in close proximity to the ATP-binding site of ACC2, suggesting hydroxylation causes a conformational change significant enough to alter this binding site and allow greater access to or retention of ATP. In addition, we

found PHD3 activates ACC2 under high nutrient conditions in order to limit FAO. Reduced PHD3 activity toward ACC2 under low nutrient conditions allows FAO to increase. We show cancer cells with very low levels of endogenous ACC2 are deficient in this nutrient switch and show persistently sustained levels of high FAO. Furthermore, we reveal that loss of PHD3 expression is a common feature of AML patient samples compared to healthy marrow. Low PHD3 expression contributes to a dramatic boost in fatty acid consumption that is necessary for AML cell survival. We find that low PHD3 expression indicates cancer cell vulnerability to FAO inhibition upon treatment with pharmacological FAO inhibitors or upon overexpression of PHD3.

The PHD3/ACC2 axis could be explored as a way the cell couples metabolic status with fat oxidation. This hypothesis is in line with previous reports suggesting sensitivity of PHD3 to high levels of α-ketoglutarate, or more generally to a high nutrient state that may be restored by addition of α-ketoglutarate. Addition of cell-permeable α-ketoglutarate restored PHD activity in cancer cells where PHDs were otherwise inhibited[48]. Further, treating mouse xenografts with cell-permeable α-ketoglutarate inhibited growth in a PHD3-dependent mechanism[49]. Thus PHD3 sensitivity to nutrient levels may have important roles in cancer biology. In this study, we highlight the ability of PHD3 to respond to the nutrient state of the cell and adjust the level of FAO accordingly. PHD3 contributes to a metabolic toggle that limits FAO when nutrients are abundant, thus enabling fuel conservation and metabolic efficiency. Low PHD3 activity under nutrient-deprived conditions contributes to amplification of FAO. Future studies may reveal whether the PHD3 response to nutrient status occurs downstream of transcriptional changes, post-translational modification, allosteric regulation or some

combination of these factors. Along these lines, further studies are also needed to identify how hydroxylation by PHD3 and phosphorylation by AMPK might cooperate to co-regulate ACC2 under various nutrient stimuli.

Finally, this study illuminates PHD3 as a fundamental regulator and predictor of the level of FAO in cancer. We find PHD3 presents a metabolic barrier to fatty acid utilization in cancer. Accordingly, reduced PHD3 expression- a common feature of AML- amplifies fatty acid consumption and to enable sustained FAO that bypasses the metabolic toggle normally regulated by PHD3. Loss of the PHD3/ACC axis thus boosts FAO in cancer, but also indicates a metabolic liability that could be targeted in cancer treatment. We show inhibition of FAO has dramatic cytotoxic effects in hematological malignancies characterized by low PHD3 expression. These data may have implications for future therapeutic strategies targeting lipid catabolism in a broad range of cancers. In addition to low PHD3 expression in AML, PHD3 is also silenced in multiple tumor types with links to high fatty acid dependency including prostate, colorectal and invasive breast cancer[50-52]. Based on the knowledge of the regulatory axis identified here, PHD3 expression could be considered as a biomarker in cancer to distinguish patients that may be successfully treated with FAO inhibitors, thus moving the field toward metabolically based treatment options in the future.

Acknowledgments

We thank Elma Zaganjor and Daniel Santos for technical assistance. We thank Qing Zhang for assistance in setting up the in vitro hydroxylation assay. We thank Peppi Karppinen at the University of Oulu, Finland, for recombinant PHD3. We thank Oliver Hankinson at the University of California, Los Angeles, for ARNT-/- hepatoma cells and

Stuart Orkin at the Dana Farber Cancer Institute/HMS for KU812 leukemia cells. This work is funded in part by the Alexander and Margaret Stewart Trust Grant. N.J.G. is supported by the National Science Foundation Graduate Research Fellowship Grant 1000087636 and NIH Training Grant T32 GM007306. S.G. is supported by NIH grant GM67945. W.G.K. is a Howard Hughes Medical Institute (HHMI) investigator and is supported by grants from the NIH. M.C.H. is supported by NIH Grant AG032375, the Glenn Foundation for Medical Research and the American Cancer Society New Scholar Award.

Materials and Methods

Reagents and constructs. For transient overexpression studies, Fugene 6 (Roche) was used to transfect 293T cells. ARNT -/- mouse hepatoma cells were transfected with Fugene HD. pcDNA3.1 empty vector and constructs containing HA-PHD1, PHD2 and PHD3 were previously described[53]. HA-PHD3 pcDNA 3.1 point mutants were generated using the QuikChange II Site-Directed Mutagenesis Kit (Agilent). ACC2 cDNA in pENTR223 vector was obtained from the Dana Farber/ Harvard Cancer Center Resource Core. For transient overexpression, ACC2 cDNA was cloned into pDEST vector (Wader Harper lab at Harvard Medical School) using Gateway LR Clonase II Enzyme Mix according to manufacturer's instructions. Briefly, 10 μl reactions containing 150 ng ACC2 pENTR223, 150 ng pDEST vector and 2 μl Clonase in TE buffer (pH 8.0) were incubated at 25˚ for 2 hr. ACC2 point mutants were generated using the QuikChange II XL Site-Directed Mutagenesis Kit (Agilent). Mutagenesis primers are listed below. For stable overexpression via retroviral infection, the HA-PHD3 construct was cloned from pCDNA3.1 into the pBABE puro vector.

MOLM14 cells were retrovirally infected via spin infection. 300,000 cells were resuspended in 2 ml of complete media supplemented with polybrene, and 500 μl virus was added. Cells were centrifuged at 37°C for 1 hr at 2250 rpm, then re-plated in fresh media in a 6-well plate.

For transient knockdown, cells were transfected with 22.5 nM siRNA and Dharmafect 1 Transfection Reagent (Dharmacon) according to manufacturer's instructions. Cells were transfected with siGENOME SMARTpool EGLN3 siRNA or control Non-Targeting siRNA Pool #2 (Dharmacon).

For stable knockdown, lentiviral shRNA against PHD3 were obtained from The RNAi Consortium at the Broad Institute/Harvard. pLKO empty vector was used as non-silencing control. Stable knockdown cell lines were generated following the Consortium instructions. Target sequences for shRNA are listed below. In experiments using one shRNA against PHD3, shPHD3.2 was used.

Primers for Mutagenesis

Point mutant	**Primer**
ACC2 P450A	F AGAAGCTTTGATCATCAATGCAAAACCAATTCTTTCTGCTGC
	R GCAGCAGAAAGAATTGGTTTTGCATTGATGATCAAAGCTTCT
ACC2 P343A	F CCGCCTGCACGGCGATTCTCTTGGC
	R GCCAAGAGAATCGCCGTGCAGGCGG
ACC2 P2131A	F GTAGGCTGAGTCTGCGAACCACACCTGTC
	R GACAGGTGTGGTTCGCAGACTCAGCCTAC
ACC2 P450G	F GGCAGCAGAAAGAATTGGTTTTGGATTGATGATCAAAGCTTCTGA
	R TCAGAAGCTTTGATCATCAATCCAAAACCAATTCTTTCTGCTGCC
PHD3 H196A	F CAGATCGTAGGAACCCAGCCGAAGTGCAGCCCT
	R AGGGCTGCACTTCGGCTGGGTTCCTACGATCTG
PHD3 R206K	F GCCCTCTTACGCAACCAAATATGCTATGACTGTCT
	R AGACAGTCATAGCATATTTGGTTGCGTAAGAGGGC

shRNA Target Sequences

Name	Clone ID	Target Sequence
shPHD3.1	TRCN0000001048	CACCTGCATCTACTATCTGAA
shPHD3.2	TRCN0000001050	GTGGCTTGCTATCCGGGAAAT

Cell culture. 293T cells and 786-O VHL$^{-/-}$ cells were cultured in 4.5 g/L glucose DMEM (Invitrogen) supplemented with 10% FBS and penicillin/streptomycin. Low glucose DMEM contained 1 g/L glucose. ARNT-deficient mouse hepatoma c4 (B13NBii1) cells previously derived from Hepa c1c7 cells[54, 55] were cultured in Minimum Essential Media alpha (Invitrogen) supplemented with 10% heat-inactivated FBS and penicillin/streptomycin. K562, MOLM14, THP1, KU812 and NB4 cells were maintained in RPMI 1640 media (Invitrogen) supplemented with 10% FBS and penicillin/streptomycin. KG1 cells were maintained in IMDM (Invitrogen) supplemented with 20% FBS and penicillin/streptomycin. HepG2 cells were cultured in Minimum Essential Medium Eagle (Sigma) supplemented with 10% FBS, penicillin/streptomycin, 1% sodium pyruvate and 1% non-essential amino acids. All cell lines were tested with the Universal Mycoplasma Detection Kit (ATCC) to ensure absence of mycoplasma.

Quantitative RT-PCR analysis. RNA was isolated by extraction with Trizol according to manufacturer instructions (Invitrogen). cDNA was synthesized using iScript cDNA synthesis kit (BioRad). Quantitative real-time PCR was performed with Sybr Green I Mastermix (Roche) or Sybr Green Fast Mix (Quanta Biosciences) on a Roche Lightcycler 480 and analyzed by using $\Delta\Delta C_t$ calculations. qPCR analyses in human cell lines are relative to the reference gene B2M. qPCR analyses in mouse ARNT -/- hepatoma cell line are relative to RPS4X. Primer sequences are provided below.

Gene	Primer
Human	
PHD1	F ACGGGCTCGGGTACGTAAG

	R CCCAGTTCTGATTCAGGTAATAGATACA
PHD2	F GACCTGATACGCCACTGTAACG
	R CCCGGATAACAAGCAACCAT
PHD3	F ATACTACGTCAAGGAGAGGT
	R TCAGCATCAAAGTACCAGA
B2M	F AGATGAGTATGCCTGCCGTGTGAA
	R TGCTGCTTACATGTCTCGATCCCA
ACC1	F ATCCCGTACCTTCTTCTACTG
	R CCCAAACATAAGCCTTCACTG
ACC2	F CTCTGACCATGTTCGTTCTC
	R ATCTTCATCACCTCCATCTC
CPT1a	F GATTTTGCTGTCGGTCTTGG
	R CTCTTGCTGCCTGAATGTGA
CPT1b	F ATTCCCACCGCGGAAGGTGC
	R GCAGCCTGGGGGCAGTCTTG
ACADM	F TCATTGTGGAAGCAGATACCC
	R CAGCTCCGTCACCAATTAAAAC
LIPG	F TGTGGAAGGAGTTTCGCAG
	R GGGATATGCTGGTGTTCTCAG
PGK1	F CCACTTGCTGT GCCAAATGGA
	R GAAGGACTTTACCTTCCAGGA
HK2	F GATTGTCCGTAACATTCTCATCGA
	R TGTCTTGAGCCGCTCTGAGAT

Mouse

RPS4X	F ACCCTGCTGGGTTTATGGATGTCA
	R TACGATGAACAGCAAAGCGACCCT
PHD3	F CAGACCGCAGGAATCCACAT
	R TTCAGCATCGAAGTACCAGACAGT

Immunoprecipitation, Western blotting and antibodies. Western blotting was performed using antibodies against ACC (Cell Signaling Technologies (CST) no. 3676), ACC1 isoform (CST no. 4190), ACC2 isoform (CST no. 8578), HA (CST no. 2367), hydroxyproline (Abcam no. ab37067), tubulin (Sigma no. T5168), HIF1α (BD no. 610959), HIF2α (CST no. 7096), actin (Sigma no. A2066), LSD1 (CST no. 2139) and PHD3 (Novus Biologicals no. NB100-139). For immunoprecipitations of transiently overexpressed HA-tagged proteins, lysates were immunoprecipitated using EZview anti-HA Affinity Gel (Sigma no. E6779). For endogenous immunoprecipitations, lysates were

immunoprecipitated with ACC antibody (CST no. 3767) or ACC2 antibody (CST no. 8578) and EZview Red Protein G Affinity Gel (Sigma no. E3403).

Mass spectrometry. To identify hydroxylated proline sites, ACC2 was transiently overexpressed in 293T cells. 48 hr later, cell lysates were collected and ACC2 was immunoprecipitated with ACC2 antibody and Protein G Affinity Gel described above. Bound material was washed and separated by SDS-PAGE. The Coomassie stained band was excised, analyzed by LC-MS2 and searched against the Uniprot Human database (downloaded August 2011) using Sequest with proline hydroxylation set as a variable modification (+15.9949 molecular weight shift).

In vitro hydroxylation assay. The in vitro hydroxylation assay was modified from a previously described assay based on the fact that hydroxylation by PHDs results in decarboxylation of α-ketoglutarate to form carbon dioxide[56]. Briefly, 250 μl reactions were performed in glass vials sealed with rubber stoppers and parafilm wax. Reaction mixtures containing 12.5 nmol synthetic peptide (Peptide 2.0), 50 mM Tris/HCl (pH 7.8), 2 mg/ml BSA, 4200 U/ml catalase, 0.1 mM DTT, 2 mM ascorbate, 500 μM $FeSO4{\cdot}7H_2O$, 0.02 μmol [1-^{14}C]α-ketoglutarate (Perkin Elmer) and 1.2 μg recombinant PHD3 were incubated at 37˚ for 30 min. Reactions were stopped by injection of 0.25 ml of 1 M KH_2PO_4 (pH 5) into vials. Vials were agitated on slow speed for 30 min at room temperature to allow capture of [^{14}C]CO_2 onto solubilized Whatman paper positioned at the top of the vials. CPM were measured by scintillation counts on filter paper.

Peptides for In Vitro Hydroxylation

Proline	**Sequence**
450	ERIGFPLMIKASEGGGGK
2131	AGQVWFPDSAYKTAQ
966	ARLELDDPSKVHPAE

ACC activity assay. Reactions were performed as previously described[57], with the exception of using 16.7 mM $MgCl_2$ instead. 50 μg protein lysate was used for each reaction. Following addition of 1 N HCl to quench reactions and convert remaining [^{14}C]bicarbonate (American Radiolabeled Chemicals) to CO_2, reactions were evaporated 2 hr at 60˚ and 15 min at 85˚ in a thermo shaker. ACC activity was calculated as incorporation of [^{14}C]bicarbonate into [^{14}C]malonyl CoA (the acid and heat stable product) as measured by scintillation counting.

ATP binding assays. ATP immunoprecipitations were performed using the ATP AffiPur Kit (Jena Bioscience), which contained aminophenyl-ATP-Agarose, C10-spacer. Procedure was done according to manufacturer's instructions, except for the following distinction. Transiently transfected 293T cells were lysed in ACC activity assay buffer[57] to promote native protein folding. Following dialysis to remove endogenous ATP and immunoprecipitation with ATP-affinity resin, bound material was washed and eluted by addition of sample buffer containing beta-mercaptoethanol. Samples were boiled 5 min at 95˚ for analysis by Western blot.

Fatty acid oxidation. For FAO assays, cells in 12 well-plates were pre-incubated with 100 μM palmitate or hexanoate and 1 mM carnitine for 4 hr in serum-free low glucose media, unless otherwise noted. Cells were then changed to 600 μl media containing 1 μCi [9,10(n)-^{3}H]palmitic acid (GE Healthcare) or 1.8 μCi n-[5,6-^{3}H]hexanoic acid (American Radiolabeled Chemicals) and 1 mM carnitine for 2 hr. The medium was collected and eluted in columns packed with DOWEX 1X2-400 ion exchange resin (Sigma) to analyze the released $^{3}H_2O$, formed during oxidation of [^{3}H]palmitate. FAO in complete media indicates media including serum was used for pre-incubation and FAO analysis. Basal

FAO indicates cells were not pre-incubated with fatty acids prior to FAO analysis. For all FAO experiments, counts per minute (CPM) were normalized to protein content in cell lysates.

Lipogenesis. Lipogenesis was performed as previously described[58] with the following modifications. Cells were pulsed for 4 hr with 4 μCi [^{14}C]acetate ± 20 μM C75, then lipids were extracted. Scintillation counts were normalized to protein concentration in parallel plates.

Drug treatment and PI staining. Cells were treated 96 hr with a range of doses of etomoxir (Cayman Chemical) or ranolazine dihydrochloride (VWR/Selleck Chemicals) or vehicle. Fresh etomoxir was spiked in at 24, 48 and 72 hr. Fresh ranolazine was spiked in at 48 hr. Dosing schedules were determined by identifying the minimum number of times drug must be re-added to observe an effect on cell viability. Cell viability at 96 hr was determined by staining cells with 1 μg/ml propidium iodide (Sigma) in PBS and flow cytometry on the BD LSR-II analyzer.

Growth rates. MOLM14 cells were plated in the wells of a 24 well plate (50,000 cells/well). At indicated times, cells were counted on the Beckman Z1 Coulter Counter.

Molecular modeling. Using CCP4mg molecular graphic software, the biotin-carboxylase domain of human ACC2 (PDB: 3JRW) was superposed with the *e. coli* biotin-carboxylase domain bound to ATP (PDB: 1DV2) to highlight the likely position of ATP in the catalytic site of human ACC2.

Statistical analysis. Unpaired two-tailed Student's t tests were used. All experiments were performed at least two to three times.

References

1. Cantor, J. R., and Sabatini, D. M. (2012). Cancer Cell Metabolism: One Hallmark, Many Faces. Cancer Discovery *2*, 881–898.

2. DeBerardinis, R. J., Lum, J. J., Hatzivassiliou, G., and Thompson, C. B. (2008). The Biology of Cancer: Metabolic Reprogramming Fuels Cell Growth and Proliferation. Cell Metabolism *7*, 11–20.

3. Ward, P. S., and Thompson, C. B. (2012). Metabolic Reprogramming: A Cancer Hallmark Even Warburg Did Not Anticipate. Cancer Cell *21*, 297–308.

4. Mullen, A. R., and DeBerardinis, R. J. (2012). Genetically-defined metabolic reprogramming in cancer. Trends in Endocrinology & Metabolism *23*, 552–559.

5. Wallace, D. C. (2012). Mitochondria and cancer. Nat Rev Cancer *12*, 685–698.

6. Carracedo, A., Cantley, L. C., and Pandolfi, P. P. (2013). Cancer metabolism: fatty acid oxidation in the limelight. Nat Rev Cancer *13*, 227–232.

7. Kaelin, W. G., Jr., and Ratcliffe, P. J. (2008). Oxygen Sensing by Metazoans: The Central Role of the HIF Hydroxylase Pathway. Molecular Cell *30*, 393–402.

8. Gorres, K. L., and Raines, R. T. (2010). Prolyl 4-hydroxylase. Critical Reviews in Biochemistry and Molecular Biology *45*, 106–124.

9. Tong, L. (2005). Acetyl-coenzyme A carboxylase: crucial metabolic enzyme and attractive target for drug discovery. Cellular and Molecular Life Sciences (CMLS) *62*, 1784–1803.

10. Liu, Y., Zuckier, L. S., and Ghesani, N. V. (2013). Dominant uptake of fatty acid over glucose by prostate cells: a potential new diagnostic and therapeutic approach. Anticancer Research, 1–6.

11. Schafer, Z. T., Grassian, A. R., Song, L., Jiang, Z., Gerhart-Hines, Z., Irie, H. Y., Gao, S., Puigserver, P., and Brugge, J. S. (2009). Antioxidant and oncogene rescue of metabolic defects caused by loss of matrix attachment. Nature *461*, 109–113.

12. Caro, P., Kishan, A. U., Norberg, E., Stanley, I. A., Chapuy, B., Ficarro, S. B., Polak, K., Tondera, D., Gounarides, J., Yin, H., et al. (2012). Metabolic Signatures Uncover Distinct Targets in Molecular Subsets of Diffuse Large B Cell Lymphoma. Cancer Cell *22*, 547–560.

13. Jeon, S.-M., Chandel, N. S., and Hay, N. (2012). AMPK regulates NADPH homeostasis to promote tumour cell survival during energy stress. Nature *485*, 661–665.

14. Zaugg, K., Yao, Y., Reilly, P. T., Kannan, K., Kiarash, R., Mason, J., Huang, P., Sawyer, S. K., Fuerth, B., Faubert, B., et al. (2011). Carnitine palmitoyltransferase

1C promotes cell survival and tumor growth under conditions of metabolic stress. Genes & Development *25*, 1041–1051.

15. Samudio, I., Harmancey, R., Fiegl, M., Kantarjian, H., Konopleva, M., Korchin, B., Kaluarachchi, K., Bornmann, W., Duvvuri, S., Taegtmeyer, H., et al. (2010). Pharmacologic inhibition of fatty acid oxidation sensitizes human leukemia cells to apoptosis induction. J. Clin. Invest. *120*, 142–156.

16. Finley, L. W. S., Carracedo, A., Lee, J., Souza, A., Egia, A., Zhang, J., Teruya-Feldstein, J., Moreira, P. I., Cardoso, S. M., Clish, C. B., et al. (2011). SIRT3 Opposes Reprogramming of Cancer Cell Metabolism through HIF1α Destabilization. Cancer Cell *19*, 416–428.

17. Losman, J. A., and Kaelin, W. G. (2013). What a difference a hydroxyl makes: mutant IDH, (R)-2-hydroxyglutarate, and cancer. Genes & Development *27*, 836–852.

18. Masson, N., and Ratcliffe, P. J. (2014). Hypoxia signaling pathways in cancer metabolism: the importance of co-selecting interconnected physiological pathways. Cancer Metab *2*, 3.

19. Vander Heiden, M. G., Lunt, S. Y., Dayton, T. L., Fiske, B. P., Israelsen, W. J., Mattaini, K. R., Vokes, N. I., Stephanopoulos, G., Cantley, L. C., Metallo, C. M., et al. (2012). Metabolic Pathway Alterations that Support Cell Proliferation. Cold Spring Harbor Symposia on Quantitative Biology *76*, 325–334.

20. Luo, W., Hu, H., Chang, R., Zhong, J., Knabel, M., O'Meally, R., Cole, R. N., Pandey, A., and Semenza, G. L. (2011). Pyruvate kinase M2 is a PHD3-stimulated coactivator for hypoxia-inducible factor 1. Cell *145*, 732–744.

21. Berra, E., Benizri, E., Ginouvès, A., Volmat, V., Roux, D., and Pouysségur, J. (2003). HIF prolyl‐hydroxylase 2 is the key oxygen sensor setting low steady‐state levels of HIF‐1α in normoxia. The EMBO Journal *22*, 4082–4090.

22. Koivunen, P., Hirsilä, M., Remes, A. M., Hassinen, I. E., Kivirikko, K. I., and Myllyharju, J. (2007). Inhibition of hypoxia-inducible factor (HIF) hydroxylases by citric acid cycle intermediates: possible links between cell metabolism and stabilization of HIF. J. Biol. Chem. *282*, 4524–4532.

23. Kikuchi, D., Minamishima, Y. A., and Nakayama, K. (2014). Prolyl-hydroxylase PHD3 interacts with pyruvate dehydrogenase (PDH)-E1β and regulates the cellular PDH activity. Biochemical and Biophysical Research Communications *451*, 288–294.

24. Brownsey, R. W., Boone, A. N., Elliott, J. E., Kulpa, J. E., and Lee, W. M. (2006). Regulation of acetyl-CoA carboxylase. Biochem. Soc. Trans. *34*, 223–227.

25. Saddik, M., Gamble, J., Witters, L. A., and Lopaschuk, G. D. (1993). Acetyl-CoA

carboxylase regulation of fatty acid oxidation in the heart. J. Biol. Chem. *268*, 25836–25845.

26. Abu-Elheiga, L., Oh, W., Kordari, P., and Wakil, S. J. (2003). Acetyl-CoA carboxylase 2 mutant mice are protected against obesity and diabetes induced by high-fat/high-carbohydrate diets. Proc. Natl. Acad. Sci. U.S.A. *100*, 10207–10212.

27. Bruick, R. K. (2001). A Conserved Family of Prolyl-4-Hydroxylases That Modify HIF. Science *294*, 1337–1340.

28. Rantanen, K., Pursiheimo, J., Hogel, H., Himanen, V., Metzen, E., and Jaakkola, P. M. (2008). Prolyl Hydroxylase PHD3 Activates Oxygen-dependent Protein Aggregation. Molecular Biology of the Cell *19*, 2231–2240.

29. Loenarz, C., and Schofield, C. J. (2011). Physiological and biochemical aspects of hydroxylations and demethylations catalyzed by human 2-oxoglutarate oxygenases. Trends in Biochemical Sciences *36*, 7–18.

30. Almarza-Ortega, D. B. (1997). Human Acetyl-CoA Carboxylase 2. Molecular Cloning, Characterization, Chromosomal Mapping, and Evidence for Two Isoforms. Journal of Biological Chemistry *272*, 10669–10677.

31. Cho, Y. S., Lee, Il, J., Shin, D., Kim, H. T., Jung, H. Y., Lee, T. G., Kang, L.-W., Ahn, Y.-J., Cho, H.-S., and Heo, Y.-S. (2010). Molecular mechanism for the regulation of human ACC2 through phosphorylation by AMPK. Biochemical and Biophysical Research Communications *391*, 187–192.

32. Thoden, J. B. (2000). Movement of the Biotin Carboxylase B-domain as a Result of ATP Binding. Journal of Biological Chemistry *275*, 16183–16190.

33. Ruderman, N., and Prentki, M. (2004). AMP kinase and malonyl-CoA: targets for therapy of the metabolic syndrome. Nat Rev Drug Discov *3*, 340–351.

34. Fullerton, M. D., Galic, S., Marcinko, K., Sikkema, S., Pulinilkunnil, T., Chen, Z.-P., O'Neill, H. M., Ford, R. J., Palanivel, R., O'Brien, M., et al. (2013). Single phosphorylation sites in Acc1 and Acc2 regulate lipid homeostasis and the insulin-sensitizing effects of metformin. Nat Med *19*, 1649–1654.

35. Yoon, M. J. (2006). Adiponectin Increases Fatty Acid Oxidation in Skeletal Muscle Cells by Sequential Activation of AMP-Activated Protein Kinase, p38 Mitogen-Activated Protein Kinase, and Peroxisome Proliferator-Activated Receptor. Diabetes *55*, 2562–2570.

36. Laurent, G., German, N. J., Saha, A. K., de Boer, V. C. J., Davies, M., Koves, T. R., Dephoure, N., Fischer, F., Boanca, G., Vaitheesvaran, B., et al. (2013). SIRT4 Coordinates the Balance between Lipid Synthesis and Catabolism by Repressing Malonyl CoA Decarboxylase. Molecular Cell *50*, 686–698.

37. Gerhart-Hines, Z., Rodgers, J. T., Bare, O., Lerin, C., Kim, S. H., Mostoslavsky, R., Alt, F. W., Wu, Z., and Puigserver, P. (2007). Metabolic control of muscle mitochondrial function and fatty acid oxidation through SIRT1/PGC-1alpha. The EMBO Journal *26*, 1913–1923.

38. Iliopoulos, O., Levy, A. P., Jiang, C., Kaelin, W. G., and Goldberg, M. A. (1996). Negative regulation of hypoxia-inducible genes by the von Hippel-Lindau protein. Proc. Natl. Acad. Sci. U.S.A. *93*, 10595–10599.

39. Wood, S. M., Gleadle, J. M., Pugh, C. W., Hankinson, O., and Ratcliffe, P. J. (1996). The role of the aryl hydrocarbon receptor nuclear translocator (ARNT) in hypoxic induction of gene expression. Studies in ARNT-deficient cells. J. Biol. Chem. *271*, 15117–15123.

40. Liu, Y. (2006). Fatty acid oxidation is a dominant bioenergetic pathway in prostate cancer. Prostate Cancer Prostatic Dis *9*, 230–234.

41. Holla, V. R., Wu, H., Shi, Q., Menter, D. G., and DuBois, R. N. (2011). Nuclear Orphan Receptor NR4A2 Modulates Fatty Acid Oxidation Pathways in Colorectal Cancer. Journal of Biological Chemistry *286*, 30003–30009.

42. Estañ, M. C., Calviño, E., Calvo, S., Guillén-Guío, B., Boyano-Adánez, M. D. C., de Blas, E., Rial, E., and Aller, P. (2014). Apoptotic Efficacy of Etomoxir in Human Acute Myeloid Leukemia Cells. Cooperation with Arsenic Trioxide and Glycolytic Inhibitors, and Regulation by Oxidative Stress and Protein Kinase Activities. PLoS ONE *9*, e115250.

43. Ramaswamy, S., Tamayo, P., Rifkin, R., Mukherjee, S., Yeang, C. H., Angelo, M., Ladd, C., Reich, M., Latulippe, E., Mesirov, J. P., et al. (2001). Multiclass cancer diagnosis using tumor gene expression signatures. Proc. Natl. Acad. Sci. U.S.A. *98*, 15149–15154.

44. Valk, P. J. M., Verhaak, R. G. W., Beijen, M. A., Erpelinck, C. A. J., Barjesteh van Waalwijk van Doorn-Khosrovani, S., Boer, J. M., Beverloo, H. B., Moorhouse, M. J., van der Spek, P. J., Löwenberg, B., et al. (2004). Prognostically useful gene-expression profiles in acute myeloid leukemia. N. Engl. J. Med. *350*, 1617–1628.

45. Andersson, A., Ritz, C., Lindgren, D., Edén, P., Lassen, C., Heldrup, J., Olofsson, T., Råde, J., Fontes, M., Porwit-MacDonald, A., et al. (2007). Microarray-based classification of a consecutive series of 121 childhood acute leukemias: prediction of leukemic and genetic subtype as well as of minimal residual disease status. Leukemia *21*, 1198–1203.

46. Holubarsch, C. J. F., Rohrbach, M., Karrasch, M., Boehm, E., Polonski, L., Ponikowski, P., and Rhein, S. (2007). A double-blind randomized multicentre clinical trial to evaluate the efficacy and safety of two doses of etomoxir in comparison with placebo in patients with moderate congestive heart failure: the

ERGO (etomoxir for the recovery of glucose oxidation) study. Clin. Sci. *113*, 205–212.

47. Nash, D. T., and Nash, S. D. (2008). Ranolazine for chronic stable angina. Lancet *372*, 1335–1341.

48. MacKenzie, E. D., Selak, M. A., Tennant, D. A., Payne, L. J., Crosby, S., Frederiksen, C. M., Watson, D. G., and Gottlieb, E. (2007). Cell-Permeating -Ketoglutarate Derivatives Alleviate Pseudohypoxia in Succinate Dehydrogenase-Deficient Cells. Molecular and Cellular Biology *27*, 3282–3289.

49. Tennant, D. A., and Gottlieb, E. (2010). HIF prolyl hydroxylase-3 mediates alpha-ketoglutarate-induced apoptosis and tumor suppression. J Mol Med *88*, 839–849.

50. Rawluszko, A. A., Bujnicka, K. E., Horbacka, K., Krokowicz, P., and Jagodziński, P. P. (2013). Expression and DNA methylation levels of prolyl hydroxylases PHD1, PHD2, PHD3 and asparaginyl hydroxylase FIH in colorectal cancer. BMC Cancer *13*, 526.

51. Huang, K. T., Mikeska, T., Dobrovic, A., and Fox, S. B. (2010). DNA methylation analysis of the HIF-1α prolyl hydroxylase domain genes PHD1, PHD2, PHD3 and the factor inhibiting HIF gene FIH in invasive breast carcinomas. Histopathology *57*, 451–460.

52. Place, T. L., Fitzgerald, M. P., Venkataraman, S., Vorrink, S. U., Case, A. J., Teoh, M. L. T., and Domann, F. E. (2011). Aberrant Promoter CpG Methylation Is a Mechanism for Impaired PHD3 Expression in a Diverse Set of Malignant Cells. PLoS ONE *6*, e14617.

53. Lee, S., Nakamura, E., Yang, H., Wei, W., Linggi, M. S., Sajan, M. P., Farese, R. V., Freeman, R. S., Carter, B. D., Kaelin, W. G., Jr., et al. (2005). Neuronal apoptosis linked to EglN3 prolyl hydroxylase and familial pheochromocytoma genes: Developmental culling and cancer. Cancer Cell *8*, 155–167.

54. Numayama-Tsuruta, K., Kobayashi, A., Sogawa, K., and Fujii-Kuriyama, Y. (1997). A point mutation responsible for defective function of the aryl-hydrocarbon-receptor nuclear translocator in mutant Hepa-1c1c7 cells. Eur. J. Biochem. *246*, 486–495.

55. Matteucci, E., Modora, S., Simone, M., and Desiderio, M. A. (2003). Hepatocyte growth factor induces apoptosis through the extrinsic pathway in hepatoma cells: favouring role of hypoxia-inducible factor-1 deficiency. Oncogene *22*, 4062–4073.

56. Zheng, X., Zhai, B., Koivunen, P., Shin, S. J., Lu, G., Liu, J., Geisen, C., Chakraborty, A. A., Moslehi, J. J., Smalley, D. M., et al. (2014). Prolyl hydroxylation by EglN2 destabilizes FOXO3a by blocking its interaction with the USP9x deubiquitinase. Genes & Development *28*, 1429–1444.

57. Pulinilkunnil, T., He, H., Kong, D., Asakura, K., Peroni, O. D., Lee, A., and Kahn, B. B. (2011). Adrenergic Regulation of AMP-activated Protein Kinase in Brown Adipose Tissue in Vivo. Journal of Biological Chemistry *286*, 8798–8809.

58. Janzer, A., German, N. J., Gonzalez Herrera, K. N., Asara, J. M., Haigis, M. C., and Struhl, K. (2014). Metformin and phenformin deplete tricarboxylic acid cycle and glycolytic intermediates during cell transformation and NTPs in cancer stem cells. Proc. Natl. Acad. Sci. U.S.A. *111*, 10574–10579.

CHAPTER IV

Metformin and phenformin deplete tricarboxylic acid cycle and glycolytic intermediates during cell transformation and NTPs in cancer stem cells

Andreas Janzer*[1], Natalie J. German*[2], Karina N. Gonzalez-Herrera[2], John M. Asara[3], Marcia C. Haigis[2] and Kevin Struhl[1]

[1] Department of Biological Chemistry and Molecular Pharmacology, Harvard Medical School, Boston, MA 02115, USA; [2] Department of Cell Biology, Harvard Medical School, Boston, MA 02115, USA; [3] Department of Medicine, Division of Signal Transduction, Beth Israel Deaconess Medical Center, Boston, MA 02215, USA.

* These authors contributed equally.

This research was originally published in *PNAS*. Andreas Janzer, Natalie J. German, Karina N. Gonzalez-Herrera, John M. Asara, Marcia C. Haigis and Kevin Struhl. (2014). Metformin and phenformin deplete tricarboxylic acid cycle and glycolytic intermediates during cell transformation and NTPs in cancer stem cells. PNAS 111(29):10574-9.

This chapter is reformatted from the originally published article and is reprinted here with kind permission from the National Academy of Sciences.

 doi: 10.1073/pnas.1409844111.

Natalie German designed and analyzed all metabolomics experiments. Andreas Janzer optimized and performed cell culture. Karina Gonzalez-Herrera assisted with Nova assays. Technicians working with John Asara at the Beth Israel Deaconess Medical Center Mass Spectrometry Facility performed metabolomics profiling.

Abstract

Metformin, a first-line diabetes drug linked to cancer prevention in retrospective clinical analyses, inhibits cellular transformation and selectively kills breast cancer stem cells (CSCs). Although a few metabolic effects of metformin and the related biguanide phenformin have been investigated in established cancer cell lines, the global metabolic impact of biguanides during the process of neoplastic transformation and in CSCs is unknown. Here, we use LC/MS/MS metabolomics (>200 metabolites) to assess metabolic changes induced by metformin and phenformin in an Src-inducible model of cellular transformation and in mammosphere-derived breast CSCs. Although phenformin is the more potent biguanide in both systems, the metabolic profiles of these drugs are remarkably similar, although not identical. During the process of cellular transformation, biguanide treatment prevents the boost in glycolytic intermediates at a specific stage of the pathway and coordinately decreases tricarboxylic acid (TCA) cycle intermediates. In contrast, in breast CSCs, biguanides have a modest effect on glycolytic and TCA cycle intermediates, but they strongly deplete nucleotide triphosphates and may impede nucleotide synthesis. These metabolic profiles are consistent with the idea that biguanides inhibit mitochondrial complex 1, but they indicate that their metabolic effects differ depending on the stage of cellular transformation.

Introduction

Altered metabolism is a hallmark of malignantly transformed cells. Cancer risk is linked to metabolic syndrome, a disease state that includes obesity, type 2 diabetes, high cholesterol, and atherosclerosis. Retrospective studies of type 2 diabetes patients treated with metformin, the most widely prescribed antidiabetic drug, show a strong correlation

between drug intake and reduced tumor incidence or reduced cancer-related deaths [1–4].

In the breast lineage, metformin inhibits growth of cancer cell lines [5–7], blocks transformation in a Src-inducible cell system [8, 9], and selectively inhibits the growth of cancer stem cells (CSCs) [8]. As a consequence of its selective effects on CSCs, combinatorial therapy of metformin and standard chemotherapeutic drugs (doxorubicin, paclitaxel, and cisplatin) increases tumor regression and prolongs remission in mouse xenografts [8, 10]. In addition, metformin can decrease the chemotherapeutic dose for prolonging tumor remission in xenografts involving multiple cancer types [10].

Phenformin, a related biguanide and formerly used diabetes drug, acts as an anticancer agent in tumors including lung, lymphoma, and breast cancer with a greater potency than metformin. Phenformin mediates antineoplastic effects at a lower concentration than metformin in cell lines, a PTEN-deficient mouse model, breast cancer xenografts, and drug-induced mitochondrial impairment [11–14]. The chemical similarities of these biguanides, as well as their similar effects in diabetes and cancer, have led to the untested assumption that phenformin is essentially a stronger version of metformin.

In a Src-inducible model of cellular transformation and CSC formation, multiple lines of evidence suggest that metformin inhibits a signal transduction pathway that results in an inflammatory response [15]. In the context of atherosclerosis, metformin inhibits NF-κB activation and the inflammatory response via a pathway involving AMP kinase (AMPK) and the tumor suppressor PTEN [16, 17]. As metformin alters energy metabolism in diabetics, we speculated that metformin might block a metabolic stress response that stimulates the inflammatory pathway [15]. However, very little is known

about the metabolic changes that inhibit the inflammatory pathway.

Previous studies on metformin-induced metabolic effects in cancer have focused on single metabolic alterations or pathways in already established cancer cell lines. Metformin leads to activation of AMPK, which plays a key role in insulin signaling and energy sensing [18]. Metformin can reduce protein synthesis via mTOR inhibition [19]. In addition, metformin may directly impair mitochondrial respiration through complex I inhibition and has been described to boost glycolysis as a compensation mechanism [14, 20]. In this regard, lactic acidosis can be a side effect of metformin and phenformin treatment of diabetic patients, presumably because inhibition of complex I prevents NADH oxidation, thereby leading to a requirement for cytosolic NADH to be oxidized by the conversion of pyruvate to lactate. There is some knowledge about the metabolic effects of metformin [21, 22], but very little is known about the specific metabolic alterations linking biguanides to inhibition of neoplastic transformation.

Here, we perform a metabolomic analysis on the effects of metformin and phenformin in a Src-inducible model of transformation and in CSCs. This inducible model permits an analysis of the transition from nontransformed to transformed cells in an isogenic cell system and hence differs from analyses of already established cancer cell lines. We studied CSCs to address why this population, which is resistant to standard chemotherapeutics and hypothesized to be a major reason for tumor recurrence, is selectively inhibited by metformin. Our results indicate the metabolic effects of metformin and phenformin are remarkably similar to each other, with only a few differences. Both biguanides dramatically decrease tricarboxylic acid (TCA) cycle intermediates in the early stages of transformation, and they inhibit the boost in select

glycolytic intermediates that normally occurs with transformation along with increases in glycerol 3-phosphate and lactate, which are metabolites branching from glycolysis. Unexpectedly, in CSCs, biguanides have only marginal effects on glycolytic and TCA cycle metabolites, but they severely decrease nucleotide triphosphates. These detailed metabolic analyses provide independent support for the idea that metformin inhibits mitochondrial complex 1 [14, 20], and they indicate that the metabolic effects of biguanides depend on the stage of the cellular transformation.

Results

Phenformin inhibits morphological transformation of ER-Src cells at a lower concentration than metformin

We previously showed metformin inhibits cellular transformation using an inducible breast cancer model [8, 9]. This model involves a derivative of the spontaneous immortalized breast epithelial cell line MCF-10A [23] expressing an ER-Src fusion gene that consists of the v-Src oncogene and the ligand-binding domain of the estrogen receptor. Activation of Src via tamoxifen results in morphological transformation and the ability to form colonies in anchorage- independent growth assays [9, 24].

As phenformin appears to be a more potent anticancer drug than metformin in various cell types [11, 12, 25], we first asked whether the related biguanide phenformin could achieve this same effect with increased potency. Indeed, soft agar assays showed that treatment with metformin or phenformin for 24 h during tamoxifen-induced Src activation reduces the number of colonies to that of cells treated only with vehicle (Figure 4.1 a). Additionally, morphologic transformation due to loss of contact inhibition is suppressed by both biguanides. Phenformin shows a comparable, and perhaps stronger,

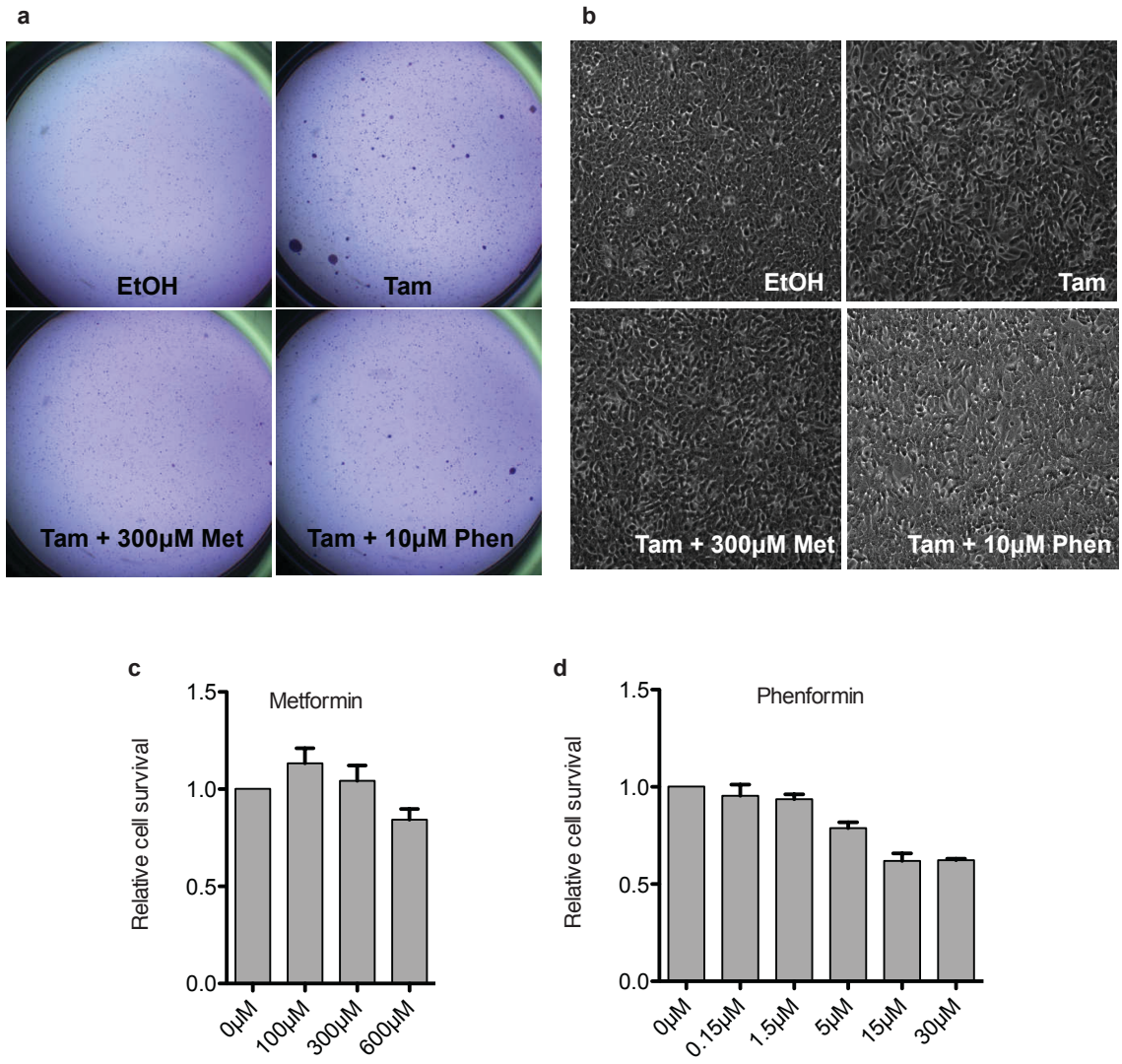

Figure 4.1 | Metformin and phenformin block malignant transformation. a-b, ERSrc cells were treated with EtOH, tamoxifen, tamoxifen + metformin, or tamoxifen + phenformin for 24 h, and soft agar assays **(a)** and morphology assays **(b)** were performed. **c-d,** Cell viability via MTT was measured after 24 h treatment of ERSrc cells with different concentrations of metformin **(c)** or phenformin **(d)**. Error bars indicate SEM.

effect, even though it is used at a 30-fold lower concentration than metformin (Figure 4.1 b). In accordance with the clinical data for diabetes treatment, phenformin is both more potent and more toxic than metformin. At the effective concentration, phenformin (10 μM) shows slightly reduced cell viability, whereas metformin (300 μM) does not affect cell survival (Figure 4.1 c and d).

Induction of cellular transformation is associated with metabolic changes typical of cancer cells

Fully transformed cancer cells commonly display the Warburg effect, characterized by a high rate of glucose consumption and lactate production [26]. Additionally, many transformed cells consume high amounts of glutamine as an additional nutrient source and consequently generate a large amount of ammonium that is secreted from the cell. In accord with these observations, analysis of media from induced ER-Src cells reveals a significant increase in glucose and glutamine uptake 24 h after Src activation (Figure 4.2 a). In addition, ammonium and lactate production are increased following Src induction (Figure 4.2 a). This switch to typical tumor cell metabolism that occurs within only 24 h of Src activation validates our inducible model for metabolic analysis of cellular transformation.

Metformin and phenformin have very similar, but nonidentical, metabolic profiles during cellular transformation

Based on their chemical relationship and a few similar effects in diabetes and cancer, it is generally assumed that phenformin is a stronger version of metformin. To address this issue in more detail and to determine the global metabolic impact of metformin and phenformin on cells undergoing transformation, we measured more than

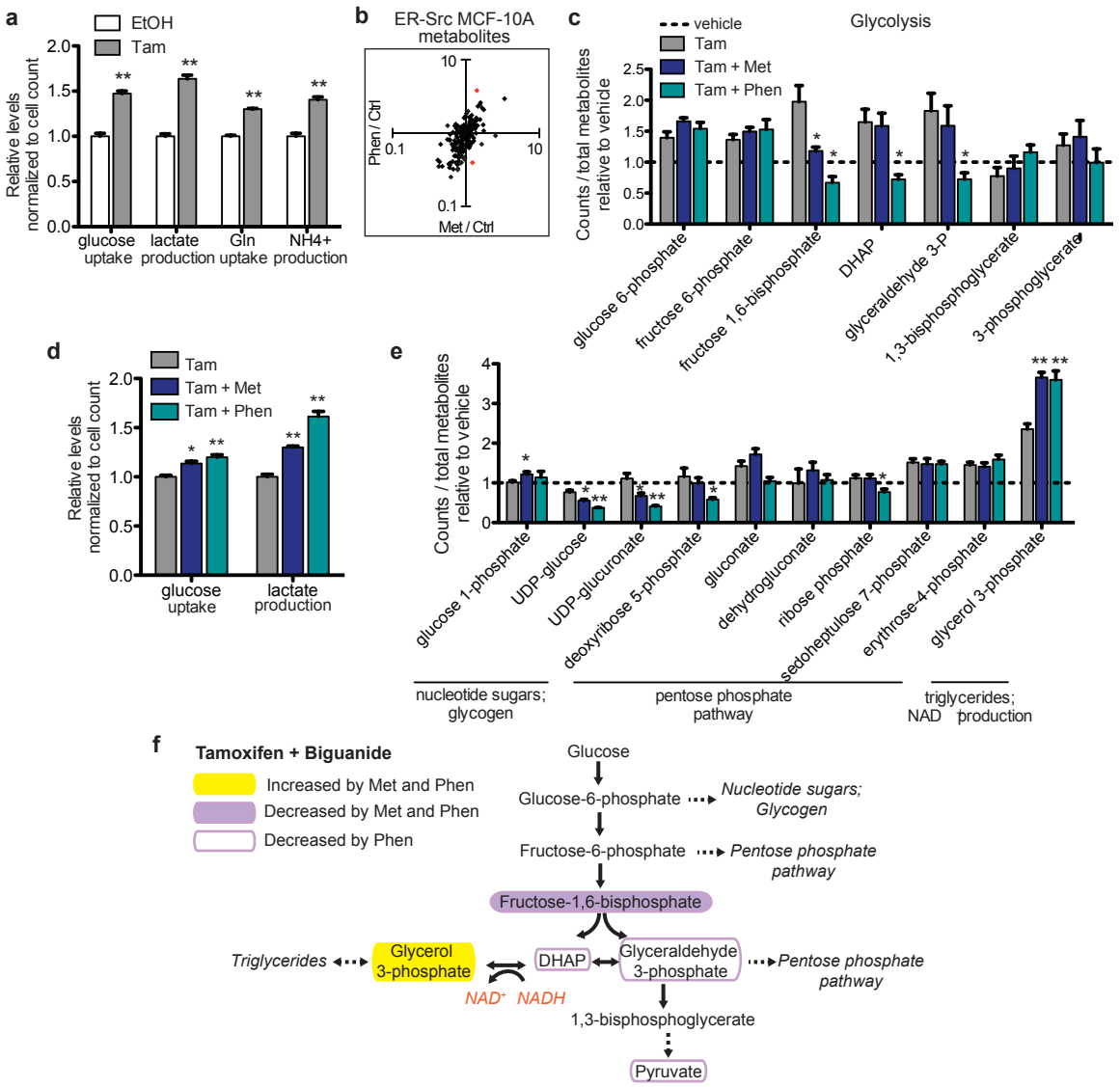

Figure 4.2 | Metformin and phenformin alter the metabolic state of the transformation process, specifically preventing an increase in some glycolytic intermediates. a, 24 h after Src induction by tamoxifen (Tam) or control treatment with ethanol (EtOH), glucose and glutamine uptake and lactate and ammonium production were measured in the media of MCF10A ERSrc cells, n = 3. **b,** To identify metformin vs. phenformin differences, fold changes of both drugs for all LS-MS/MS metabolites over the tamoxifen-only sample were determined and ratios were calculated. Red dots indicate differentially regulated metabolites outside of a 99.7% CI generated over all ratios. **c,** Relative levels of glycolytic intermediates measured with LC-MS/MS for tamoxifen ± metformin or phenformin and vehicle (ethanol)-treated samples, n = 4. **d,** Glucose uptake and lactate production were measured in the media 24 h after Src induction ± metformin , n = 3. **e,** Relative levels of metabolites branching from glycolysis with tamoxifen ± metformin or phenformin and vehicle-treated samples, n = 4. **f,** Diagram of glycolytic intermediates altered by metformin or phenformin treatment. The role of glycerol 3-phosphate production in regeneration of NAD^+ is indicated in orange. For all panels, *p < 0.05 and **p < 0.01 compared with control sample. Error bars indicate SEM.

200 metabolites by LC/MS/MS 24 h after tamoxifen treatment in the presence or absence of biguanides (Table 4.1). Fold change values for each biguanide vs. tamoxifen-only treatment were determined for all metabolites (Figure 4.2 b). Taking into account the consistently stronger potency of phenformin over metformin, the vast majority of metabolites behave similarly with the two biguanides. Only two metabolites appear to be differentially affected ($P < 0.003$), namely serine and anthranilate, and a similar analysis in a stably transformed breast cancer cell line, CAMA-1, reveals five differentially affected metabolites.

Metformin and phenformin prevent the tamoxifen-induced boost in glycolytic intermediates

To identify metabolic pathways altered by biguanides during the initial stages of transformation, we focused on significantly changed metabolites in biguanide-treated samples compared with tamoxifen-only treatment ($p < 0.05$). As expected, levels of multiple glycolytic intermediates are increased during transformation (Figure 4.2 c and Figure S4.1 a). Interestingly, increases in glycolytic intermediates are only observed for the early part of the pathway. All intermediates preceding 1,3 bisphosphoglycerate are increased during transformation, whereas this and all subsequent intermediates including pyruvate are not.

Addition of either biguanide causes a decrease in specific glycolytic intermediates, but not in the entire pathway (Figure 4.2 c). With phenformin treatment, three successive intermediates in the middle of glycolysis—fructose 1,6-bisphosphate, dihydroxyacetone phosphate (DHAP), and glyceraldehyde-3-phosphate— are significantly reduced compared with tamoxifen-only treatment and even lower than the untransformed state

Table 4.1 | Metabolites analyzed by LC-MS/MS

1-methyl-histidine
1-methyladenosine
1,3-diphosphateglycerate
2-aminooctanoic acid
2-dehydro-D-gluconate
2-deoxyglucose-6-phosphate
2-hydroxy-2-methylbutanedioic acid
2-hydroxygluterate
2-isopropylmalic acid
2-keto-isovalerate
2-ketohaxanoic acid
2-oxo-4-methylthiobutanoate
2-oxobutanoate
2,3-dihydroxybenzoic acid
2,3-diphosphoglyceric acid
3-methylphenylacetic acid
3-phospho-serine
3-phosphoglycerate
3-S-methylthiopropionate
4-aminobutyrate
4-pyridoxic acid
5-methoxytryptophan
5-methyl-THF
5-phosphoribosyl-1-pyrophosphate
6-phospho-D-gluconate
7-methylguanosine
7,8-dihydrofolate
a-ketoglutarate
acadesine
acetoacetate
acetyl-CoA
acetylcarnitine
acetyllysine
acetylphosphate
aconitate
adenine
adenosine
adenosine 5-phosphosulfate
ADP
ADP-D-glucose
alanine
allantoate
allantoin
aminoadipic acid
aminoimidazole carboxamide ribonucleotide
AMP
anthranilate
arginine
ascorbic acid
asparagine
aspartate
ATP
atrolactic acid
betaine
betaine aldehyde
biotin
carbamoyl phosphate
carnitine
CDP
CDP-choline
CDP-ethanolamine
cholesteryl sulfate
choline
citraconic acid
citrate
citrulline
CMP
coenzyme A
creatine
creatinine
CTP
cyclic-AMP
cystathionine
cysteine
cystine
cytidine
cytosine
D-erythrose-4-phosphate
D-glucarate
D-gluconate
D-glucono-lactone-6-phosphate
D-glucosamine-1-phosphate
D-glucosamine-6-phosphate
D-glyceraldehdye-3-phosphate
D-sedoheptulose-1-7-phosphate
dAMP
dATP
dCDP
dCMP
dCTP
deoxyadenosine
deoxyguanosine
deoxyinosine
deoxyribose-phosphate
deoxyuridine
dephospho-CoA
dephospho-CoA
dGDP
dGMP
dGTP
dihydroorotate
dihydroxy-acetone-phosphate
dimethylglycine
dTDP
dTMP
dTMP
dTTP
dUMP
ethanolamine
FAD
flavone
folate
fructose-1,6-bisphosphate
fructose-6-phosphate
fumarate
GDP
geranyl-PP
glucono-lactone
glucosamine
glucose-1-phosphate
glucose-6-phosphate
glutamate
glutamine
glutathione
glutathione
glutathione disulfide
glutathione disulfide
glycerate
glycerophosphocholine
glycolate
glyoxylate
GMP
GTP
guanidoacetic acid
guanine
guanosine
guanosine 5-diphosphate,3-diphosphate
hexose-phosphate
histidine
homocysteic acid
homocysteine
homoserine
hydroxyisocaproic acid
hydroxyphenylacetic acid
hydroxyphenylpyruvate
hydroxyproline
hypoxanthine
IDP
imidazole
imidazoleacetic acid
IMP
indole
indole-3-carboxylic acid
indoleacrylic acid
inosine
isocitrate
kynurenic acid
kynurenine
L-arginino-succinate
lactate
lipoate
lysine
malate
maleic acid
methionine
methionine sulfoxide
methylcysteine
methylmalonic acid
methylnicotinamide
myo-inositol
N-acetyl spermidine
N-acetyl spermine
N-acetyl-glucosamine
N-acetyl-glucosamine-1-phosphate
N-acetyl-glutamate
N-acetyl-glutamine
N-acetyl-L-alanine
N-acetyl-L-ornithine
N-carbamoyl-L-aspartate
N6-acetyl-L-lysine
NAD+
NADH
NADP+
NADPH
nicotinamide
nicotinamide ribotide
nicotinate
O-acetyl-L-serine
ornithine
orotate
orotidine-5-phosphate
oxaloacetate
p-aminobenzoate
p-hydroxybenzoate
pantothenate
phenylalanine
phenyllactic acid
phenylpropiolic acid
phosphoenolpyruvate
phosphorylcholine
pipecolic acid
proline
purine
putrescine
pyridoxamine
pyridoxine
pyroglutamic acid
pyrophosphate
pyruvate
quinolinate
riboflavin
ribose-phosphate
S-adenosyl-L-homocysteine
S-adenosyl-L-homocysteine
S-adenosyl-L-methionine
S-methyl-5-thioadenosine
S-ribosyl-L-homocysteine
S-ribosyl-L-homocysteine
sarcosine
sedoheptulose-bisphosphate
serine
shikimate
sn-glycerol-3-phosphate
spermidine
spermine
succinate
succinyl-CoA
taurine
thiamine pyrophosphate
thiamine-phosphate
threonine
thymine
trans, trans-farnesyl diphosphate
trehalose-6-phosphate
trehalose-sucrose
tryptophan
tyrosine
UDP
UDP-D-glucose
UDP-D-glucuronate
UDP-N-acetyl-glucosamine
UMP
uracil
urea
uric acid
uridine
UTP
valine
xanthine
xanthosine
xanthurenic acid

(dotted line). With metformin treatment, fructose 1,6-bisphosphate is significantly reduced, albeit to a lesser extent than with phenformin, and DHAP and glyceraldehyde-3-phosphate are slightly reduced. Neither biguanide has an effect on the earliest glycolytic intermediates that are increased during transformation nor on later glycolytic intermediates whose levels are unaffected during transformation.

The decrease in specific glycolytic intermediates is not due to a defect in glucose uptake. Analysis of cell culture media 24 h after tamoxifen treatment shows that phenformin and (to a lesser extent) metformin actually increase glucose uptake (Figure 4.2 d), consistent with previous reports that metformin increases the dependency on glycolysis [4]. Lactate production is also increased in the presence of biguanides, again with phenformin having the stronger effect (Figure 4.2 d). Thus, despite promoting increased glucose consumption and lactate production, metformin and phenformin ultimately decrease specific glycolytic intermediates, suggesting rapid glucose processing that depletes intermediates from key junctions in glycolysis.

Biguanide treatment increases glycerol 3-phosphate and lactate production during transformation

We asked whether decreased glycolytic intermediates in the presence of biguanides during transformation might be due to increased partitioning to metabolites branching from glycolysis. Surprisingly, although a number of anabolic precursors of the pentose phosphate pathway, nucleotide sugars, or glycogen synthesis are depleted with biguanide treatment, glycerol 3-phosphate is increased by both metformin and phenformin (Figure 4.2 e and f). Glycerol 3-phosphate, which is generated from the glycolytic intermediate DHAP, can serve as an intermediary between glucose and lipid metabolism. However,

analysis of ^{14}C-glucose incorporation into the lipid fraction reveals that biguanides instead decrease de novo lipogenesis (Figure S4.1 b), indicating that glycerol 3-phosphate levels are increased for an alternate purpose. As conversion of DHAP to glycerol 3-phosphate regenerates NAD^+ from NADH (shown in orange, Figure 4.2 f), we hypothesize increased glycerol 3-phosphate levels promote NAD^+ regeneration, which is required to maintain glycolysis.

Although glycerol 3-phosphate is increased with both drugs, UDP-glucose and UDP-glucuronate, branching out of glycolysis at the glucose 6-phosphate step via glucose 1-phosphate, are decreased. As UDP-glucose is a metabolic precursor for glycogen synthesis, biguanides may direct glycolytic intermediates away from glycogen synthesis, which is a nutrient storage pathway that normally occurs in cells during energy abundance. UDP-glucuronate feeds in the pentose phosphate pathway, but this pathway is not significantly affected by either biguanide (Figure 4.2 e).

Metformin and phenformin decrease the level of TCA cycle intermediates

In addition to boosting glycolysis, cancer cells must allocate nutrients toward the TCA cycle to generate ATP and intermediates necessary for macromolecule biosynthesis [27]. Along with glucose-derived pyruvate, glutamine flux contributes substantially to fueling the TCA cycle in many cancer cells. Strikingly, nearly all TCA cycle metabolites are strongly decreased with both metformin and phenformin (Figure 4.3 a and b). Decreased levels of TCA cycle intermediates correlate with decreased pyruvate (with phenformin), increased shunting of glucose-derived carbons toward lactate, and decreased levels of glutamate and (marginally) glutamine (Figure 4.3 b). Glutamine uptake is not decreased by biguanides, indicating there is no defect in glutamine transport

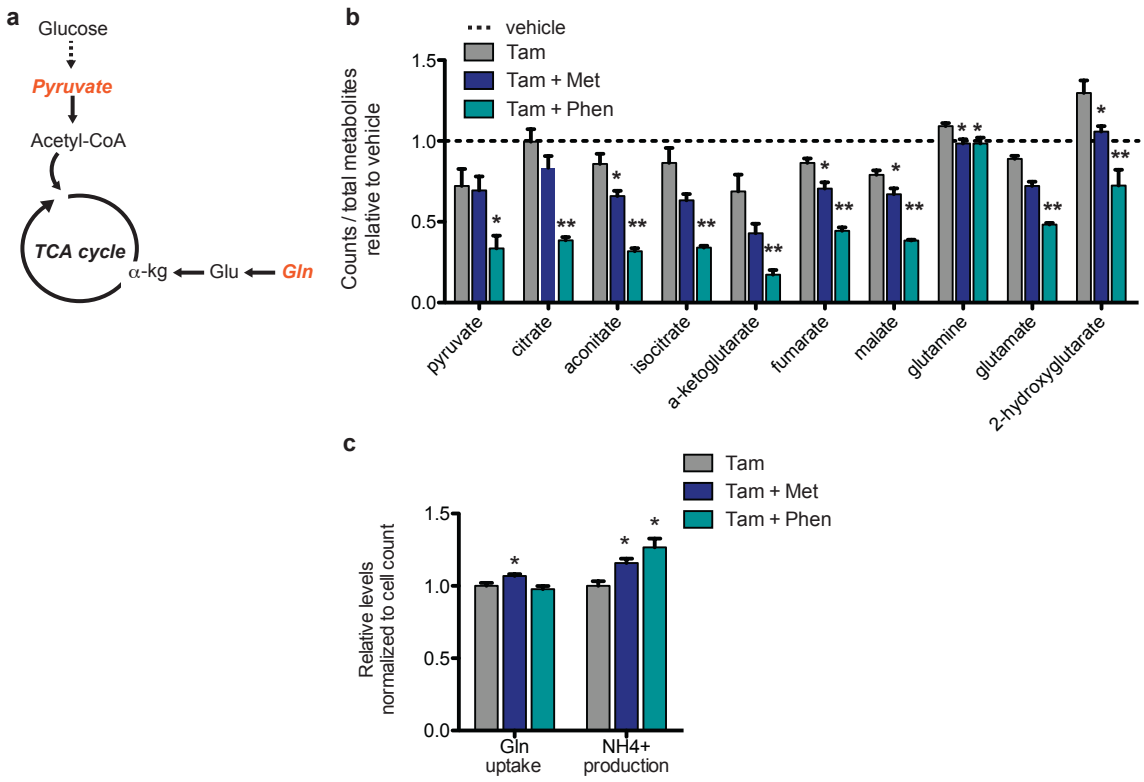

Figure 4.3 | Metformin and phenformin decrease TCA cycle intermediates. a, Schematic of the TCA cycle with key molecules fueling the cycle indicated in orange. **b,** Relative levels of TCA cycle intermediates following treatment with tamoxifen ± metformin or phenformin as measured by LC-MS/MS, n = 4. **c,** Glutamine uptake and NH4+ production were measured in the media 24 h after Src induction ± metformin or phenformin, n = 3. *p < 0.05 and **p < 0.01 compared with tamoxifen treatment alone. Error bars indicate SEM.

across the cell membrane (Figure 4.3 c). Ammonium production is increased by biguanide treatment (Figure 4.3 c), suggesting increased utilization of glutamine as an attempt to refuel the TCA cycle via anaplerosis.

Our results appear to differ from a previous report in prostate cancer suggesting that metformin does not inhibit the TCA cycle but rather alters the fuel source by decreasing the oxidation of glucose-derived pyruvate and increasing glutamine anaplerosis [28]. We considered the possibility that this apparent difference in TCA cycle inhibition might be due to analysis of stably transformed cancer cells as opposed to cells early in the process of transformation. However, biguanide treatment of a stably transformed breast cancer cell line (CAMA-1) leads to a decrease in TCA cycle intermediates (Figure S4.2), suggesting that the metabolic reduction of the TCA cycle by biguanides may be important for inhibiting transformation.

Biguanides induce a CSC-specific depletion of nucleotide triphosphates

Metformin selectively kills breast CSCs and, as a consequence, can act together with standard chemotherapeutic drugs to increase tumor regression and prolong relapse in mouse xenografts [8, 10]. CSCs represent a minor population of cancer cells either in primary tissue or cancer cell lines, but they are enriched in mammospheres that form when cultivated in nonadherent and non-differentiating conditions [29, 30]. We performed metabolic profiling on 7-day-old mammospheres from the transformed breast cancer cell line CAMA-1 that were treated with metformin, phenformin, or vehicle for 24 h; as a control, we analyzed the CAMA-1 parental cell line. In accordance with observations during cellular transformation (Figure 4.2 b), the vast majority of metabolites are similarly regulated with both drugs (Figure 4.4 a).

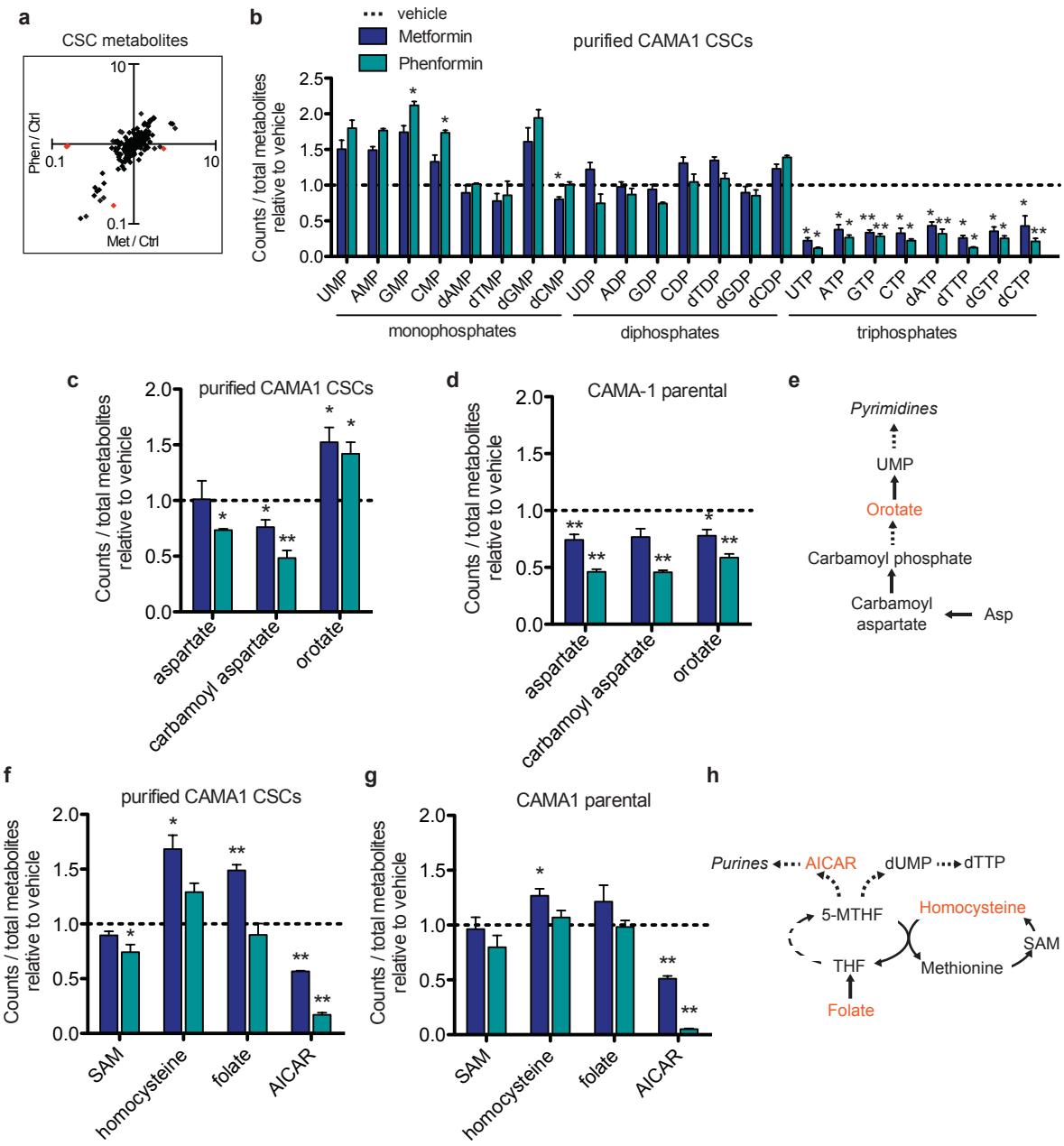

Figure 4.4 | Metformin and phenformin alter the metabolic state of breast cancer stem cells and deplete NTPs. a, Fold change comparisons identify metabolites differently regulated in metformin vs. phenformin samples measured by LC-MS/MS after 24 h of treatment in breast CSCs. Red diamonds represent differentially altered metabolites. **b,** Relative levels of nucleoside monophosphates, diphosphates, and triphosphates in metformin- or phenformin-treated CAMA-1 CSCs compared with untreated CSCs, n = 4. **c-d,** Relative levels of pyrimidine precursors in CAMA-1 CSCs **(c)** and parental CAMA-1 **(d)** treated with metformin or phenformin, n = 4. **e,** Schematic of key metabolites in pyrimidine synthesis. **f-g,** Relative levels of folate metabolites in CAMA-1 CSCs **(f)** and parental CAMA-1 **(g)** treated with metformin or phenformin for 24 h, n = 4. **h,** Schematic depicting of folate and regeneration of 5-MTHF in purine and dTTP synthesis . *p < 0.05 and **p < 0.01 compared with vehicle control. Error bars indicate SEM.

Surprisingly, the degree of the metabolic effects induced by biguanides differs considerably between the transformation and CSC systems. CSCs treated with biguanides show only marginal effects on glycolytic and TCA cycle intermediates (Figure S4.3). In contrast and unexpectedly, levels of all ribonucleotide and deoxyribonucleotide triphosphates (NTPs) are strongly decreased on biguanide treatment, with the effects of phenformin being stronger than metformin. Conversely, levels of all ribonucleotide and some deoxyribonucleotide monophosphates trend toward being increased by biguanide treatment, whereas little if any effect is seen on nucleotide diphosphates (Figure 4.4 b). Importantly, this depletion of NTPs by metformin and phenformin occurs specifically in CSCs and not in the parental CAMA-1 cell line (Figure S4.4 a). Although isolated effects on nucleotide metabolism are observed during tamoxifen-induced transformation (Figure S4.4 b), the magnitude and extent of NTP pool depletion are much greater in CSCs (Figure 4.4 b). Biguanide treatment also increases the levels of early precursors in nucleotide metabolic pathways, including orotate (Figure 4.4 c and e). Although the orotate precursors aspartate and carbamoyl aspartate are similarly regulated in CSCs and parental CAMA-1 cell line, the increased orotate level is specific to CSCs (Figure 4.4 c and d). These observations indicate that CSCs have distinct responses to biguanides and, in particular, appear to be defective in converting nucleotide precursors to NTPs.

Folate metabolism and aminoimidazole carboxamide ribonucleotide levels are altered by biguanides

Analysis of metabolites that feed into purine and pyrimidine synthesis reveals that CSCs treated with metformin, but not phenformin, have a buildup of folate (Figure 4.4 f and h). Folate is enzymatically reduced to tetrahydrofolate (THF) and subsequently

converted to N5-methyl-THF (5-MTHF) to serve as a methyl donor for both purine and dTTP synthesis. 5-MTHF can also serve as a 1-carbon donor to homocysteine to produce methionine, and conversely, homocysteine can be regenerated from methionine via the intermediate S-adenosyl-methionine (SAM). In both CSCs and parental CAMA1 cells, we observed increased folate and homocysteine with metformin treatment, possibly indicating a defect in entry of folate into the THF-cycling pathway for nucleotide synthesis. Interestingly altered folate metabolism in the Escherichia coli food source has been implicated in metformin-mediated benefits in Caenorhabditis elegans [31]. Additionally, both phenformin and metformin decrease aminoimidazole carboxamide ribonucleotide (AICAR), an intermediate required for purine synthesis (Figure 4.4 f–h). As decreased AICAR is observed in both CSCs and the parental line, the CSC-specific depletion of NTPs suggests that this population may have greater NTP utilization and hence be more sensitive to AICAR levels.

Discussion

Phenformin and metformin have remarkably similar metabolic profiles, with phenformin having increased potency

It has been assumed that phenformin is essentially a stronger version of metformin, but the evidence is limited to their chemical similarity and a few common effects in diabetes and cancer contexts. Our detailed metabolic analysis (>200 metabolites) indicates that the metabolic profiles of metformin and phenformin are remarkably similar, with phenformin causing stronger effects even when used at a 30-fold lower concentration. At least in part, this likely reflects the slightly greater lipophilic character of phenformin relative to metformin that facilitates drug uptake. Although both

biguanides use the OCT1 transporter for cellular entry, phenformin may be more readily taken up to reach its cellular targets [32, 33]. However, it is possible that phenformin may also have a stronger effect on the cellular target(s) per se.

Despite the remarkably similar metabolic profiles, a very small number of metabolites are uniquely altered by only one biguanide. Although metabolites that appear to be specifically affected by phenformin might simply reflect a quantitative difference between the two biguanides, metabolites such as anthranilate that are only affected by metformin cannot be explained in such a manner. These rare examples, which could be considered to occur from off-target effects of the drugs, have the potential to differentially affect medical outcomes. Nevertheless, the remarkably similar metabolic profiles, together with other lines of evidence, suggest that phenformin be considered as a more powerful alternative to metformin as an anti-cancer agent.

Biguanides lead to a depletion of glycolytic and TCA cycle intermediates during cellular transformation

The process of neoplastic transformation creates a demand for increased synthesis of macromolecules, and this is accommodated by increased uptake of glucose and glutamine from the medium. Tamoxifen-induced transformation causes increased levels of all metabolites involved in glycolysis up to and including the step mediated by triose phosphate isomerase, presumably a consequence of increased glucose uptake. However, glycolytic intermediates after this step are not increased, even though the cells produce more lactate. It is possible that increased lactate production is not simply due to increased flux through the entire glycolytic pathway but rather involves differences in the competition for pyruvate to be converted to lactate or to citrate for entry into the TCA

cycle (see below). Alternatively, the latter glycolytic intermediates may not accumulate due to rapid processing toward lactate.

Interestingly, the biguanides selectively decrease three consecutive metabolites in the middle of the glycolytic pathway. For each drug, the levels of these three metabolites are reduced to a comparable extent, an observation that could be explained by a decrease in the step that converts fructose 6-phosphate to fructose 1,6-diphosphate. Alternatively, it might reflect biguanide-induced partitioning of glucose-derived carbons toward glycerol 3-phosphate, a metabolite whose level is significantly increased by metformin and phenformin.

Both biguanides cause a quantitatively similar decrease in all TCA metabolites tested, strongly suggesting decreased flux into the TCA cycle. Reduced levels of some TCA metabolites have been observed previously with metformin treatment [22]. There are two explanations, which are not mutually exclusive, to explain the effects on the TCA cycle. First, biguanides lead to decreased levels of pyruvate and increased levels of lactate production, presumably by increasing the conversion of pyruvate to lactate. As pyruvate directly leads into the TCA cycle, lowering its intracellular levels is expected to reduce the levels of all TCA metabolites. Second, biguanides decrease the levels of glutamate, a metabolite that leads directly into the TCA cycle on conversion to α-ketoglutarate. Thus, biguanides may decrease input into the TCA cycle by inhibiting precursors generated either by carbon or nitrogen metabolism (pyruvate and glutamate, respectively), and hence reduce ATP production and anabolic metabolites necessary for cell growth that are derived from the TCA cycle.

Transformation in the inducible ER-Src model is mediated by an inflammatory

response that depends on NF-κB and STAT3 [9, 24], and metformin blocks this response by an unknown mechanism [15]. Our results indicate that this inflammatory response is associated with increased glucose uptake and increased glycolytic intermediates, although the mechanistic connection is unknown. Further, they suggest that the biguanide-mediated effects on metabolism effectively decrease the inflammatory stimuli or signal transduction pathway that is required for transformation.

Biguanides differently affect the transformation process and CSCs, suggesting unique metabolic states of these two systems

As the biguanides presumably affect the same target(s) in all cells, we were surprised to find different metabolic profiles during the transformation process and in CSCs. Although TCA cycle and glycolysis were mainly affected during transformation, the biguanides more specifically affected NTP levels in the CSCs. The decreased NTP levels in CSCs are likely to limit the availability for energetics, RNA, DNA, and biosynthesis of cofactors such as FAD, NADH, and CoA. In addition, metformin causes a defect in folate utilization in CSCs, as evidenced by increased levels of folate pathway metabolites. Consistent with this observation, the folate derivative 5-formimino-tetrahydrofolate increases in metformin-treated breast cancer cell lines [34], and patients treated with metformin have a higher serum level of homocysteine, a metabolite involved in folate cycling [35].

The differential metabolic effects of biguanides strongly suggest that CSCs have a distinct metabolic state compared with other cancer cells. We speculate that CSCs might have reduced requirements for glycolysis and the TCA cycle, perhaps analogous to yeast cells growing on nonfermentative carbon sources, and increased dependence for NTPs,

perhaps due to a reduced energy state. It is also tempting to speculate that the severe defect in NTP levels (and perhaps the defect in folate metabolism) underlies the increased sensitivity of CSCs to metformin treatment compared with typical cancer cells. More generally, our observations suggest that the metabolic effects of metformin may differ considerably among cancer cell types and states.

Evidence for mitochondrial complex 1 being a target of biguanides and future use of metabolic profiles

The direct target(s) of metformin is unknown, although mitochondrial complex I is the best candidate at present [14, 20]. A defect in complex I will decrease oxidation of NADH to NAD^+, a critical reaction to maintain the function of the TCA cycle, and ultimately inhibit oxidative phosphorylation leading to ATP. Several observations in this paper are consistent with the hypothesis that biguanides target complex I. First, biguanides decrease the levels of all TCA intermediates, suggesting an overall defect in TCA cycle function due to the relative inability to oxidize NADH to NAD^+. Second, decreased TCA cycle function is likely to result in preferential conversion of pyruvate to lactate as opposed to entering the TCA cycle, and this is observed in biguanide-treated cells. In this regard, inhibition of complex I by rotenone boosts lactate production [36] and reduces TCA cycle intermediates [37], allowing an alternate way to produce ATP when the electron transport chain is not functional. Third, the increased lactate production and increased levels of glycerol-3-phosphate may reflect stimulation of two key reactions that effectively oxidize NADH to NAD^+, thereby compensating for lower levels of NAD^+ due to decreased complex I activity. Fourth, the strong decrease in NTPs in CSCs suggests a major defect in energy state necessary, likely reflecting a defect in oxidative

phosphorylation.

Our detailed metabolic profiling provides independent support for the idea that complex I is a target of biguanides. As a complement to biochemical studies, examining metabolic profiles conferred by drugs with known targets (e.g., rotenone) or caused by functional inhibition or deletion of an individual gene should be very helpful for identifying the physiological target of biguanides. In addition, metabolic profiles conferred by biguanide treatment should be very useful for identifying new drugs with similar metabolic properties, and such drugs might have potential for treatment of diabetes or cancer.

Materials and Methods

Cell lines and culture conditions. MCF-10A ER-Src cells were grown as previously described in DMEM/F12 media supplemented with charcoal stripped FBS, penicillin/streptomycin, puromycin, EGF, hydrocortisone, insulin and cholera toxin [10]. Transformation via Src activation was induced by addition to 1 μM tamoxifen (Sigma) for 24 h. Metformin (300 μM) or phenformin (10 μM) were added together with tamoxifen. CAMA-1 cells were grown in DMEM media containing 10% FBS and antibiotics.

Mammosphere culture conditions. CAMA-1 cells were trypsinized, counted, and 10,000 cells/ml were seeded in ultra-low attachment plates in serum free mammosphere media as previously described [10]. Cells were passaged every 7 days, collected in 50 ml tubes, and the plate was washed once with PBS and combined with the collected cells. Spheres were collected by gentle centrifugation and resuspended in 0.5% Trypsin for 8 minutes. Trypsin was quenched with media containing FBS, pelleted by centrifugation, and

resuspended in mammosphere media. Cells were further dissociated mechanically by passing through a 23G syringe 6 times, and single cell suspension verified microscopically. Mammospheres were passaged multiple times to ensure enrichment for CSCs.

Metabolic profiling by target liquid-chromatography mass spectrometry. Cells were washed once with PBS and lysed in 80% (v/v) methanol at -78°C to extract intracellular polar metabolites. Cell debris was removed by centrifugation at 13000 rpm at 4°C. The supernatant containing metabolites was evaporated using a refrigerated Speed Vac. LC/MS/MS-based metabolomics analysis was done as previously described by [38].

Lipogenesis. De novo lipogenesis was measured as previously described [39]. Briefly, lipogenesis was measured in in MCF-10A ERSrc cells 24 hours after treatment +/- tamoxifen and +/- biguanide. Cells were pulsed for 4 hours with 0.8μCi ^{14}C-glucose (Perkin Elmer) per 800ul media +/- biguanide. Cells were rinsed twice with PBS then lysed in 0.5% Triton X-100. The lipid fraction was obtained by chloroform and methanol (2:1 v/v) extraction, followed by the addition of water. Samples were centrifuged, and the bottom phase was collected to measure ^{14}C incorporation into lipids. All scintillation counts were normalized to protein concentrations.

Statistical analysis. To identify significantly altered metabolites with either metformin or phenformin treatment in comparison to control treatment, metabolites from each sample were normalized to total metabolite counts. A student *t*-test was performed, and changed metabolites with a $P < 0.05$ were used for further analysis. To identify unique effects of one biguanide over the other, unbiased by a consistent potency effect, fold-changes of metformin or phenformin over control cells for all metabolites were plotted against each

other. Ratios of these two-fold changes for each metabolite were calculated and a 99.7% confidence interval over all measured metabolites was determined to address whether some metabolites are uniquely altered by either biguanide. Metabolites outside of this interval were considered to be differentially regulated.

Glucose, glutamine, lactate and ammonia measurement (NOVA analysis). Cell supernatant was collected 24 hours post tamoxifen and biguanide treatment, and cells were counted for normalization. Analysis was performed using the BioProfile FLEX analyzer (Nova Biomedicals) as previously described [40].

Acknowledgements

We thank Min Yuan for metabolomics technical assistance. A.J. was supported by a fellowship from the Postdoc Programme of the German Academic Exchange Service (DAAD), N.J.G. by National Science Foundation Graduate Research Fellowship Grant 1000087636, K.N.G.-H. by the Paul & Daisy Soros Fellowship for New Americans, M.C.H. by National Institutes of Health (NIH) Grant AG032375, the American Cancer Society New Scholar Award, and the Glenn Foundation for Medical Research, and K.S. by NIH Grant CA 107486.

References

1. Evans, J. M., Donnelly, L.A., Emslie-Smith, A.M., Alessi, D.R., and Morris, A.D. (2005). Metformin and reduced risk of cancer in diabetic patients. BMJ 330, 1304–1305.

2. Jiralerspong, S., Palla, S.L., Giordano, S.H., Meric-Bernstam, F., Liedtke, C., Barnett, C.M., Hsu, L., Hung, M.C., Hortobagyi, G.N., and Gonzalez-Angulo, A.M. (2009). Metformin and pathologic complete responses to neoadjuvant chemotherapy in diabetic patients with breast cancer. J Clin Oncol *27,* 3297–3302.

3. Dowling, R.J., Niraula, S., Stambolic, V., and Goodwin, P.J. (2012). Metformin in cancer: Translational challenges. J Mol Endocrinol *48,* R31–R43.

4. Pollak, M.N. (2012). Investigating metformin for cancer prevention and treatment: The end of the beginning. Cancer Discov *2,* 778–790.

5. Alimova, I.N., Liu, B., Fan, Z., Edgerton, S.M., Dillon, T., Lind, S.E., and Thor, A.D. (2009). Metformin inhibits breast cancer cell growth, colony formation and induces cell cycle arrest in vitro. Cell Cycle 8, 909–915.

6. Liu, B., Fan, Z., Edgerton, S.M., Deng, X.S., Alimova, I.N., Lind, S.E., and Thor, A.D. (2009). Metformin induces unique biological and molecular responses in triple negative breast cancer cells. Cell Cycle 8, 2031–2040.

7. Zakikhani, M., Dowling, R., Fantus, I.G., Sonenberg, N., Pollak, M. (2006). Metformin is an AMP kinase-dependent growth inhibitor for breast cancer cells. Cancer Res *66,* 10269–10273.

8. Hirsch, H.A., Iliopoulos, D., Tsichlis, P.N., Struhl, K. (2009). Metformin selectively targets cancer stem cells, and acts together with chemotherapy to block tumor growth and prolong remission. Cancer Res *69,* 7507–7511.

9. Hirsch, H.A., Iliopoulos, D., Joshi, A., Zhang, Y., Jaeger, S.A., Bulyk, M., Tsichlis, P.N., Shirley Liu, X., and Struhl, K. (2010). A transcriptional signature and common gene networks link cancer with lipid metabolism and diverse human diseases. Cancer Cell *17,* 348–361.

10. Iliopoulos, D., Hirsch, H.A., Struhl, K. (2011). Metformin decreases the dose of chemotherapy for prolonging tumor remission in mouse xenografts involving multiple cancer cell types. Cancer Res *71,* 3196–3201.

11. Huang, X., Wullschleger, S., Shpiro, N., McGuire, V.A., Sakamoto, K., Woods, Y.L., McBurnie, W., Fleming, S., and Alessi, D.R. (2008). Important role of the LKB1-AMPK pathway in suppressing tumorigenesis in PTEN-deficient mice. Biochem J *412,* 211–221.

12. Appleyard, M.V., Murray, K.E., Coates, P.J., Wullschleger, S., Bray, S.E., Kernohan, N.M., Fleming, S., Alessi, D.R., and Thompson, A.M. (2012). Phenformin as prophylaxis and therapy in breast cancer xenografts. Br J Cancer *106,* 1117–1122.

13. Dykens, J.A., Jamieson, J., Marroquin, L., Nadanaciva, S., Billis, P.A., and Will, Y. (2008). Biguanide-induced mitochondrial dysfunction yields increased lactate production and cytotoxicity of aerobically-poised HepG2 cells and human hepatocytes in vitro. Toxicol Appl Pharmacol *233,* 203–210.

14. Owen, M.R., Doran, E., Halestrap, A.P. (2000). Evidence that metformin exerts its anti-diabetic effects through inhibition of complex 1 of the mitochondrial respiratory chain. Biochem J *348,* 607–614.

15. Hirsch, H.A., Iliopoulos, D., Struhl, K. (2013). Metformin inhibits the inflammatory response associated with cellular transformation and cancer stem cell

growth. Proc Natl Acad Sci USA *110,* 972–977.

16. Li, S.N., Wang, X., Zeng, Q.T., Feng, Y.B., Cheng, X., Mao, X.B., Wang, T.H., and Deng, H.P. (2009). Metformin inhibits nuclear factor kappaB activation and decreases serum high-sensitivity C-reactive protein level in experimental atherogenesis of rabbits. Heart Vessels *24,* 446–453.

17. Kim, S.A., Choi, H.C. (2012). Metformin inhibits inflammatory response via AMPK-PTEN pathway in vascular smooth muscle cells. Biochem Biophys Res Commun *425,* 866–872.

18. Hardie, D.G. (2008). Role of AMP-activated protein kinase in the metabolic syndrome and in heart disease. FEBS Lett *582,* 81–89.

19. Larsson, O., Morita, M., Topisirovic, I., Alain, T., Blouin, M.J., Pollak, M., and Sonenberg, N. (2012). Distinct perturbation of the translatome by the antidiabetic drug metformin. Proc Natl Acad Sci USA *109,* 8977–8982.

20. El-Mir, M.Y., Nogueira, V., Fontaine, E., Avéret, N., Rigoulet, M., and Leverve, X. (2000). Dimethylbiguanide inhibits cell respiration via an indirect effect targeted on the respiratory chain complex I. J Biol Chem *275,* 223–228.

21. Scotland, S., Saland, E., Skuli, N., de Toni, F. Boutzen, H., Micklow, E., Sénégas, I., Peyraud, R., Peyriga, L., Théodoro, F., et al. (2013). Mitochondrial energetic and AKT status mediate metabolic effects and apoptosis of metformin in human leukemic cells. Leukemia *27,* 2129–2138.

22. Zakikhani, M., Bazile, M., Hashemi, S., Javeshghani, S., Avizonis, D., St Pierre, J., and Pollak, M.N. (2012). Alterations in cellular energy metabolism associated with the antiproliferative effects of the ATM inhibitor KU-55933 and with metformin. PLoS ONE *7,* e49513.

23. Soule, H.D., Maloney, T.M., Wolman, S.R., Peterson, W.D. Jr., Brenz, R., McGrath, C.M., Russo, J., Pauley, R.J., Jones, R.F., and Brooks, S.C. (1990). Isolation and characterization of a spontaneously immortalized human breast epithelial cell line, MCF-10. Cancer Res *50,* 6075–6086.

24. Iliopoulos, D., Hirsch, H.A., Struhl, K. (2009). An epigenetic switch involving NF-kappaB, Lin28, Let-7 MicroRNA, and IL6 links inflammation to cell transformation. Cell *139,* 693–706.

25. Rosilio, C., Lounnas, N., Nebout, M., Imbert, V., Hagenbeek, T., Spits, H., Asnafi, V., Pontier-Bres, R., Reverso, J., Michiels, J.F., et al. (2013). The metabolic perturbators metformin, phenformin and AICAR interfere with the growth and survival of murine PTEN-deficient T cell lymphomas and human T-ALL/T-LL cancer cells. Cancer Lett *336,* 114–126.

26. Warburg, O. (1956). On respiratory impairment in cancer cells. Science *124,* 269–

270.

27. Lunt, S.Y., Vander Heiden, M.G. (2011). Aerobic glycolysis: Meeting the metabolic requirements of cell proliferation. Annu Rev Cell Dev Biol *27,* 441–464.

28. Fendt, S.M., Bell, E.L., Keibler, M.A., Davidson, S.M., Wirth, G.J., Fiske, B., Mayers, J.R., Schwab, M., Bellinger, G., Csibi, A., et al. (2013). Metformin decreases glucose oxidation and increases the dependency of prostate cancer cells on reductive glutamine metabolism. Cancer Res *73,* 4429–4438.

29. Liao, M.J., Zhang, C.C., Zhou, B., Zimonjic, D.B., Mani, S.A., Kaba, M., Gifford, A., Reinhardt, F., Popescu, N.C., Guo, W., Eaton, E.N., Lodish, H.F., Weinberg, and R.A. (2007). Enrichment of a population of mammary gland cells that form mammospheres and have in vivo repopulating activity. Cancer Res *67,* 8131–8138.

30. Grimshaw, M.J., Cooper, L., Papazisis, K., Coleman, J.A., Bohnenkamp, H.R., Chiapero-Stanke, L., Taylor-Papadimitriou, J., and Burchell, J.M. (2008). Mammosphere culture of metastatic breast cancer cells enriches for tumorigenic breast cancer cells. Breast Cancer Res *10,* R52.

31. Cabreiro, F., Au, C., Leung, K.Y., Vergara-Irigaray, N., Cochemé, H.M., Noori, T., Weinkove, D., Schuster, E., Greene, N.D., and Gems, D. (2013). Metformin retards aging in C. elegans by altering microbial folate and methionine metabolism. Cell *153,* 228–239.

32. Shu, Y., Sheardown, S.A., Brown, C., Owen, R.P., Zhang, S., Castro, R.A., Ianculescu, A.G., Yue, L., Lo, J.C., Burchard, E.G., Brett, C.M., and Giacomini, K.M. (2007). Effect of genetic variation in the organic cation transporter 1 (OCT1) on metformin action. J Clin Invest *117,* 1422–1431.

33. Shitara, Y., Nakamichi, N., Norioka, M., Shima, H., Kato, Y., and Horie, T. (2013). Role of organic cation/carnitine transporter 1 in uptake of phenformin and inhibitory effect on complex I respiration in mitochondria. Toxicol Sci *132,* 32–42.

34. Corominas-Faja, B., Quirantes-Piné, R., Oliveras-Ferraros, C., Vazquez-Martin, A., Cufí, S., Martin-Castillo, B., Micol, V., Joven, J., Segura-Carretero, A., and Menendez, J.A. (2012). Metabolomic fingerprint reveals that metformin impairs one-carbon metabolism in a manner similar to the antifolate class of chemotherapy drugs. Aging (Albany, NY Online) *4,* 480–498.

35. Sahin, M., Tutuncu, N.B., Ertugrul, D., Tanaci, N., Guvener, N.D. (2007). Effects of metformin or rosiglitazone on serum concentrations of homocysteine, folate, and vitamin B12 in patients with type 2 diabetes mellitus. J Diabetes Complications *21,* 118–123.

36. Xu, Q., Vu, H., Liu, L., Wang, T.C., Schaefer, W.H. (2011). Metabolic profiles show specific mitochondrial toxicities in vitro in myotube cells. J Biomol NMR *49,* 207–219.

37. Basu, S.S., Blair, I.A. (2011). Rotenone-mediated changes in intracellular coenzyme A thioester levels: Implications for mitochondrial dysfunction. Chem Res Toxicol *24,* 1630–1632.

38. Shyh-Chang N, et al. (2013) Influence of threonine metabolism on S-adenosylmethionine and histone methylation. Science *339,* 222–226.

39. Laurent, G., German, N. J., Saha, A. K., de Boer, V. C. J., Davies, M., Koves, T. R., Dephoure, N., Fischer, F., Boanca, G., Vaitheesvaran, B., et al. (2013). SIRT4 Coordinates the Balance between Lipid Synthesis and Catabolism by Repressing Malonyl CoA Decarboxylase. Molecular Cell *50*, 686–698.

40. Finley, L.W., Carracedo, A., Lee, J., Souza, A., Egia, A., Zhang, J., Teruya-Feldstein, J., Moreira, P.I., Cardoso, S.M., Clish, C.B., et al. (2011). SIRT3 opposes reprogramming of cancer cell metabolism through HIF1α destabilization. Cancer Cell *19,* 416–428.

CHAPTER V

Discussion

Altered metabolism is at the heart of cancer, from the early stages of cancer onset to the late stages of an established tumor. The process of metabolic reprogramming enables cancer cells to ramp up nutrient uptake and processing in order to amass biomolecules and fuel pathways that maintain cancer cell survival. In many cases, these metabolic adaptations originated throughout evolution to enable organismal survival under harsh, nutrient-limited conditions, but have been hijacked by cancer cells to fuel their own growth and proliferation, even at the expense of the host[1, 2]. In cancer, metabolic regulatory nodes are frequently altered in a way that defies the normal constraints intended to maintain metabolic homeostasis. However, it has recently been realized and clinically verified that these junctions of metabolic misregulation can be identified, understood and targeted to fight back against cancer.

During the course of my dissertation studies, I completed three studies focused on uncovering novel metabolic regulatory pathways with the goal of shedding light on the utility of these nodes as potential therapeutic targets in cancer. In Chapter II, I started from a blank slate and aimed to identify metabolic enzymes that may be regulated by SIRT4, a protein linked to nutrient homeostasis and tumor suppression. In Chapter III, I described the discovery of a fundamental mechanism by which PHD3 limits fatty acid catabolism, and showed that loss of PHD3 in acute myeloid leukemia (AML) promotes cancer cell survival by enabling unhindered uptake and oxidation of fatty acids. In Chapter IV, I analyzed the global metabolic effects of the diabetes drug metformin on tumor-initiating cells to help solve the mystery of how this small molecule impedes

cancer onset.

SIRT4 coordinates the mitochondrial acetylome and PC activity

In Chapter II, we performed an acetylomics survey of mitochondrial proteins in wild type (WT) and SIRT4 knockout (KO) liver and brown adipose tissue (BAT) to identify putative substrates of SIRT4 deacetylase activity. Contrary to the view in the sirtuin field that SIRT4 is a weak deacetylase, our data suggest SIRT4 may be a biologically relevant, substrate-specific deacetylase with major impact on cellular bioenergetics. We find SIRT4 loss increases acetylation of select mitochondrial proteins, the majority of which are enzymes in the TCA cycle, fatty acid metabolism and the electron transport chain (ETC). While future biochemical studies are necessary to validate these substrates, the metabolic pathways identified by this study fit with known biologies of SIRT4. SIRT4 KO mice are known to have increased fatty acid oxidation but decreased lipid synthesis, increased levels of TCA cycle intermediates and overall hyperactived mitochondrial metabolism. By coordinating multiple enzymes in these pathways, SIRT4 could potentially establish greater metabolic regulation.

A major finding in this study is that SIRT4 binds and represses pyruvate carboxylase (PC). PC is a key anaplerotic enzyme that provides an alternate route for pyruvate to enter the TCA cycle. Our data support a developing theme in sirtuin research that the major function of SIRT4 is to limit mitochondrial oxidative metabolism. While most sirtuins promote oxidative metabolism in response to low nutrient conditions, SIRT4 is emerging as a counterbalance that limits oxidative metabolism in the presence of adequate nutrients. In the case of PC, we hypothesize SIRT4 may limit oxidative metabolism by interfering with formation of the active PC homotetramer and therefore

limiting anaplerotic flux into TCA cycle. Because PC has strong relevance in cancer and diabetes, it will be interesting for future studies to assess whether SIRT4-mediated repression of PC contributes to these diseases.

Further studies are also needed to validate other putative SIRT4 targets identified in our acetylation proteomics analysis. Nicotinamide nucleotide transhydrogenase (NNT) warrants particular interest because it has already been validated as a SIRT4 target in vitro[3] and was the most dramatically hyperacetylated protein in SIRT4 KO mice in our study. By coordinating the balance of NAD(H) and NADP(H), NNT modulates the cellular redox status. Thus, through NNT, SIRT4 could potentially direct the cellular balance of catabolic versus anabolic pathways. NNT is increasingly being recognized as a key contributor to cancer cell metabolism. In tumors experiencing hypoxia or mitochondrial defects, NNT is a major source of NADPH to drive reductive carboxylation to maintain anaplerosis[4, 5]. Therefore, further studies could explore the role of the SIRT4/NNT axis in coordinating reverse TCA cycling in cancer.

More broadly, our results in Chapter II raise the question of how SIRT4 coordinates activity toward potentially multiple substrates to regulate organismal metabolism. It is now known that SIRT4 has a handful of metabolic targets, and our data raises the possibility of dozens of new substrates that may be validated in the future. However it is not clear how SIRT4, or in fact how any sirtuin, directs its activity toward select substrates at specific times. Because metabolism is regulated with intricate and sophisticated precision, we consider it unlikely that SIRT4 simply acts on all of its substrates at once with no preference or selectivity under different scenarios. We propose that in response to certain environmental or nutrient stresses, SIRT4 activity is directed to

enzymes in particular metabolic pathways to appropriately restore homeostasis. Future studies are needed to identify factors that guide the preferred enzymatic activity and substrates of SIRT4 in response to a range of stimuli.

PHD3 hydroxylates and activates ACC2 to limit fatty acid oxidation in cancer

In Chapter III we identified PHD3 as a fundamental regulator of fatty acid metabolism in response to the cellular metabolic state. Our findings diverge from traditional views of PHDs as predominantly serving to modulate hypoxia inducible factor (HIF) and glycolysis. Here, we show instead that PHD3 plays a major role in lipid metabolism by hydroxylating and activating ACC2 to limit fatty acid oxidation (FAO). We find this mode of repressing FAO is particularly important under high nutrient conditions, raising the intriguing possibility that PHD3 may act as a nutrient sensor to coordinate fuel utilization. One candidate molecule that may coordinate PHD3 activity is the PHD co-substrate α-ketoglutarate. Abundant α-ketoglutarate could signal that the TCA cycle is sufficiently fueled, and high local concentrations of this metabolite might be sensed by PHD3 to limit further, unnecessary catabolism of fatty acids. There is currently little knowledge of how the cell dually incorporates information about fat metabolism and the TCA cycle to coordinate fuel choice. My research presents the innovative hypothesis that the PHD3/ACC axis allows these pathways to be concordantly regulated.

A key insight of Chapter III is that PHD3 is frequently suppressed in AML. We show loss of PHD3 contributes to high FAO, a metabolic pathways that is essential for survival of these cancer cells. In the immediate future, we are pursuing ongoing mouse studies to evaluate whether reinstating the PHD3/ACC2 regulatory axis limits AML

severity. As we observed in human AML, we have found that several mouse models of AML show strongly decreased levels of PHD3 compared to normal cd11b^{+} myeloid cells. Thus, we are evaluating whether PHD3 overexpression in a mouse model of leukemia impedes onset and severity of AML. We are using a mouse model in which primary mouse bone marrow cells are transduced with MLL-AF9 ex vivo and transplanted into mice to induce AML. Overexpression of PHD3 or empty vector in tandem with MLL-AF9 transduction will allow us to assess whether PHD3 impedes leukemogenesis. Additionally, we will assess whether modulation PHD3 in primary human AML cells limits engraphment upon tail vein injection in immune-compromised NOD/SCID gamma mice. This experiment will assess whether PHD3 activation has therapeutic potential in the treatment of existing AML.

This study raises several questions and possibilities about the role of PHD3 and FAO in cancer. First, what is the purpose of elevated FAO in cancer, and why is its upregulation particularly essential for specific tumor types? FAO has been proposed as a mechanism to generate ATP, build TCA cycle intermediates or other fats or produce the antioxidant molecule NADPH. Additionally, other studies suggest FAO is required to maintain the quality of the mitochondrial membrane. Future studies are needed to explore these hypotheses, perhaps aided by targeted screens to identify pathways that rescue FAO inhibition in cancer cells otherwise dependent on this pathway. Second, based on the results in Chapter III, could low PHD3 expression serve as a biomarker to indicate cancers with high FAO? In ongoing analyses of AML patient gene expression profiles, we find approximately 80% of patients have very low levels of PHD3, and this subset of patients shows striking, significant upregulation of oxidative phosphorylation gene

programs. This supports the findings in Chapter III and further suggests low PHD3 is a promising clinical marker of AML dependency on oxidative metabolism. Finally, could FAO inhibitors be used to treat AML characterized by low PHD3 expression? Currently metabolically-targeted therapeutics are not a standard part of treatment in AML, and furthermore there are no ongoing clinical trials testing the efficacy of FAO inhibitors in AML. There is great need for more clinical options for patients with AML. In 2015, over 20,000 people are expected to be diagnosed with AML in the US, and over 10,000 patients with AML are expected to die[6]. Our work, combined with the work of others on the role of FAO in leukemia, provides ample support that FAO inhibitors should be explored as treatment options for this deadly disease.

Metformin and phenformin alter the metabolic state and impede neoplastic transformation and cancer stem cell viability

The diabetes drug metformin and the related, more potent biguanide phenformin have received much attention for their anti-cancer properties in biochemical studies, animal models and even retrospective patient studies. In Chapter IV, we set out to define the metabolic alterations caused by metformin and phenformin that may bear insight to how these drugs inhibit the induction of a cancerous cellular state. We also analyzed the drugs' unique metabolic effects on cancer stem cells, a small population of cells that possesses predominant tumor-initiation capacity and, importantly, is selectively inhibited by metformin treatment.

One surprising insight from our metabolomics analysis is that the ability of metformin and phenformin to block neoplastic transformation is linked to a forced dependency on glycolysis and an ensuing nutrient crisis. In a breast cell culture model of

Src-induced transformation, metformin and phenformin block the transition to a cancer cell state. In this system, we find biguanide treatment increases glucose uptake and lactate production. This strong upregulation of glycolysis may occur as a cellular adaptation to low ETC flux. This hypothesis fits with the major dogma in the field that biguanides inhibit Complex I of the ETC. Our data indicate that the glycolytic switch induced by biguanides cannot fulfill the metabolic and bioenergetic demands required for transformation. In the presence of biguanides, cells undergoing transformation become depleted of glycolytic intermediates and TCA cycle metabolites. We hypothesize this nutrient crisis prevents the cell from achieving a transformed state.

Our work also highlights the complex role of glycolysis in cancer. Numerous studies have shown upregulated glycolysis and the Warburg effect fuel growth and survival of multiple cancer subtypes. However, we show here that a strong switch to glycolytic metabolism is not amenable to the early stages of cellular transformation. Indeed, we find metformin and phenformin greatly upregulate glycolysis, but block transformation. This suggests the amount of glycolysis that promotes cancer development requires a fine balance. Some level of upregulation is needed to boost the biosynthetic processes that are characteristic of the transformed state, but extreme dependency on glycolysis due to blocks in the ETC can limit transformation. Our observation that metformin induces nutrient deprived state in order to prevent cancer fit with studies in the Pollack lab[7]. This group recently showed serine metabolism is upregulated in cells to compensate for the nutrient deficiencies induced by biguanide treatment. Furthermore, a serine-free diet enhanced the anti-neoplastic effects of metformin treatment in mice, which we suggest might amplify the glycolytic and TCA cycle deficits caused by

biguanides to exacerbate the nutrient crisis and restrict the onset of cancer.

A second finding from Chapter IV that calls for further study is the intriguing increase in glycerol 3-phosphate upon metformin and phenformin treatment during transformation induction. Glycerol 3-phopshate is a glucose-derived molecule that can be used for lipid synthesis. While most anabolic molecules are decreased with biguanide treatment, the level of this particular biosynthetic molecule is strongly increased. We propose two hypotheses for why glycerol 3-phosphate may be upregulated by biguanide treatment. First, generating glycerol 3-phopshate also produces NAD^+. Thus, producing glycerol 3-phosphate can enable continued glycolysis similar to the way in which lactate production sustains glycolysis. Alternatively, glycerol 3-phosphate levels may be increased to help fuel the electron transport chain in a way that bypasses Complex I inhibition. Glycerol 3-phosphate can travel to the mitochondria and be converted to dihydroxyacetone phosphate (DHAP) by mitochondrial glycerol 3-phosphate dehydrogenase (GPDH-M), directly contributing electrons to the quinol pool in the ETC. In this way, we hypothesize glycerol 3-phosphate drives a cellular adaptation to compensate for Complex I inhibition. Interestingly, recent studies by the Shulman lab suggest metformin leads to downstream inhibition of GPDH-M by 50% in mice[8]. Future studies are needed to examine the role of glycerol 3-phosphate in response to biguanides, and more importantly to understand whether increased glycerol 3-phosphate provides a possible mechanism of resistance that a cancer cell may adapt to bypass the effects of biguanide treatment.

A final conclusion of our metabolomics analysis is that biguanides induce different metabolic effects in transforming cells compared to cancer stem cells (CSCs). Unlike

cells undergoing transformation, CSCs treated with metformin or phenformin did not show broad decreases in glycolytic and TCA cycle metabolites. Instead, the most striking metabolic alteration in CSCs is depletion of nucleotide triphosphates (NTPs). This correlates with dramatically decreased levels of AICAR, a biosynthetic intermediate in purine synthesis. Intriguingly, NTP levels were unaffected in the parental CAMA1 cell line from which the CSCs were derived, despite similar decreases in AICAR. Our study raises the hypothesis that biguanide treatment may cause CSCs to rely heavily on NTPs, leading to a precipitous decrease in NTPs that is not amenable to survival. We propose that CSCs require high levels of NTPs to maintain growth and stemness. This hypothesis fits with studies in developmental biology showing NTPs are key signaling molecules in hematopoietic and neural stem cells[9-11]. For example, exogenous UTP added to hematopoietic stem cells promotes migration and bone marrow engraphment[11]. We propose the following model for how biguanides may alter NTP levels and induce CSC death: when biguanides inhibit Complex I, ATP production by oxidative phosphorylation is impeded. To compensate, CSCs use other NTPs to make ATP. Thus, NTPs are unavailable to perform other functions that are key for maintaining CSC survival. Eventually, NTP depletion combined with a low bioenergetic state may cause selective growth inhibition in CSCs. Further studies are needed to test this hypothesis and determine the role of NTPs in CSCs, with the potential of discovering new avenues to explore in cancer therapeutics.

Conclusions

In the last decade, the advances in cancer metabolism have been monumental. Much has been learned about the molecular drivers that boost fuel uptake and direct

nutrient fate in order to promote cancer onset and progression. There is great momentum to push this research toward the clinic and hopefully yield therapeutic outcomes that improve upon the current standard of care. The findings in this dissertation contribute to the field of tumor metabolism through the discovery and characterization of pathways and regulatory nodes guiding nutrient utilization in cancer cells. This work reveals a clearer picture of how metabolic programs are altered in cancer to promote proliferation and survival, and also how metabolism can be targeted in strategies for cancer treatment.

References

1. Efeyan, A., Comb, W. C., and Sabatini, D. M. (2015). Nutrient-sensing mechanisms and pathways. Nature *517*, 302–310.

2. Gomes, A. P., and Blenis, J. (2015). A nexus for cellular homeostasis: the interplay between metabolic and signal transduction pathways. Current Opinion in Biotechnology *34*, 110–117.

3. Rauh, D., Fischer, F., Gertz, M., Lakshminarasimhan, M., Bergbrede, T., Aladini, F., Kambach, C., Becker, C. F. W., Zerweck, J., Schutkowski, M., et al. (2013). An acetylome peptide microarray reveals specificities and deacetylation substrates for all human sirtuin isoforms. Nat Comms *4*.

4. Mullen, A. R., Hu, Z., Shi, X., Jiang, L., Boroughs, L. K., Kovacs, Z., Boriack, R., Rakheja, D., Sullivan, L. B., Linehan, W. M., et al. (2014). Oxidation of Alpha-Ketoglutarate Is Required for Reductive Carboxylation in Cancer Cells with Mitochondrial Defects. Cell Reports *7*, 1679–1690.

5. Gameiro, P. A., Laviolette, L. A., Kelleher, J. K., Iliopoulos, O., and Stephanopoulos, G. (2013). Cofactor balance by nicotinamide nucleotide transhydrogenase (NNT) coordinates reductive carboxylation and glucose catabolism in the tricarboxylic acid (TCA) cycle. Journal of Biological Chemistry *288*, 12967–12977.

6. Adult Acute Myeloid Leukemia Treatment. National Cancer Institute at the National Institutes of Health. www.cancer.gov. [Accessed March 23, 2015].

7. Gravel, S. P., Hulea, L., Toban, N., Birman, E., Blouin, M. J., Zakikhani, M., Zhao, Y., Topisirovic, I., St-Pierre, J., and Pollak, M. (2014). Serine Deprivation Enhances Antineoplastic Activity of Biguanides. Cancer Research *74*, 7521–7533.

8. Madiraju, A. K., Erion, D. M., Rahimi, Y., Zhang, X.-M., Braddock, D. T.,

Albright, R. A., Prigaro, B. J., Wood, J. L., Bhanot, S., MacDonald, M. J., et al. (2014). Metformin suppresses gluconeogenesis by inhibiting mitochondrial glycerophosphate dehydrogenase. Nature *510*, 542–546.

9. Mishra, S. K. (2006). Extracellular nucleotide signaling in adult neural stem cells: synergism with growth factor-mediated cellular proliferation. Development *133*, 675–684.

10. Gampe, K., Stefani, J., Hammer, K., Brendel, P., Pötzsch, A., Enikolopov, G., Enjyoji, K., Acker-Palmer, A., Robson, S. C., and Zimmermann, H. (2014). NTPDase2 and Purinergic Signaling Control Progenitor Cell Proliferation in Neurogenic Niches of the Adult Mouse Brain. Stem Cells *33*, 253–264.

11. Rossi, L., Manfredini, R., Bertolini, F., Ferrari, D., Fogli, M., Zini, R., Salati, S., Salvestrini, V., Gulinelli, S., Adinolfi, E., et al. (2007). The extracellular nucleotide UTP is a potent inducer of hematopoietic stem cell migration. Blood *109*, 533–542.

APPENDIX I

SIRT4 coordinates the balance between lipid synthesis and catabolism by repressing malonyl CoA decarboxylase

Gaëlle Laurent,[1] Natalie J. German,[1] Asish K. Saha,[3] Vincent C.J. de Boer,[1,7] Michael Davies,[4] Timothy R. Koves,[4] Noah Dephoure,[1] Frank Fischer,[5] Gina Boanca,[5] Bhavapriya Vaitheesvaran,[6] Scott B. Lovitch,[2] Arlene H. Sharpe,[2] Irwin J. Kurland,[6] Clemens Steegborn,[5] Steven P. Gygi,[1] Deborah M. Muoio,[4] Neil B. Ruderman,[3] and Marcia C. Haigis[1]

[1]Department of Cell Biology, [2]Department of Microbiology and Immunobiology, Harvard Medical School, Boston, MA 02115, USA; [3]Diabetes Research Unit, Section of Endocrinology, Department of Medicine, Boston University Medical Center, Boston, MA 02118, USA; [4]Departments of Medicine and Pharmacology and Cancer Biology, Sarah W. Stedman Nutrition and Metabolism Center, Duke University Medical Center, Durham, NC 27710, USA; [5]Department of Biochemistry, University of Bayreuth, 95440 Bayreuth, Germany; [6]Department of Medicine, Diabetes Center, Stable Isotope and Metabolomics Core Facility, Albert Einstein College of Medicine, Bronx, NY 10461, USA; [7]Present address: Laboratory of Genetic Metabolic Diseases, Academic Medical Center, 1105 AZ Amsterdam, The Netherlands

This research was originally published in *Molecular Cell.* Gaëlle Laurent, Natalie J. German, Asish K. Saha, Vincent C.J. de Boer, Michael Davies, Timothy R. Koves, Noah Dephoure, Frank Fischer, Gina Boanca, Bhavapriya Vaitheesvaran, Scott B. Lovitch,

Arlene H. Sharpe, Irwin J. Kurland, Clemens Steegborn, Steven P. Gygi, Deborah M. Muoio, Neil B. Ruderman, and Marcia C. Haigis. (2013). SIRT4 coordinates the balance between lipid synthesis and catabolism by repressing malonyl CoA decarboxylase. Molecular Cell 50, 686-698.

 doi: 10.1016/j.molcel.2013.05.012.

Gaëlle Laurent conceived the project and performed experiments. Natalie German assisted with design of deacetylation studies and performed biochemistry experiments to validate MCD as the first known SIRT4 deacetylation substrate. This chapter is reprinted with kind permission of Elsevier Inc.

Molecular Cell
Article

SIRT4 Coordinates the Balance between Lipid Synthesis and Catabolism by Repressing Malonyl CoA Decarboxylase

Gaëlle Laurent,[1] Natalie J. German,[1] Asish K. Saha,[3] Vincent C.J. de Boer,[1,7] Michael Davies,[4] Timothy R. Koves,[4] Noah Dephoure,[1] Frank Fischer,[5] Gina Boanca,[5] Bhavapriya Vaitheesvaran,[6] Scott B. Lovitch,[2] Arlene H. Sharpe,[2] Irwin J. Kurland,[6] Clemens Steegborn,[5] Steven P. Gygi,[1] Deborah M. Muoio,[4] Neil B. Ruderman,[3] and Marcia C. Haigis[1,*]
[1]Department of Cell Biology
[2]Department of Microbiology and Immunobiology
Harvard Medical School, Boston, MA 02115, USA
[3]Diabetes Research Unit, Section of Endocrinology, Department of Medicine, Boston University Medical Center, Boston, MA 02118, USA
[4]Departments of Medicine and Pharmacology and Cancer Biology, Sarah W. Stedman Nutrition and Metabolism Center, Duke University Medical Center, Durham, NC 27710, USA
[5]Department of Biochemistry, University of Bayreuth, 95440 Bayreuth, Germany
[6]Department of Medicine, Diabetes Center, Stable Isotope and Metabolomics Core Facility, Albert Einstein College of Medicine, Bronx, NY 10461, USA
[7]Present address: Laboratory of Genetic Metabolic Diseases, Academic Medical Center, 1105 AZ Amsterdam, The Netherlands
*Correspondence: marcia_haigis@hms.harvard.edu
http://dx.doi.org/10.1016/j.molcel.2013.05.012

SUMMARY

Lipid metabolism is tightly controlled by the nutritional state of the organism. Nutrient-rich conditions increase lipogenesis, whereas nutrient deprivation promotes fat oxidation. In this study, we identify the mitochondrial sirtuin, SIRT4, as a regulator of lipid homeostasis. SIRT4 is active in nutrient-replete conditions to repress fatty acid oxidation while promoting lipid anabolism. SIRT4 deacetylates and inhibits malonyl CoA decarboxylase (MCD), an enzyme that produces acetyl CoA from malonyl CoA. Malonyl CoA provides the carbon skeleton for lipogenesis and also inhibits fat oxidation. Mice lacking SIRT4 display elevated MCD activity and decreased malonyl CoA in skeletal muscle and white adipose tissue. Consequently, SIRT4 KO mice display deregulated lipid metabolism, leading to increased exercise tolerance and protection against diet-induced obesity. In sum, this work elucidates SIRT4 as an important regulator of lipid homeostasis, identifies MCD as a SIRT4 target, and deepens our understanding of the malonyl CoA regulatory axis.

INTRODUCTION

According to the bioenergetic demands of the organism, tissues must appropriately adjust their metabolism to either store lipids or catabolize fatty acids to generate more energy (Duncan et al., 2007; Long and Zierath, 2006). This balance between lipid anabolic and catabolic processes is coordinately and precisely regulated, in part by the cellular levels of the metabolite malonyl CoA (Saggerson, 2008; Saha and Ruderman, 2003). To undergo β-oxidation, fatty acids must cross both the inner and outer mitochondrial membranes, and this rate-limiting step is catalyzed by carnitine palmitoyltransferase 1 (CPT1), which is allosterically inhibited by malonyl CoA. In addition, malonyl CoA serves as the chain-elongating unit for fatty acid synthesis. Thus, regulation of malonyl CoA levels provides a means to control the balance between fat synthesis and fat oxidation. Two enzymes regulate cellular malonyl CoA levels: acetyl CoA carboxylase (ACC) converts acetyl CoA to malonyl CoA, and malonyl CoA decarboxylase (MCD) converts it back to acetyl CoA. The regulation of ACC activity through phosphorylation by AMPK is well characterized (Hardie, 2011), whereas the regulation of MCD activity is much less studied.

Sirtuins are NAD^+-dependent deacylases and ADP-ribosyltransferases involved in many biological processes, mediating adaptive responses to the cellular environment (Houtkooper et al., 2012; Lombard et al., 2011). Proteomic surveys revealed that a majority of mitochondrial metabolic enzymes are differentially acetylated according to the nutritional state of the cell (Wang et al., 2010; Yang et al., 2011; Zhao et al., 2010), suggesting that acetylation may regulate global cellular metabolism and coordinates fuel switching. Three of the mammalian sirtuins (SIRT3, SIRT4, and SIRT5) are located in the mitochondria and may play roles as sensors of energy status in this organelle (Houtkooper et al., 2012; Lombard et al., 2011). SIRT4 is one of the least-characterized mitochondrial sirtuins (Haigis et al., 2006; Ahuja et al., 2007). Previously, it was shown that SIRT4 represses fat catabolism (Nasrin et al., 2010), but the direct substrates involved and the physiological significance remain unknown. Importantly, the role of SIRT4 in lipid synthesis and storage has never been investigated.

In this study, we demonstrate a novel function for SIRT4 in the regulation of lipid metabolism. We find that SIRT4 represses fatty acid oxidation in skeletal muscle and stimulates lipogenesis

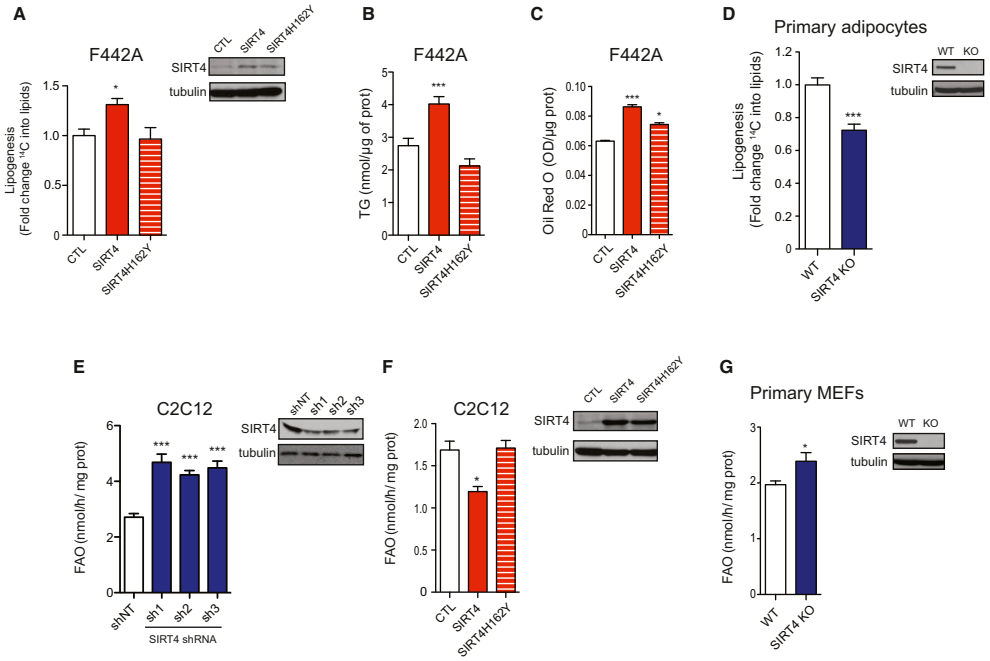

Figure 1. SIRT4 Regulates Lipid Metabolism

(A–C) (A) Lipogenesis from ^{14}C-acetate (n = 3) (A), triglyceride levels (n = 6) (B), and oil red O staining (n = 6) (C) were determined using F442A adipocytes stably expressing empty vector control (CTL, open bar), SIRT4 (red bar), or the catalytic inactive mutant of SIRT4, SIRT4H162Y (red striped bar).

(D) Lipogenesis was measured using ^{14}C-acetate in WT (open bar) and SIRT4 KO (blue bar) primary adipocyte lines (n = 3).

(E) Fatty acid oxidation (FAO) was measured in C2C12 cells expressing control shRNA (shNT, open bar) or shRNAs targeted against SIRT4 (blue bars) (n = 3).

(F) FAO was measured in C2C12 cells overexpressing empty vector control, SIRT4, or SIRT4H162Y (n = 3).

(G) FAO was determined using WT and SIRT4 KO primary MEF lines (n = 3). Levels of SIRT4 protein were determined by western blotting using antibodies to SIRT4 and tubulin as a loading control. In each panel, data represent mean ± SEM; *p < 0.05, **p < 0.01, ***p < 0.001.

in white adipose tissue (WAT), indicating that SIRT4 can regulate the balance between fat oxidation and fat synthesis. To achieve this regulation, SIRT4 directly binds, deacetylates, and represses malonyl CoA deacarboxylase (MCD). As a consequence, SIRT4 KO mice display deregulation of crucial physiologic aspects of lipid metabolism, leading to increased tolerance to an exercise challenge and protection against diet-induced obesity.

RESULTS

SIRT4 Promotes Lipid Synthesis and Represses Fatty Acid Oxidation

To assess the role of SIRT4 on lipid homeostasis, we initially examined its effects on de novo lipid synthesis. As WAT is the major organ responsible for lipid synthesis and storage, we tested the role of SIRT4 on lipogenesis in the mouse adipocyte cell line, F442A. We found that overexpression of SIRT4 leads to an increase in lipogenesis, as measured by [^{14}C]-acetate incorporation into the lipid fraction (Figure 1A), and an increase in accumulation of trigycerides (TGs) and stored lipids (Figures 1B and 1C). This increase was not observed in cells overexpressing the catalytically inactive mutant of SIRT4, SIRT4H162Y (Ahuja et al., 2007). To confirm these results using a primary model, we examined lipogenesis using adipocytes freshly isolated from WAT from SIRT4 WT and KO mice. As observed in F442A cells, lipid synthesis was decreased in SIRT4 KO primary adipocytes (Figure 1D). Together, these results suggest that SIRT4 activity promotes fat anabolism.

To assess the role of SIRT4 in lipid catabolism, we measured fatty acid oxidation in C2C12 cells, a mouse myocyte cell line. As muscles rely primarily on fatty acids for energy, myocytes provide a good model to study fatty acid oxidation. We found that the oxidation of palmitate, a saturated long-chain fatty acid, was significantly higher in C2C12 cells in which SIRT4 expression was stably reduced by lentiviral expression of

three independent shRNAs against SIRT4 compared to control cells (Figure 1E). Conversely, palmitate oxidation was diminished in C2C12 cells stably overexpressing SIRT4, but not in cells overexpressing SIRT4H162Y (Figure 1F). Similarly, fatty acid oxidation was elevated in primary SIRT4 KO mouse embryonic fibroblasts (MEFs) (Figure 1G). These data demonstrate for the first time that SIRT4 promotes lipogenesis and represses fatty acid oxidation, indicating that SIRT4 may coordinate the balance between lipid catabolic and anabolic pathways.

SIRT4 Represses Malonyl CoA Decarboxylase

As SIRT4 represses palmitate oxidation and stimulates lipogenesis, we reasoned that SIRT4 regulates an enzyme positioned at the interface between oxidative and synthetic pathways. One major branchpoint in lipid homeostasis is the interconversion of acetyl CoA to malonyl CoA, a metabolite that inhibits fat oxidation, while promoting fat synthesis (Figure 2A). Two enzymes regulate cellular malonyl CoA levels: ACC converts acetyl CoA to malonyl CoA, and MCD converts it back to acetyl CoA. Together these enzymes constitute a highly responsive control system modulating the levels of malonyl CoA and thereby the rate of fatty acid catabolism or synthesis (Figure 2A). To test this idea, we determined whether SIRT4 physically binds with ACC or MCD in coimmunoprecipitation studies. We did not detect an interaction between SIRT4 and ACC (see Figure S1A online). Whereas MCD localizes both to the cytosol and the mitochondrial matrix, in skeletal muscle the majority of MCD activity resides within mitochondria (Kerner and Hoppel, 2002). Thus, we investigated and observed a physical interaction between SIRT4 and SIRT4H162Y with mitochondrial MCD (Figures 2B and 2C). We confirmed that SIRT4 and MCD colocalize in mitochondria using confocal microscopy (Figure 2D). In contrast to SIRT4, the other mitochondrial sirtuins, SIRT3 and SIRT5, showed no detectable physical association with MCD in control immunoprecipitations under these conditions, further indicating a specific interaction between SIRT4 and MCD.

We next investigated the importance of MCD activity in SIRT4-mediated regulation of lipid homeostasis. We observed that overexpression of MCD in C2C12 and F442A cells increases fatty acid oxidation rates and repressed lipogenesis, respectively (Figures S1B–S1D). Thus, MCD overexpression phenocopied SIRT4 deletion. To assess directly whether SIRT4 regulates lipid homeostasis through MCD, we analyzed fatty acid oxidation in SIRT4 WT and KO MEFs in which MCD expression was stably reduced by lentiviral expression of shRNA against MCD (Figure S1E). Reduction of MCD abrogated the increased fatty acid oxidation found in SIRT4 KO cells to levels comparable to those of WT cells (Figure 2E), demonstrating that the increased fatty acid oxidation in SIRT4 KO cells required MCD activity.

Based on these findings, we hypothesized that MCD activity would be elevated in SIRT4 KO cells, decreasing malonyl CoA levels, subsequently increasing fat oxidation. In agreement with this model, MCD activity was elevated 2-fold in SIRT4 KO MEFs compared to WT MEFs (Figure 2F). Next, to confirm that acute modulation of SIRT4 activity can regulate MCD, we treated cells with a pansirtuin inhibitor nicotinamide (NAM). We found that MCD activity was significantly increased in the WT cells treated with NAM compared to the untreated cells. This is due to inhibition of SIRT4, as NAM had no further effect in SIRT4 KO cells (Figure 2F). To confirm these findings, we further examined the effect of SIRT4 on MCD activity in muscle and adipocyte cells, using C2C12 and F442A cell lines stably expressing WT or H162Y SIRT4. In both cell types, overexpression of SIRT4 resulted in reduced MCD activity, whereas overexpression of the catalytic mutant had no effect (Figures 2G and 2H). Taken together, these data suggest that SIRT4 represses MCD activity in muscle and adipocyte cell lines.

SIRT4 Deacetylates MCD

Our results demonstrate that in cells SIRT4 binds MCD and represses its enzymatic activity. We sought to assess whether this repression is mediated by posttranslational modification. Although they belong to the same protein family, sirtuins exhibit several enzymatic activities, including deacetylation, deacylation, and ADP-ribosylation. Previous reports found that SIRT4 is a weak ADP-ribosyltransferase but not a BSA or histone deacetylase (Ahuja et al., 2007; Haigis et al., 2006; Schwer et al., 2002). To identify posttranslational modifications of MCD, we immunoprecipitated MCD from C2C12 cells and analyzed posttranslational modifications by mass spectrometry. MCD was previously shown to be acetylated on six different lysines (K58, K167, K210, K316, K388, and K444) (Nam et al., 2006). Our analysis identified additional acetylation on lysine residue 471 (Figure S2A) but did not detect ADP-ribosylation, malonylation, or succinylation. Notably, K471 is one of the most conserved lysines of MCD and is invariant from *D. Rerio* to humans (Figure S2B). Hence, we speculated that SIRT4 may have a substrate-specific deacetylase activity, as has been demonstrated for SIRT6 and SIRT7 (Barber et al., 2012; Zhong et al., 2010).

To test whether MCD acetylation level is regulated by SIRT4, we stably expressed a FLAG-tagged murine MCD in MEFs and treated cells with or without NAM. MCD acetylation was measured after immunoprecipitation of MCD by western blotting with anti-acetyl lysine antibody. We found that NAM treatment increased MCD acetylation levels (Figure 3A). We also detected an increase in the acetylation level of MCD in the SIRT4 KO cells compared to the WT cells (Figure 3B). Furthermore, SIRT4 overexpression reduced MCD acetylation (Figure 3C). These data demonstrate that SIRT4 regulates the acetylation levels of MCD in cells.

To test whether SIRT4 can directly deacetylate MCD, we assessed the ability of SIRT4 to deacetylate MCD protein in vitro. We incubated MCD-FLAG with SIRT4-FLAG and SIRT4H162Y-FLAG immunoprecipitated from HEK293T cells in the presence of NAD^+. We observed that SIRT4 directly deacetylates MCD in vitro, whereas SIRT4H162Y does not (Figure 3D). Since SIRT4 interacts with SIRT3 (Ahuja et al., 2007), we wanted to exclude the possibility that the observed deacetylation was due to a contamination by SIRT3. We performed in vitro deacetylation assays using SIRT4 immunoprecipitated from HEK293T cells where SIRT3 was stably reduced by shRNA (Figure S2C) and immunoprecipitated MCD-FLAG from SIRT3 KO cells. We then observed that SIRT4 isolated from SIRT3-deficient cells could deacetylate MCD (Figure S2D). Next, to determine

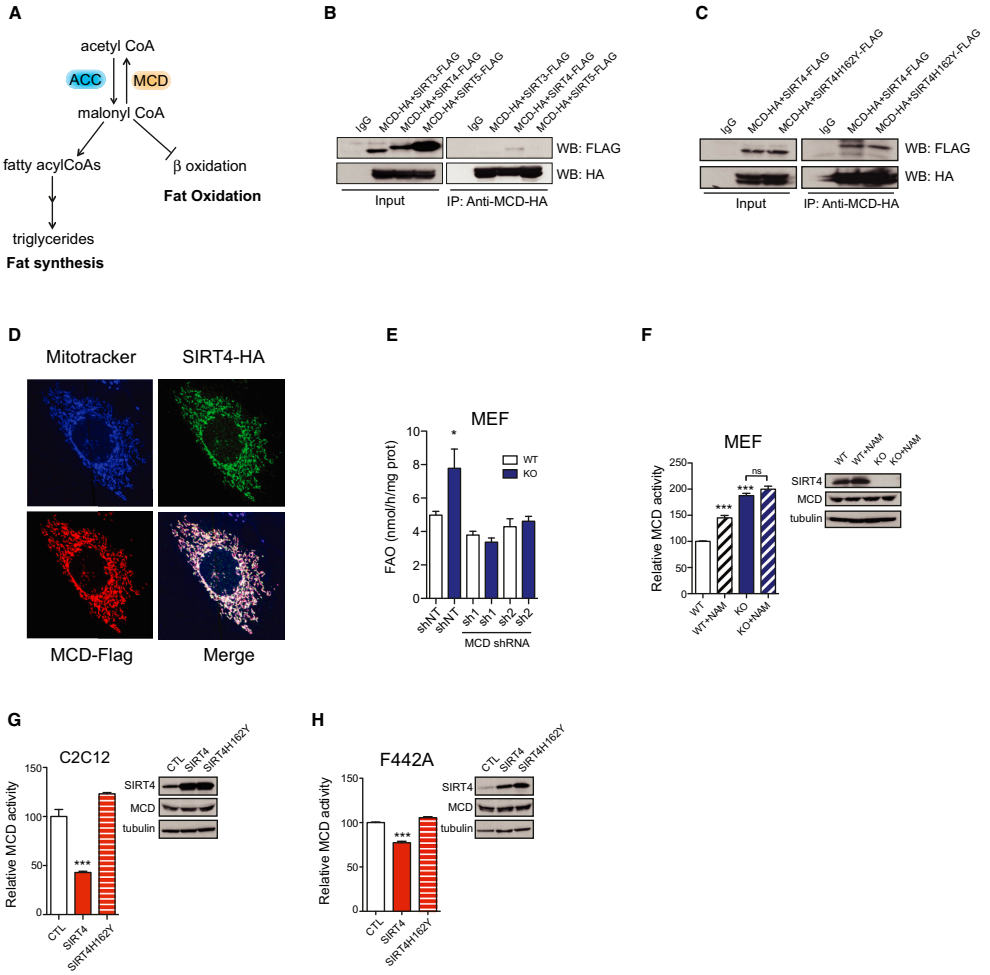

Figure 2. SIRT4 Interacts with and Represses MCD Activity

(A) Schematic of the regulation of lipid homeostasis and malonyl CoA by acetyl-CoA carboxylase (ACC) and malonyl CoA decarboxylase (MCD).

(B) Sirtuin-MCD interactions were assessed by cotransfecting expression vectors for SIRT3, SIRT4, or SIRT5 (FLAG-tagged at the C terminus) with an expression vector for C-terminal HA-tagged MCD in HEK293T cells. HA-tagged MCD was immunoprecipitated, and interactions were detected by immunoblotting with antibodies against FLAG.

(C) Expression vectors containing SIRT4 or SIRT4H162Y (FLAG-tagged) were cotransfected with C-terminal HA-tagged MCD in HEK293T cells, and SIRT4-MCD binding was assessed by immunoprecipitation of MCD-HA and western blotting with FLAG antibodies.

(D) The subcellular localization of SIRT4-HA (green) and MCD-FLAG (red) stably overexpressed in immortalized MEFs was examined by immunofluorescence using HA and FLAG antibodies and the mitochondrial marker Mitotracker (pseudocolored in blue).

(E) FAO rates were assessed in WT and SIRT4 KO primary MEFs treated with control shRNA (shNT) or two shRNAs against MCD (sh1 and sh2) as indicated (n = 3).

(F) Relative MCD activity in SIRT4 WT and SIRT4 KO immortalized MEFs treated or not with nicotinamide (NAM; striped bars) (n = 3).

(G and H) Relative MCD activity in C2C12 (n = 3) (G) or in F442A cells (n = 3) (H) overexpressing empty vector control, SIRT4, or SIRT4H162Y. Levels of SIRT4 and MCD proteins were determined by western blotting using antibodies for SIRT4 and MCD and tubulin as a loading control. In each panel, data represent mean ± SEM; *p < 0.05, **p < 0.01, ***p < 0.001. See also Figure S1.

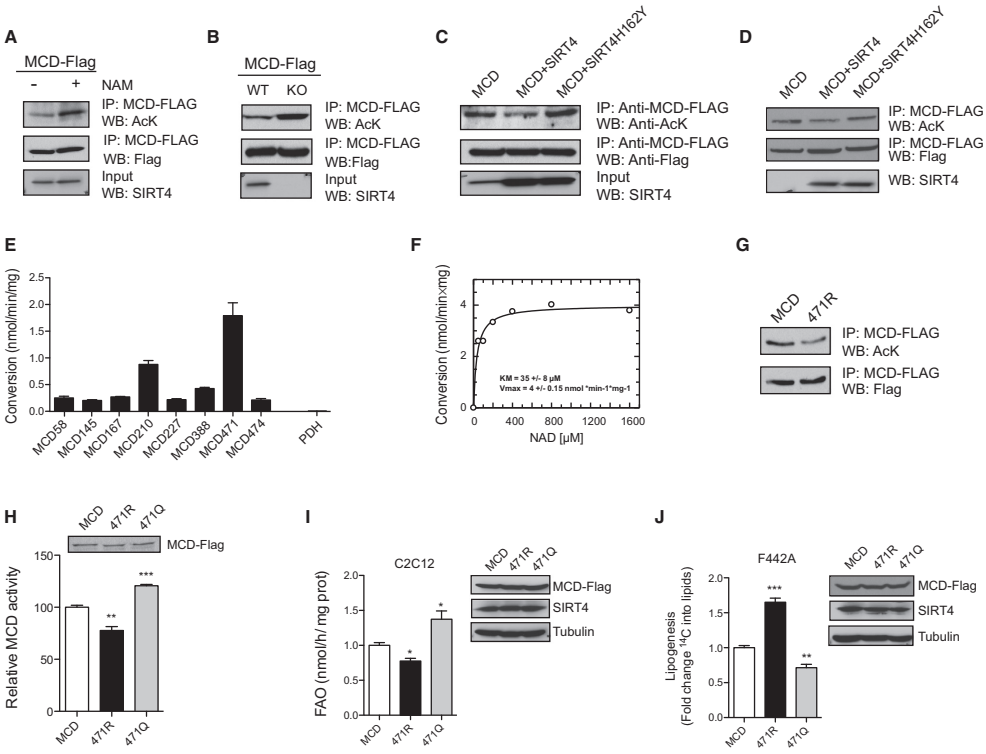

Figure 3. SIRT4 Deacetylates MCD

(A) MCD acetylation was measured in WT immortalized MEFs before or after treatment with NAM. FLAG-tagged MCD was stably overexpressed in WT MEFs treated with (+) or without (–) NAM and immunoprecipitated using antibodies against FLAG. MCD acetylation levels were assessed with antibodies against acetyl-lysine (AcK).

(B) MCD acetylation was assessed using WT and SIRT4 KO MEFs as described for (A).

(C) MCD acetylation was measured in C2C12 cells stably overexpressing FLAG-tagged MCD and SIRT4 or SIRT4H162Y. After immunoprecipitation of MCD with anti-FLAG antibodies, acetylation was measured as for (A).

(D) In vitro deacetylation assay was performed using immunopurified MCD and SIRT4. FLAG-MCD was immunoprecipitated from MEFs and incubated with FLAG-SIRT4 and FLAG-SIRT4H162Y immunoprecipitated from HEK293 cells and MCD acetylation status assessed by western blot.

(E) Recombinant SIRT4 was incubated with synthesized acetylated peptides of MCD, and peptide deacetylation was assessed using mass spectrometry. Acetylated peptide from pyruvate dehydrogenase (PDH) was included as a negative control (n = 3).

(F) Acetylated peptide was incubated with SIRT4, and NAD^+ concentrations were varied as indicated. Peptide deacetylation levels were analyzed by LC-MS.

(G) Constructs encoding MCD, MCD K471R, or MCD K471Q were expressed in HEK293T cells, and MCD activity was measured (n = 4).

(H and I) Retrovirus used to generate stable C2C12 (H) and F442A (I) cell lines overexpressing MCD, MCD K471R, or MCD K471Q where FAO rates and lipogenesis were assessed (n = 3). In each panel, data represent mean ± SEM; *p < 0.05, **p < 0.01, ***p < 0.001. See also Figures S2 and S6.

whether the deacetylation of MCD by SIRT4 regulates its activity, we measured MCD activity after in vitro deacetylation by SIRT4. MCD activity was reduced after incubation with SIRT4, but not with SIRT4H162Y (Figure S2E). Together, these results demonstrate that SIRT4 has a substrate-specific deacetylase activity, and that MCD is a target of SIRT4.

To elucidate which residues on MCD are deacetylated by SIRT4, we performed a series of mass spectrometry-based deacetylation assays using chemically synthesized acetylated peptides of MCD. We found that SIRT4 deacetylated lysine 471 of MCD with the highest efficiency but presented little activity against other acetylated MCD peptides (Figure 3E, Figure S2F, and Table S1). Providing an additional negative control, SIRT4 did not deacetylate pyruvate dehydrogenase (PDH), which is readily deacetylated by SIRT3 (data not shown), suggesting that SIRT4 deacetylase activity is substrate specific (Figure 3E), and

also not due to contaminant deacetylase activity. Moreover, this activity was NAD^+ dependent, and the recombinant SIRT4 used in this assay showed a K_m for NAD^+ comparable to that of other sirtuins (Figure 3F). Next we investigated the contribution of K471 to the total acetylation level and enzymatic activity of MCD. We tested the acetylation level of K471R MCD mutant, which cannot be acetylated on that residue, and found that K471R MCD was notably less acetylated than wild-type MCD (Figure 3G). To confirm the significance of K471 deacetylation to MCD enzyme function, we tested the enzymatic activity of K471R and K471Q MCD mutants, which mimic constitutive deacetylation and acetylation, respectively. K471R MCD had a reduced enzymatic activity (Figure 3H), whereas the K471Q variant had elevated activity (Figure 3H). These data indicate that SIRT4 possesses direct deacetylase activity on K471 of MCD in vitro and that acetylation of this residue accounts for a significant contribution to the total level of MCD acetylation and activity.

Finally, we examined the consequences of K471 acetylation status on palmitate oxidation and lipogenesis. In accordance with the effect observed on its enzymatic activity, the K471R MCD variant diminished fat oxidation, whereas K471Q MCD enhanced fat oxidation (Figure 3I). Similarly, lipogenesis was promoted by K471R MCD and repressed by K471Q MCD (Figure 3J). Of note, mutation of K210 in MCD, which was a weaker peptide SIRT4 substrate, did not alter fat oxidation or lipogenesis (Figures S2D and S2E). These results show that the acetylation status of the K471 residue of MCD regulates both lipogenesis and FAO.

SIRT4 Deacetylates MCD In Vivo during the Fed State

We next sought to understand the physiological relevance of the biochemical regulation of MCD by SIRT4. During periods of nutritional abundance, when surplus metabolic intermediates funnel into fatty acid synthesis and energy storage, the steady-state levels of malonyl CoA rise (Saggerson, 2008). This in turn prevents entry of fatty acids into mitochondria and dampens fat oxidation, while promoting fat synthesis (Figure 4A, left panel). Conversely, in the fasted state, when malonyl CoA is low, fatty acids are transported into the mitochondria and undergo β-oxidation (Figure 4A, right panel). Thus, malonyl CoA level is tightly linked to the nutritional state of the organism. As malonyl CoA is the substrate for MCD, we hypothesized that the regulation of MCD by SIRT4 might be linked to nutritional status of mice. To test this idea, we measured SIRT4 protein levels during the fed and fasting state in WT mice. SIRT4 levels decreased with fasting in muscle (Figure 4B) and WAT (Figure 4C), supporting the idea that SIRT4 may be important for the regulation of lipid metabolism during nutrient-rich conditions.

As SIRT4 represses MCD activity via deacetylation, we reasoned that MCD acetylation would be regulated by nutrient status. We assessed the acetylation level of MCD in muscle and WAT in WT mice under fed and fasted conditions. Proteins were immunoprecipitated with monoclonal anti-acetyl-lysine antibody and analyzed by western blot with MCD antibody. We found that MCD was deacetylated in muscle and WAT of fed mice (Figures 4D and 4E). Importantly, MCD is hyperacetylated in muscle and WAT of SIRT4 KO mice compared to WT (Figures 4F and 4G), demonstrating that SIRT4 is necessary for MCD deacetylation in vivo under fed conditions.

To determine whether SIRT4 represses MCD activity in vivo, we measured MCD activity in muscle and WAT of WT and SIRT4 KO mice in the fed state and found that, as in cells, MCD activity was significantly increased in SIRT4 KO compared to WT tissues (Figures 4H and 4I). Since MCD regulates lipid metabolism by lowering malonyl CoA levels, we hypothesized that SIRT4 may control malonyl CoA levels in response to nutrient availability. As expected, in both muscle and WAT of WT mice, malonyl CoA levels diminished with fasting (Figures 4J and 4K). Strikingly, SIRT4 deletion reduced malonyl CoA levels in both muscle and WAT during the fed state and abolished the switch between high and low malonyl CoA levels in the fed versus fasted state (Figures 4J and 4K). Thus, these studies identify SIRT4 as a physiological regulator of malonyl CoA levels in vivo.

Alteration of Lipid Metabolism in SIRT4 KO Mice

As MCD activity and malonyl CoA levels were altered in SIRT4 KO mouse, we examined potential physiological indicators of dysregulation in lipid metabolism. We measured the lipid composition of WAT and skeletal muscle isolated from WT and SIRT4 KO mice under fed and fasted conditions and observed that the levels of triglycerides and phospholipids in SIRT4 KO mice under fed conditions trended to the levels observed in WT and SIRT4 KO mice under fasting conditions (Figures 5A–5C). Moreover, the differences between fed and fasted levels of triglycerides and phospholipids were blunted in SIRT4 KO tissues. These observations indicated that SIRT4 loss in WAT and muscle may in part mimic a fasted state of lipid metabolism during fed conditions, and dampens the physiological switch to low nutrient conditions.

We next examined the physiological relevance of low malonyl CoA levels in fat oxidation and lipid synthesis. Exercise capacity is one well-established physiological readout of fatty acid oxidation. For example, AMPK activation increases skeletal muscle oxidative capacity and exercise endurance in mice (Narkar et al., 2008; Thomson et al., 2007). As SIRT4 loss increased MCD activity, resulting in low malonyl CoA level, we speculated that a metabolic shift toward lipid utilization in SIRT4 KO mice might augment exercise performance. Using untrained SIRT4 KO and WT littermate controls, we found that SIRT4 KO mice ran 20% further distance and longer running times during a graded, maximal treadmill challenge (Figures 5D and 5E). Whole-body indirect calorimetry showed that the respiratory exchange ratio (RER) of SIRT4 KO mice trended lower at high workloads and throughout 15 min of recovery (Figures 5F and 5G), suggesting increased lipid oxidation during these periods. We did not detect any major changes in the fiber types of SIRT4 WT and KO mice (Figure S3A). As well, blood glucose and lactate levels, measured 15 min after exercise, were similar between genotypes (Figure S3B). To test the possibility that these phenotypes stem from a general increase in mitochondrial content or function, we examined mitochondrial DNA content but did not observe differences in muscle or WAT of SIRT4 WT and KO mice (Figure S3C). In addition, we did not detect gross abnormalities in mitochondrial ultrastructure analyzed by electron microscopy (Figure S3D). Finally, we do not see a significant difference in mitochondrial and fat oxidation gene

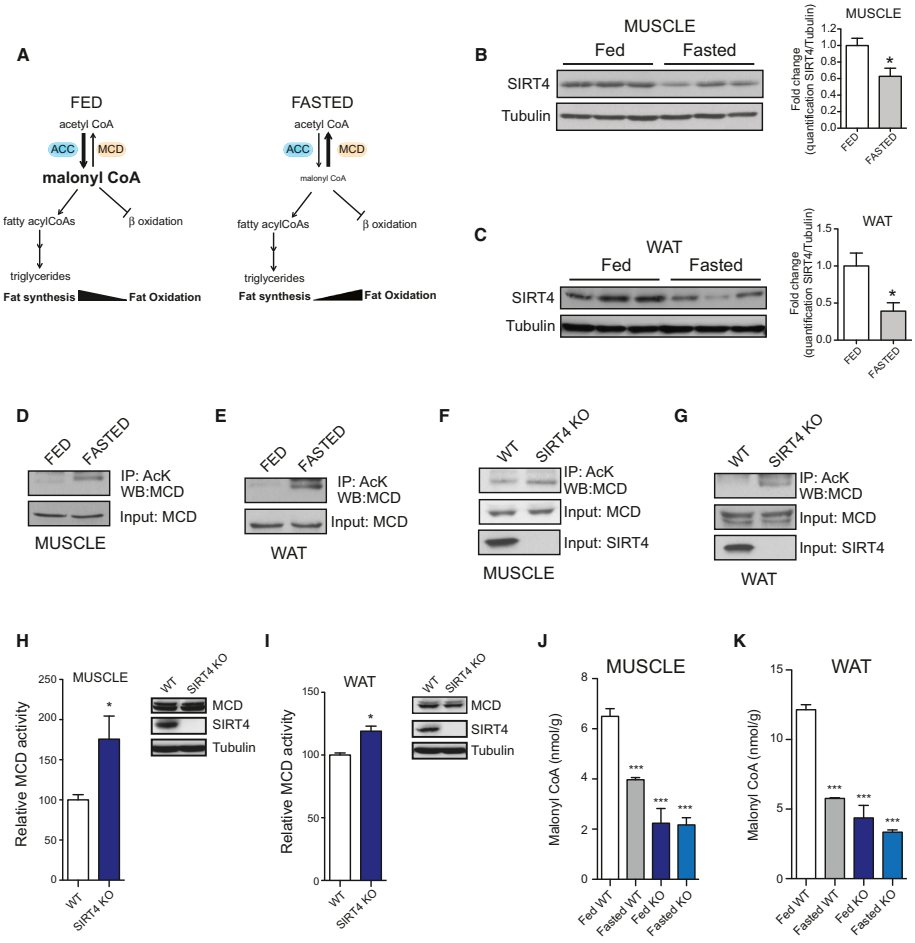

Figure 4. SIRT4 Deacetylates MCD In Vivo during the Fed State, Controlling Malonyl CoA Levels

(A) Schematic of the regulation of lipid homeostasis during fed and fasted state.

(B and C) Muscle (soleus) and WAT were harvested from mice under fed or fasted conditions and analyzed for SIRT4 expression by western blot and normalized to tubulin. Images were quantified (right panels) for the SIRT4/tubulin ratio using ImageJ.

(D and E) Muscle (soleus) and WAT extracts from WT mice fed or fasted were immunoprecipitated with a monoclonal AcK antibody and blotted for MCD.

(F and G) Muscle (soleus) and WAT extracts from WT and SIRT4 KO fed mice were immunoprecipitated with a monoclonal AcK antibody and blotted for MCD.

(H and I) Relative MCD activity in muscle (quadriceps) and WAT from WT and SIRT4 KO fed mice (n = 4 per genotype).

(J and K) Malonyl CoA levels were measured in muscle (quadriceps) and WAT from WT (open and gray bars) and SIRT4 KO (dark and light blue bars) mice under fed and fasted conditions (n = 4 per genotype, per condition). In each panel, data represent mean ± SEM; *p < 0.05, **p < 0.01, ***p < 0.001.

expression in the muscle of SIRT4 KO mice compared to WT muscle (Figure S3E). Thus, these results are consistent with an increase in fat oxidation in SIRT4 KO mice, leading to higher exercise capacity.

To examine whether SIRT4 loss affected lipid synthesis in vivo, we monitored de novo lipogenesis by measuring incorporation of deuterated water into palmitate, as previously described (Edmond et al., 1998; Lee et al., 1994). Deuterium atoms

exchange with hydrogen atoms on different carbon positions of glucose metabolites as they go through the glycolytic/gluconeogenic pathways and the TCA cycle (Radziuk and Pye, 2002), and the accumulation of these deuterated metabolites can contribute to deuterium labeling of fatty acids during de novo lipogenesis. The extent of labeled palmitate, representing de novo lipid synthesis, can be measured by GC-MS. We observed a 50% reduction in the percentage of newly synthesized lipids in SIRT4 KO WAT compared to WT tissue, highlighting the importance of SIRT4 to de novo lipogenesis in vivo (Figure 5H). This effect is not observed in liver and plasma, where we found that palmitate synthesis was identical in WT and SIRT4 KO animals (Figures 5I and 5J). Malonyl CoA levels were also not different in livers of SIRT4 KO mice (Figure S3F), consistent with previous studies identifying a major role for MCD in organs other than the liver (Ruderman et al., 2003). Overall, these results suggest that SIRT4 plays a major role in lipid homeostasis by repressing fat oxidation and promoting lipid anabolism in vivo.

SIRT4 Deletion Protects against Dietary-Induced Obesity

Increased lipogenesis can contribute to obesity. We therefore investigated whether the decrease in lipogenesis observed in SIRT4 KO mice would correspond with a change in weight gain. On a standard low-fat diet (LFD), SIRT4 KO mice have normal growth curves (Figure 6A), and do not display differences in adipose fat mass (Figures S4A–S4D) or serum lipid profiles (Figures S4E–S4H). Strikingly, when SIRT4 KO mice were placed on a high-fat diet (HFD), their weight gain remained similar to the mice under LFD, and was significantly less than the weight gain of WT mice under HFD (Figure 6A). Thus, we show for the first time that loss of SIRT4 protects mice from HFD-induced obesity.

To better understand the mechanism of protection against obesity in SIRT4 KO mice, we assessed the body composition of animals fed a HFD using computed tomography (CT) scans. The percentage of fat mass was significantly lower in SIRT4 KO mice compared to control animals (Figures 6B and 6C). By contrast, absence of SIRT4 did not appear to affect the percentage of brown adipose tissue (BAT) (Figure S4I). In addition, while liver weight was not affected by SIRT4 loss (Figure S4J), weight of epididymal WAT was significantly lower in the SIRT4 KO mice compared to WT animals (Figure 6D). We found that WAT in SIRT4 KO mice appears normal, and we did not detect increased signs of apoptosis, structural alterations, or inflammation (Figure 6E and Figures S4K and S4L).

To test whether protection from adiposity was due to difference in food intake, we analyzed food consumption. SIRT4 KO mice ate equivalent amounts (or slightly more) as WT controls (Figure 6F). Likewise, we did not detect differences in their RER or physical activity (Figures S4M and S4N). By contrast, analysis of energy expenditure revealed that SIRT4 KO mice have a significant increase in energy expenditure during the dark cycle (Figures 6G–6I); this increased energy burning phenotype is consistent with our cellular data and provides an explanation for the protection against a HFD. As the dark cycle corresponds to the fed state in mice, this result also supports the role of SIRT4 function during nutrient abundance. Interestingly, despite protection against diet-induced obesity, the SIRT4 KO mice were equally susceptible to glucose and insulin intolerance when compared to their WT counterparts (Figures S5A–S5E).

Finally, we assessed MCD acetylation levels in SIRT4 WT and KO mice under HFD in WAT. As expected, we found that MCD was hyperacetylated in SIRT4 KO mice compared to WT mice (Figure 6J). Measurement of MCD activity demonstrated an elevated activity (Figure 6K and Figure S5F), and consistently malonyl CoA levels (Figure 6L and Figure S5G) were lower in SIRT4 KO compared to WT mice. These data demonstrate that SIRT4 loss increases MCD acetylation and activity during a high-fat dietary challenge.

DISCUSSION

In this study, we identify a clear role for the mitochondrial sirtuin, SIRT4, in the metabolic reprogramming toward anabolic lipid processes to promote lipogenesis while inhibiting fatty acid oxidation (Figure 1). Mechanistically, SIRT4 mediates this switch in lipid homeostasis by binding, deacetylating K471, and inhibiting MCD activity (Figures 2 and 3). Interestingly, only a few cases of protein deacetylation have been described to result in decreased enzymatic activity (Zhao et al., 2010; Kim et al., 2012). K471 is at close distance to the malonyl CoA entry point (PDB ID code 2YGW), and its acetylation might help gate the ligand entry (Figure S6). In addition, we discovered that SIRT4 regulates MCD activity and malonyl CoA levels in vivo (Figure 4). SIRT4 represses MCD in the fed state (Figure 4), promoting lipid synthesis and storage while inhibiting lipid catabolism. SIRT4 KO mice are deficient for this switch between fed and fasted states (Figure 5) and demonstrate decreased lipogenesis in vivo (Figure 5). As a consequence, when placed under HFD, SIRT4 KO mice are resistant to diet-induced obesity (Figure 6).

Sirtuins possess multiple enzymatic activities, and this is the first study to demonstrate that SIRT4 possesses deacetylase activity. SIRT5 was reported to have deacetylase activity (Nakagawa et al., 2009), but recent work demonstrated that SIRT5 is also a demalonylase and desuccinylase (Du et al., 2011; Peng et al., 2011). Similarly, SIRT6 was initially thought to function solely as an ADP-ribosyltransferase, but later studies identified a substrate-specific deacetylase activity (Zhong et al., 2010). No deacetylase activity was reported for SIRT4 using histone or BSA substrates (Haigis et al., 2006; Ahuja et al., 2007; Schwer et al., 2002). However, our data suggest that the absence of deacetylase activity for SIRT4 may have been a reflection of the lack of an appropriate substrate. Here, we show for the first time that SIRT4 has a susbstrate-specific deacetylase activity, as SIRT4 deacetylates MCD directly and regulates the levels of its acetylation in cells and organs. In the future, it will be interesting to assess whether SIRT4 possesses other deacylase activities.

Maintenance of metabolic homeostasis requires a coordinated regulation of energy intake, storage, and expenditure. Metabolic pathways are designed to sense incoming nutritional and environmental cues and to respond appropriately. Due to their dependency on NAD^+, sirtuins are critical modulators of metabolism, sensing changes in metabolic cues in order to exert adaptive responses (Houtkooper et al., 2012). Our work reveals that SIRT4 mediates the switch between anabolic and catabolic

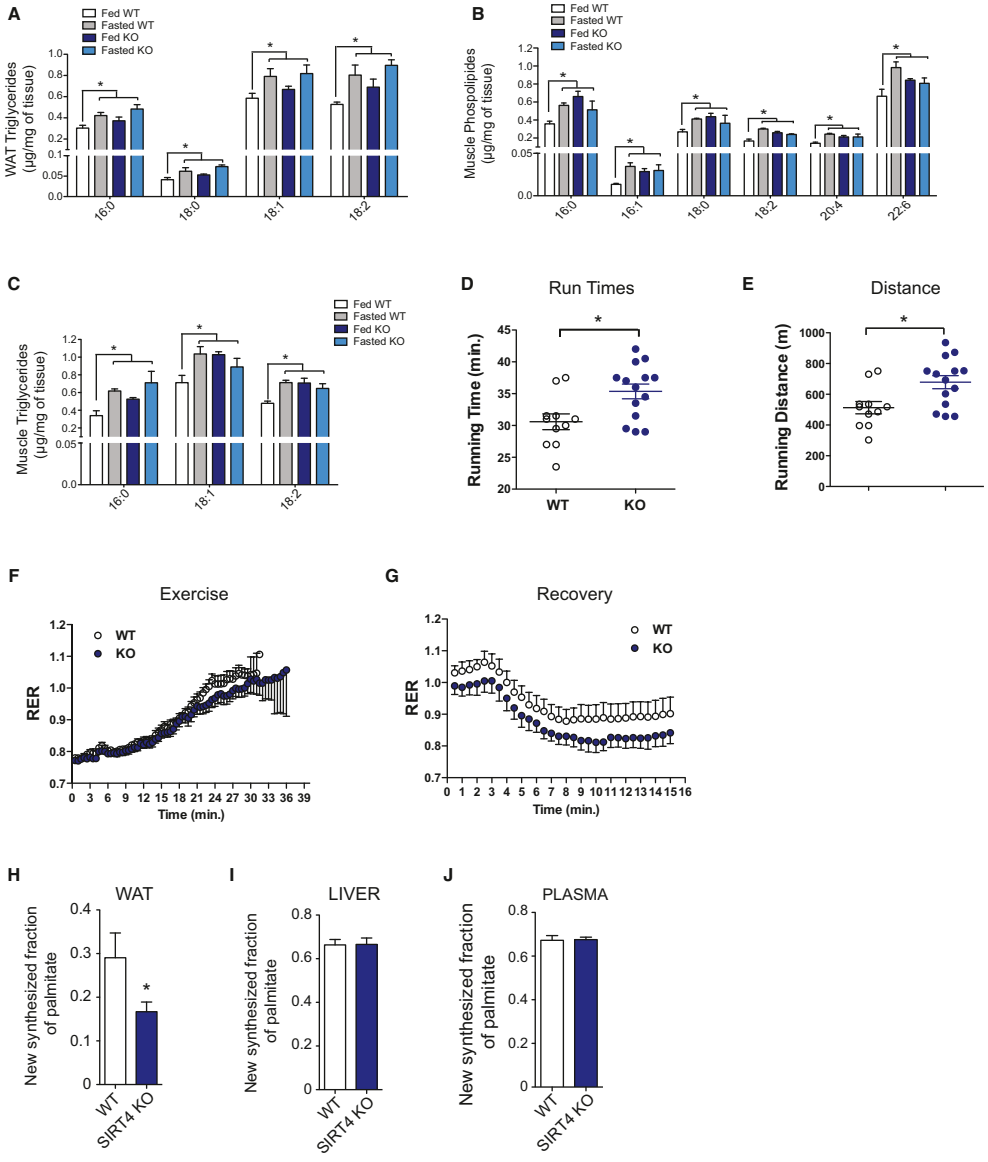

Figure 5. SIRT4 KO Mice Display an Altered Lipid Metabolism In Vivo

(A) Triglyceride composition from WAT from WT and SIRT4 KO fed and fasted mice (n = 3 mice per genotype, per condition).

(B and C) Skeletal muscle (quadriceps) phospholipid and triglyceride composition from WT and SIRT4 KO fed and fasted mice (n = 3 mice per genotype, per condition).

(legend continued on next page)

pathways through the regulation of MCD. It was proposed that AMPK may regulate MCD activity, but this regulation remains unclear (Kuhl et al., 2006; Habinowski et al., 2001; Sambandam et al., 2004; Saha et al., 2000). We uncovered a distinct regulation of MCD via acetylation. Thus, it will be interesting for future studies to examine how MCD acetylation may synergize with differences in AMPK activity.

Our data suggest that the mitochondrial form of MCD is important for control of lipid metabolism, shedding new light on the significance of mitochondrial malonyl CoA. Our findings indicate that influencing mitochondrial malonyl CoA can affect both fat oxidation and lipogenesis. Indeed, we show that changes in mitochondrial MCD activity clearly affect total malonyl CoA levels (2- to 3-fold in SIRT4 KO muscle and WAT). However, little is known about how the mitochondrial pool of malonyl CoA regulates these pathways. Of note, a recent study similarly showed that changes in mitochondrial lipogenesis protected against diet-induced obesity (Smith et al., 2012). It will be important for future studies to examine the mechanisms that control mitochondrial versus cytoplasmic malonyl CoA, such as involvement of transporters or shuttle systems, and dissect their role in lipid homeostasis.

Strikingly, loss of SIRT4 increases exercise capacity. Exercise training activates a number of pathways that contribute to metabolic reprogramming of lipid handling (Bassel-Duby and Olson, 2006). Of relevance, decreased malonyl CoA has been observed in muscle after exercise, increasing fat oxidation (Dean et al., 2000; Hutber et al., 1997). A study showed that these changes were associated with increased MCD activity (Kuhl et al., 2006). In line with these observations, we show that deletion of SIRT4 leads to decreased malonyl CoA levels and increased exercise capacity, suggesting that SIRT4 might play a role in metabolic reprogramming during exercise training.

The adaptations that improve exercise performance are typically expected to protect against obesity and related metabolic disorders, making it important to identify proteins involved in this reprogramming to treat metabolic diseases. However, the glucose homeostasis of SIRT4 KO mice on a HFD resemble that of WT mice on a HFD (Figure S6), demonstrating that while SIRT4 loss protects against diet-induced adiposity, it does not protect the animals against metabolic dysfunction that arises with high-fat challenge. Thus, SIRT4 loss appears to uncouple metabolic fitness from obesity. Interestingly, and in line with our observation, deletion of MCD protects against insulin resistance (Koves et al., 2008). Likewise, increased mitochondrial flux and fatty acid oxidation are associated with some models of insulin resistance (Sunny et al., 2011; Koves et al., 2008). To understand this uncoupling, it will be important for future studies to probe the role of SIRT4 and MCD in glucose and insulin homeostasis and to assess further the potential therapeutic consequences of modulating SIRT4 or MCD function. In sum, our work uncovers an aspect of lipid metabolic reprogramming mediated by SIRT4 deacetylation of MCD.

EXPERIMENTAL PROCEDURES

Cell Culture

MEFs were isolated from SIRT4 WT and KO littermate embryos as described (Xu, 2005) and were immortalized using the SV40 large T antigen. F442A cells were differentiated as previously described (Djian et al., 1985). Isolation of primary adipocytes was performed as previously described (Eguchi et al., 2011). All primary cell cultures were performed using a minimum of two independently generated cell lines per genotype. For NAM treatments, cells were incubated overnight with a final concentration of 20 mM NAM. Lentiviral shRNA against SIRT4 clones were purchased from Openbiosystems and lentiviral shRNA against MCD was obtained from The RNAi Consortium (TRC) at the Broad Institute/Harvard. Stable knockdown cell lines were generated according to TRC instructions. MCD cDNA was purchased from Openbiosystems and cloned into pBabe vector for stable expression and pcDNA (HA tag) for transient transfection. Cells overexpressing SIRT4 and SIRT4H162Y were generated by retroviral infection by pBabe vector. Commercial antibodies were used to analyze acetyl-lysine (ImmuneChem for western blotting and PTM biolabs for immunoprecipitation), and antibodies raised against murine SIRT4 were described previously (Haigis et al., 2006).

Measurement of De Novo Lipogenesis in Cells, Triglyceride Content, and Oil Red O Staining

For the measurement of lipogenesis, F442A cells and primary adipocytes were placed overnight in low-glucose low-serum media, then labeled with 1-^{14}C acetic acid (Perkin Elmer) while stimulated with insulin and high glucose for 1 hr. Cells were washed twice with PBS before lysis in 0.5% Triton X-100. The lipid fraction was extracted by the addition of chloroform and methanol (2:1 v/v), followed by the addition of water. Samples were centrifuged, and ^{14}C incorporation was measured in the bottom, lipid-containing phase using a scintillation counter. Each condition was normalized to protein concentrations. Triglycerides were measured using the adipogenesis assay kit from Biovison (K610-100), and oil red O staining was performed using the adipogenesis assay kit from Millipore (ECM950).

Fatty Acid Oxidation

C2C12 cells were differentiated in 2% horse serum media and incubated overnight in culture medium containing 100 μM palmitate (C16:0) and 1 mM carnitine. In the final 2 hr of incubation, cells were pulsed with 1.7 μCi [9,10(n)-^{3}H]palmitic acid (GE Healthcare), and the medium was collected and eluted on ion exchange columns packed with DOWEX 1X2-400 resin (Sigma) to analyze the released $^{3}H_2O$, formed during cellular oxidation of [^{3}H]palmitate. For FAO assays in MEFs, primary MEFs were used below passage 5.

MCD Activity Assay and Determination of Malonyl CoA Levels

MCD activity was tested using a radiochemical assay (Kerner and Hoppel, 2002). Briefly, protein lysates are incubated with [2-^{14}C]malonyl CoA which is decarboxylated by MCD into [2-^{14}C]acetyl-CoA, which is converted to [2-^{14}C]acetylcarnitine in the presence of excess L-carnitine (Sigma) and carnitine acetyltransferase (Roche). The positively charged radiolabeled product, acetylcarnitine, is separated from negatively charged excess radiolabeled substrate through an exclusion column, and the radioactivity is measured by scintillation counting. MCD activity assays were performed on 50 μg of protein from cell or tissue lysates. Malonyl CoA was determined by the method previously described (McGarry et al., 1978; Saha et al., 1995) to measure malonyl CoA-dependent incorporation of [^{3}H]acetyl CoA into fatty acids, and results were normalized by protein content (Linn, 1981).

(D and E) Exercise tolerance assays were performed on WT and SIRT4 KO mice (n = 11–14 per genotype).
(F and G) RER in WT and SIRT4 KO mice during exercise (F) and recovery (G) (n = 11–14).
(H–J) De novo lipogenesis in vivo was measured by determining incorporation of deuterated water into palmitate in WAT (H), liver (I), and plasma (J) (n = 6 per genotype). New synthesized fraction has a max value of 1, where the number of observed deuteriums on palmitate measured equals the number of maximal deuterium atoms incorporated. In each panel, data represent mean ± SEM; *p < 0.05, **p < 0.01, ***p < 0.001. See also Figure S3.

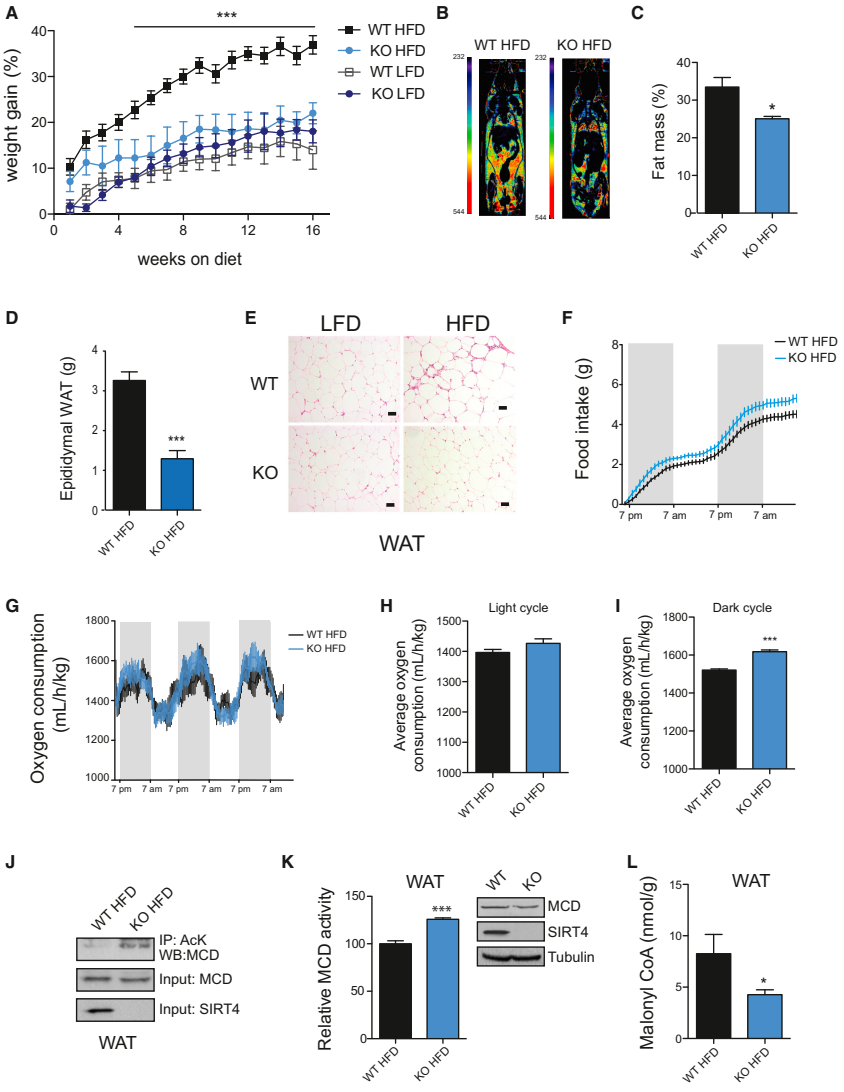

Figure 6. SIRT4 KO Mice Are Protected from Diet-Induced Weight Gain

(A) Body weight of WT and SIRT4 KO mice on a low-fat diet (LFD) and high-fat diet (HFD) (n = 10–12 per genotype).

(B) Representative images of CT scan of WT and SIRT4 KO mice on a HFD with fat mass highlighted. Red represents the highest value in the range of WAT density and in blue the lowest.

(C) Percentage of fat mass analyzed by CT scan of WT and SIRT4 KO mice on a HFD (n = 6 per genotype).

(D) Epididymal WAT weights from WT and SIRT4 KO mice on a HFD (n = 6 per genotype).

(E) Representative hematoxylin and eosin staining slides of WAT of WT and SIRT4 KO mice under LFD and HFD. Scale bar, 50 μM.

(F) Food intake in WT and SIRT4 KO mice on a HFD (n = 6 per genotype).

(legend continued on next page)

Animal Studies

Studies were performed according to protocols approved by the Institutional Animal Care and Use Committee, the Standing Committee on Animals at Harvard. Three- to four-month-old SIRT4 WT and KO male littermates (n = 6) fed a normal chow diet (PicoLab Diet 5053) were used for all LFD studies. For fasting experiments, food was removed just before the dark cycle (7 p.m.), and mice were subjected to fasting conditions overnight before sacrifice. For lipid composition, organs were analyzed by the Vanderbilt Mouse Metabolic Phenotyping Center (MMPC) using GCMS. For HFD experiments, SIRT4 WT and KO male littermates (n = 6) mice were fed D12492 from Research diets for 16 weeks, and studies were performed with two to three separate cohorts of mice. Body weight was measured weekly. CT scan studies were performed at the Longwood SAIF (Boston). SIRT4 WT and KO male mice fed a HFD (n = 6) were used. Results were analyzed using InVivoScope software.

Exercise Tolerance Assays

Male SIRT4 KO and littermate controls (n = 11–14) were habituated to the metabolic treadmills (Columbus Instruments) for 3 days prior to exercise testing. Each 15 min habituation session consisted of a 5 min exploration session at 0 m/min, 5 min at 6 m/min, and 5 min at 15 m/min at a constant 10° incline. A mild electrical stimulus was applied to trained mice to remain on the moving treadmill belt. O_2 and CO_2 gas sensors (Columbus Instruments) were calibrated before every test, and testing started at 8 a.m. each morning following removal of food for 1 hr. After collection of resting gasses, the treadmill was started at a speed of 6 m/min and was increased by 3 m/min every 3 min until mice could no longer maintain the set workload. Animals were allowed to recover for 15 min in the metabolic treadmills, after which blood glucose (Accu-Check Aviva) and lactate (Nova Biomedicals) were obtained from tail blood. All procedures were approved by Duke University Institutional Animal Care and Use Committee.

Lipogenesis In Vivo

De novo lipogenesis studies were done by measuring palmitate (C16:0) enrichments using gas chromatography (GC)-electron impact ionization (EI) mass spectrometry (MS) as previously described (Lee et al., 1994; Edmond et al., 1998). Briefly, mice were injected with 6% body water of deuterated water followed by 4% D_20 in the drinking water for 14 days. After harvesting the organs, petroleum ether extractions of the fatty acids were performed after acidification of the saponified tissue. Fatty acid methyl esters (FAMEs) were prepared by adding 200 μl methanolic HCl (Supelco) to the dried fatty acid fraction and were then heated at 100°C for at least 1 hr. FAME was then dried with nitrogen, redissolved in hexane as solvent, and analyzed by GC/MS.

Statistical Analysis

Analyses were performed using an unpaired Student's t test and ANOVA test for lipid composition. Significant differences are as follows: *p < 0.05, **p < 0.01, and ***p < 0.001. All experiments were performed at least two to three times.

SUPPLEMENTAL INFORMATION

Supplemental Information includes six figures, one table, Supplemental Experimental Procedures, and Supplemental References and can be found with this article at http://dx.doi.org/10.1016/j.molcel.2013.05.012.

ACKNOWLEDGMENTS

We thank Hong Lu for technical assistance and Carla Harris (Vanderbilt MMPC Lipid Lab, DK59637) for lipid composition analysis. We thank the Nikon Imaging Center at Harvard Medical School. We thank Lydia Finley and the members of the Haigis lab for helpful discussions and constructive comments on the paper. G.L. was supported by Human Frontier Science Program, N.J.G. by National Science Fondation graduate research fellowship, V.C.J.d.B. by grants from the Netherlands Organization for Scientific Research (grants 916.10.065 and 825.07.005), and M.D. by NIDDK grant 1F32DK093256-01. I.J.K. was supported by grants DK58132-01A2, U19AI091175-01, and P60DK020541 (Einstein DRTC). N.B.R. and A.K.S. were supported by USPHS grants RO1DK19514 and RO1DK67509. T.R.K. was supported by Ellison Foundation grant AG-NS-0548-09. D.M.M. was supported by NIH grants 1RO1HL101189 and 2PO1DK05398. M.C.H. was supported by funding from NIH grant AG032375, Ellison Foundation AG-NS-0573-09, Glenn Foundation for Medical Research, and funding from SIRTRIS-GSK.

Received: December 18, 2012
Revised: March 22, 2013
Accepted: May 2, 2013
Published: June 6, 2013

REFERENCES

Ahuja, N., Schwer, B., Carobbio, S., Waltregny, D., North, B.J., Castronovo, V., Maechler, P., and Verdin, E. (2007). Regulation of insulin secretion by SIRT4, a mitochondrial ADP-ribosyltransferase. J. Biol. Chem. *282*, 33583–33592.

Barber, M.F., Michishita-Kioi, E., Xi, Y., Tasselli, L., Kioi, M., Moqtaderi, Z., Tennen, R.I., Paredes, S., Young, N.L., Chen, K., et al. (2012). SIRT7 links H3K18 deacetylation to maintenance of oncogenic transformation. Nature *487*, 114–118.

Bassel-Duby, R., and Olson, E.N. (2006). Signaling pathways in skeletal muscle remodeling. Annu. Rev. Biochem. *75*, 19–37.

Dean, D., Daugaard, J.R., Young, M.E., Saha, A., Vavvas, D., Asp, S., Kiens, B., Kim, K.H., Witters, L., Richter, E.A., and Ruderman, N. (2000). Exercise diminishes the activity of acetyl-CoA carboxylase in human muscle. Diabetes *49*, 1295–1300.

Djian, P., Phillips, M., and Green, H. (1985). The activation of specific gene transcription in the adipose conversion of 3T3 cells. J. Cell. Physiol. *124*, 554–556.

Du, J., Zhou, Y., Su, X., Yu, J.J., Khan, S., Jiang, H., Kim, J., Woo, J., Kim, J.H., Choi, B.H., et al. (2011). Sirt5 is a NAD-dependent protein lysine demalonylase and desuccinylase. Science *334*, 806–809.

Duncan, R.E., Ahmadian, M., Jaworski, K., Sarkadi-Nagy, E., and Sul, H.S. (2007). Regulation of lipolysis in adipocytes. Annu. Rev. Nutr. *27*, 79–101.

Edmond, J., Higa, T.A., Korsak, R.A., Bergner, E.A., and Lee, W.N. (1998). Fatty acid transport and utilization for the developing brain. J. Neurochem. *70*, 1227–1234.

Eguchi, J., Wang, X., Yu, S., Kershaw, E.E., Chiu, P.C., Dushay, J., Estall, J.L., Klein, U., Maratos-Flier, E., and Rosen, E.D. (2011). Transcriptional control of adipose lipid handling by IRF4. Cell Metab. *13*, 249–259.

Habinowski, S.A., Hirshman, M., Sakamoto, K., Kemp, B.E., Gould, S.J., Goodyear, L.J., and Witters, L.A. (2001). Malonyl-CoA decarboxylase is not a substrate of AMP-activated protein kinase in rat fast-twitch skeletal muscle or an islet cell line. Arch. Biochem. Biophys. *396*, 71–79.

Haigis, M.C., Mostoslavsky, R., Haigis, K.M., Fahie, K., Christodoulou, D.C., Murphy, A.J., Valenzuela, D.M., Yancopoulos, G.D., Karow, M., Blander, G., et al. (2006). SIRT4 inhibits glutamate dehydrogenase and opposes the effects of calorie restriction in pancreatic beta cells. Cell *126*, 941–954.

(G–I) Energy expenditure in WT and SIRT4 KO mice on a HFD (n = 6 per genotype).
(J) WAT extracts from WT and SIRT4 KO mice under HFD were immunoprecipitated with a monoclonal AcK antibody and western blotted for MCD.
(K) MCD activity in WAT of WT and SIRT4 KO mice under HFD.
(L) Malonyl CoA levels in WAT of WT and SIRT4 KO mice under HFD. In each panel, data represent mean ± SEM; *p < 0.05, **p < 0.01, ***p < 0.001. See also Figures S4 and S5.

Hardie, D.G. (2011). Sensing of energy and nutrients by AMP-activated protein kinase. Am. J. Clin. Nutr. *93*, 891S–896S.

Houtkooper, R.H., Pirinen, E., and Auwerx, J. (2012). Sirtuins as regulators of metabolism and healthspan. Nat. Rev. Mol. Cell Biol. *13*, 225–238.

Hutber, C.A., Rasmussen, B.B., and Winder, W.W. (1997). Endurance training attenuates the decrease in skeletal muscle malonyl-CoA with exercise. J. Appl. Physiol. *83*, 1917–1922.

Kerner, J., and Hoppel, C.L. (2002). Radiochemical malonyl-CoA decarboxylase assay: activity and subcellular distribution in heart and skeletal muscle. Anal. Biochem. *306*, 283–289.

Kim, E.Y., Kim, W.K., Kang, H.J., Kim, J.H., Chung, S.J., Seo, Y.S., Park, S.G., Lee, S.C., and Bae, K.H. (2012). Acetylation of malate dehydrogenase 1 promotes adipogenic differentiation via activating its enzymatic activity. J. Lipid Res. *53*, 1864–1876.

Koves, T.R., Ussher, J.R., Noland, R.C., Slentz, D., Mosedale, M., Ilkayeva, O., Bain, J., Stevens, R., Dyck, J.R., Newgard, C.B., et al. (2008). Mitochondrial overload and incomplete fatty acid oxidation contribute to skeletal muscle insulin resistance. Cell Metab. *7*, 45–56.

Kuhl, J.E., Ruderman, N.B., Musi, N., Goodyear, L.J., Patti, M.E., Crunkhorn, S., Dronamraju, D., Thorell, A., Nygren, J., Ljungkvist, O., et al. (2006). Exercise training decreases the concentration of malonyl-CoA and increases the expression and activity of malonyl-CoA decarboxylase in human muscle. Am. J. Physiol. Endocrinol. Metab. *290*, E1296–E1303.

Lee, W.N., Bassilian, S., Guo, Z., Schoeller, D., Edmond, J., Bergner, E.A., and Byerley, L.O. (1994). Measurement of fractional lipid synthesis using deuterated water (2H2O) and mass isotopomer analysis. Am. J. Physiol. *266*, E372–E383.

Linn, T.C. (1981). Purification and crystallization of rat liver fatty acid synthetase. Arch. Biochem. Biophys. *209*, 613–619.

Lombard, D.B., Tishkoff, D.X., and Bao, J. (2011). Mitochondrial sirtuins in the regulation of mitochondrial activity and metabolic adaptation. Handb. Exp. Pharmacol. *206*, 163–188.

Long, Y.C., and Zierath, J.R. (2006). AMP-activated protein kinase signaling in metabolic regulation. J. Clin. Invest. *116*, 1776–1783.

McGarry, J.D., Stark, M.J., and Foster, D.W. (1978). Hepatic malonyl-CoA levels of fed, fasted and diabetic rats as measured using a simple radioisotopic assay. J. Biol. Chem. *253*, 8291–8293.

Nakagawa, T., Lomb, D.J., Haigis, M.C., and Guarente, L. (2009). SIRT5 deacetylates carbamoyl phosphate synthetase 1 and regulates the urea cycle. Cell *137*, 560–570.

Nam, H.W., Lee, G.Y., and Kim, Y.S. (2006). Mass spectrometric identification of K210 essential for rat malonyl-CoA decarboxylase catalysis. J. Proteome Res. *5*, 1398–1406.

Narkar, V.A., Downes, M., Yu, R.T., Embler, E., Wang, Y.X., Banayo, E., Mihaylova, M.M., Nelson, M.C., Zou, Y., Juguilon, H., et al. (2008). AMPK and PPARdelta agonists are exercise mimetics. Cell *134*, 405–415.

Nasrin, N., Wu, X., Fortier, E., Feng, Y., Bare', O.C., Chen, S., Ren, X., Wu, Z., Streeper, R.S., and Bordone, L. (2010). SIRT4 regulates fatty acid oxidation and mitochondrial gene expression in liver and muscle cells. J. Biol. Chem. *285*, 31995–32002.

Peng, C., Lu, Z., Xie, Z., Cheng, Z., Chen, Y., Tan, M., Luo, H., Zhang, Y., He, W., Yang, K., et al. (2011). The first identification of lysine malonylation substrates and its regulatory enzyme. Mol. Cell. Proteom. *10*. http://dx.doi.org/10.1074/mcp.M111.012658, M111.012658.

Radziuk, J., and Pye, S. (2002). Quantitation of basal endogenous glucose production in type II diabetes: importance of the volume of distribution. Diabetologia *45*, 1053–1084.

Ruderman, N.B., Park, H., Kaushik, V.K., Dean, D., Constant, S., Prentki, M., and Saha, A.K. (2003). AMPK as a metabolic switch in rat muscle, liver and adipose tissue after exercise. Acta Physiol. Scand. *178*, 435–442.

Saggerson, D. (2008). Malonyl-CoA, a key signaling molecule in mammalian cells. Annu. Rev. Nutr. *28*, 253–272.

Saha, A.K., and Ruderman, N.B. (2003). Malonyl-CoA and AMP-activated protein kinase: an expanding partnership. Mol. Cell. Biochem. *253*, 65–70.

Saha, A.K., Kurowski, T.G., and Ruderman, N.B. (1995). A malonyl-CoA fuel-sensing mechanism in muscle: effects of insulin, glucose, and denervation. Am. J. Physiol. *269*, E283–E289.

Saha, A.K., Schwarsin, A.J., Roduit, R., Masse, F., Kaushik, V., Tornheim, K., Prentki, M., and Ruderman, N.B. (2000). Activation of malonyl-CoA decarboxylase in rat skeletal muscle by contraction and the AMP-activated protein kinase activator 5-aminoimidazole-4-carboxamide-1-beta -D-ribofuranoside. J. Biol. Chem. *275*, 24279–24283.

Sambandam, N., Steinmetz, M., Chu, A., Altarejos, J.Y., Dyck, J.R., and Lopaschuk, G.D. (2004). Malonyl-CoA decarboxylase (MCD) is differentially regulated in subcellular compartments by 5'AMP-activated protein kinase (AMPK). Studies using H9c2 cells overexpressing MCD and AMPK by adenoviral gene transfer technique. Eur. J. Biochem. *271*, 2831–2840.

Schwer, B., North, B.J., Frye, R.A., Ott, M., and Verdin, E. (2002). The human silent information regulator (Sir)2 homologue hSIRT3 is a mitochondrial nicotinamide adenine dinucleotide-dependent deacetylase. J. Cell Biol. *158*, 647–657.

Smith, S., Witkowski, A., Moghul, A., Yoshinaga, Y., Nefedov, M., de Jong, P., Feng, D., Fong, L., Tu, Y., Hu, Y., et al. (2012). Compromised mitochondrial fatty acid synthesis in transgenic mice results in defective protein lipoylation and energy disequilibrium. PLoS ONE *7*, e47196. http://dx.doi.org/10.1371/journal.pone.0047196.

Sunny, N.E., Parks, E.J., Browning, J.D., and Burgess, S.C. (2011). Excessive hepatic mitochondrial TCA cycle and gluconeogenesis in humans with nonalcoholic fatty liver disease. Cell Metab. *14*, 804–810.

Thomson, D.M., Porter, B.B., Tall, J.H., Kim, H.J., Barrow, J.R., and Winder, W.W. (2007). Skeletal muscle and heart LKB1 deficiency causes decreased voluntary running and reduced muscle mitochondrial marker enzyme expression in mice. Am. J. Physiol. Endocrinol. Metab. *292*, E196–E202.

Wang, Q., Zhang, Y., Yang, C., Xiong, H., Lin, Y., Yao, J., Li, H., Xie, L., Zhao, W., Yao, Y., et al. (2010). Acetylation of metabolic enzymes coordinates carbon source utilization and metabolic flux. Science *327*, 1004–1007.

Xu, J. (2005). Preparation, culture, and immortalization of mouse embryonic fibroblasts. Curr. Protoc. Mol. Biol. *Chapter 28*, Unit 28 21.

Yang, L., Vaitheesvaran, B., Hartil, K., Robinson, A.J., Hoopmann, M.R., Eng, J.K., Kurland, I.J., and Bruce, J.E. (2011). The fasted/fed mouse metabolic acetylome: N6-acetylation differences suggest acetylation coordinates organ-specific fuel switching. J. Proteome Res. *10*, 4134–4149.

Zhao, S., Xu, W., Jiang, W., Yu, W., Lin, Y., Zhang, T., Yao, J., Zhou, L., Zeng, Y., Li, H., et al. (2010). Regulation of cellular metabolism by protein lysine acetylation. Science *327*, 1000–1004.

Zhong, L., D'Urso, A., Toiber, D., Sebastian, C., Henry, R.E., Vadysirisack, D.D., Guimaraes, A., Marinelli, B., Wikstrom, J.D., Nir, T., et al. (2010). The histone deacetylase Sirt6 regulates glucose homeostasis via Hif1alpha. Cell *140*, 280–293.

Molecular Cell, Volume *50*

Supplemental Information

SIRT4 Coordinates the Balance between Lipid Synthesis and Catabolism by Repressing Malonyl CoA Decarboxylase

Gaëlle Laurent, Natalie J. German, Asish K. Saha, Vincent C.J. de Boer, Michael Davies, Timothy R. Koves, Noah Dephoure, Frank Fischer, Gina Boanca, Bhavapriya Vaitheesvaran, Scott B. Lovitch, Arlene H. Sharpe, Irwin J. Kurland, Clemens Steegborn, Steven P. Gygi, Deborah M. Muoio, Neil B. Ruderman, and Marcia C. Haigis

Inventory of Supplemental Information

Figure S1: SIRT4 interacts with and represses MCD activity.
Related to Figure 2.

Figure S2: SIRT4 deacetylates MCD on the highly conserved K471 residue.
Related to Figure 3.

Figure S3: SIRT4 KO mice do not show changes in muscle fibers types, blood glucose and lactate levels after exercise. SIRT4 KO mice do not show alteration in mitochondrial content. Malonyl CoA levels are unaltered in liver of SIRT4 KO mice.
Related to Figure 5.

Figure S4: Metabolic parameters of SIRT4 WT and KO mice under LFD and HFD.
Related to Figure 6.

Figure S5: Glucose homeostasis, MCD activity and malonyl-coa levels in muscle of SIRT4 WT and KO mice under HFD.
Related to Figure 6.

Figure S6: Structural depiction of the location of the K471 equivalent (K472) in human MCD (PDB: 2YGW) complexed with Acetyl CoA.
Related to Figure 3.

Table S1: List of acetylated peptides used in deacetylation experiments. *Related to Figure 3.*

Supplemental Experimental Procedures

Supplemental References

Figure S1

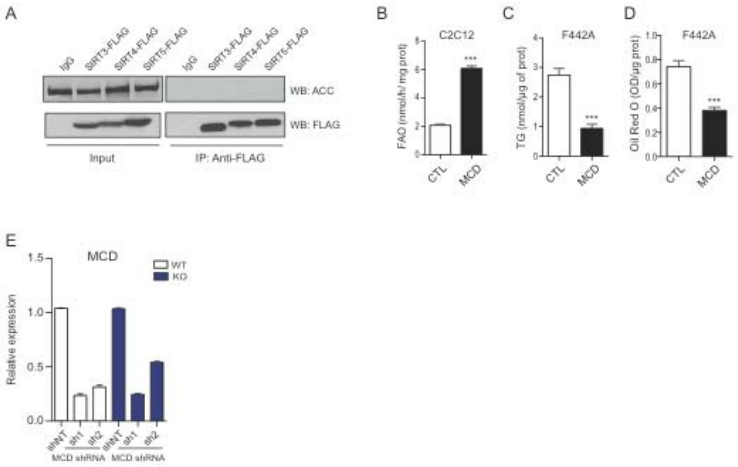
A
IgG
SIRT3-FLAG
SIRT4-FLAG
SIRT5-FLAG
IgG
SIRT3-FLAG
SIRT4-FLAG
SIRT5-FLAG
WB: ACC
WB: FLAG
Input
IP: Anti-FLAG
B
C2C12
FAO (nmol/h/ mg prot)
CTL
MCD
C
F442A
TG (nmol/µg of prot)
CTL
MCD
D
F442A
Oil Red O (OD/µg prot)
CTL
MCD
E
MCD
WT
KO
Relative expression
shNT
sh1
sh2
shNT
sh1
sh2
MCD shRNA
MCD shRNA

Figure S2

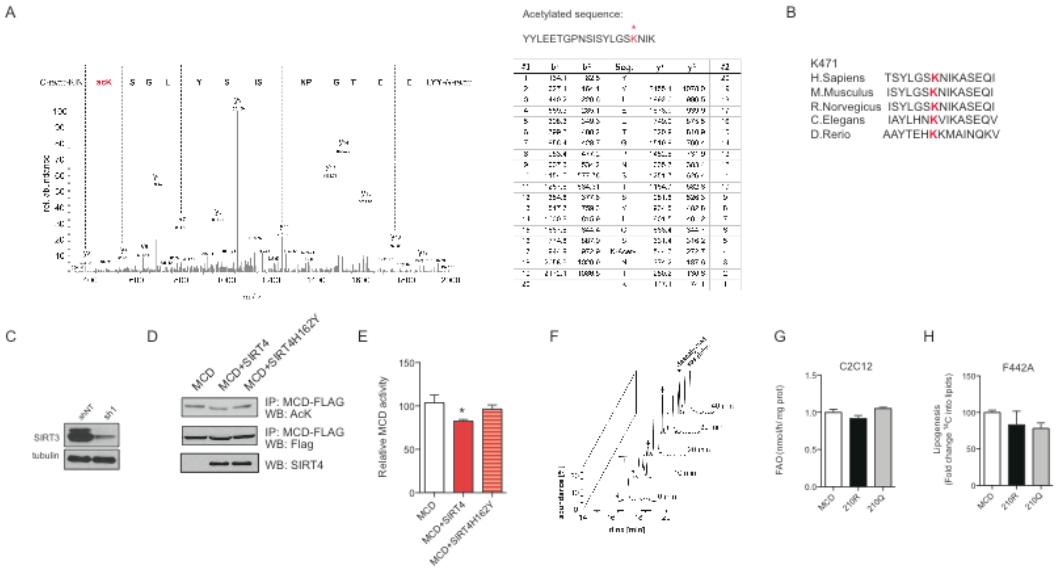
A
Acetylated sequence:
YYLEETGPNSISYLGSKNIK
B
K471
H.Sapiens TSYLGSKNIKASEQI
M.Musculus ISYLGSKNIKASEQI
R.Norvegicus ISYLGSKNIKASEQI
C.Elegans IAYLHNKVIKASEQV
D.Rerio AAYTEHKKMAINQKV
C
siNT
siS1
SIRT3
tubulin
D
MCD
MCD+SIRT4
MCD+SIRT4H162Y
IP: MCD-FLAG
WB: AcK
IP: MCD-FLAG
WB: Flag
WB: SIRT4
E
Relative MCD activity
MCD
MCD+SIRT4
MCD+SIRT4H162Y
F
G
C2C12
FAO (nmol/h/ mg prot)
MCD
210R
210Q
H
F442A
Lipogenesis
(Fold change -% into lipids)
MCD
210R
210Q

Figure S3

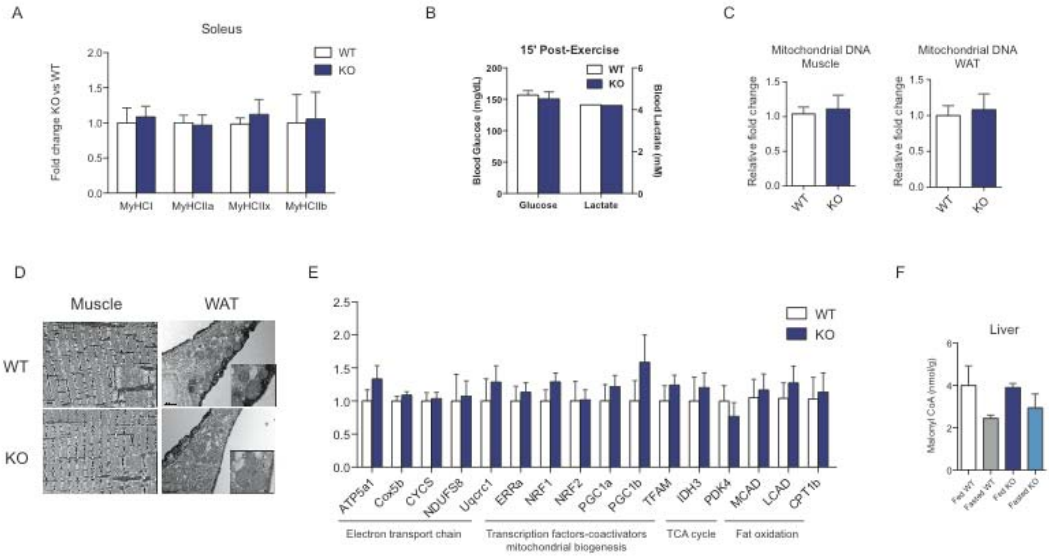
A
Soleus
WT
KO
Fold change KO vs WT
MyHCI
MyHCIIa
MyHCIIx
MyHCIIb
B
15' Post-Exercise
WT
KO
Blood Glucose (mg/dL)
Blood Lactate (mM)
Glucose
Lactate
C
Mitochondrial DNA Muscle
Mitochondrial DNA WAT
Relative fold change
WT
KO
D
Muscle
WAT
WT
KO
E
WT
KO
ATP5a1
Cox5b
CYCS
NDUFS8
Uqcrc1
ERRa
NRF1
NRF2
PGC1a
PGC1b
TFAM
IDH3
PDK4
MCAD
LCAD
CPT1b
Electron transport chain
Transcription factors-coactivators mitochondrial biogenesis
TCA cycle
Fat oxidation
F
Liver
Malonyl CoA (nmol/g)
Fed WT
Fasted WT
Fed KO
Fasted KO

Figure S4

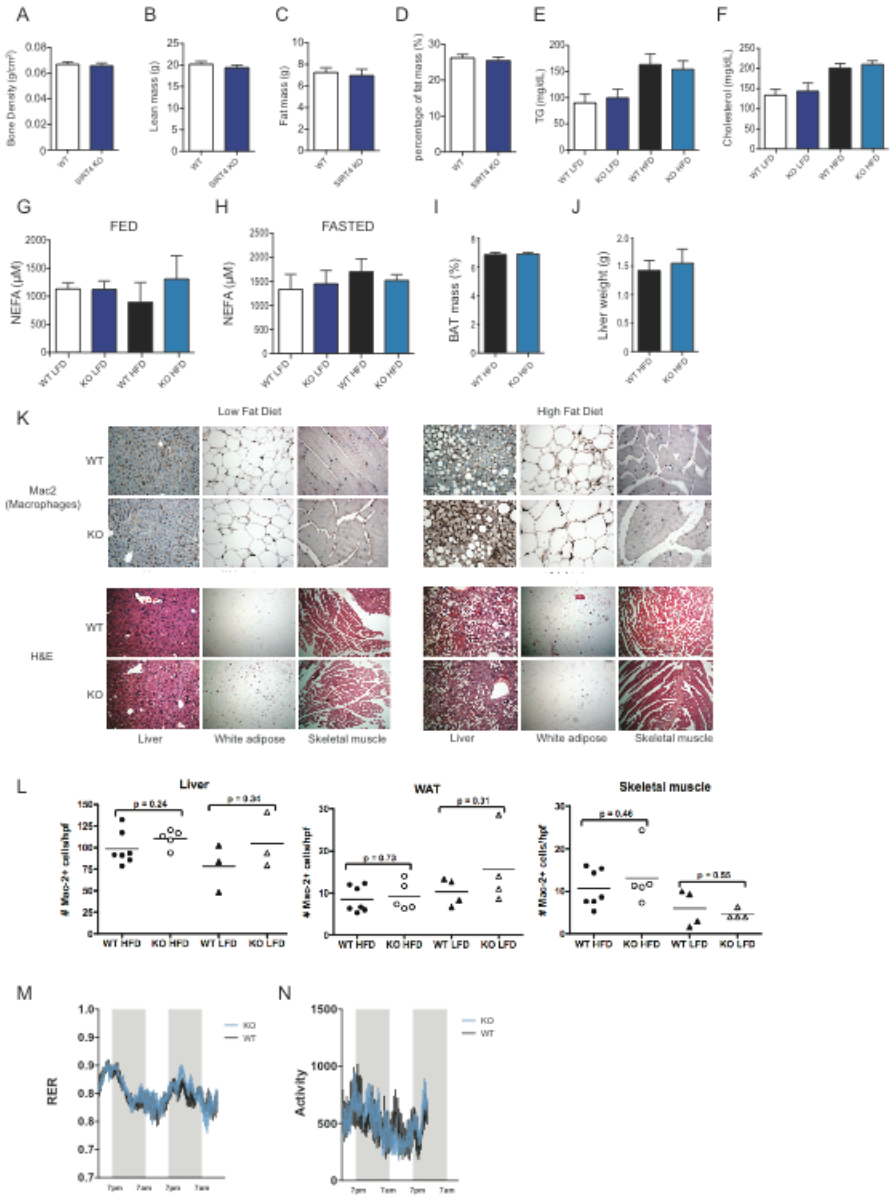
A
B
C
D
E
F
Bone Density (g/cm²)
Lean mass (g)
Fat mass (g)
percentage of fat mass (%)
TG (mg/dL)
Cholesterol (mg/dL)
WT
SIRT4 KO
WT LFD
KO LFD
WT HFD
KO HFD
G
H
I
J
FED
FASTED
NEFA (μM)
BAT mass (%)
Liver weight (g)
K
Low Fat Diet
High Fat Diet
Mac2 (Macrophages)
H&E
WT
KO
Liver
White adipose
Skeletal muscle
L
Liver
WAT
Skeletal muscle
# Mac-2+ cells/hpf
p = 0.24
p = 0.34
p = 0.79
p = 0.31
p = 0.46
p = 0.55
M
N
RER
Activity

Figure S5

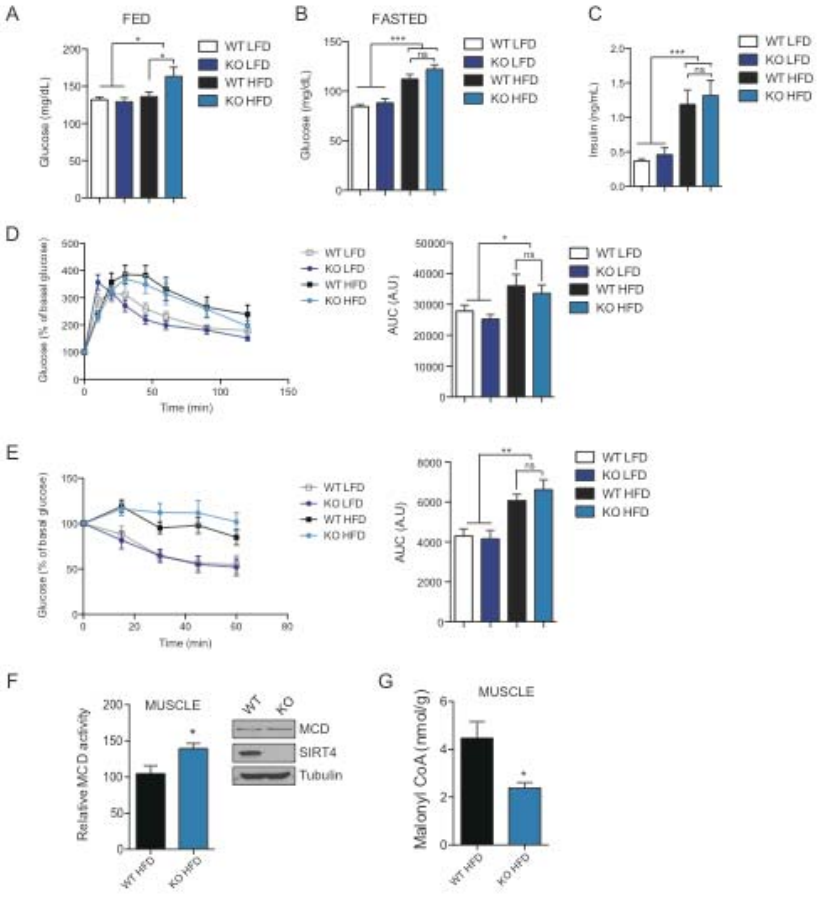
A
FED
Glucose (mg/dL)
WT LFD
KO LFD
WT HFD
KO HFD
B
FASTED
Glucose (mg/dL)
C
Insulin (ng/mL)
D
Glucose (% of basal glucose)
Time (min)
AUC (A.U)
E
Glucose (% of basal glucose)
Time (min)
AUC (A.U)
F
MUSCLE
Relative MCD activity
WT
KO
MCD
SIRT4
Tubulin
G
MUSCLE
Malonyl CoA (nmol/g)

Figure S6

A

B

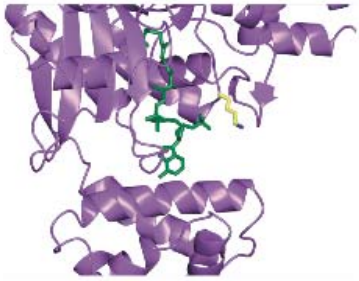

Table S1

substrate peptides	
MCDK210	PCEVLQ-{Lys(Ac)}-ISEAEA
MCDK388	EWVQSE-{Lys(Ac)}-LVRALQ
MCDK167	LEAQAL-{Lys(Ac)}-LVEGPD
MCDK58	AYELRE-{Lys(Ac)}-TPAPAE
MCDK145	LFHHIS-{Lys(Ac)}-LDGGVR
MCDK227	KNWMDM-{Lys(Ac)}-RRVGPY
MCDK471	ISYLGS-{Lys(Ac)}-NIKASE
MCDK474	LGSKII-{Lys(Ac)}-ASEQVL
NNTMK100	GAGEAS-{Lys(Ac)}-FSDDHY
PDH	KADQLY-{Lys(AC)}-QKFIRG

Figure S1.

(A) Expression vectors for wild type SIRT4 and SIRT4H162Y (C-terminal, FLAG-tagged) were transfected in HEK293T and assessed for interaction with ACC by immunoprecipitation. (B) Fatty acid oxidation in C2C12 cells overexpressing empty vector control (CTL, open bar) or MCD (black bar). (C-D) Triglyceride levels and Oil Red O staining in F442A adipocytes stably expressing empty vector control (CTL, open bars) or MCD (black bars). (E) MCD expression tested by RT-qPCR in WT cells (open bars) and KO cells (blue bars) treated with a control shRNA (shNT) or two shRNAs against MCD (sh1 and sh2). Data represent mean ± SEM. (*) $p < 0.05$; (**) $p < 0.01$, (***) $p < 0.001$.

Figure S2.

Mass spectrometry analysis identified one new site of MCD acetylation. (A) Summary peptide fragment table from acetylated lysine residue and m/z spectra obtained from mass spectrometry analysis of MCD purified from C2C12 cells. (B) K471 is highly conserved in many species. (C) SIRT3 expression in 293T cells treated with shRNA control (shNT) and shRNA targeting SIRT3. (D) FLAG-MCD immunoprecipitated from SIRT3 KO fibroblasts was incubated with FLAG-SIRT4 and FLAG-SIRT4H162Y immunoprecipitated from HEK293T cells knock down for SIRT3 and MCD acetylation status assessed. (E) MCD activity was assessed after deacetylation assay in vitro by SIRT4 and SIRT4H162Y. (F) Time course of the K471 deacetylation in presence of SIRT4. Reaction was stopped every 10 minutes until 40 minutes and the deacetylated product analyzed by mass

spectrometry. (G-H) Vectors containing wild-type MCD, MCD K210R or MCD K210Q were stably expressed in C2C12 cells (G) and F442A cells (H) and FAO rates and lipogenesis were assessed, respectively. Data represent mean ± SEM. (*) $p < 0.05$; (**) $p < 0.01$, (***) $p < 0.001$.

Figure S3.

(A) Fibers types were analyzed by quantitative RT-PCR in SIRT4 WT vs KO soleus. Relative expression values were normalized to WT mice. (B) SIRT4 WT vs. KO blood glucose and lactate levels were measured 15 minutes after exercise. (C) Mitochondrial DNA content was assessed in muscle (soleus) and WAT of SIRT4 WT and KO mice. (D) Representative EM images of mitochondria in red muscle (left panel) and WAT (right panel) of SIRT4 WT and KO mice. Scale bar is 1 μM. (E) Gene expression assessed by qRT-PCR of mitochondrial genes in muscle (quadriceps) of SIRT4 WT and KO mice. (F) Malonyl CoA levels in liver of SIRT4 WT and KO fed and fasted mice. Data represent mean ± SEM. (*) $p < 0.05$; (**) $p < 0.01$, (***) $p < 0.001$.

Figure S4.

Bone density (A), lean mass (B), fat mass (C) and percentage of fat mass (D) were analyzed by Dexascan for SIRT4 WT and KO mice. (E) Plasma triglycerides were measured from SIRT4 KO and WT mice on a HFD or LFD (F) Plasma cholesterol was measured from SIRT4 KO and WT mice on a HFD or LFD. (G-H) Plasma non-esterified fatty acids (NEFA) were measured from SIRT4

KO and WT mice on a HFD or LFD diet in mice that were fed (G) or fasted overnight (H). (I) Brown Adipose Tissue (BAT) mass was analyzed by CT scan in SIRT4 WT and KO mice under HFD and normalized to total body weight. (J) Liver weight was measured from SIRT4 WT and KO mice after HFD. (K) Representative images of Mac2 immunostaining and Hematoxylin and Eosin (H&E) staining from liver, WAT and muscle (quadriceps) of SIRT4 WT and KO mice after LFD and HFD. (L) Quantification of cells stained with Mac2 in liver, WAT and muscle of SIRT4 WT and KO mice under LFD and HFD. (M) Respiratory Exchange Ratio (RER) in SIRT4 WT and KO mice under HFD (n=6). (N) Locomotor activity of SIRT4 WT and KO mice. Data represent mean ± SEM. (*) $p < 0.05$; (**) $p < 0.01$, (***) $p < 0.001$.

Figure S5.

(A-B) Blood glucose levels in SIRT4 WT and KO mice on a LFD and HFD in a fed state (A) or after on overnight fast (B). (C) Plasma insulin levels were measured from SIRT4 WT and KO mice on a LFD and HFD after on overnight fast. Glucose tolerance test (D) and Insulin tolerance test (E) was performed using SIRT4 WT and KO mice on a LFD and HFD. In each experiment, n=5-7 mice per condition. (F) MCD activity in muscle (quadriceps) of SIRT4 WT and KO under HFD (G) Malonyl CoA levels in muscle (quadriceps) of SIRT4 WT and KO under HFD. Data represent mean ± SEM. (*) $p < 0.05$; (**) $p < 0.01$, (***) $p < 0.001$.

Figure S6.

MCD structure. To assess the possible relevance of K471 residue, we superimposed the MCD crystal structure (PDB: 2YGW) with the structurally homologous CurA protein from the cyanobacteria L. majuscula (PDB: 2REF). By overlaying the MCD and CurA structures, we found that K472 of human MCD (the equivalent of K471 of mouse MDC) is at close distance to the putative malonyl CoA entry point. MCD is represented in purple, the ligand in green and K472 is in yellow.

Table S1.

Peptide sequences used for peptide deacetylation assays.

Supplemental Experimental Procedures

SIRT4 recombinant protein

The cDNA corresponding to SIRT4 residues 25-314 were cloned into pET15b (Merck Biosciences), resulting in an N-terminal HIS-tag. SIRT4 (25-314) protein was produced overnight at 20 °C in *E. coli* BL21(DE3)Star (Invitrogen) through induction with 0.5 mM IPTG at an OD_{600} of 0.8. Harvested cells were lysed in 25 mM Hepes, pH 7.0, 150 mM NaCl, and 10 mM imidazole. The protein was incubated with Talon resin (Clontech), the resin washed with 25 mM Hepes pH 7.0, 150 mM NaCl, 20 mM imidazole, and bound protein eluted with the same buffer with an increased imidazol concentration of 200 mM. The protein was then applied to a Superdex200 size exclusion column (GE Healthcare) in 20 mM Hepes pH 7.0, 150 mM NaCl. SIRT4 protein eluted at the volume expected for a monomer and was concentrated in amicon units (Millipore) and snap frozen in liquid nitrogen for storage at -80 °C.

Peptide deacetylation assay

Standard assays contained 20 mM Tris/HCl pH 7.8, 150 mM NaCl, 1 mM NAD^+, 2 mM DTT, 0.5 mM substrate peptide and 5 µg to 20 µg SIRT4. For NAD^+ or peptide titrations concentrations were varied as indicated and SIRT4 amounts adjusted to obtain well measurable deacetylation levels. Reactions were incubated at 37 °C and aliquots stopped after different time points (up to 120 min) by adding trifluoro-acetic acid (TFA) (0.2 % v/v). Samples were diluted 1:1000 with 0.1 % formic acid (FA) (v/v) and analyzed on an LC-ESI-MS consisting of a Shimadzu prominence HPLC (Shimadzu) connected to a Thermo

LCQ mass spectrometer (Thermo Fisher Scientific). Peptide species were separated using a linear gradient from 0% to 45% buffer B within 30 min (buffer A: 0.1 % TFA, 0.02 % HFBA; buffer B: 70 % ACN, 0.1 % TFA, 0.02 % HFBA) and a 100 µm ID capillary reversed phase column (Reprosil C18, AQ, 3µm; Dr. Maisch, Germany) with a flow rate of 300 µl/min. Extracted ion chromatograms with mass windows ± 2 m/z were generated for the acetylated and deacetylated peptide, peak areas determined using Xcalibur, and time-courses analyzed in Excel and GraFit (Erithacus Software).

Analysis of MCD modifications

In gel tryptic digests of MCD-IPs were prepared as described previously (Schluesener et al., 2005). Peptide separation on an Accela U-HPLC connected to an LTQ XL Orbitrap Velos (Thermo Fisher Scientific) was achieved with a linear gradient from 0 % to 40 % buffer B within 90 min (buffer A: 2 % ACN 0.1 % FA; buffer B: 70 % ACN, 0.1 % FA) on a heated (45 °C) 75 µm ID capillary reversed phase column (Luna C_{18}, Phenomenex) with a flow rate of 250 µl/min. A full MS scan between 300 and 2000 m/z was acquired for the precursor ion (R = 60 000) using Velos method files, followed by MS/MS scans of the top 20 ions using standard CID fragmentation settings. Fragment identification was performed using the SEQUEST algorithm in Proteome discoverer 1.2 (Thermo Fisher Scientific).

Immunofluorescence

In brief, cells were fixed in 4% paraformaldehyde (PFA) for 30 min, permeabilized in 0.01% triton for 10 min, rinsed twice in phosphate buffered saline (PBS)

solutions and blocked for 30 min in 5% BSA. Cells were stained with MitoTracker Far-Red (Molecular Probes), together with specific antibody recognizing HA tag (Cell Signaling) for SIRT4 detection and FLAG tag (Sigma) for MCD detection. Images were acquired with identical exposure times and settings.

Metabolic parameters

Blood was collected from fed or overnight fasted mice and serum was separated by centrifugation. Blood glucose was read directly from the tail vein using a glucose meter (OneTouch Ultra 2, Lifescan). Glucose tolerance tests were performed after an overnight fast by injecting mice intraperitoneally with 2 g/kg BW glucose. Insulin tolerance tests were performed on animals in the fed state by intraperitoneal injection with 0.75 U/kg BW of insulin (Sigma). In each case, blood glucose was read from the tail vain using a glucose meter. Plasma NEFA, triglycerides and cholesterol levels were analyzed using commercial kits (WAKO diagnostics). Lipid composition in muscle and WAT was analyzed by the Vanderbilt Mouse Metabolic Phenotyping Center (MMPC) Lipid Lab. Insulin levels were analyzed by the Specialized Assay Core (Joslin Diabetes Center). Metabolic cages analyses were performed using the TSE LabMaster (TSE Systems). Mice were acclimated to the chambers for 2 days and then gas exchanges and locomotor activity were measured every 27 min for 48 h. Mice were fed every day while in the cages. Body composition of the LFD mice was analyzed by dual energy X-ray absorptiometry (Lunar, PIXImus).

Immunohistochemistry

Organs were fixed in 4% PFA and embedded in paraffin. Sections were stained with hematoxylin and eosin (H&E) in accordance with standard procedures. Immunohistochemistry was performed using antibodies against Mac2, a marker of macrophages and images were manually quantified.

Electron Microscopy

Tissues were immersion fixed in 2.5% glutaraldehyde, 2% PFA, in 0.1M cacodylate buffer pH 7.4 (modified Karnovsky's fixative) for at least 1hr at room temperature before being placed in a 4ºC refrigerator. To continue processing, tissues were washed 4x for 10 minutes each in 0.1M cacodylate buffer, and then fixed secondarily in 1% osmium tetroxide in buffer, for 1 hour at 4ºC. Tissues were washed 4x for 10 minutes in deionized water before being immersed in 2% aqueous uranyl acetate to be contrast fixed over night at 4ºC. The following day the tissues were washed 4x10 minutes in deionized water, then taken through a dehydration series including 30%, 50%, 70%, 95%, and 100% ethanol, 10 minutes each at 4ºC. Next, tissues were brought to room temperature to continue dehydrating with 100% ethanol 3x 10 minutes each and 100% propylene oxide twice for 15 minutes. Infiltration proceeded with 1:1 propylene oxide and LX112 Epon resin, tissues being rotated overnight at room temperature. The following day, the sample containers' caps' were left off to evaporate the propylene oxide over the course of the day before removing the remaining resin and adding 100% freshly made resin. Samples were recapped and rotated overnight. Before embedding the next day, samples were placed in a vacuum oven at 60ºC for 2

hours. Tissues were embedded in flat molds and cured at 60ºC over 48 hrs. Cured blocks were sectioned using a Leica Ultracut E ultramicrotome with a diamond knife set to cut sections at 80nm thickness, which reflected a light gold color. Sections were put on 2mm x 0.5mm formvar coated copper slot grids that had been carbon coated and glow discharged. Grids were contrast stained with 2% uranyl acetate for 10minutes and lead citrate for 5minutes. Grids were imaged on a JEOL 1400 TEM equipped with a side mount Gatan Orius SC1000 digital camera.

Gene expression and mtDNA analysis

RNA from skeletal muscle tissue were extracted with Trizol (Invitrogen) and cleaned up with RNeasy mini kit (QIAGEN) according to the instructions. cDNA was synthesized with the iScript cDNA synthesis kit (BioRad) using 500ng of RNA. Quantitative RT-PCR reactions were performed using 1µM of primers and LightCycler® 480 SYBR Green Master (Roche) on an LightCycler® 480 detection system (Roche). Calculations were performed by a comparative method (2-$\Delta\Delta$CT) using actin as an internal control. For mtDNA analysis, total DNA from skeletal muscle tissue and WAT were extracted with DNeasy blood and tissue kit (QIAGEN). mtDNA was amplified using primers specific for the mitochondrial cytochrome c oxidase subunit 2 (COX2) gene and normalized to genomic DNA by amplification of the ribosomal protein s18 (rps18) nuclear gene. Primers sequences available upon request.

Modeling of MCD and ligand binding site.

Initial atomic coordinates and files for MCD, CurA and acetyl-CoA were obtained from the RCSB protein data bank and modeled using CCP4mg molecular graphics software (McNicholas et al., 2011). Acetyl-CoA from CurA was positioned into the 2.80Å MCD structure by superposing the structures as a guide.

Supplemental References

McNicholas, S., Potterton, E., Wilson, K.S., and Noble, M.E. (2011). Presenting your structures: the CCP4mg molecular-graphics software. Acta Crystallogr D Biol Crystallogr *67*, 386-394.

Schluesener, D., Fischer, F., Kruip, J., Rogner, M., and Poetsch, A. (2005). Mapping the membrane proteome of Corynebacterium glutamicum. Proteomics *5*, 1317-1330.

APPENDIX II

Supplemental data tables and figures to accompany Chapters II-IV.

Table S2.1 | Significantly increased or decreased acetylation sites by >50% in SIRT4 KO BAT compared to WT

* = acetylated lysine residue. Hyperacetylated sites are denoted by the fold change in blue boxes.

Protein name	Description	Normalized fold change	AcK site	Peptide	Raw intensity				Raw intensity pvalue
					WT 1	WT 2	KO 1	KO 2	
TCA cycle and Anaplerosis									
ACO2	aconitase 2, mitochondrial	3.1	304, 305	MK*K*YLSK	259540	223489	2184570	1994430	0.003
ACO2	aconitase 2, mitochondrial	2.2	605	CTTDHISAAGPWLK*FR	473437	540894	3213210	3119620	0.000
ACO2	aconitase 2, mitochondrial	1.9	138	VAVPSTIHCDHLIEAQVGGEK*DLR	195585	239471	1079350	1296720	0.013
ACO2	aconitase 2, mitochondrial	1.9	587	LQLLEPFDKWDGKDLEDLQILIK*VK	94700	85200	516718	460552	0.005
ACO2	aconitase 2, mitochondrial	1.9	573	LQLLEPFDK*WDGKDLEDLQILIK	3582470	3019640	19552200	15507300	0.020
ACO2	aconitase 2, mitochondrial	1.9	577	LQLLEPFDKWDGK*DLEDLQILIK	3582470	3019640	19552200	15507300	0.020
ACO2	aconitase 2, mitochondrial	1.8	305	MKK*YLSK	2383730	1728540	11053500	9483340	0.011
ACO2	aconitase 2, mitochondrial	1.6	652	YYKK*HGIR	1362220	1233150	4976560	6651250	0.033
ACO2	aconitase 2, mitochondrial	1.6	689	AIITK*SFAR	1528820	1371300	5828550	7000930	0.014
ACO2	aconitase 2, mitochondrial	0.6	228	CPK*VIGVK	1206400	1294630	1898100	2023270	0.011
ACSS1	acyl-CoA synthetase short-chain family member 1	2.6	389	LLLK*YGDAWVK	78565	131754	869107	664238	0.025
ACSS3	acyl-CoA synthetase short-chain family member 3 iso 1	3.1	210	IDHAK*PK	17400	19500	172000	150000	0.006
CS	citrate synthase	4.1	103	GYSIPECQK*MLPK	103570	75082	842566	1219190	0.038
CS	citrate synthase	1.5	393	IVPNILLEQGK*AK	102230	119679	520099	440466	0.012
CS	citrate synthase	0.6	382	LVAQLYK*IVPNILLEQGK	7007740	5894620	11032400	9701940	0.046
DLAT	dihydrolipoamide S-acetyltransferase	1.5	461	ELNK*MLEGK	486539	504323	2089630	2172370	0.001
DLD	dihydrolipoamide dehydrogenase	3.2	122	LNLEK*MMEQK	221991	155621	1717120	1676910	0.001
DLD	dihydrolipoamide dehydrogenase	1.8	104	ALLNNSHYYHMAHGK*DFASR	253047	189412	1002620	1251050	0.019
DLD	dihydrolipoamide dehydrogenase	1.5	127	MMEQK*HSAVK	29209	29842	111319	144390	0.027
DLD	dihydrolipoamide dehydrogenase	0.6	273	FK*LNTK	2820180	2882820	5146110	4920120	0.003
DLST	dihydrolipoamide S-succinyltransferase	2.8	268, 274	ARHK*DAFLKK*	33400	39600	276000	295000	0.002
DLST	dihydrolipoamide S-succinyltransferase	2.4	268, 273	HK*DAFLK*K	362179	257082	2452440	1705170	0.043
DLST	dihydrolipoamide S-succinyltransferase	2.1	227	SEHREK*MNR	6486	7249	40597	40998	0.000
DLST	dihydrolipoamide S-succinyltransferase	2.1	273	HKDAFLK*K	5782620	5338260	32153100	33363700	0.001
FH	fumarate hydratase 1	1.8	77	STMNFK*IGGATER	406601	493182	2332340	2301250	0.001
IDH1; IDH2	isocitrate dehydrogenase 1 (NADP+), soluble	2.2	93; 133	MWK*SPNGTIR	169814	112321	765854	964723	0.020
IDH2	isocitrate dehydrogenase 2 (NADP+), mitochondrial	5.5	45	IK*VEKPVVEMDGDEMTR	53821	53654	950392	710379	0.023
IDH2	isocitrate dehydrogenase 2 (NADP+), mitochondrial	1.5	133	KMWK*SPNGTIR	123744	144052	558937	609977	0.004
IDH3A	isocitrate dehydrogenase 3 (NAD+) alpha	1.5	85	WMIPPEAK*ESMDKNK	210611	212996	944246	894759	0.001
IDH3A	isocitrate dehydrogenase 3 (NAD+) alpha	0.7	90	ESMDK*NK	88581	83592	155045	174631	0.016
IDH3A	isocitrate dehydrogenase 3 (NAD+) alpha	0.7	223	EVAENCK*DIK	613062	600213	1033010	1289430	0.050
IDH3B	isocitrate dehydrogenase 3, beta subunit	1.7	373	DMGGYSTTTDFIK*SVIGHLHPHGG	294221	275375	1163320	1503100	0.025
IDH3G	isocitrate dehydrogenase 3 (NAD+), gamma	1.5	50	ISSQQTIPPSAK*YGGR	21843	24306	81303	110860	0.039
MDH2	malate dehydrogenase 2, NAD (mitochondrial)	4.1	338	ASIKKGEDFVKNMK*	16100	16309	164112	209272	0.017
MDH2	malate dehydrogenase 2, NAD (mitochondrial)	2.4	335	KGEDFVK*NMK	173615	142447	1124680	999727	0.005
MDH2	malate dehydrogenase 2, NAD (mitochondrial)	2.0	328	ASIK*KGEDFVK	83096	93046	524827	486827	0.002
MDH2	malate dehydrogenase 2, NAD (mitochondrial)	2.0	328, 329	ASIK*K*GEDFVK	222360	147401	889244	1186340	0.031
MDH2	malate dehydrogenase 2, NAD (mitochondrial)	1.7	329	ASIKK*GEDFVK	347016	401690	1833940	1668600	0.004
MDH2	malate dehydrogenase 2, NAD (mitochondrial)	0.7	185	ANTFVAELK*GLDPAR	2252320	2364000	4366820	4242130	0.002
PC	pyruvate carboxylase	1.5	316	QVGYENAGTVEFLVDK*HGK	182905	68006	586101	449504	0.048
PC	pyruvate carboxylase	1.5	1090	SILVK*DTQAMK	155763	128599	600994	565679	0.003
PDHA1	pyruvate dehydrogenase E1 alpha 1	1.8	244	AAASTDYYK*R	223868	237512	1300560	1066720	0.015
PDHA1	pyruvate dehydrogenase E1 alpha 1	1.6	336	MVNSNLASVEELK*EIDVEVR	73530	90543	345468	414309	0.014
PDHA1	pyruvate dehydrogenase E1 alpha 1	1.6	267	EATK*FAAAYCR	261972	260369	1279160	1060830	0.014
PDHA1; PDHA2	pyruvate dehydrogenase E1 alpha 1	2.5	77; 78	MELK*ADQLYK	503846	588540	3992960	3688450	0.002
SCS-beta	succinate-Coenzyme A ligase, ADP-forming, beta subunit	1.6	88	SSDEAYAIAK*K	1719960	1862680	7957730	8690000	0.003
SCS-beta	succinate-Coenzyme A ligase, ADP-forming, beta subunit	0.7	267	YDATMVEINPMVEDSDGK*VLCMDAK	260909	373209	626551	592267	0.038
SCS-beta	succinate-Coenzyme A ligase, ADP-forming, beta subunit	0.7	216	K*EQAVTLAQK	130950	134851	265492	231789	0.021
SDHA	succinate dehydrogenase Fp subunit	3.0	498	ANAGEESVMNLDK*LR	39988	58600	342427	489027	0.038
SDHA	succinate dehydrogenase Fp subunit	2.8	517	LNMQK*SMQNHAAVFR	95382	126755	1003090	781053	0.020
SDHA	succinate dehydrogenase Fp subunit	1.8	182	FGK*GGQAHR	734985	543886	3321440	3065880	0.004

Table S2.1 (Continued).

Lipid metabolism									
ACAA2	acetyl-CoA acyltransferase 2 (mitochondrial 3-oxoacyl-CoA thiolase)	2.4	171	LPMGMTAENLAAK*YNISREDCDRYALQSQQR	258087	156131	1263630	1545820	0.015
ACAA2	acetyl-CoA acyltransferase 2 (mitochondrial 3-oxoacyl-CoA thiolase)	0.6	240	LPSVFK*K	1653280	1672470	2732950	2954350	0.009
ACAA2	acetyl-CoA acyltransferase 2 (mitochondrial 3-oxoacyl-CoA thiolase)	0.6	191	WK*AANEAGYFNEEMAPIEVK	688755	720450	1269920	1136900	0.018
ACAD10	acyl-Coenzyme A dehydrogenase family, member 10	4.9	1052	FADGPDEVHQLTVAK*MELK	19722	20700	302076	254878	0.008
ACADL	long-chain acyl-CoA dehydrogenase	3.0	156	EQIEK*FIPQMTAGK	53966	63041	498180	479218	0.001
ACADL	long-chain acyl-CoA dehydrogenase	1.9	318	K*AFGKTVAHIQTVQHK	141000	116000	800000	587000	0.034
ACADL	long-chain acyl-CoA dehydrogenase	1.8	279	AQDTAELFFEDVRLPANALLGEENK*GF	75154	699803	2116450	1824330	0.044
ACADL	long-chain acyl-CoA dehydrogenase	1.5	322	AFGK*TVAHIQTVQHK	333673	264414	1417130	1193350	0.013
ACADM	medium-chain acyl-CoA dehydrogenase	2.3	307	ALDEATKYALDRK*TFGK	38488	57738	302694	331099	0.004
ACADM	medium-chain acyl-CoA dehydrogenase	1.7	420	EHIEKYK*N	454928	466398	2164940	2302790	0.002
ACADM	medium-chain acyl-CoA dehydrogenase	1.5	301	ALDEATK*YALDRK	658259	647589	2973640	2506640	0.012
ACADM	medium-chain acyl-CoA dehydrogenase	0.7	175	TK*AEKKGDEYVINGQK	44200	34400	72900	80000	0.026
ACADS	short-chain acyl-CoA dehydrogenase	0.6	306	NAFGAPLTK*LQNIQFK	1329260	1249060	2398550	2283820	0.004
ACADSB	acyl-Coenzyme A dehydrogenase, short/branched chain	1.5	284	IGHGYK*YAIGSLNEGR	682177	1016340	3932470	3039240	0.031
ACADVL	acyl-Coenzyme A dehydrogenase, very long chain	2.0	52	AREATQAVLDK*PETLSSDASTR	1067250	1433450	7212740	6915520	0.002
ACADVL	acyl-Coenzyme A dehydrogenase, very long chain	1.9	248	SSAIPSPCGKYYTLNGSK*	210000	195000	1290000	890000	0.047
ACADVL	acyl-Coenzyme A dehydrogenase, very long chain	1.5	279	EK*ITAFVVER	346457	431608	1632980	1701520	0.002
ACADVL	acyl-Coenzyme A dehydrogenase, very long chain	1.5	373	TQFGDK*IHNFGVIQEK	224094	254814	1128270	888196	0.024
ACADVL	acyl-Coenzyme A dehydrogenase, very long chain	1.5	383	TQFGDKIHNFGVIQEK*	224094	254814	1128270	888196	0.024
CPT1B	carnitine palmitoyltransferase 1b, muscle	0.5	404	QTFFSSGK*NK	54270	46119	72213	76764	0.035
CPT2	carnitine O-palmitoyltransferase	1.6	69	YLSAQK*PLLNDSQFR	167632	160006	740795	719627	0.000
CPT2	carnitine O-palmitoyltransferase	0.6	305	QK*LIHGGNEETLR	367220	382322	681414	642712	0.005
DCI	dodecenoyl-Coenzyme A delta isomerase	3.1	229	SVMTK*WLAIPDHSR	736507	964189	6154690	8500250	0.032
DCI	dodecenoyl-Coenzyme A delta isomerase	0.5	48	VLVETEGPAGVAVMK*LR	258291	292022	412445	371130	0.049
DECR1	2,4-dienoyl CoA reductase 1	4.2	260	FEK*EMIDRIPCGR	121069	131018	1477830	1544630	0.001
DECR1	2,4-dienoyl CoA reductase 1	0.6	246	TK*GAFSR	610379	558145	1085110	931406	0.035
ECH1	enoyl coA hydratase 1, peroxisomal	2.4	195	YCTQDAFFQIK*EVDMGLAADVGTLQRLPK	115735	58209	528762	648059	0.017
ECH1	enoyl coA hydratase 1, peroxisomal	1.6	147	DLISK*YQK	232000	214000	951000	1120000	0.011
ECH1	enoyl coA hydratase 1, peroxisomal	0.7	97	ISK*DSDCR	106786	137715	215267	255765	0.047
ECHS1	enoyl CoA hydratase, short chain, 1, mitochondrial	2.0	101	AFAAGADIK*EMQNR	650656	534750	3758200	2991660	0.019
FASN	fatty acid synthase	2.0	786	SSCTIIPLMK*R	34400	48300	273951	196279	0.039
GPD2	glycerol-3-phosphate dehydrogenase 2, mitochondrial	0.7	262	KTDPETGK*ER	5270	5670	11100	9780	0.019
GPD2	glycerol-3-phosphate dehydrogenase 2, mitochondrial	0.6	510	TYGDKAFEVAK*MASVTGK	83810	77241	144538	131425	0.016
HADHA	mitochondrial trifunctional protein, alpha subunit	5.5	406, 411	GQQQVFK*GLNDK*VK	27800	42600	568883	523079	0.002
HADHA	mitochondrial trifunctional protein, alpha subunit	2.5	457	HK*VLKEVESVTPEHCIFASNTSALPINQIAAVSKRPEK	17813	23800	149774	141079	0.002
HADHA	mitochondrial trifunctional protein, alpha subunit	2.2	129	MFEK*LEK	143736	141519	863288	882103	0.000
HADHA	mitochondrial trifunctional protein, alpha subunit	2.0	516	VIGMHYFSPVDKMQLLEIITTDK*TSK	168407	115032	827605	792036	0.002
HADHA	mitochondrial trifunctional protein, alpha subunit	2.0	759	KYESAYGTQFTPCQLLLDHANNSSK*KFYQ	36123	53783	251756	247108	0.002
HADHA	mitochondrial trifunctional protein, alpha subunit	1.7	249	TIEYLEEVAVNFAK*GLADRK	136840	147609	759078	618480	0.016
HADHA	mitochondrial trifunctional protein, alpha subunit	1.7	303	GLYPAPLK*IIDAVK	1067910	823070	4415290	4471720	0.001
HADHA	mitochondrial trifunctional protein, alpha subunit	0.7	436	DSIFSNLIGQLDYK*GFEK	526642	504460	862278	1071410	0.050
HADHA	mitochondrial trifunctional protein, alpha subunit	0.6	60	INSPNSK*VNTLNK	147292	145372	223207	244134	0.014
HADHB	mitochondrial trifunctional protein, beta subunit	2.0	333	ALAMGYK*PK	941909	725916	4795230	4733660	0.001
HADHB	mitochondrial trifunctional protein, beta subunit	0.6	294	LK*PAFIKPYGTVTAANSSFLTDGASAMLIMSEDR	955588	1222320	1889480	1890800	0.027
HADHB	mitochondrial trifunctional protein, beta subunit	0.6	299	LKPAFIK*PYGTVTAANSSFLTDGASAMLIMSEDR	955588	1222320	1889480	1890800	0.027
HADHSC	L-3-hydroxyacyl-Coenzyme A dehydrogenase	1.8	185	LVEVIK*TPMTSQK	128860	165871	806358	715237	0.006
HADHSC	L-3-hydroxyacyl-Coenzyme A dehydrogenase	1.8	206	TFESLVDFCKTLGK*HPVSCKDTPGFIVNR	426026	399701	2269650	1917250	0.011
PCCA	propionyl-Coenzyme A carboxylase, alpha polypeptide	1.8	492	FVK*GDISTK	424287	470093	2195080	2407520	0.003
PCCA	propionyl-Coenzyme A carboxylase, alpha polypeptide	1.5	150	AQAVHPGYGFLSENKEFAK*R	475909	599455	2059410	2347440	0.009
PECR	peroxisomal trans-2-enoyl-CoA reductase	0.6	83	K*EEEVSNLVK	253813	218808	388253	396766	0.013
PISD	phosphatidylserine decarboxylase proenzyme	0.5	309	VVLTGDWK*HGFFSL	172686	183194	269312	280605	0.006
THEM2	acyl-CoA thioesterase 13	0.5	127	TTGK*LIAQGR	131351	107928	179642	189106	0.036
THEM2	acyl-CoA thioesterase 13	0.5	37	VTLVSAAPEK*LICEMK	134738	143299	170128	183383	0.041
Electron transport chain and energy production									
ATP5A1	ATP synthase F1 complex, α subunit, iso 1	0.5	539	ISEQSDAK*LK	59570	58372	91250	80088	0.041
ATP5B	mitochondrial ATP synthase beta subunit	0.6	133	VLDSGAPIK*IPVGPETLGR	116677	109975	190108	181293	0.006
ATP5C	ATP synthase F1 complex, γ subunit iso b	2.4	55	MVAAAK*YAR	10490	11279	67681	82818	0.014
ATP5D	ATP synthase F1 complex, δ subunit precursor	1.5	136	ANLEK*AQSELSGAADEAAR	293147	437691	1683690	1339220	0.026
ATP5F1	ATP synthase F0 complex, subunit b, iso 1	3.2	154	QIQDAIDMEK*AQQALVQKR	35600	27258	334343	234279	0.037
ATP5F1	ATP synthase F0 complex, subunit b, iso 1	2.5	221	RKEEEHMIDWVEK*HVVK	29680	21726	174316	183698	0.002

Table S2.1 (Continued).

ATP5F1	ATP synthase F0 complex, subunit b, iso 1	1.9	244	CIEDLK*LLAK	100234	138604	589296	677556	0.009
ATP5F1	ATP synthase F0 complex, subunit b, iso 1	1.5	53	PLPPLPEYGGK*VR	14300	10800	54600	54200	0.002
ATP5H	ATP synthase F0 complex, subunit d	1.7	72	ANVAKPGLVDDFEK*K	198413	227859	1182940	832156	0.046
ATP5H	ATP synthase F0 complex, subunit d	1.5	117	IQEYEK*QLEK	272371	287448	1189920	1242830	0.001
ATP5H	ATP synthase F0 complex, subunit d	1.5	149	K*YPYWPHQPIENL	341003	387488	1660210	1389920	0.014
COX6C	cytochrome c oxidase, subunit VIc	3.2	61	NYDSMK*DFEEMRK	33350	53188	398662	393959	0.001
COX7C	cytochrome c oxidase, subunit VIIc	0.5	25	SHYEEGPGK*NLPFSVENK	256495	251821	381180	391422	0.002
ETFA	electron transferring flavoprotein, alpha polypeptide	2.0	162	CDEK*VKVFSVR	573568	573324	2819360	3739770	0.028
ETFB	electron transferring flavoprotein, beta polypeptide	0.7	176	LK*LPAVVTADLR	340743	447392	733759	714651	0.026
ETFB	electron transferring flavoprotein, beta polypeptide	0.6	110	VLAK*LAEK	177805	159458	302907	279332	0.015
ETFDH	electron transferring flavoprotein, dehydrogenase	2.2	496	GSDSDQLK*PAK	18746	34751	185441	152475	0.016
NDUFA10	NADH dehydrogenase (ubiquinone) 1 alpha subcomplex 10	1.5	122	FYDDPK*SNDGNSYR	91890	83947	371900	383298	0.001
NDUFA10	NADH dehydrogenase (ubiquinone) 1 alpha subcomplex 10	0.5	75	LAK*EIAQQLGMK	68076	62289	83034	89843	0.041
NDUFA5	NADH dehydrogenase (ubiquinone) 1 alpha subcomplex, 5	2.1	46	K*YTEQITNEKLDMVKAEPDVK	37575	38100	224839	223513	0.000
NDUFA5	NADH dehydrogenase (ubiquinone) 1 alpha subcomplex, 5	1.5	36	TLDILK*HFPK	1642000	2161640	9061750	7570250	0.015
NDUFB6	NADH dehydrogenase (ubiquinone) 1 beta subcomplex, 6	1.5	24	WLK*DQELSPR	434105	567265	2036280	2082990	0.002
NDUFS1	NADH dehydrogenase (ubiquinone) Fe-S protein 1	2.9	84	MCLVEIEK*APK	199258	218345	1823560	1610550	0.005
NDUFV1	NADH dehydrogenase ubiquinone flavoprotein 1	2.9	104	WSFMNK*PSDGRPK	181190	167069	1422670	1476520	0.000
NDUFV1	NADH dehydrogenase ubiquinone flavoprotein 1	2.1	81	EILLKGPDWILGEMK*TSGLR	115000	132000	656856	838634	0.021
NDUFV1	NADH dehydrogenase ubiquinone flavoprotein 1	1.8	375	LIEFYK*HESCGQCTPCR	83945	70586	360254	421622	0.010
NUEM	NADH dehydrogenase (ubiquinone) 1 alpha subcomplex, 9	2.1	254	GIVNATK*DPDAVGK	27820	40881	237292	176120	0.031
SDHB	succinate dehydrogenase complex, subunit B, iron sulfur	2.0	53	FAIYRWDPDK*TGDKPR	32300	41500	224000	192000	0.009
UQCRC2	ubiquinol cytochrome c reductase core protein 2	0.7	98	GASSFK*ITR	481013	443929	894033	827789	0.009
UQCRHL	ubiquinol-cytochrome c reductase hinge protein	0.5	40	EHCEQLEK*CVK	1429330	1573450	2264430	2202190	0.011
UQCRQ	ubiquinol-cytochrome c reductase, complex III subunit VII	1.5	33	AFPSYFSK*GIPNVLRR	744610	1072500	3604840	3847740	0.005
VDAC-3	voltage-dependent anion channel 3	0.6	226	YK*LDCR	28591200	32534000	58736500	50846100	0.032
VDAC-3	voltage-dependent anion channel 3	0.5	63	YK*VCNYGLTFTQK	557790	524298	768705	770881	0.005
Amino acid metabolism									
AASS	aminoadipate-semialdehyde synthase precursor	2.2	286	KTDGVYDPVEYEK*YPER	19360	29295	157331	138960	0.007
ACAT1	acetyl-Coenzyme A acetyltransferase 1 precursor	0.7	171	GATPYGGVK*LEDLIVKDGLTDVYNK	1684490	1849720	3445290	3120000	0.014
ALDH4A1	aldehyde dehydrogenase 4A1	2.8	118	KEWDLK*PMADR	15200	11800	105000	109000	0.001
ALDH4A1	aldehyde dehydrogenase 4A1	2.5	113	K*EWDLKPMADR	120665	127826	872881	875539	0.000
ALDH4A1	aldehyde dehydrogenase 4A1	1.7	357	LYVPK*SLWPQIK	441000	416682	2077210	1931520	0.002
ALDH4A1	aldehyde dehydrogenase 4A1	0.7	551	ETHK*PLGDWR	352782	371325	699427	648346	0.008
ALDH6A1	aldehyde dehydrogenase family 6, subfamily A1	0.7	55	SDK*WIDIHNPATNEVVGR	273729	309082	585684	527159	0.016
ALDH6A1	aldehyde dehydrogenase family 6, subfamily A1	0.7	113	YQQLIK*ENLK	164222	154810	272750	314412	0.024
ALDH6A1	aldehyde dehydrogenase family 6, subfamily A1	0.6	117	ENLK*EIAR	916814	929386	1629510	1518390	0.007
AUH	AU RNA binding protein/enoyl-Coenzyme A hydratase	2.2	88	MLSK*AVDALKSDKK	88824	47002	377611	455416	0.016
AUH	AU RNA binding protein/enoyl-Coenzyme A hydratase	0.6	75	AYGK*NALSK	216076	234875	403942	394309	0.004
AUH	AU RNA binding protein/enoyl-Coenzyme A hydratase	0.6	84	NLLK*MLSK	201000	247750	362281	394019	0.032
BCKDHB	branched chain keto acid dehydrogenase E1 beta	2.4	162	GLLLSCIEDK*NPCIFFEPK	22925	52406	287715	219111	0.029
BCKDK	branched chain ketoacid dehydrogenase kinase	2.1	192	YFLDK*TLTSR	124494	121733	755400	735289	0.000
CCBL2	cysteine conjugate-beta lyase 2	1.6	117	ALSCLYGK*IYQR	1098140	1200350	5696280	4984720	0.007
CCBL2	cysteine conjugate-beta lyase 2	1.6	427	SKPHFEK*LVR	21161	9479	66626	71343	0.013
FAHD2A	fumarylacetoacetate hydrolase domain containing 2A	2.3	202	NGK*QWLLGK	207835	224429	1455250	1297130	0.005
GCDH	glutaryl-Coenzyme A dehydrogenase	4.0	240	GFILEK*GMR	10500	19800	198821	144572	0.030
HIBCH	3-hydroxyisobutyryl-Coenzyme A hydrolase	1.5	352	AVLIDK*DQTPK	523151	502935	2043760	2198730	0.002
IVD	isovaleryl coenzyme A dehydrogenase	0.6	147	NGNEAQK*EK	20856	22690	37963	37578	0.003
MCCC1	methylcrotonoyl-Coenzyme A carboxylase 1 (alpha)	2.0	577	DGSYDMQIDNK*SFR	26654	25434	172654	128423	0.030
MCCC1	methylcrotonoyl-Coenzyme A carboxylase 1 (alpha)	0.6	180	SIMAAAGVPVVEGYHGK*DQSDQCLR	47453	44837	78209	87991	0.018
MUT	methylmalonyl-Coenzyme A mutase	1.5	604	RVNK*FMER	14130	20775	61571	85524	0.046
OXCT1	3-oxoacid CoA transferase 1	1.7	271	LIK*GEKYEK	43811	29304	156502	198655	0.024
OXCT1	3-oxoacid CoA transferase 1	1.7	274	LIKGEK*YEK	43811	29304	156502	198655	0.024
PRODH	proline dehydrogenase	1.5	356	FTEEEEQQMK*R	6215	6240	27427	25001	0.004
SHMT2	serine hydroxymethyltransferase 2 (mitochondrial)	1.7	469	LQDFK*SFLLKDPETSQR	22042	27295	109716	132229	0.014
Signaling									
AK3	adenylate kinase 3	2.6	29, 34	ITK*HFELK*HLSSGDLLR	57631	41528	364620	371847	0.001
AK3	adenylate kinase 3	1.8	34	HFELK*HLSSGDLLR	2537260	2263010	12869200	11196400	0.008
AK3	adenylate kinase 3	1.5	171	TVGIDDLTGEPLIQREDDKPETVIK*R	20039	20966	72819	98578	0.037
S100A4	S100 calcium binding protein A4	0.6	28	FK*LNKT	2820180	2882820	5146110	4920120	0.003

Table S2.1 (Continued).

SgK269	NKF3 kinase family member	1.8	1698	RTLLMIKFAEK*SLDR	17865	11801	79092	68071	0.011
Transcription and RNA processing									
DDX47	DEAD (Asp-Glu-Ala-Asp) box polypeptide 47	2.5	450	VAGGKMK*K	10500	13926	85220	84100	0.001
LRPPRC	leucine-rich PPR motif-containing protein	1.5	462	NVQGIIDILK*IMNK	150267	138690	587809	643664	0.004
PHC3	polyhomeotic-like 3	0.1	826	K*PDNQSLGHR	442214	409000	129102	174125	0.010
TRIP8	jumonji domain containing 1C	2.1	1645	K*QNDLQKR	114705	74969	582786	563424	0.002
VARS2	valyl-tRNA synthetase 2, mitochondrial	2.3	548	VIGENAEDDRK*ECWVVGR	34118	36581	220490	240522	0.003
Other small molecule metabolism									
BPHL	biphenyl hydrolase-like (serine hydrolase)	1.9	126	DAKDAVDLMK*ALQFK	63127	45486	244243	341905	0.041
BPHL	biphenyl hydrolase-like (serine hydrolase)	0.6	243	HLLPLVQCPTLIVHGEK*DPLVPR	22203	21592	39078	34305	0.025
C21orf33	es1 protein	1.5	152	NLSTFAVDGKDCK*VNKEVER	78500	68900	327000	286000	0.008
Fmo5	flavin containing monooxygenase 5	0.5	97	MYAK*EFDLLK	236497	225327	332628	363140	0.019
ZADH2	zinc binding alcohol dehydrogenase, domain containing 2	2.2	35	TMQK*LVVTR	526216	431858	3046860	3023540	0.000
Carrier and transport proteins									
SLC25A1	tricarboxylate transport protein, mitochondrial	2.3	277	AFYK*GTVPR	192951	160396	1343220	1001310	0.028
SLC25A1	tricarboxylate transport protein, mitochondrial	0.6	97	GLSSLLYGSIPK*AAVR	904005	1026840	1444360	1609050	0.032
SLC25A3	phosphate carrier protein, mitochondrial	5.3	204	MYK*EEGLNAFYK	60080	58994	867117	930028	0.001
SLC25A32	mitochondrial folate transporter	1.5	175	IYK*YEGVR	130668	139607	499602	675004	0.036
SLC25A4; SLC25A5	solute carrier family 25, member	1.7	272	AFFK*GAWSNVLR	1096110	1576060	7080260	5805820	0.017
SLC25A5	ADP/ATP translocase 2	2.0	272	DEGSKAFFK*GAWSNVLR	445809	477625	2351030	2783800	0.010
Chaperone									
HSP60	heat shock protein 1 (chaperonin)	1.5	387	RIQEITEQLDITTSEYEK*EKLNER	78548	128747	476522	427581	0.010
HSP75	TNF receptor-associated protein 1	2.0	326	YIAQAYDK*PR	28500	28436	183238	140637	0.025
HSPA9	heat shock protein 9	3.8	300	ETGVDLTK*DNMALQR	162787	238101	2055510	2197960	0.002
HSPA9	heat shock protein 9	1.8	610	MEEFKDQLPADECNK*LKEEISK	58138	50056	319609	239446	0.030
Waste and ROS clearance									
CA3	carbonic anhydrase III	1.7	212	LK*EPMTVSSDQMAK	393963	335238	1674240	1741980	0.001
SOD2	superoxide dismutase 2, mitochondrial	3.2	130	DFGSFEK*FKEK	275877	248499	2237190	2542790	0.005
SOD2	superoxide dismutase 2, mitochondrial	3.2	132	DFGSFEKFK*EK	275877	248499	2237190	2542790	0.005
TXNRD2	thioredoxin reductase 2 precursor	1.8	153	VK*YFNIK	590531	552932	3120600	2805880	0.004
Proteolysis									
ADAMTS20; TTLL2	a disintegrin-like and metalloprotease with thrombospondin type 1 motifs 20	0.6	1642; 210	YK*CDLR	28591200	32534000	58736500	50846100	0.032
AFG3L2	AFG3(ATPase family gene 3)-like 2	1.7	299	VLK*DEIDVK	51765	60399	269597	284621	0.002
PITRM1	pitrilysin metallepetidase 1	1.6	770	K*YLLNCDNMR	17900	18000	79477	85519	0.002
Translation regulation									
eEF1G	eukaryotic translation elongation factor 1 gamma	0.6	434	AVNQGK*IFK	162203	174101	265760	283087	0.010
IARS2	mitochondrial isoleucine tRNA synthetase	2.4	241	SYK*PVYWSPSSR	411157	351770	2334780	2756280	0.010
IARS2	mitochondrial isoleucine tRNA synthetase	1.7	540	TK*DEYLINSQTTEHIIK	47000	47600	206066	252939	0.016
Apoptosis									
BCAP29	B-cell receptor-associated protein 29	0.6	177, 178	FMEENEKLKLGLRNDNAEEHLLEAENK*K*	62480	68789	113099	125959	0.017
LETMD1	LETM1 domain containing 1	1.5	304	LGIGQLTAQEVK*SACYLR	190488	162578	850381	686374	0.019
SHARPIN	SHANK-associated RH domain interacting protein	1.5	240	SSSAHVSLK*	9133	7932	35227	37498	0.002
Cytoskeleton/architecture/structural protein									
FOP	Fgfr1 oncogene partner	0.6	64	K*FLNTK	2820180	2882820	5146110	4920120	0.003
IMMT	inner membrane protein, mitochondrial	0.6	674	QLK*PPAELYPEDINTFK	165551	234550	357746	354183	0.046
Nucleotide binding									
ATAD3A	AAA-ATPase TOB3	4.0	490	MYFDK*YVLKPATEGK	46700	43300	546023	473871	0.006
DNA repair									
TDP1	tyrosyl-DNA phodphodiesterase 1	1.9	57	KVAHK*R	106244	89984	440285	594070	0.032

Table S2.1 (Continued).

Ubiquitin conjugation									
RNF220	ring finger protein 220	0.6	476, 496	TCK*NSDIEKITEESAVTTFEALK*ARVR	1876260	1780750	2739600	3096090	0.028
Unknown function									
9330129D05Rik; ACAD10	PREDICTED: hypothetical protein LOC338350 isoform 1	3.7	538, 542; 1052, 1056	VAK*MELK*NQSR	17100	9100	137194	138407	0.001
9330129D05Rik; ACAD10	PREDICTED: hypothetical protein LOC338350 isoform 1	1.5	267; 776	YGTEEQK*AR	61188	57691	219218	271622	0.019
CLYBL	citrate lyase beta like	1.7	56	RAVLYVPGNDEKK*IR	68400	77200	362000	336000	0.002
LOC727947; UQCRB	PREDICTED: hypothetical protein	1.7	12	SAVSASSK*WLDGFR	420341	457605	2136730	2003490	0.002
SLC25A6; SLC25A5	predicted gene, EG433923	1.6	155	EFK*GLGDCLVK	1313960	1096370	5329970	5667500	0.002
SLC25A6; SLC25A5	predicted gene, EG433923	1.5	105	QIFLGGVDK*R	318744	391985	1559900	1364010	0.009
SLC25A6; SLC25A5	predicted gene, EG433923	0.7	96	YK*QIFLGGVDKR	39637	48205	83018	85844	0.012
SLC25A6; SLC25A5	predicted gene, EG433923	0.6	166	IYK*SDGIK	240141	240167	352294	395180	0.025

Table S2.2 | Significantly increased or decreased acetylation sites by >50% in SIRT4 KO liver compared to WT

* = acetylated lysine residue. Hyperacetylated sites are denoted by the fold change in blue boxes.

Protein name	Description	Normalized fold change	AcK site	Peptide	Raw intensity				Raw intensity pvalue
					WT 1	WT 2	KO 1	KO 2	
Lipid metabolism									
ACAD11	acyl-Coenzyme A dehydrogenase family, member 11	0.5	175	YGTGVGYCK*R	394481	397769	235261	216982	0.003
ACADM	medium-chain acyl-CoA dehydrogenase	0.7	173	CVTEPSAGSDVAAIK*TK	82714	79411	56147	61026	0.017
ACADS	short-chain acyl-CoA dehydrogenase	0.5	262	ENLLGEPGMGFK*IAMQTLDMGR	1716080	1898340	1012350	911946	0.015
ACADVL	acyl-Coenzyme A dehydrogenase, very long chain	0.6	373	TQFGDK*IHNFGVIQEK	159366	151401	103987	100901	0.006
ACADVL	acyl-Coenzyme A dehydrogenase, very long chain	0.6	383	TQFGDKIHNFGVIQEK*	159366	151401	103987	100901	0.006
ACADVL	acyl-Coenzyme A dehydrogenase, very long chain	0.5	279	EK*ITAFVVER	3014970	2710000	1750000	1490000	0.025
ACADVL	acyl-Coenzyme A dehydrogenase, very long chain	0.5	277	TPIKDAATGAVK*EK	105385	111808	63692	57784	0.008
ACOX1; ACOX1 iso3	acyl-Coenzyme A oxidase 1	0.7	159	GLETTATYDPK*TQEFILNSPTVTSIK	786441	835116	570661	590458	0.013
CROT	carnitine O-octanoyltransferase	0.6	501	DCSHGK*GFDR	139777	152123	98056	83831	0.028
EHHADH	enoyl CoA, hydratase/3-hydroxyacyl CoA dehydrogenase	0.7	355	SGQASAK*PNLR	503831	562658	363383	400059	0.049
EHHADH	enoyl CoA, hydratase/3-hydroxyacyl CoA dehydrogenase	0.6	605	ETHHIK*QR	45789	49335	33257	32044	0.015
EHHADH	enoyl CoA, hydratase/3-hydroxyacyl CoA dehydrogenase	0.6	329	VGIPVVAVESDPK*QLDTAK	1008620	975302	631643	713016	0.018
EHHADH	enoyl CoA, hydratase/3-hydroxyacyl CoA dehydrogenase	0.6	274	ALQYAFFAEK*SANK	2857570	2690340	2024620	1706110	0.037
HADHA	mitochondrial trifunctional protein, alpha subunit	1.9	460	VLK*EVESVTPEHCIFASNTSALPINQIAAVSKRPEK	138231	170675	344077	297455	0.028
HADHSC	L-3-hydroxyacyl-Coenzyme A dehydrogenase	1.6	206	TFESLVDFCKTLGK*HPVSCKDTPGFIVNR	797463	779362	1321540	1307240	0.000
HMGCS2	hydroxymethylglutaryl-CoA synthase 2	1.6	350	GLKLEETYTNK*DVDKALLK	4582870	4442780	7362320	7575170	0.002
HSD17B13	alcohol dehydrogenase PAN1B-like	0.6	79	GVEETADK*CR	188987	194017	115910	118151	0.001
SCP2	sterol carrier protein 2, liver	0.6	443	K*LEEEGEQFVKK	2072980	2119920	1251690	1555150	0.046
SCP2	sterol carrier protein 2, liver	0.6	438	ANLVFK*EIEK	3621140	3880890	2355220	2383400	0.009
SCP2	sterol carrier protein 2, liver	0.5	453	KLEEEGEQFVK*K	893644	979273	438613	586380	0.038
SCP2	sterol carrier protein 2, liver	0.5	491	GSVLPNSDK*K	1343400	1379820	747823	732430	0.001
SCP2	sterol carrier protein 2, liver	0.5	432	SSAGDGFK*ANLVFK	3324710	2880160	1767740	1489300	0.030
Electron transport chain and energy production									
ATP5O; Gm5436	ATP synthase F1 complex, O subunit	1.6	172	SFLSPNQILK*LEIK	2755120	2890210	4377940	4958250	0.025
COX5A	cytochrome c oxidase, subunit Va	1.6	145	AGPHKEIYPYVIQELRPTLNELGISTPEELGLDK*V	240000	202000	359000	391128	0.025
CYCS; CYCT	cytochrome c, somatic	1.9	87	MIFAGIK*K	96357	94195	199452	188540	0.003
CYP2C19; Cyp2c50	cytochrome P450, family 2. subfamily c, polypeptide 37	0.4	200	DRDFLNLMEK*LNEITK	1091210	1039420	454900	464508	0.002
NNT	nicotinamide nucleotide transhydrogenase	152.8	70	EIFQNEK*R	35100	27700	5450000	4780000	0.004
NNT	nicotinamide nucleotide transhydrogenase	7.0	433	DGK*VIFPAPTPK	59500	66228	527830	412556	0.020
UCP1	uncoupling protein 1 (mitochondrial, proton carrier)	2.5	151	MQAQSHLHGIK*PR	25797	20160	65067	59734	0.010
Waste and ROS clearance									
catalase	catalase	0.7	306	VWPHK*DYPLIPVGK	2877040	2767710	2090370	1905860	0.017
catalase	catalase	0.6	476	DAQLFIQK*K	6392650	5733400	3953580	3917840	0.023
CPS1	carbamoyl-phosphate synthetase 1	0.7	307	EPLFGISTGNIITGLAAGAK*SYK	3611900	3951500	2739770	2761550	0.026
ETHE1	ETHE1 protein	1.5	172	TDFQQGCAK*TLYHSVHEK	311533	328790	553019	486580	0.028
GSTM1	glutathione S-transferase mu 1	0.4	173	MFEPK*CLDAFPNLR	537546	566485	258642	259759	0.002
OTC	ornithine transcarbamylase	1.6	88	SLGMIFEK*R	7002400	8080000	14250600	12073200	0.044
TXNRD2	thioredoxin reductase 2 precursor	1.5	153	VK*YFNIK	1112490	1170950	1931260	1769700	0.014

Table S2.2 (Continued).

TCA cycle and Anaplerosis									
DLST	dihydrolipoamide S-succinyltransferase	2.2	268, 273	HK*DAFLK*K	446635	551597	1129640	1173990	0.008
GOT2	glutamate oxaloacetate transaminase 2, mitochondrial	1.8	107	NLDKEYLPIGGLAEFCK*ASAELALGENNEVLK	857238	1034700	1945590	1761770	0.019
OGDH; OGDHL	oxoglutarate dehydrogenase (lipoamide)	0.5	276; 282	KWSSEK*R	318414	264580	135912	154071	0.036
PC	pyruvate carboxylase	0.5	152	MGDK*VEAR	217517	258913	131624	111675	0.037
Amino acid metabolism									
AASS	aminoadipate-semialdehyde synthase precursor	0.5	707	DSIK*YAEIYGISSAHTLLR	5238960	5486120	3006970	3139310	0.004
ALDH6A1	aldehyde dehydrogenase family 6, subfamily A1	1.6	113	YQQLIK*ENLK	416092	395160	739331	627533	0.039
IVD	isovaleryl coenzyme A dehydrogenase	1.5	149	NGNEAQKEK*YLPK	118013	124369	188759	202699	0.010
Transcription and RNA processing									
NACA	nascent polypeptide-associated complex alpha subunit isoform a	2.3	1180	K*ASKTAAPK	13300	15000	33400	34600	0.003
SND1	staphylococcal nuclease domain containing 1	0.7	193	HFVDSHHQK*PVNAIIEHVR	357304	358662	239696	282383	0.045
Other small molecule metabolism									
BPHL	biphenyl hydrolase-like (serine hydrolase)	1.8	126	DAKDAVDLMK*ALQFK	1881350	1934430	4075460	3325560	0.041
Carrier and transport proteins									
SLC12A3	phosphate carrier protein, mitochondrial	0.6	866	ISLLSK*FR	1778360	1665060	1110630	1173860	0.012
Signaling									
TAO3	TAO kinase 3	2.0	830	ELQK*LEQR	408370	375249	858731	813434	0.004
Chaperone									
HSP60	heat shock protein 1 (chaperonin)	1.8	369	GKGDKAHIEK*R	38407	33967	71190	66305	0.010
Translation regulation									
MGC17403	TFS2-M domain-containing protein 1	0.6	4	MSDK*NQIIAR	864000	807000	582354	559386	0.013
Adhesion or extracellular matrix protein									
FGG	fibrinogen gamma chain	0.6	405, 431	SRWYSMK*ETTMKIIPFNRLSIGEGQQHHMGGSK*	1830000	1996450	1160000	1145990	0.012
Proteolysis									
SERPINA1	serine (or cysteine) proteinase inhibitor, clade A, member 1a	1.6	292	ELISK*FLLNR	561234	678166	1141590	989358	0.043
Unknown function									
9330129D05Rik; ACAD10	PREDICTED: hypothetical protein LOC338350 isoform 1	1.8	542; 1056	MELK*NQSR	274558	402650	662810	642321	0.040
A230051G13Rik	hypothetical protein LOC216792	1.7	222	GQLGDLQDYHK*YR	577782	538197	1003760	980827	0.003
EG620143	PREDICTED: hypothetical protein	6.7	24; 30; 69	KQLATK*AAR	247101	250061	1719220	1846890	0.002
EG620143	PREDICTED: hypothetical protein	3.2	19, 24; 25, 30; 64, 69	K*QLATK*AAR	3303060	3364100	12275700	10684400	0.009
EG544973	PREDICTED: hypothetical protein	4.2	10, 15; 16, 21; 55, 60	K*STGGK*APR	1969650	1728440	8585560	8138010	0.002
KIAA1751	hypothetical protein LOC544678	0.7	55	ESK*GAEK	55920	58222	41286	39653	0.007
LOC240549	hypothetical protein LOC240549	1.6	43	LK*ALVDKWPDFNTVVVRPR	218024	273959	442676	414682	0.028

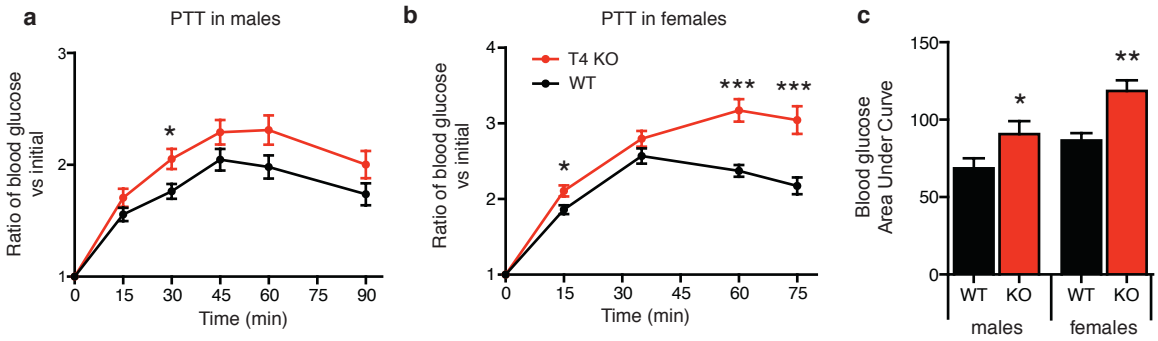

Figure S2.1 | SIRT4 KO mice show increased blood glucose levels in pyruvate tolerance tests. a-b, Pyruvate tolerance tests in 6-month WT and SIRT4 KO male and female mice. Mice were fasted overnight, then injected intraperitoneally with 2 g/kg pyruvate. Tail vein blood glucose was monitored at15 min intervals. Values are represented as the ratio of blood glucose versus initial for each mouse. n=22-29. **c,** Area under the curve calculated from PTT graphs. * $p < 0.05$, ***$p < 0.001$. Error bars indicate SEM.

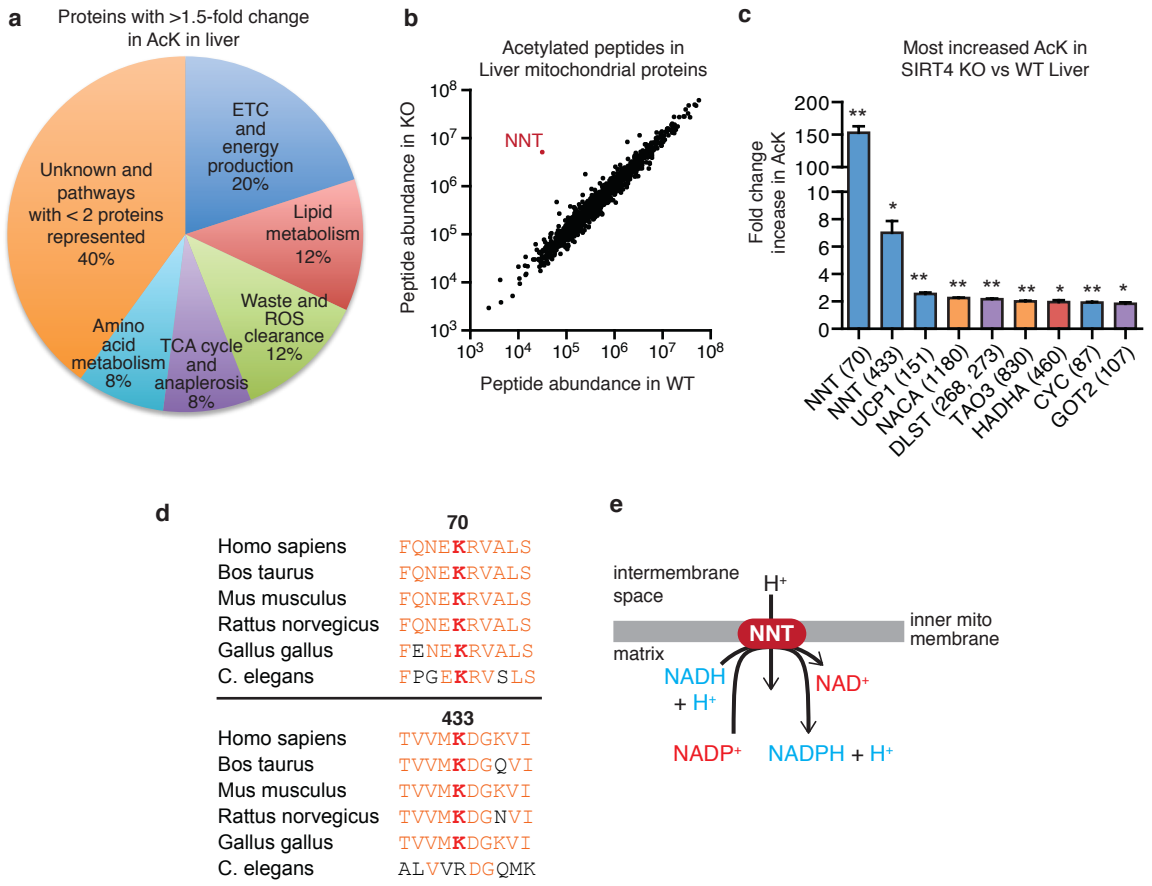

Figure S2.2 | NNT is a strongly hyperacetylated protein in SIRT4 KO liver. a, Pie chart depicting the pathways represented by the 24 mitochondrial proteins with significantly increased lysine acetylation in SIRT4 KO versus WT liver. Enzymes involved in lipid metabolism, ETC and energy production represent the greatest portion. **b,** Raw intensity of acetylated peptides in WT versus SIRT4 KO liver mitochondrial proteins. Each point represents one acetylated peptide. While most protein changes are <8-fold, NNT is particularly highly acetylated in SIRT4 KO liver. **c,** AcK sites with the greatest increase in SIRT4 KO liver, based on the median-centered normalized fold change values. The acetylated residue is listed in parenthesis. **d**, Conservation of K70 and K433 in NNT. K70 is conserved from C. elegans to Homo sapiens. K433 is conserved in several vertebrate species. K70 and K433 are highlighted in red. Other conserved residues are in orange. **e,** Schematic depicting NNT function. NNT acts as a proton pump at the the inner mitochondrial membrane and is linked to ETC function. Protons moved to the intermembrane space by the ETC can be returned to the matrix not only via ATP synthase but also via NNT. NNT concomitantly interconverts $NADP^+$ and NADH to NADPH and NAD^+. *$p < 0.05$, **$p < 0.01$. Error bars indicate SEM.

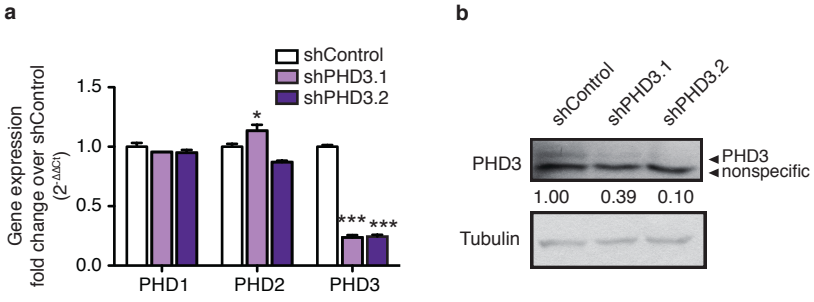

Figure S3.1 | Extent of PHD3 knockdown in 293T cells. a-b, PHD gene expression **(a)** and PHD3 protein levels **(b)** in 293T cells stably expressing shRNA against PHD3 (shPHD3.1 and shPHD3.2) or non-targeting control (shControl). *$p < 0.05$, ***$p < 0.001$ Error bars indicate SEM.

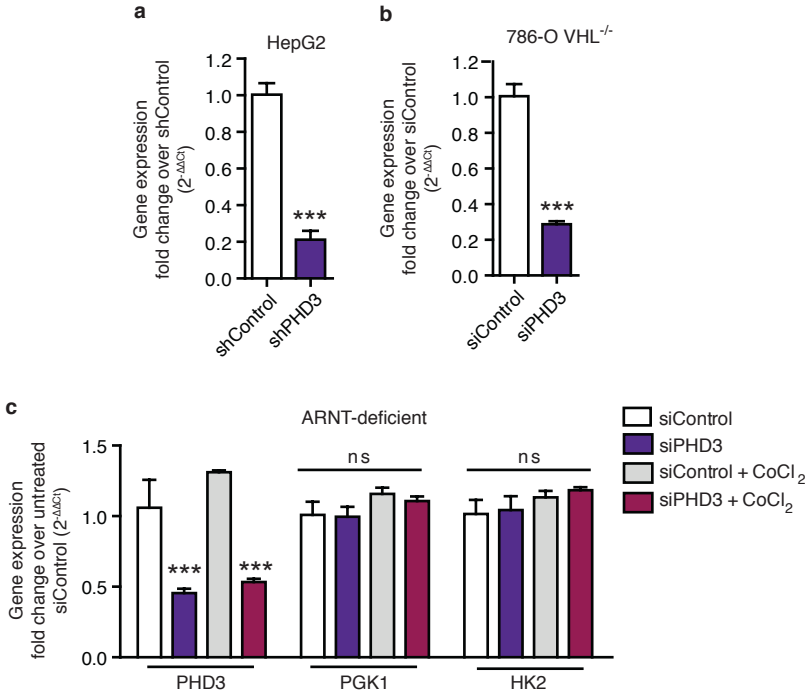

Figure S3.2 | Extent of PHD3 knockdown by shRNA or siRNA in several cell lines. a, PHD3 gene expression in HepG2 cells stably expressing shRNA against PHD3 (shPHD3.2) or non-targeting control (shControl). **b,** PHD3 gene expression in 786-O $VHL^{-/-}$ cells transiently transfected with siRNA against PHD3 or control. **c,** PHD3 gene expression and HIF target gene expression in ARNT-deficient cells transiently transfected with siRNA against PHD3 or control, and also treated +/- the HIF stabilizing compound $CoCl_2$. ***$p < 0.001$. Error bars indicate SEM.

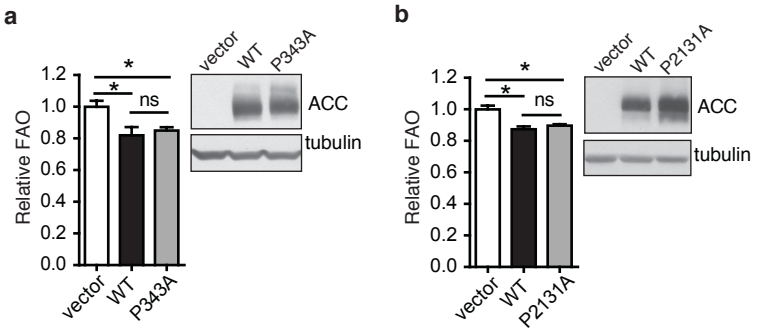

Figure S3.3 | Site-specific mutagenesis of sites P343 and P2131 in ACC2 does not alter the ability of ACC2 to repress FAO. a-b, Palmitate oxidation in complete media in 293T cells transiently overexpressing wild type ACC2 or ACC2 lacking the P343 **(a)** or P2131 **(b)** putative hydroxylation sites (n = 3). Western blots show levels of overexpressed ACC2 (n = 3). *$p < 0.05$. Error bars indicate SEM.

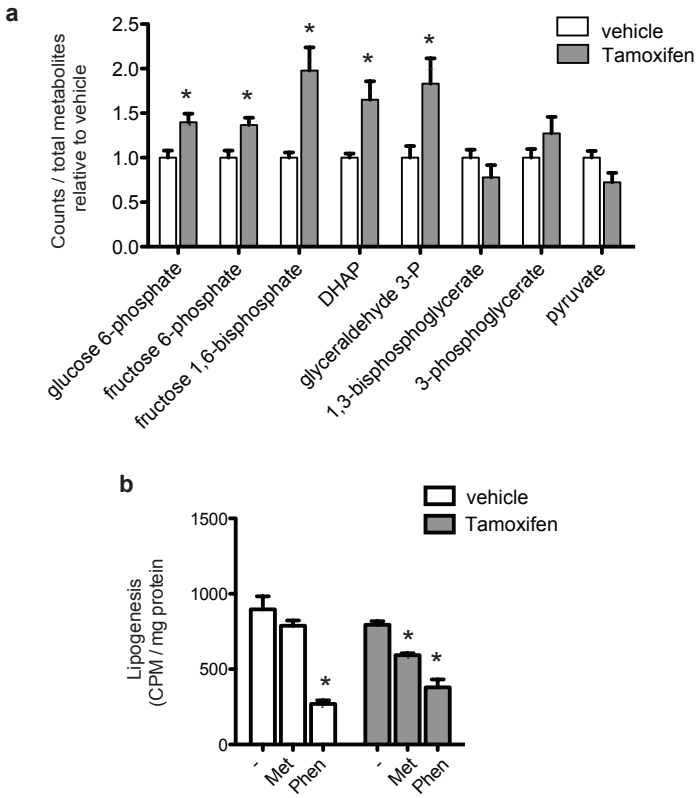

Figure S4.1 | Glycolytic induction during transformation and decrease in lipogenesis with phenformin treatment. a, Relative levels of glycolytic intermediates measured by LC-MS/MS in MCF10A ER-Src cells treated with tamoxifen or ethanol for 24 hr, n=4. **b,** De novo lipogenesis from ^{14}C-glucose in ER-Src cells pre-treated with tamoxifen or ethanol +/- biguanide for 24 hr prior to 4 hr lipogenesis analysis, n=3. *$p < 0.05$ compared to vehicle control. Error bars indicate SEM.

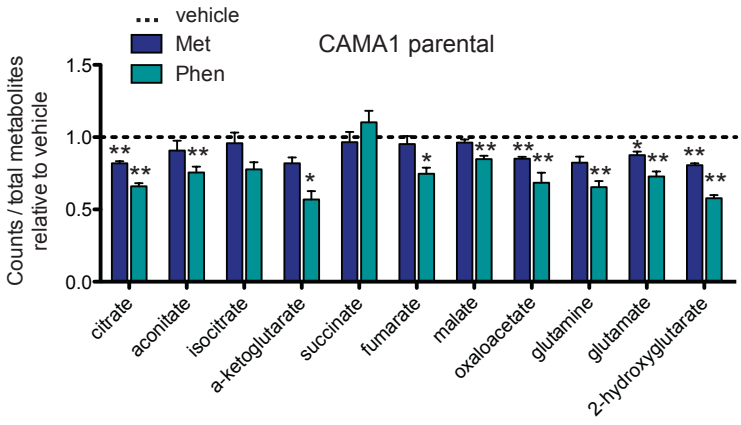

Figure S4.2 | TCA cycle regulation by biguanides in transformed CAMA-1 breast cancer cells. 24 hours after metformin or phenformin treatment TCA cycle intermediates were measured in CAMA-1 breast cancer cells, n=4. *$p < 0.05$, **$p < 0.01$ compared to vehicle control. Error bars indicate SEM.

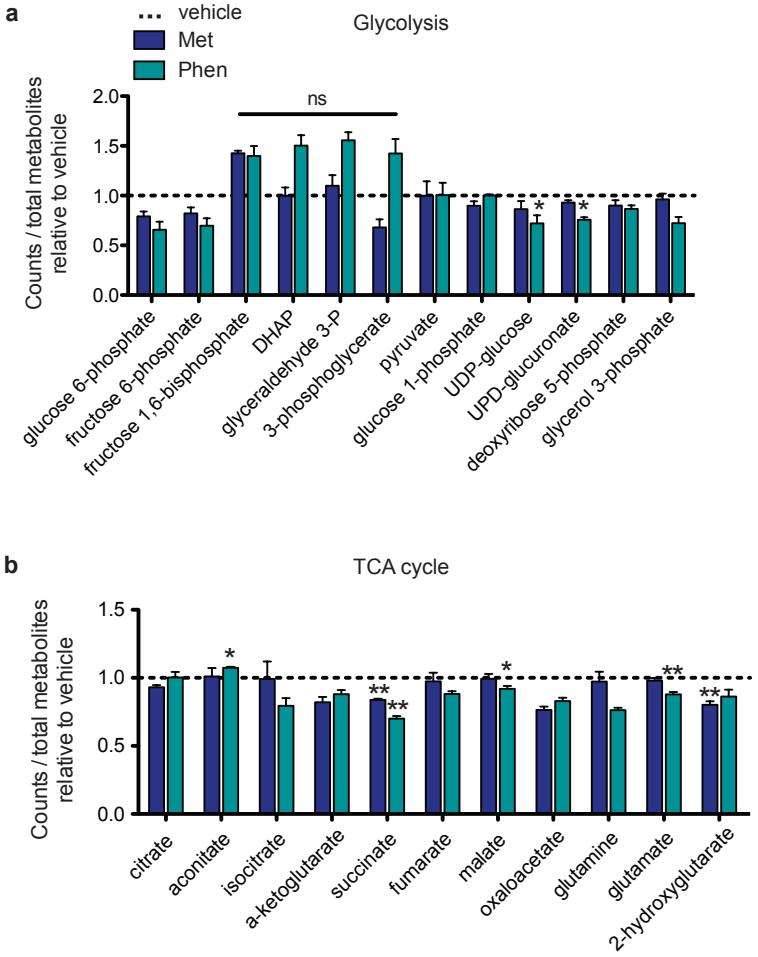

Figure S4.3 | Glycolysis and TCA cycle regulation by metformin and phenformin in CSCs. a-b, After 24 hr treatment with metformin and phenformin, intermediates of glycolysis **(a)** and TCA cycle **(b)** in cancer stem cells were measured, n=3. *p < 0.05, **p < 0.01 compared to vehicle control. Error bars indicate SEM.

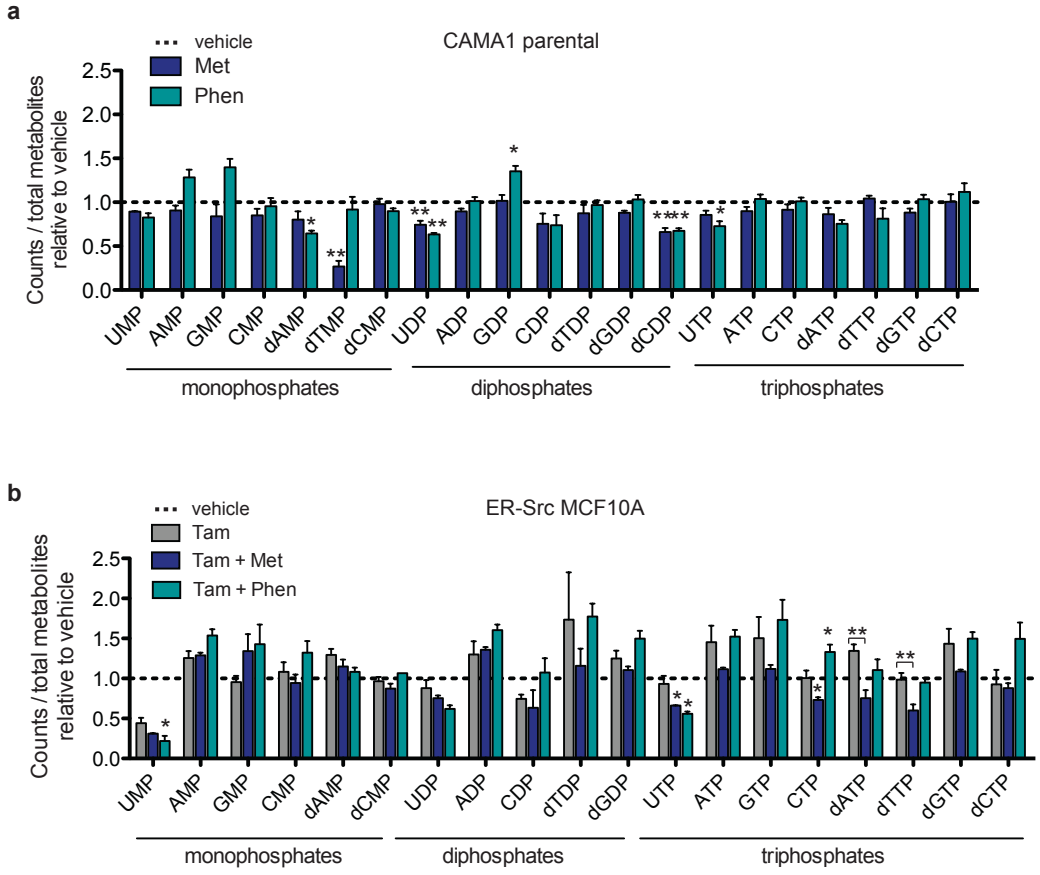

Figure S4.4 | Nucleoside regulation by metformin and phenformin in parental CAMA-1 cells and during the transformation process of MCF-10A ER-Src. a-b, Parental CAMA-1 **(a)** and transformation induced MCF-10A ER-Src **(b)** cells were treated with metformin or phenformin for 24hr and changes in nucleotide metabolism were measured, n=4. *$p < 0.05$, **$p < 0.01$ compared to tamoxifen treatment alone. Error bars indicate SEM.